DISSERTATION

MECHANISMS OF INTERACTION BETWEEN BENTONITE AND ANIONIC POLYMERS IN ENHANCED GEOSYNTHETIC CLAY LINERS

Submitted by

Anna Norris

Department of Civil and Environmental Engineering

In partial fulfillment of the requirements

For the Degree of Doctor of Philosophy

Colorado State University

Fort Collins, Colorado

Spring 2021

Doctoral Committee:

Advisor: Joseph Scalia
Co-Advisor: Charles Shackelford

Travis Bailey
Craig Benson
Thomas Borch

ABSTRACT

MECHANISMS OF INTERACTION BETWEEN BENTONITE AND ANIONIC POLYMERS IN ENHANCED GEOSYNTHETIC CLAY LINERS

Polymer enhanced bentonites (EBs) are a potential solution to the chemical incompatibility of natural bentonite in many containment applications. Relative to conventional (natural or un-enhanced) bentonites, EBs have shown improved (lower) hydraulic conductivity to high strength waste liquids, but the mechanisms underlying these improvements are not well understood. The EB geosynthetic clay liners (EB-GCLs) evaluated in this study were produced with linear anionic polymers poly(acrylic acid) (PA) and sodium carboxymethylcellulose (CMC), as well as a covalently crosslinked PA (PAx), using multiple mixing methods (dry-sprinkle, dry mix, and wet mix) and percent polymer enhancements (5-10% by mass). The results of hydraulic conductivity tests based on permeation with concentrated inorganic solutions, viz., 500 mM NaCl and 167 mM $CaCl_2$, indicated that specific combinations of polymer type and mixing methods in the EB-GCLs produced a low hydraulic conductivity ($\leq 5.0\times10^{-11}$ m/s) for a given applied hydraulic gradient and permeant solution. The use of a lower hydraulic gradient (i.e., 30 vs. 300) also was shown to have the potential to yield a lower hydraulic conductivity of EB-GCLs, suggesting that EB-GCLs are sensitive to the applied hydraulic gradient in a way that conventional GCLs containing unamended sodium bentonite (NaB) are not. The reason for this difference is that there is less likelihood of any hydrogel existing within the EB-GCL being flushed from the EB-GCL at the lower hydraulic gradient. Batch adsorption tests were conducted with 16.7 and 167 mM $CaCl_2$, 500 mM NaCl, 12.3 mM $CaSO_4$ and 167 mM Na_2SO_4 solutions to compare the adsorption behavior with respect to cation and anion species and concentration. Poly (acrylic acid) adsorption onto NaB increased with increasing Ca^{2+} concentration (12.5 mM $CaSO_4$ < 16.67 mM $CaCl_2$ < 167 mM $CaCl_2$), resulting in increasing solid (adsorbed) phase concentration of PA. Sodium bentonite tested with NaCl exhibited limited adsorption capacity for PA. Total

carbon (TC) analysis was confirmed to be an accurate technique for measuring polymer loading of both as-prepared and hydrated/permeated EB-GCLs. A multiple lines of evidence approach was used to determine the mechanisms controlling the hydraulic conductivity of EB-GCLs. The results of the hydraulic conductivity testing were paired with measurements of polymer retention and qualitative measurements of hydrogel formation to understand the variables controlling polymer migration within and through the EB-GCL and the relationship between polymer retention and hydraulic conductivity. The results indicated that the low hydraulic conductivity of EB-GCLs ($\leq 5.0\times10^{-11}$ m/s) is controlled by a combination of pore blocking (mechanical entrapment) and adsorption of polymer hydrogel. The reduction in long-term hydraulic conductivity of EB-GCLs relative to unamended GCLs in aggressive inorganic solutions was determined to be the result of several factors, including (1) the formation of hydrogel, (2) the clogging of the largest (most conductive) pores by the hydrogel, (3) the balancing of seepage forces that are sufficient to mobilize the hydrogel into the pores but not sufficiently high to untangle and mobilize the hydrogel due to shear thinning or dislodging by inertial forces, and (4) the kinetics of hydrogel formation and adsorption of polymer to the surface of bentonite. This study illuminates the myriad of interconnected factors that can and must be optimized for EB-GCLs to provide effective long-term containment of aggressive inorganic wastes.

ACKNOWLEDGEMENTS

Professors Joseph Scalia and Charles Shackelford, thank you for your guidance, mentorship, and patience, during my time at Colorado State University. My dissertation would not exist without you and your support. Much gratitude is also due to my PhD committee: Professors Thomas Borch and Travis Bailey from Colorado State University and Professor Craig Benson from the University of Virginia.

I would like to acknowledge multiple graduate students current and past who guided me and assisted over the past four years. Mohammad Reza Hassanzadeh Gorakhi and Neelufar Aghazamani, present and past PhD students at Colorado State University, thank you most of all for your friendship as well as your never-ending support and encouragement in my journey to complete my PhD. Monika Popang, Joel Conzelmann, Emily Cook, and Ragan Anthony, thank you for your friendship and generosity with your time in the lab. Theresa O'Donnell, my undergraduate research assistant at Colorado State University, thank you for all your time and effort spent in the lab during and after my maternity leave. I could not have finished my PhD without you.

I would like to thank my parents Joseph and Barbara Norris, my sisters, Sarah and Rachel Norris, and my family and friends in the USA and abroad for their love and never-ending confidence in me as I pursued my PhD. Finally, I would like to thank my husband, Stefan Van Oyen and daughter, Lucie Van Oyen. No words can adequately describe the gratitude I feel for having such a loving and supportive family.

To all my current and past professors, along with everyone else I could not thank on this page, thank you for everything you have done to allow me to pursue this journey.

TABLE OF CONTENTS

LIST OF TABLES

LIST OF FIGURES

Executive Summary

INTRODUCTION

Engineered containment systems are essential to manage the waste products of an industrialized society. To prevent potential damage to the environment, and impacts to human health, containment systems should prohibit contaminant migration for hundreds to thousands of years. Bentonite barrier layers are used in environmental containment systems due to the low permeability of bentonite to water. Unfortunately, the low hydraulic conductivity of bentonites may be increased by exposure to liquid chemistries typical of many containment applications, hindering the long-term effectiveness of many containment systems (Benson et al. 2010a, Bouazza and Gates 2014, Chen et al. 2019). To design for potential compatibility issues over long-time scales requires a thorough understanding of the mechanisms governing transport and fate of contaminants within the barrier system.

Enhanced bentonites, or bentonites blended with polymers or high molecular-weight organic molecules, are a potential solution to the instability of natural bentonite in many containment applications (e.g., Scalia et al. 2018); products containing enhanced bentonites have already been adopted by industry (Donovan et al. 2016a,b; Yu et al. 2019; Donovan et al. 2020). These materials have shown improved hydraulic conductivity to waste liquids, but the mechanisms underlying these improvements are not well understood (Flynn and Carter 1998; Trauger and Darlington 2000; Katsumi et al. 2001, 2008; Di Emidio 2010; Di Emidio et al. 2010; Scalia et al. 2014; Scalia and Benson 2016; Tian et al. 2016a,b; Scalia and Benson 2017; Tian et al. 2017; Scalia et al. 2018; Tian et al. 2019; Yu et al. 2019). Understanding these mechanisms is fundamental to the safe adoption of enhanced bentonites in long-term barrier applications, to developing future generations of these materials, and to adequately design barrier systems for societies' ever-growing portfolio of wastes.

The aim of this research was to better understand the mechanisms underlying the improvement of hydraulic behavior in geosynthetic clay liners (GCLs) containing anionic-polymer-enhanced bentonites (henceforth termed EB-GCLs). Laboratory testing completed in this study supports the primary mechanism of pore blocking by polymer hydrogels as the mechanism controlling the low hydraulic conductivity of EB GCLs, and that effective pore blocking dependent on variables underlying anionic polymer hydrogel formation, structure, and adsorption to bentonite.

The completed work had four primary objectives: (1) explore the effects of anionic polymer types, properties, and enhancement methods (i.e. dry sprinkling, dry mixing, wet mixing, in-situ polymerization) for creation of EB-GCLs on hydraulic conductivity and chemical compatibility; (2) determine the potential for adsorption of anionic polymers on bentonite in high concentration solutions; (3) investigate the micro-scale mechanisms controlling hydraulic conductivity and chemical compatibility of enhanced bentonite geosynthetic clay liners and (4) develop a model to predict long-term hydraulic conductivity and chemical compatibility of GCLs comprising polyacrylate enhanced bentonites for field applications.

METHODS

Enhanced bentonites were prepared using two types of linear anionic polymers, poly(acrylic acid) and sodium carboxymethyl cellulose. Poly(acrylic acid) (PA) EBs were prepared with three different molecular weights (MoW): (1) low weight (LW, MoW~5000 g/mol), (2) medium weight (MW, MoW~50000 g/mol) and (3) high weight (HW, MoW~345000 g/mol). Sodium carboxymethylcellulose (CMC) EBs were prepared with high and low viscosity grade CMCs. A covalently crosslinked poly(acrylic acid) (PAx) was also used to produce an EB. Finally, an in-situ polymerized bentonite polymer composite (Scalia et al. 2011, Scalia et al. 2014, and Bohnhoff et al. 2013) was used for comparison.

Sodium bentonite was modified using three mixing methods: dry mixing (DM), dry sprinkling (DS), and wet mixing (WM). Dry mixed EBs were prepared by adding a percentage (by mass) of air-dry polymer to air-dry bentonite. Dry sprinkle EBs were prepared by sprinkling a known percentage of dried polymer in an even layer at the inflow side of the GCL before placing the air dry NaB atop (downstream).

Wet mix EBs were created by first mixing a known percentage of polymer into DIW in a mechanical stirrer to allow for the dispersion and hydration of the dried polymer. Dried NaB was then added and mixed. Finally, the WM EBs were then dried and ground.

Enhanced bentonites were tested for hydraulic conductivity in the form of a GCL. Hydraulic conductivity testing of the lab prepared EB-GCLs was conducted at low effective stress (27 kPa) in with concentrated NaCl and $CaCl_2$ solutions (500mM and 167 mM, respectively), following ASTM D6766-18 (ASTM 2018) (falling head, constant tail water elevation but without backpressure). A target average hydraulic gradient (i) of 300 was applied via gravity head using glass burettes (falling head). Each specimen was permeated until ASTM D6766 termination criteria were met. Specimens with high hydraulic conductivities ($>10^{-8}$ m/s) were tested for preferential flow with Rhodamine WT dye.

Batch adsorption tests were conducted with HW PA to determine the degree of adsorption of the anionic polymer on NaB in concentrated inorganic salt solutions and the effect the cation or anion species can have on adsorption. Batch adsorption tests were conducted with 16.67 and 167 mM $CaCl_2$, 500 mM NaCl, 12.25 mM $CaSO_4$ and 167 mM Na_2SO_4 solutions to compare the adsorption behavior. Pyrophyllite was tested for adsorption capacity to determine the effect of the net negative surface charge of the montmorillonite. Homoionized sodium bentonite also was tested for adsorption capacity to determine the potential for adsorption in a system devoid of multi-valent cations.

Four methods were analyzed for use to quantify polymer in EB-GCLs pre- and post-permeation, (1) component loss on ignition (LOI), (2) component A total carbon analysis (TC), (3) component B TC, and (4) a composite TC method. The relative merits of these methods are compared.

A variety of hydrogel formation tests also were conducted to evaluate hydrogel development in the hydrating and permeant solutions tested. Each test method was designed to make observations regarding the factors (kinetics, solution chemistry, polymer type) governing hydrogel properties.

MAJOR FINDINGS

This study is presented in four chapters. The first chapter, titled "Considerations for the effective design of sodium bentonite geosynthetic clay liners enhanced with anionic polymers," presents the results of a range of long-term hydraulic conductivity tests on EB-GCLs permeated with concentrated salt solutions (500 mM NaCl and 167 mM $CaCl_2$). The EB-GCLs were produced with linear anionic polymers PA and CMC, and a covalently crosslinked PAx, using multiple mixing methods and percent polymer enhancements (5-10%). An in-situ polymerized BPC was also tested for comparison and was used as a dry mixed enhancement at 5% polymer content. The results of hydraulic conductivity testing indicated that best combinations of polymer type and mixing methods in EB-GCLs produced a low hydraulic conductivity for a given applied gradient and permeant solution. The higher molecular weight PAs provided the best performance of the linear anionic polymers tested, requiring a low percent (5-8%) polymer addition to reduce hydraulic conductivity to the concentrated solutions tested. Covalently crosslinked PAx slightly outperformed linear PA in concentrated NaCl but not in $CaCl_2$. The BPC produced a low hydraulic conductivity but did not out-perform the other tested EB-GCLs prepared by simpler methods. The dry sprinkle method provided the best performance with the least amount of required effort of the mixing methods tested. The use of dry mixing to produce the EB-GCL posed potential risk for the formation of intergranular flow paths through the elution of polymer during permeation. Wet mixing was less effective than dry mixing methods.

The second chapter, titled "Effects of ion species on the adsorption of poly(acrylic acid) onto sodium montmorillonite," presents the results of batch adsorption tests conducted with a HW PA to determine the degree of adsorption of the anionic polymer on sodium montmorillonite (primary mineral in sodium bentonite) in concentrated inorganic salt solutions and the effect the cation or anion species can have on adsorption. Batch adsorption tests were conducted with in 16.7 and 167 mM $CaCl_2$, 500 mM NaCl, 12.23 mM $CaSO_4$ and 167 mM Na_2SO_4 solutions to compare the adsorption behavior. Pyrophyllite, was tested for adsorption capacity to determine (by difference) the effect of the net negative surface charge of the montmorillonite. Homoionized sodium bentonite also was tested for adsorption capacity to determine the potential for adsorption in a system devoid of multi-valent cations. The results of this study are

consistent with previous studies completed with anionic polymer adsorption onto negatively charged particles/surfaces at higher liquid to solid ratios. Poly(acrylic acid) adsorption onto sodium bentonite increased with increasing Ca^{2+} concentration (12.5 mM $CaSO_4$ < 16.67 mM $CaCl_2$ < 167 mM $CaCl_2$), resulting in increasing solid (adsorbed) phase concentration of PA. In systems dominated by Na^+, sodium bentonite exhibited limited adsorption capacity for PA, while in systems dominated by Ca^{2+}, sodium bentonite had a higher adsorption capacity for PA. Limited adsorption was exhibited by both pyrophyllite and homoionized sodium bentonite. The primary adsorption mechanism exhibited by the anionic polymers onto sodium bentonite in GCLs hydrated and permeated with high concentration monovalent and divalent solutions is likely cation-bridging.

The third chapter, titled "Corroboration of polymer quantification methods for sodium bentonite GCLs enhanced with anionic polymers," presents the results of a method comparison between loss on ignition (LOI) and total carbon (TC) analysis for use to evaluate polymer content in EB-GCLs for initial and post permeation analysis. Results were compared to recent recommendations for use of total carbon (TC) for polymer quantification. Different mixtures of polymer and bentonite (enhanced bentonites; EBs) were tested containing different anionic polymer types including, HW, MW, and LW PA, HV and LV CMC, and PAx. The deviations in measured polymer content using the composite and component TC methods for post-permeation EB-GCLs, permeated with either 500 mM NaCl or 167 mM $CaCl_2$, prepared using wet mixing methods, also were analyzed. The results of this study confirm the bias of the component LOI method; the linear anionic polymers tested exhibited higher mass loss when ignited individually than when ignited in the bentonite-polymer mixtures. As recommended by others, the composite TC method was confirmed to be a more accurate method for measurement of the polymer loading of both un-hydrated and hydrated/permeated, commercial EB-GCL products. The three TC methods tested, composite, component A, and component B, produced similar final polymer contents in post-permeation EB-GCLs with slight deviations in measured post-permeation polymer content by different methods depending on polymer type and permeant solution.

The fourth chapter, titled "Mechanisms controlling the hydraulic conductivity of sodium bentonite geosynthetic clay liners enhanced with anionic polymer," presents the results of the mechanistic analysis of the EB-GCLs produced in this study. To determine the mechanisms controlling the hydraulic conductivity of EB-GCLs, the results of the hydraulic conductivity testing were paired with measurements of polymer retention (via component B TC analysis) to identify the variables controlling polymer movement within and out of the EB-GCL and the relationship between polymer retention and hydraulic conductivity. Physical (pore-clogging) and chemical (adsorption) polymer retention mechanisms were considered. Hydraulic conductivity tests also were conducted with a granular sodium bentonite and pyrophyllite to determine the effect of intergranular pore size and surface charge, respectively. A variety of hydrogel formation tests also were conducted to evaluate hydrogel development in the hydrating and permeant solutions tested. The results of the hydrogel formation tests confirmed that PA hydrogel was formed in both NaCl and $CaCl_2$ solutions during hydration. The results of the hydraulic conductivity testing and polymer retention analysis indicated that the low hydraulic conductivity of EB-GCLs is controlled by a combination of pore blocking (mechanical entrapment) and adsorption of polymer hydrogel. When an EB-GCL produces a low hydraulic conductivity, the effective pore size of the bentonite at equilibrium must be less than the smallest remaining hydrogel. The effective "filtration" of the polymer hydrogel and ultimately the reduction in long-term hydraulic conductivity was determined to be dependent on (1) the formation of hydrogel, (2) the random insertion of the hydrogels into the pores such that the largest pores are blocked, (3) a balance of seepage forces that are sufficient to mobilize the hydrogels into the pores but not so large that the hydrogels untangle due to shear thinning or are dislodged by inertial forces, and (4) the kinetics of hydrogel formation and adsorption of polymer to the surface of bentonite.

REFERENCES

ASTM. 2018. Standard test method for evaluation properties of geosynthetic clay liners permeated with potentially incompatible liquids. D6766, West Conshohocken, Pennsylvania, USA.

Benson, C., Oren, A., and Gates, W. 2010. Hydraulic conductivity of two geosynthetic clay liners permeated with a hyperalkaline solution. *Geotextiles and Geomembranes*, 28(2), 206-218.

Bouazza, A., and Gates, W. 2014. Overview of performance compatibility issues of GCLs with respect to leachates of extreme chemistry. *Geosynthetics International*, 21(2), 151-167.

Chen, J., Salihoglu, H., Benson, C., Likos, W., and Edil, T. 2019. Hydraulic conductivity of bentonite-polymer composite geosynthetic clay liners permeated with coal combustion product leachates. *Journal of Geotechnical and Geoenvironmental Engineering*, 145(9), 04019038.

Di Emidio, G. 2010. Hydraulic conductivity and chemico-osmotic performance of polymer treated clays, Ph.D. Dissertation, University of Ghent, Ghent, Belgium.

Di Emidio, G., Van Impe, W., and Mazzieri, F. 2010. A polymer enhanced clay for impermeable geosynthetic clay liners. Proceedings, Sixth International Environmental Geotechnics Conference, International Society for Soil Mechanics and Geotechnical Engineers, New Delhi, India.

Donovan, M., Valorio, R., and Gebka, B. 2016a. Polymer enhanced geosynthetic clay liners for extreme leachate chemistries. Proceedings, EuroGeo6 Conference, International Geosynthetics Society, Jupiter, Florida, USA.

Donovan, M., Valorio, R., and Gebka, B. 2016b. Chemical compatibility of polymer modified GCLs in coal combustion residual leachates. Proceedings, GeoAmericas 2016 Conference., International Geosynthetics Society, Jupiter, Florida, USA.

Donovan, M., Gebka, B., and Wind, D. 2020. New lighter, longer GCLs for mining applications. Proceedings, Tailings and Mine Waste 2020, Colorado State University, Fort Collins, Colorado, USA.

Flynn, B. and Carter, G. 1998. Waterproofing material and method of fabrication thereof. US Patent Number: 6,537,676 B1.

Katsumi, T., Onikata, M., Hasegawa, S., Lin, L., Kondo, M., and Kamon, M. 2001. Chemical compatibility of modified bentonite permeated with inorganic chemical solutions. *Geoenvironmental Impact Management*, Thomas Telford, London, 419-424.

Katsumi, T., Ishimori, H., Onikata, M., and Fukagawa, R. 2008. Longterm barrier performance of modified bentonite materials against sodium and calcium permeant solutions. *Geotextiles and Geomembranes*, 26(1), 14-30.

Scalia, J., and Benson, C. 2016. Evaluation of Na-bentonite-polyacrylate mixtures to enhance the chemical resistance of geosynthetic clay liners, Proceedings, Geo-Chicago 2016, GSP No. 271, ASCE, Reston, Virginia, USA, 388-397.

Scalia, J., and Benson, C. 2017. Polymer fouling and hydraulic conductivity of mixtures of sodium bentonite and a bentonite-polymer composite. *Journal of Geotechnical and Geoenvironmental Engineering*, 143(4), 04016112.

Scalia, J., Benson, C., Bohnhoff, G., Edil, T., and Shackelford, C. 2014. Long-term hydraulic conductivity of a bentonite-polymer composite permeated with aggressive inorganic solutions. *Journal of Geotechnical and Geoenvironmental Engineering,* 140(3), 04013025.

Scalia, J., Bohnhoff, G., Shackelford, C., Benson, C., Sample-Lord, K., Malusis, M., and Likos, W. 2018. Enhanced bentonites for containment of inorganic wastes by GCLs. *Geosynthetics International*, 25(4), 392-411.

Tian, K., Benson, C. and Likos, W. 2016a. Hydraulic conductivity of geosynthetic clay liners to low-level radioactive waste leachate. *Journal of Geotechnical and Geoenvironmental Engineering*, 142(8), 1-12.

Tian, K., Likos, W., and Benson, C. 2016b. Pore-scale imaging of polymer-modified bentonite in saline solutions, Proceedings, Geo-Chicago 2016, GSP No. 271, ASCE, Reston, Virginia, USA, 468-477.

Tian, K., Benson, C. and Likos, W. 2017. Effect of anion ratio on the hydraulic conductivity of a bentonite-polymer geosynthetic clay liner. Proceedings, Geo-Frontiers 2017, Orlando, FL, USA, GSP No. 276, ASCE, Reston, VA, USA, pp. 180-189.

Tian, K., Likos, W., and Benson, C. 2019. Polymer elution and hydraulic conductivity of bentonite-polymer composite geosynthetic clay liners. *Journal of Geotechnical and Geoenvironmental Engineering,* 145(10), 04019071.

Yu, B., El-Zein, A., and Rowe, R. 2020. Effect of added polymer on the desiccation and healing of a geosynthetic clay liner subject to thermal gradients. *Geotextiles and Geomembranes*, in press.

Chapter 1

Impact of polymer mixing method and mass loading on hydraulic performance of geosynthetic clay liners comprising anionic polymer-enhanced bentonites

SUMMARY

The hydraulic performance of geosynthetic clay liners (GCLs) comprising anionic polymer-enhanced bentonites (EBs) based on permeation with concentrated electrolyte solutions (500 mM NaCl and 167 mM $CaCl_2$) at low effective stress (27 kPa) was evaluated. The EBs included a powdered sodium bentonite (NaB) enhanced with one of seven anionic polymers, including linear, non-crosslinked poly(acrylic acid) (PA) with low, medium, and high molecular weights (PALW, PAMW, PAHW), sodium carboxymethylcellulose (CMC) with either low viscosity (CMCLV) or high viscosity (CMCHV), a covalently crosslinked, sodium polyacrylate (PAx), and an in-situ polymerized bentonite polymer composite (BPC). The polymers were added to the NaB at mass loadings of 5, 8, and/or 10 % using dry sprinkling (DS), dry mixing (DM), and/or wet mixing (WM) methods. The lowest hydraulic conductivities for the EB-GCLs prepared with PA based on permeation with 500 mM NaCl and 167 mM $CaCl_2$ were 1.3×10^{-11} m/s and 4.0×10^{-11} m/s, respectively, for the PAHW added at 5% via DS and 2.9×10^{-11} m/s and 4.7×10^{-11} m/s, respectively, for the PAMW added at 8% via DS. The viscosity grade of CMC did not impact the hydraulic conductivity of the EB-GCLs. All EB-GCLs eluted polymer during permeation, regardless of mixing method or polymer type. The DS mixing method provided the best hydraulic performance. Observations of hydrogel in multiple effluent samples and at the outflow end of specimens support pore clogging within the EB-GCL specimens by hydrogel. Polymer elution was correlated with preferential interaggregate flow paths in multiple EB-GCL specimens, indicating the importance of polymer retention in maintaining low hydraulic conductivity of EB-GCLs. Since standard termination criteria for the measurement of the hydraulic conductivity of conventional, unenhanced GCLs (e.g., ASTM D 6766) do not include the potential impact of polymer elution from EB-GCLs, caution should be exercised when

adapting these criteria to measure the hydraulic conductivity of EB-GCLs such as those evaluated in this study.

1.1 INTRODUCTION

Geosynthetic clay liners (GCLs) comprising natural sodium bentonite (NaB) have been used extensively as engineered barriers or components of engineered barrier systems in waste containment applications (e.g., liners for landfills). However, conventional GCLs have proven to be ineffective hydraulic barriers to aggressive inorganic solutions, such as hypersaline (high salt concentration) solutions (e.g., brines) or extremely acidic or basic leachates, especially under low confining stresses (Shackelford et al. 2000; Benson et al. 2010; Bouazza and Gates 2014; Chen et al. 2019). The hydraulic incompatibility between natural NaB and liquids with aggressive chemistry has motivated the production of a plethora of chemically enhanced bentonites (EBs) for use in GCLs for the purpose of improving hydraulic performance. The types of chemical enhancements that have been evaluated include organic compounds such as propylene and glycerol carbonate, and anionic polymers such as sodium carboxymethylcellulose (CMC) and poly(acrylic acid) (PA).

Scalia et al. (2018) compared measured hydraulic conductivity results from multiple sources for conventional GCLs as well as enhanced-bentonite GCLs (EB-GCLs) permeated with solutions with a range of ionic strengths, I (= $\frac{1}{2}\Sigma c_i z_i^2$, where c_i = molar concentration of ionic species i, and z_i = charge of ionic species i). Although the hydraulic conductivity of conventional GCLs was low ($\leq 5\times10^{-11}$ m/s) at low ionic strengths ($I \leq 20$ mM), the hydraulic conductivity was higher and more variable for higher ionic strength solutions. The hydraulic performance of the EB-GCLs was better than that for conventional GCLs in some cases, but significant variability in hydraulic conductivity (1.0×10^{-13} m/s $\leq k \leq 9.0\times10^{-6}$ m/s) was evident for $I > 20$ mM, especially for commercially produced contaminant resistant clays with proprietary amendments. These results illustrate that not all EB-GCLs are equally effective, and that the hydraulic conductivity of EB-GCLs can vary considerably based on the properties of the polymer (e.g., molecular weight, degree of polymerization), method of preparing the EB, and the properties of the hydrating and

permeant solution. Also, the mechanisms underlying the hydraulic compatibility of EBs and EB-GCLs to aggressive inorganic solutions differ from those of natural NaB, thereby rendering traditional indicator parameters, such as swell index, ineffectual for EBs (Onikata et al. 1996, 1999; Trauger and Darlington 2000; Katsumi et al. 2001, 2008; Schroeder et al. 2001; Ashmawy et al. 2002; Kolstad et al. 2004; Guyonnet et al. 2009; Di Emidio et al. 2010, 2011; Mazzieri et al. 2010; Naismith et al. 2011; Scalia et al. 2011; Bohnhoff et al. 2013; Scalia et al. 2014; Tian et al. 2016a,b; Scalia et al. 2018; Chai and Prongmanee 2019; Tian et al. 2019; Reddy et al. 2020).

The objective of this chapter is to evaluate the effects of the material properties and method of preparation on the hydraulic conductivity of EB-GCLs comprising anionic-polymer (PA or CMC) EBs based on permeation with concentrated inorganic chemical solutions (500 mM NaCl and 167 mM $CaCl_2$). The hydraulic conductivity values of the anionic-polymer EB-GCLs also are compared with those of an EB-GCL comprising bentonite polymer composite (BPC), an in-situ polymerized EB (e.g., Bohnhoff 2012; Bohnhoff and Shackelford 2013; Bohnhoff et al. 2014; Scalia et al. 2014). The results of this study demonstrate that changes in hydraulic behavior of anionic-polymer EBs and EB-GCLs can be related to differences in (i) polymer type and properties (e.g., molecular weight), (ii) polymer mass loading, (iii) method of specimen preparation, and (iv) chemical composition of permeant solution.

1.2 MATERIALS

Several materials were used in this study, including NaB, CMC with low viscosity (CMCLV) and high viscosity (CMCHV), non-crosslinked linear PA with low, medium, and high molecular weights (PALW, PAMW, PAHW), a cross-linked PA (PAx), and the BPC. The polymer mass loadings representing the mass percentage of the polymer added to the NaB to comprise the EB were 5, 8, and/or 10%, which is indicated by the number appended to the aforementioned designations. For example, PALW5 indicates that 5% of the PALW by mass was added to 95% of the NaB by mass. Finally, the EBs are designated as DS, DM, and WM to indicate the method of preparation as dry sprinkling, dry mixing, and wet mixing, respectively. In addition to these solid materials, different chemical solutions were used as hydrating and permeating liquids. Further details on these materials follow.

1.2.1 Sodium bentonite

The NaB used in this study was obtained from Colloid Environmental Technologies Company (CETCO, Hoffman Estates, IL, USA), and is the same NaB used in Bentomat® GCLs as well as other studies on GCL behavior (Scalia et al. 2011; Bohnhoff 2012; Bohnhoff and Shackelford 2013; Bohnhoff et al. 2014; Scalia et al. 2014). The NaB was evaluated in a powdered form. Two particle-size distributions (PSDs) for the NaB are shown in Figure 1.1, viz., a dry PSD based on a dry analysis by passing the NaB through a stack of sieves in accordance with the procedure for coarse-grained materials (e.g., see Howell et al. 1997; Shackelford et al. 2000, Scalia et al. 2011), and a wet PSD from Bohnhoff (2012) based on traditional hydrometer analysis (ASTM D422; ASTM 2007). Both dry and wet PSDs are consistent with that of a fine-grained soil. As shown in Table 1.1, the NaB exhibited a swell index in deionized water (DIW) of 31.4 mL/2 g, and a cation exchange capacity (CEC) of 78 $cmol^{+}/kg$. The exchange sites were occupied by approximately 44% Na, 36% Ca, 17% Mg, and 2% K.

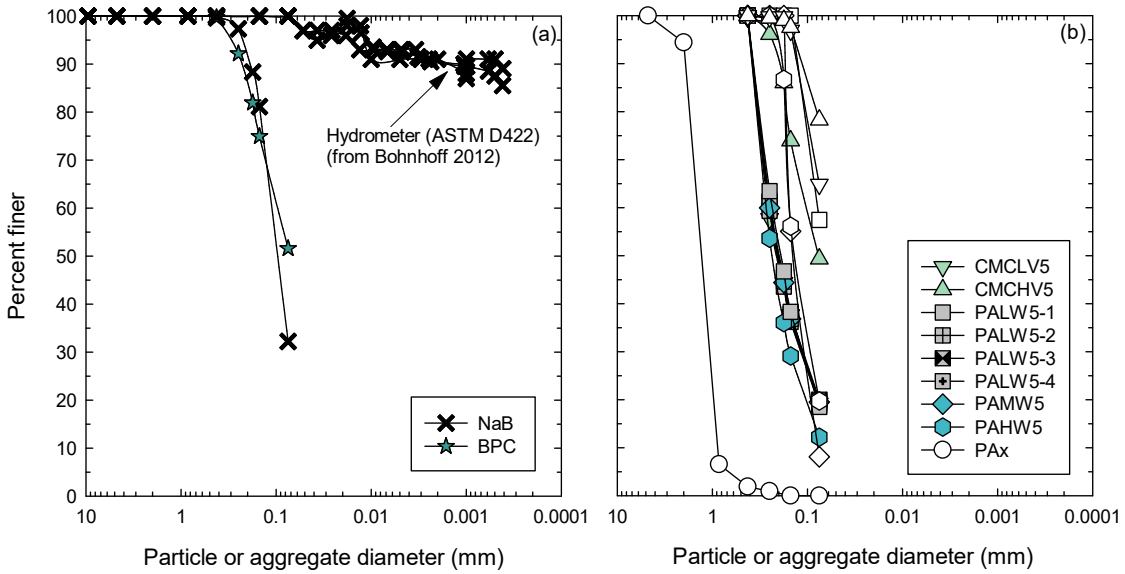

Figure 1.1: Particle-size distributions based on mechanical sieve analysis of dry materials unless otherwise indicated: (a) sodium bentonite (NaB) and bentonite polymer composite (BPC); (b) raw polymers (open symbols), wet mixed enhanced bentonites at 5% polymer mass loading (closed symbols) produced using NaB, sodium carboxymethylcellulose with low viscosity (CMCLV) or high viscosity (CMCHV), poly(acrylic acid) with low, medium, or high molecular weights (PALW, PAMW, PAHW), and covalently crosslinked PA (PAx).

Table 1.1: Selected properties of the sodium bentonite (NaB) used in this study versus those for the bentonite polymer composite (BPC) (adapted from Scalia et al. 2014).

Property	Standard/Method	NaB	BPC
Swell index (mL/2 g)	ASTM D5890-06	31.4	72.7
Atterberg limits [a]:	ASTM D4318-10		
Liquid limit, *LL*		420	255
Plasticity index, *PI*		381	NM[b]
Unified Soil Classification	ASTM D2487-11	CH	CH
Carbonate content (%)	ASTM D4373-14	1.3	0.0
Montmorillonite content (%)	X-ray diffraction (10 samples)	85-91	73-77
Cation exchange capacity, CEC ($cmol^+/kg$)	ASTM D7503-18	78.0	142.6
Soluble metals ($cmol^+/kg$):	ASTM D7503-18		
Ca		0.2	9.5
Mg		0.1	1.6
Na		18.1	118
K		0.4	0.4
Bound/exchangeable metals (mole fraction):	ASTM D7503-18		
Ca		0.36	0.06
Mg		0.17	0.02
Na		0.44	0.90
K		0.02	0.02

[a] From Bohnhoff 2012; [b] NM = not measurable.

1.2.2 Sodium carboxymethylcellulose

The CMCLV used in this study is produced by Calbiochem® (Millipore Sigma, Burlington, MA, USA) and the CMCHV is produced by MP Biomedical (Irvine, CA, USA). Carboxymethylcellulose can be differentiated by degree of substitution (DoS), i.e., the number of carboxymethyl groups substituted per anhydroglucose unit, and a weighted average molecular weight which describes the average chain degree of polymerization (DP) (Buchholz and Graham 1998). The technical specifications for the CMCHV are shown in Table 1.2, whereas those for the CMCLV were not provided by the manufacturer. The particle

sizes for the two CMCs were not altered from the manufacturer provided material, and the resulting PSDs of both CMCs are shown in Figure 1.1b.

Table 1.2: Parameters of polymers used in this study.

Polymer type	DoS (-)	DP (-)	Molecular Weight (g/mol)
CMCHV	0.65-0.85[a]	3200[a]	685290-736500[c]
PALW	NA	29.9	5000[a]
PAMW	NA	[b]	50000[a]
PAHW	NA	[b]	345000[a]

Notes: DoS = degree of substitution; DP = average chain degree of polymerization; Molecular weight = molecular weight; CMCHV = high viscosity sodium carboxymethylcellulose; PALW, PAMW, PAHW = low, medium, high molecular weight polyacrylate; PAx = covalently crosslinked polyacrylate; NA = not applicable.
[a] Reported by the manufacturer; [b] Not provided by manufacturer; [c] Molecular weight of CMC calculated as $[C_6H_7O_2(OH)_x(OCH_2COONa)_y]_n$ where n is DP, x + y =3, and y is DoS.

1.2.3 Poly(acrylic acid)

The PA ($[\text{-}CH_2CH(CO_2H)\text{-}]_n$) used in this study is a synthetic polymer of acrylic acid. The negatively charged carboxylic moiety (COO^-) on the polymer repeating unit (R) is satisfied by a proton (H^+). Commercial PA is differentiated primarily by molecular weight and DP (Buchholz and Graham 1998). Poly(acrylic acid) that is covalently crosslinked is known as crosslinked PA (PAx).

Technical specifications of the PAs provided by the manufacturer are given in Table 1.2. The PALW, PAMW, and PAHW were supplied by Polysciences Inc. (Warrington, Pennsylvania, USA), and the manufacturer reported molecular weights were approximately 5,000, 50,000, and 345,000 g/mol, respectively. All the PAs are linear, i.e., non-crosslinked.

When used as an enhancement, the PA in solution was air dried until solidified and then ground and screened. Grinding of the polymer was completed using a rotary blade grinder (KitchenAid BCG211OB; Benton Harbor, Michigan, USA). The PA was ground to achieve a PSD similar to that for the base NaB to allow for homogeneous mixing (Malusis and Scalia 2007). The PSD of each dried PA also is shown in Figure 1.1.

A crosslinked PAx also was used in this study for comparison with the linear, non-crosslinked PAs. The PAx was a partial sodium salt-graft-poly(ethylene oxide) (sodium salt) from Aldrich Chemistry (St. Louis, MO, USA). Properties of the PAx (e.g., molecular weight) were not provided by the manufacturer.

1.2.4 Bentonite polymer composite

The BPC used in this study was prepared by the polymerization of acrylic acid within a bentonite slurry, and is the same BPC used in previous studies (Scalia et al. 2011, 2014; Bohnhoff et al. 2013). The BPC, which comprised approximately 28.5% of polyacrylate polymer (Scalia et al. 2014), was tested as a dry-mixed enhancement of NaB at 5% polymer by mass (i.e., EB with 17.3% BPC). Properties of the granular NaB used to prepare the BPC can be found in Scalia et al. (2014). Both the swell index with DIW and CEC of the BPC were high (72.7 mL/2 g and 142.6 $cmol^{+}/kg$), with Na occupying approximately 90% of the exchange sites (see Table 1.1). For use in this study, the BPC was ground to a powdered form by mortar and pestle with 51.6% of the particles < 0.075 mm (see Figure 1.1a).

1.2.5 Hydrating and permeant solutions

Concentrated inorganic solutions, i.e., 167 mM $CaCl_2$ and 500 mM NaCl, with I = 500 mM were used as hydrating and permeant solutions to evaluate the hydraulic conductivity of the EB-GCL specimens. The electrical conductivity (EC) and pH of the 167 mM $CaCl_2$ solution were 3280 mS/m and 5.8, respectively, whereas the respective EC and pH of the 500 mM NaCl were 4850 mS/m and 6.2. The $CaCl_2$ solution was prepared by dissolving $CaCl_2$ di-hydrate, $CaCl_2 \bullet 2H_2O$ (Alfa Aesar; Ward Hill, Massachusetts, USA) in DIW. The NaCl solution was prepared by dissolving anhydrous NaCl (Fisher Chemical; Hampton, New Hampshire, USA) in DIW. The prepared solutions were stored in collapsible carboys with no headspace to limit interaction with the atmosphere.

1.3 METHODS

1.3.1 Bentonite modification

The NaB was enhanced with an anionic polymer using three mixing methods, viz., dry mixing, dry sprinkling, and wet mixing. Dry-mixed (DM) EBs were prepared by adding a percentage (by mass) of air-dried polymer to air-dried NaB. The masses were not corrected for the gravimetric, air-dried (hygroscopic) water content for the NaB of 8.0%. The mixture was rotated end-over-end in a sealed container at 30 rpm for 1 min. Dry-sprinkled (DS) EBs were prepared by sprinkling a known percentage (by mass) of air-dried polymer evenly as a layer at the inflow side (bottom) of the GCL specimen before placing the air-dried NaB on top.

Wet-mixed (WM) EBs were created by first adding a known, target percentage of 5% of air-dry polymer by mass of air-dry NaB into 350 mL of DIW. For wet-mixed EBs prepared with both CMCHV and CMCLV, the air-dried CMC was added to 350 mL of DIW in a mechanical stirrer (Hamilton Beach Single Spindle Drink Mixer, Glen Allen, VA, USA) set to the highest operating speed (18,000 rpm). The CMCs and DIW were mixed for 5 min to allow for the dispersion and hydration of the dried polymer. After 5 min, 50 g of air-dried NaB was added in the mechanical stirrer cup with another 150 mL of DIW and mixed at 18,000 rpm for 10 min, resulting in a total of 500 mL of DIW and a total mixing time of 15 min.

The EBs wet-mixed with PA were prepared in a similar manner to those wet-mixed with CMC, except the total volumes of DIW for the mixtures containing PALW and PAMW were reduced due to the excessive foam produced by the high shear mixing of PA and DIW. First, the PA was added to 350 mL of DIW in the hydrated form provided by the manufacturer with a target polymer content of 5% or 8% by mass. Then, after 1 min of mixing (shortened from 5 min due to foaming), 50 g of air-dried NaB was added to the mechanical stirrer. Finally, an additional 75 mL or 150 mL of DIW was added for the mixtures containing PAMW or PAHW, respectively, and mixing continued for an additional 14 min for a total period of 15 min, which was the same as that for the EBs wet-mixed with CMC. The total volumes of DIW, i.e., 350, 425, and 500 mL for the PALW, PAMW, and PAHW mixtures, respectively, reflected the maximum amount of DIW that could be added to the mixture to fill the cup without losing slurry while mixing. The

wet-mixed EBs then were oven dried at 105 ºC for 24 h and ground using the rotary blade grinder until 100% passed the U.S. No. 40 sieve (0.420 mm).

All the PSDs of the wet-mixed EBs, shown in Figure 1.1, were similar. Four batches of the PALW5 were prepared separately to evaluate the consistency of the rotary grinder (labelled PALW5-1 to PALW5-4 in Figure 1.1). Based on the results shown in Figure 1.1, the rotary grinder produced consistent PSDs.

1.3.2 Geosynthetic clay liner preparation

Enhanced bentonites prepared using the dry and wet mixing methods were tested for hydraulic conductivity in the form of a conventional, unreinforced GCL specimens. Schematic representations of the specimens are shown in Figure 1.2. The layers of a typical GCL were reproduced with each EB following the method described in Scalia et al. (2014). A non-woven, calendared geotextile (PolySpun heavy-duty landscape fabric) with a mass per area of 0.08 kg/m^2 was placed below and then above a layer of EB. An additional non-woven geotextile with a mass per area of 1 kg/m^2 was placed below and above the GCL to serve as the bounding drainage layers in place of porous stones and filter paper as per Scalia et al. (2014). Specimens were prepared in flexible-wall permeameters with a 152.4 mm diameter in an even layer at 4.5 kg/m^2. This bentonite mass per area is similar to that for commercial GCLs (e.g., Koerner 2005).

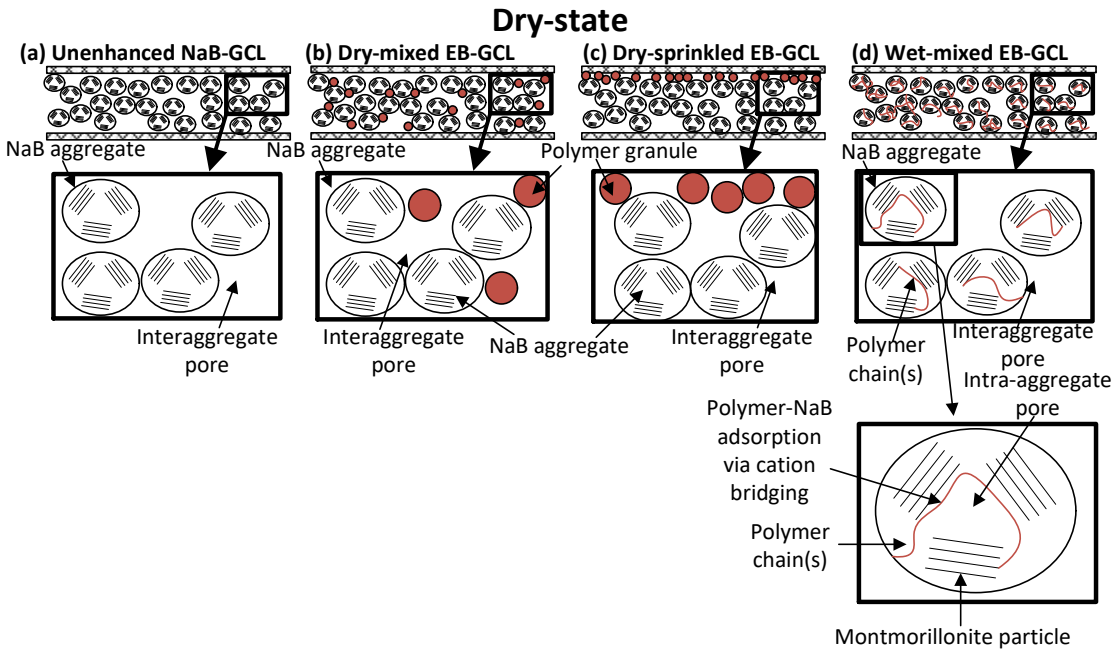

Figure 1.2 Schematic cross-sections of geosynthetic clay liners (GCLs) in the dry-state assembled with (a) unenhanced sodium bentonite (NaB) or enhanced-bentonite GCLs (EB-GCL) using (b) dry-mixing, (c) dry-sprinkling, or (d) wet-mixing methods.

1.3.3 Hydraulic conductivity

Hydraulic conductivity tests were performed using flexible-wall permeameters following ASTM D6766-18 (ASTM 2018) and the falling headwater, constant tailwater method except backpressure was not applied (e.g., Kolstad et al. 2004; Lee and Shackelford 2005; Meer and Benson 2007; Bradshaw and Benson 2013; Scalia et al. 2014; Tian et al. 2016). Prior to permeation, each specimen was hydrated with the permeant solution for 48 h under an average effective confining stress of 27 kPa. A total confining stress of 34.3 kPa was applied during hydration and throughout the hydraulic conductivity test via gravity head applied by an elevated water tank. Hydration was promoted by flushing hydrating liquid across the lower (inflow) boundary of the GCL specimen, whereas the upper (outflow) lines were not flushed to reduce a possible loss of polymer from the system prior to permeation. As per Jo et al. (2005), 6.4-mm (0.25-in)-diameter tubing was used to prevent clogging of the tubing with eluted polymer during permeation. For most tests, a target, average hydraulic gradient of 200 was applied via gravity head using glass burettes (falling head). The target hydraulic gradient was based on an assumed typical hydrated GCL thickness of 7.5 mm. A hydraulic gradient of 200 to 300 is typical for hydraulic conductivity testing of GCLs due to the typically

low k (Shackelford et al. 2000; Scalia et al. 2014). However, the final average hydraulic gradients for the permeated specimens ranged from 242 to 327 due to thinner-than-expected final thicknesses (i.e., 4.30 to 6.84 mm) resulting from a significant reduction in swelling of the NaB in the aggressive inorganic solutions as well as material loss via polymer elution.

Each specimen was permeated from bottom (inflow) to top (outflow) at least until the ASTM D6766 termination criteria were achieved. The primary termination criteria include: (1) a ratio of outflow to inflow within 1.00±0.25; (2) at least two pore volumes of flow (PVF) passed through the specimen; and (3) establishment of chemical equilibrium between the outflow and the inflow based on a ratio of outflow-to-inflow EC within 1.0±0.1. Other requirements include: (i) at least three values of flow rate; (ii) flux and hydraulic conductivity determined over a minimum time period of 8 h; (iii) no significant upward or downward trend in the hydraulic conductivity for the last three measurements; (iv) none of the last three flow rate values less than 0.75 times nor greater than 1.25 times the average flow rate; and (v) flux and hydraulic conductivity based on the average of the last three consecutive measured values. However, since the potential impact of polymer elution is not considered by the ASTM D6766 termination criteria, permeation was continued beyond the duration required by ASTM D6766 for all but one specimen to evaluate the applicability of the ASTM D6766 termination criteria for EB-GCLs. The potential for preferential flow also was evaluated by adding 5 mg/L Rhodamine WT dye to the influent as described in Scalia and Benson (2011).

1.4 RESULTS

1.4.1 Hydraulic conductivity

A summary of the measured specimen properties and results of the hydraulic conductivity tests are provided in Tables 1.3 and 1.4 for specimens permeated with 500 mM NaCl and 167 mM $CaCl_2$ solutions, respectively. The reported values are for the following parameters: GCL specimen designation, polymer type and relative molecular weight or viscosity, initial polymer content by mass, specimen preparation (mixing) method, final thickness (L_f), final water content (w_f), and the values for the testing duration (t), *PVF*, and hydraulic conductivity (k) based on both the ASTM D6766 termination criteria and the end-of-the-test conditions. Unless otherwise noted, all hydraulic conductivity values referred to subsequently are those based on ASTM D6766 termination criteria, i.e., k_{6766}.

Table 1.3: Properties and hydraulic conductivity test results of conventional geosynthetic clay liner (GCL) comprising sodium bentonite (NaB) and enhanced-bentonite GCL (EB-GCL) specimens permeated with 500 mM NaCl.

Specimen Designation	Specimen Properties							Elapsed Time, t (d)		Pore Volumes of Flow, PVF		Hydraulic Conductivity, k ($\times 10^{-10}$ m/s)		k_{6766}/k_f	$k_{EB\text{-}GCL}/k_{GCL}$
	Polymer type	Molecular weight or Viscosity	P_i (%)	Mixing method	d_f (mm)	L_f (mm)	w_f	t_{6766}	t_f	PVF_{6766}	PVF_f	k_{6766}	k_f [b,c]		
NaB	NA	NA	NA	NA	152.4	6.10	0.86	1.7	4.8	2.6	5.9	2.8	1.6	1.8	NA
CMCLV5DM	CMC	LV	5	DM	150.0	5.51	0.91	196	214	14.8	25.8	0.85	1.2	0.71	0.30
CMCLV5WM	CMC	LV	5	WM	151.6	6.10	1.03	120	126	3.1	4.9	0.69	0.67	1.0	0.25
CMCLV5DS	CMC	LV	5	DS	151.8	4.80	0.79	62.5	66.7	9.3	14.6	1.2	1.4	0.86	0.43
CMCHV5DM	CMC	HV	5	DM	145.9	5.75	0.96	199	216	18.7	31.3	1.2	1.4	0.86	0.43
CMCHV5WM	CMC	HV	5	WM	150.1	6.84	1.18	30.5	77.3	3.0	6.9	0.33	0.23	1.4	0.12
PALW5DS	PA	LW	5	DS	149.9	5.30	0.94	2.7	18.0	6.6	19.1	2.4	1.4	1.7	0.86
PALW8DS[a]	PA	LW	8	DS	-	-	-	3.5	4.7	2.4	3.6	3.7	3.4	1.1	2.1
PALW5WM	PA	LW	5	WM	154.1	5.50	0.97	5.9	21.0	2.4	7.3	0.78	0.49	1.6	0.28
PAMW5DS	PA	MW	5	DS	145.7	5.20	0.79	41.4	73.6	5.8	12.5	0.26	0.27	0.96	0.093
PAMW8DS	PA	MW	8	DS	150.0	4.80	0.80	20.9	59.2	6.7	18.1	0.29	0.33	0.88	0.10
PAMW5WM	PA	MW	5	WM	153.7	6.90	1.06	22.4	85.0	4.5	11.5	0.48	0.35	1.4	0.17
PAHW5DS	PA	HW	5	DS	150.2	4.60	0.76	34.6	66.4	3.3	8.1	0.13	0.18	0.72	0.046
PAHW5WM	PA	HW	5	WM	152.1	6.34	1.08	16.4	188	5.3	20.4	0.52	0.15	3.5	0.19
PAx5DS	PAx	Unknown	5	DS	149.7	7.00	0.95	88.9	136	5.4	7.9	0.25	0.25[c]	1.0	0.089
BPC5DM	PA	Unknown	5	DM	149.1	6.20	0.82	61.5	143	2.9	11.5	0.11	0.19	0.58	0.039

Notes: NA = not applicable; NaB = sodium bentonite; PA = polyacrylate; CMC = carboxymethylcellulose; PAx = polyacrylate; BPC = bentonite polymer composite; Molecular weight = molecular weight; HW = high Molecular weight; MW = medium Molecular weight; LW = low Molecular weight; HV = high viscosity; LV = low viscosity DS = dry sprinkling; WM = wet mixing; DM = dry mixing; P_i = initial polymer content based on mass of polymer added; d_f = final diameter; L_f = final thickness; w_f = final gravimetric water content; t_{6766}, PVF_{6766}, k_{6766} = values based on ASTM D6766 termination criteria; t_f, PVF_f, k_f = final values at the end of testing; $k_{GCL} = k_{6766}$ of NaB GCL specimen; $k_{EB\text{-}GCL} = k_{6766}$ of polymer-amended EB-GCL specimen.

[a] Test still ongoing; [b] Preferential flow; [c] Hydrogel visible on geotextiles and/or permeameter.

Table 1.4: Properties and hydraulic conductivity test results of conventional, geosynthetic clay liner (GCL) comprising sodium bentonite (NaB) and enhanced-bentonite GCL (EB-GCL) specimens permeated with 167 mM $CaCl_2$.

GCL Designation	Specimen Properties							Elapsed Time, t (d)		Pore Volumes of Flow, PVF		Hydraulic Conductivity, k ($\times 10^{-10}$ m/s)		k_{6766}/k_f	$k_{EB\text{-}GCL}/k_{GCL}$
	Polymer type	Molecular weight or Viscosity	P_i (%)	Mixing method	d_f (mm)	L_f (mm)	w_f	t_{6766}	t_f	PVF_{6766}	PVF_f	k_{6766}	k_f [b,c]		
NaB	NA	NA	NA	NA	150.3	6.80	0.80	1.6	5.6	3.0	9.2	5.5	4.8	1.1	NA
CMCLV5DM	CMC	LV	5	DM	150.3	5.10	0.91	3.0	4.4	3.2	16.2	1.4	31[b]	0.047	0.26
CMCLV5WM[a]	CMC	LV	5	WM	-	-	-	4.3	1.5	4.5	6.5	5.9	6.0	0.98	1.1
CMCHV5DM	CMC	HV	5	DM	149.0	5.60	0.97	65.4	65.5	14.2	21.4	135	181[b]	0.78	24.5
CMCHV5WM	CMC	HV	5	WM	152.0	6.60	1.06	8.4	8.8	5.7	6.2	3.7	3.8	0.97	0.67
PALW5DS	PA	LW	5	DS	150.7	4.30	0.76	1.4	3.7	8.2	16.1	5.7	3.4[c]	1.7	1.0
PALW10DS	PA	LW	10	DS	150.0	6.20	0.75	3.5	4.3	3.9	5.5	4.1	4.0	1.0	0.75
PALW5WM	PA	LW	5	WM	154.0	5.30	0.85	2.5	3.3	5.0	7.0	3.3	3.8	0.87	0.60
PAMW5DS	PA	MW	5	DS	150.4	4.67	0.75	1.7	2.4	12.4	15.3	4.7	4.1	1.1	0.85
PAMW8DS	PA	MW	8	DS	150.8	4.91	0.75	84.9	117	7.1	13.0	0.11	0.11[c]	1.0	0.020
PAMW10DS	PA	MW	10	DS	148.2	6.27	0.74	48.7	112	3.8	10.1	0.25	0.27	0.93	0.045
PAMW8DM[a]	PA	MW	8	DM	-	-	-	4.3	5.1	3.9	4.8	2.3	2.3	1.0	0.15
PAMW8WM[a]	PA	MW	8	WM	-	-	-	5.1	6.5	3.8	5.1	0.85	0.82	1.0	0.15
PAHW5DS	PA	HW	5	DS	153.3	4.81	0.79	50.2	50.2	13.3	13.3	0.40	0.40[c]	1.0	0.073
PAHW8DS	PA	HW	8	DS	148.6	6.18	0.79	24.6	71.3	3.8	10.7	0.46	0.34	1.4	0.084
PAHW5WM	PA	HW	5	WM	151.5	5.25	0.86	1.5	3.3	2.6	5.7	3.1	2.5	1.2	0.56
PAx5DS[a]	PAx	Unknown	5	DS	-	-	-	4.2	5.1	2.4	3.2	2.2	2.3	0.97	0.48
BPC5DM	BPC	Unknown	5	DM	148.0	5.90	0.69	44.0	77.0	4.1	11.5	0.32	0.55	0.58	0.058

Notes: NA = not applicable; NaB = sodium bentonite; PA = polyacrylate; CMC = carboxymethylcellulose; PAx = polyacrylate; BPC = bentonite polymer composite; Molecular weight = molecular weight; HW = high Molecular weight; MW = medium Molecular weight; LW = low Molecular weight; HV = high viscosity; LV = low viscosity DS = dry sprinkling; WM = wet mixing; DM = dry mixing; P_i = initial polymer content based on mass of polymer added; d_f = final diameter; L_f = final thickness; w_f = final gravimetric water content; t_{6766}, PVF_{6766}, k_{6766} = values based on ASTM D6766 termination criteria; t_f, PVF_f, k_f = final values at the end of testing; $k_{GCL} = k_{6766}$ of NaB GCL specimen; $k_{EB\text{-}GCL} = k_{6766}$ of polymer-amended EB-GCL specimen.

[a] Test still ongoing; [b] Preferential flow; [c] Hydrogel visible on geotextiles and/or permeameter.

1.4.2 ASTM D6766 termination criteria

The hydraulic conductivity of the GCL specimens based on ASTM D6766 termination criteria are shown versus those at the end of testing in Figure 1.3. In general, but not universally, the ASTM D6766 termination criteria appear to capture the hydraulic conductivity of the permeated specimens to within a factor of approximately ±2 (i.e., $0.5 \leq k_{6766}/k_f \leq 2$), excluding the two noted outliers (see Tables 1.3 and 1.4). The two outliers include the wet-mixed PAHW5 specimen permeated with 500 mM NaCl and the dry-mixed CMCLV5 specimen permeated with 167 mM $CaCl_2$. These specimens produced respective decreasing and increasing trends in hydraulic conductivity after achievement of the ASTM D6766 termination criteria. For these two specimens, the effect of polymer migration through and elution from the EB-GCL specimens on the hydraulic conductivity was not captured by the ASTM D6766 termination criteria. Nonetheless, the ASTM D6766 termination criteria mostly captured the hydraulic conductivity at equilibrium for the EB-GCL specimens. The effects of polymer elution on the representativeness of the termination criteria for EB-GCLs with higher percentage enhancements and/or permeated with lesser concentrated inorganic solutions than evaluated in this study remains unclear. Also, the potential impact of polymer elution on the long-term behavior of EB-GCLs is still unknown. Thus, although the ASTM D6766 termination criteria appear useful for EB-GCLs, these termination criteria are insufficient to provide conservative (high) hydraulic conductivities for all EB-GCLs.

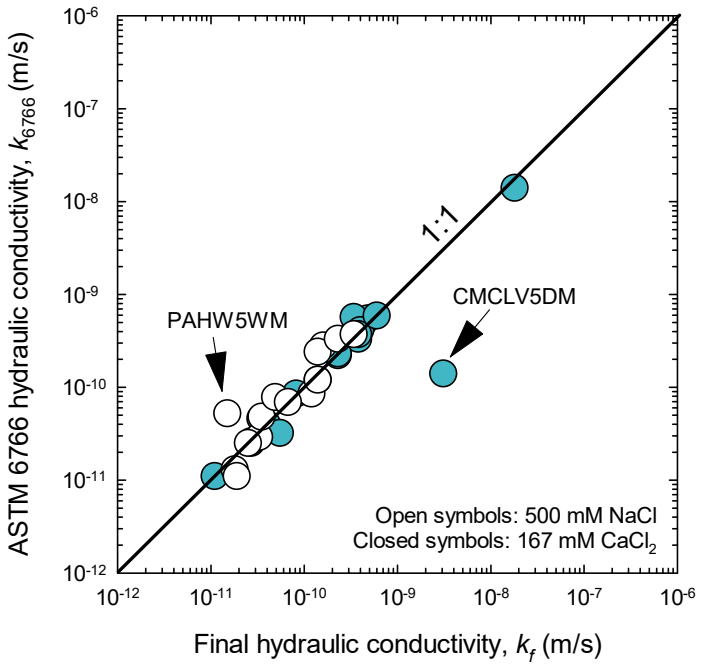

Figure 1.3: Hydraulic conductivity based on ASTM D6766 termination criteria versus that at the end of testing for all GCL specimens.

1.4.2.1 Conventional GCL with unenhanced NaB

The results for the conventional GCL specimens comprising the unenhanced NaB are summarized in Tables 1.3 and 1.4 and shown in Fig. 1.4. The hydraulic conductivity to 500 mM NaCl and 167 mM $CaCl_2$ were 2.8×10^{-10} m/s and 5.5×10^{-10} m/s, respectively. The order-of-magnitude similarity in these values is likely attributable to the equivalent ionic strength (I = 500 mM) of both permeant solutions, and the higher hydraulic conductivity to 167 mM $CaCl_2$ can be attributed to the greater detrimental impact of the Ca^{2+} versus Na^{+} cation (e.g., Shackelford 1994). As illustrated in (Fig. 1.4c,d), both specimens achieved the ASTM D6766 termination criterion with respect to electrical conductivity (as well as all other termination criteria).

The measured hydraulic conductivity values are lower than those reported in other studies for similar NaB permeated with similarly aggressive solutions. For example, for a GCL comprising granular bentonite with Atterberg limits (LL = 430, PI = 393) similar to those for the NaB used in this study (Table

1.1), Lee and Shackelford (2005) reported a mean hydraulic conductivity for duplicate specimens permeated with 100 mM $CaCl_2$ of 3.4×10^{-9} m/s, which is 6.1 times higher than the hydraulic conductivity of 5.5×10^{-10} m/s measured in this study to 167 mM $CaCl_2$. This difference in measured hydraulic conductivity can be attributed, in part, to the initial aggregate size of the NaB, i.e., the NaB in this study is powdered, whereas that in the study by Lee and Shackelford (2005) was granular. As noted by Shackelford et al. (2000), the initial aggregate size of NaB can impact the swelling of the NaB and ultimately the measured hydraulic conductivity, with a larger initial aggregate size generally correlating with lesser swell and higher hydraulic conductivity.

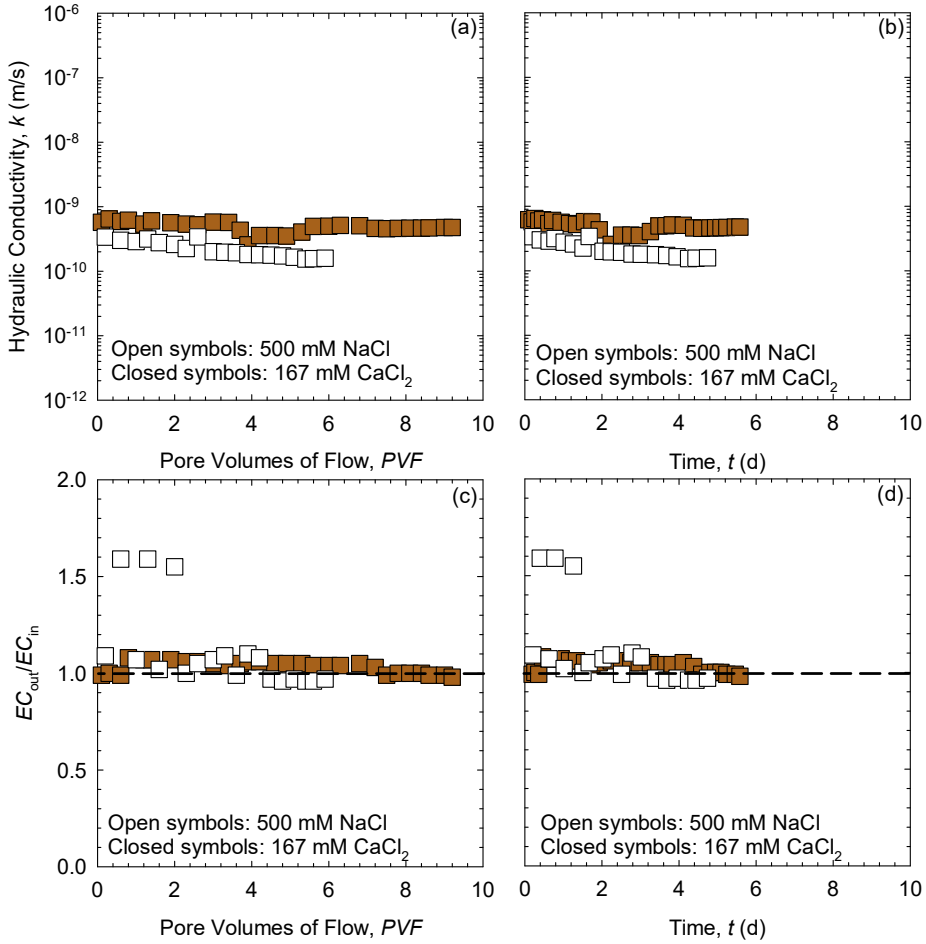

Figure 1.4: Hydraulic conductivity (k) test results as a function of pore volumes of flow (PVF) and elapsed time (t) for conventional GCL specimens permeated with 500 mM NaCl and 167 mM $CaCl_2$ solutions: (a) k versus PVF; (b) k versus t; (c) ratio of outflow-to-inflow electrical conductivity (EC_{out}/EC_{in}) versus PVF; (d) EC_{out}/EC_{in} versus t.

1.4.2.2 EB-GCLs enhanced with CMC

The results of the hydraulic conductivity tests for the EB-GCLs enhanced with CMC are summarized in Tables 1.3 and 1.4 and shown in Figure 1.5. Only a single test was conducted for a specimen prepared using the dry sprinkling method, viz., specimen CMCLV5DS permeated with 500 mM NaCl (Figure 1.5a,b). The hydraulic conductivity of this specimen based on the ASTM D6766 termination criteria was about two times lower than that for the conventional GCL with unenhanced NaB ($k_{EB\text{-}GCL}/k_{GCL} = 0.43$). In contrast, the hydraulic conductivity at the end of testing of 1.4×10^{-10} m/s for the CMCLV5DS specimen was almost the same as that (1.6×10^{-10} m/s) for the conventional GCL specimen (Table 1.3).

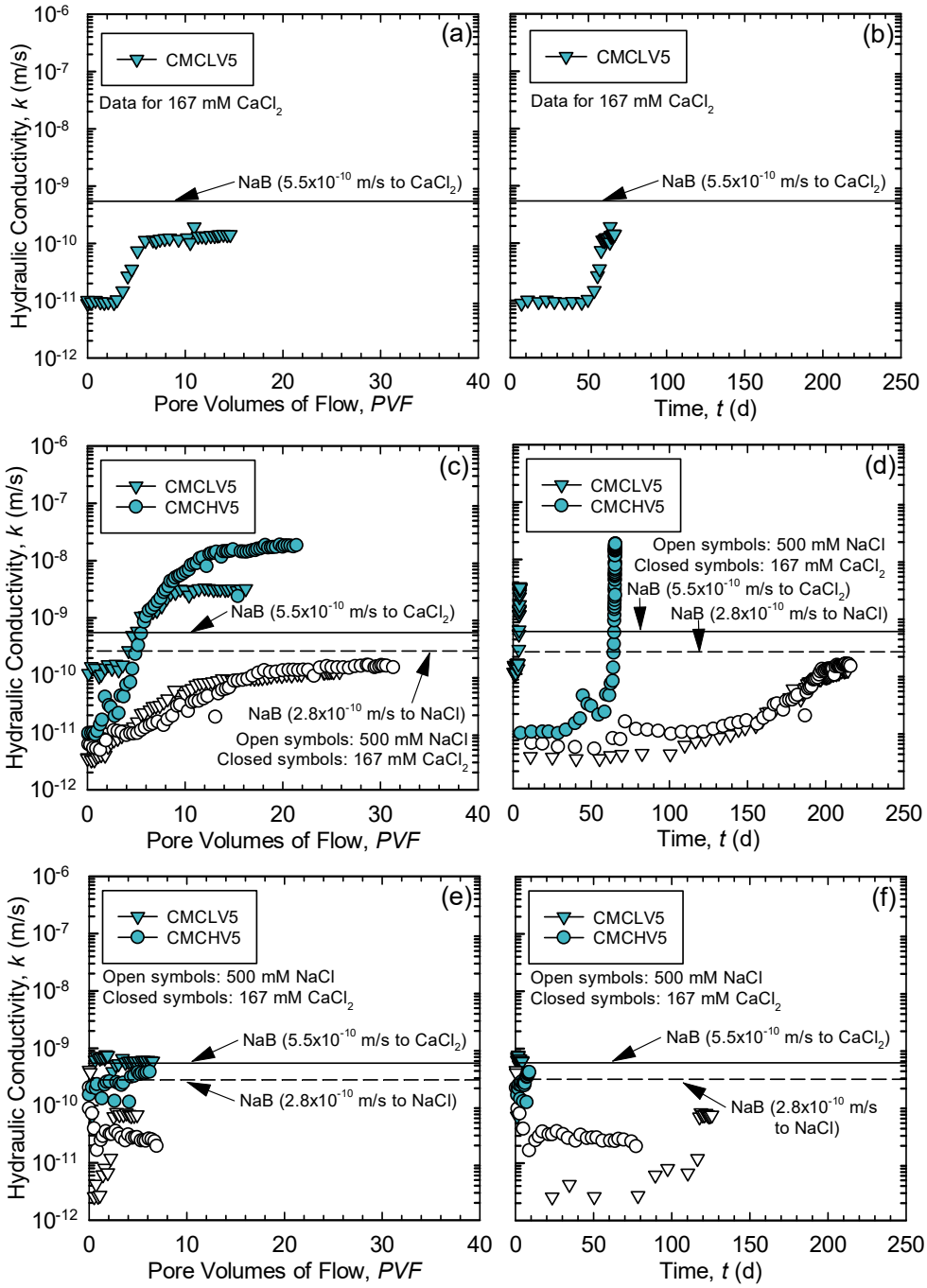

Figure 1.5: Hydraulic conductivity test results as a function of pore volumes of flow and elapsed time for EB-GCL specimens comprising sodium carboxymethylcellulose with high viscosity (CMCHV) and low viscosity (CMCLV) at 5% polymer mass loading and permeated with 500 mM NaCl and/or 167 mM $CaCl_2$ solutions: (a,b) dry-sprinkled specimens; (c,d) dry-mixed specimens; (e,f) wet-mixed specimens. Standardized hydraulic conductivity (k_{6766}) values for the conventional GCL specimens comprising unenhanced sodium bentonite (NaB) permeated with 500 mM NaCl and 167 mM $CaCl_2$ also are indicated.

For tests conducted with specimens prepared by dry mixing with CMC (Figure 1.5c,d), viz., CMCLV5DM and CMCHV5DM, all the k_{6766} values based on permeation with either 500 mM NaCl or 167 mM $CaCl_2$ were lower than the respective values for the conventional GCL (i.e., $0.26 \leq k_{EB\text{-}GCL}/k_{GCL} \leq 0.43$), except for specimen CMCHV5DM permeated with 167 mM $CaCl_2$, which resulted in $k_{EB\text{-}GCL}/k_{GCL} = 24.5$. In this case, the hydraulic conductivity increased over the course of 10 *PVF* to a final hydraulic conductivity (k_f) of 1.8×10^{-8} m/s ($k_{6766} = 1.4\times10^{-8}$ m/s). As illustrated subsequently, this high hydraulic conductivity was associated with preferential flow in one area of that specimen, which likely occurred due to the elution of polymer. The same trend and behavior in hydraulic conductivity was observed for specimen CMCLV5DM permeated with 167 mM $CaCl_2$, such that the k_f of 3.1×10^{-9} m/s also was greater than that of 4.8×10^{-10} m/s for the conventional GCL, even though the k_{6766} of 1.4×10^{-10} m/s was lower than that of 5.5×10^{-10} m/s for the conventional GCL (i.e., $k_{EB\text{-}GCL}/k_{GCL} = 0.26$). These results illustrate, that the termination criteria in ASTM D6766 can result in significantly unconservative (low) values of hydraulic conductivity for polymer amended EB-GCLs when the polymer is eluted from the specimen.

For tests conducted with specimens prepared by wet mixing with CMC (Figure 1.5e,f), viz., CMCLV5WM and CMCHV5WM, the test involving permeation of specimen CMCLV5WM with 167 mM $CaCl_2$ is still ongoing. Thus, any discussion of the results for this test is premature. For the other specimens, the k_{6766} values for CMCLV5WM permeated with 500 mM NaCl and the CVCHV5WM permeated with 500 mM NaCl and 167 mM $CaCl_2$ were lower than the respective values for the conventional GCL (i.e., $k_{EB\text{-}GCL}/k_{GCL} = 0.25$, $k_{EB\text{-}GCL}/k_{GCL} = 0.12$, and $k_{EB\text{-}GCL}/k_{GCL} = 0.67$, respectively). The k_f values to 500 mM NaCl of 6.7×10^{-11} m/s for the CMCLV5WM specimen and 3.3×10^{-11} m/s for the CMCHV5WM specimen also were lower relative to that of 1.6×10^{-10} m/s for the conventional GCL specimen, whereas the value of 3.8×10^{-10} m/s to 167 mM $CaCl_2$ for the CMCHV5WM specimen was only slightly lower relative to that of 4.8×10^{-10} m/s for the conventional GCL specimen. Thus, the hydraulic conductivity values of the wet-mixed CMC specimens were lower than that for the conventional GCL.

The temporal trend in hydraulic conductivity for the CMCHV5WM specimen was not the same as that for the CMCHV5DM specimen (Figure 1.5c,d), but the CMCHV5WM specimen was permeated only for 6.2 *PVF* compared to 21.4 *PVF* for the CMCHV5DM specimen, even though both specimens were not terminated before the criteria in ASTM D6766 had been achieved. This difference is likely related to the difference in the two preparation methods, i.e., wet mixing versus dry mixing.

1.4.2.3 EB-GCLs enhanced with PA

The results of the hydraulic conductivity tests for EB-GCLs enhanced with PA are summarized in Tables 1.3 and 1.4 and shown in Figure 1.6. For tests conducted with specimens prepared using the dry sprinkling method (Figure 1.6a,b), specimens PALW5DS, PALW8DS, PAMW5DS, PAMW8DS, and PAHW5DS were permeated with 500 mM NaCl (Table 1.3), whereas specimens PALW5DS, PALW10DS, PAMW5DS, PAMW8DS, PAMW10DS, PAHW5DS, and PAHW8DS were permeated with 167 mM $CaCl_2$ (Table 1.4). Based on the results for all these specimens, the percentage of PA necessary to reduce the hydraulic conductivity relative to that for the conventional GCL (i.e., $k_{EB\text{-}GCL}/k_{GCL} < 1$) varied with the molecular weight of PA and type of permeant solution (NaCl vs. $CaCl_2$).

Based on the results for all these specimens permeated with either 500 mM NaCl or 167 mM $CaCl_2$, only specimen PALW5DS permeated with 167 mM $CaCl_2$ did not achieve a lower hydraulic conductivity than that for the conventional GCL, with the k_{6766} values being essentially the same ($k_{EB\text{-}GCL}/k_{GCL} = 1.0$). For all the other specimens, the $k_{EB\text{-}GCL}/k_{GCL}$ values were lower than unity, and in some cases, significantly lower. For all the specimens permeated with 500 mM NaCl, $0.046 \leq k_{EB\text{-}GCL}/k_{GCL} \leq 0.86$, whereas for all the specimens permeated with 167 mM $CaCl_2$ (except PALW5DS), $0.020 \leq k_{EB\text{-}GCL}/k_{GCL} \leq 0.85$. In general, k_{6766} tended to decrease with increasing molecular weight of PA and/or increasing mass loading of PA.

For permeation with 500 mM NaCl, the greatest decrease in k_{6766} for the EB-GCL specimens relative to that for the conventional GCL specimen occurred with specimens PAMW5DS, PAMW8DS, PAHW5DS, i.e., $0.046 \leq k_{EB\text{-}GCL}/k_{GCL} \leq 0.10$, versus $k_{EB\text{-}GCL}/k_{GCL} = 0.86$ for specimen PALW5DS. Thus, the higher molecular weight PA specimens resulted in significantly lower k_{6766} values. However, polymer

mass loading did not have as significant an effect as polymer molecular weight, since the $k_{EB\text{-}GCL}/k_{GCL}$ for the PAHW5DS specimen was 0.046, which is about half the values of 0.093 and 0.10 for specimens PAMW5DS and PAMW8DS, respectively.

Similar results were obtained for the specimens permeated with 167 mM $CaCl_2$. For these specimens, the greatest decrease in k_{6766} for the EB-GCL specimens relative to that for the conventional GCL specimen of $0.020 \leq k_{EB\text{-}GCL}/k_{GCL} \leq 0.084$ occurred for specimens PAMW8DS, PAMW10DS, PAHW5DS, and PAHW8DS versus $0.75 \leq k_{EB\text{-}GCL}/k_{GCL} \leq 1.0$ for specimens PALW5DS, PALW10DS, and PAMW5DS. However, in contrast to the results based on permeation with 500 mM NaCl, polymer mass loading seemed to have a somewhat greater effect on the results. For example, $k_{EB\text{-}GCL}/k_{GCL} = 0.85$ for the PAMW5DS specimen permeated with 167 mM $CaCl_2$, which is 9.1 times greater than that of 0.093 based on permeation with 500 mM NaCl, whereas $k_{EB\text{-}GCL}/k_{GCL} = 0.020$ for the PAMW8DS specimen permeated with 167 mM $CaCl_2$. Thus, increasing the polymer mass loading of the dry-sprinkled PAMW specimens from 5 to 8 % significantly improved the hydraulic performance of these specimens permeated with 167 mM $CaCl_2$, but had minimal effect on the hydraulic performance of the same specimens permeated with 500 mM NaCl. This requirement for more polymer to achieve a similar hydraulic conductivity may be due to the lower molecular weight of the PAMW (~50000 g/mol) relative to that of the PAHW (~345000 g/mol), which equates to a reduction in polymer chain length. For example, increasing the mass loading of PAHW for the dry-sprinkled EB-GCL specimens from 5% to 8% did not significantly impact the hydraulic performance of these specimens permeated with 167 mM $CaCl_2$, with a k_{6766} of 4.0×10^{-11} m/s at 5% versus 4.6×10^{-11} m/s at 8%.

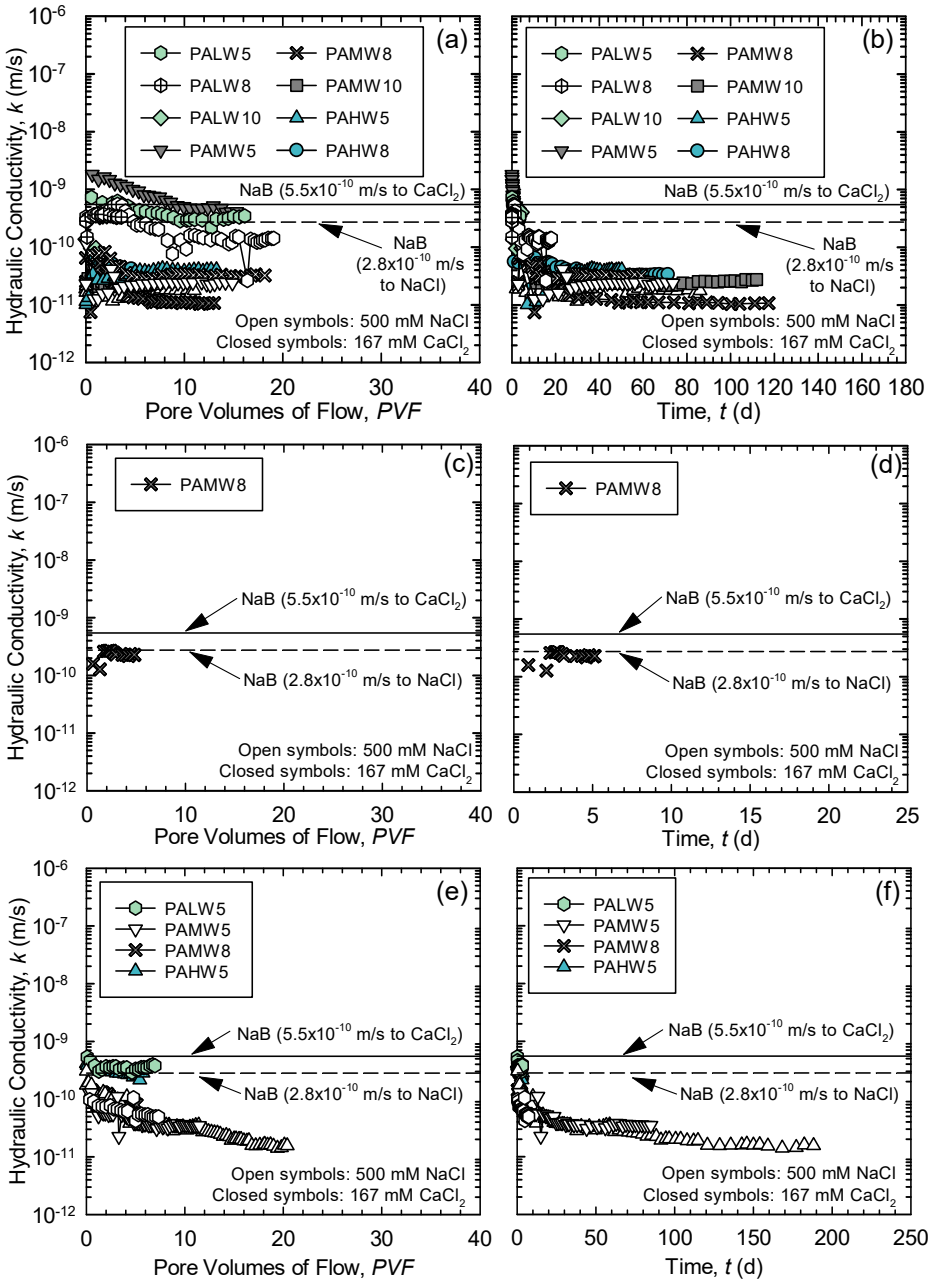

Figure 1.6: Hydraulic conductivity test results as a function of pore volumes of flow and elapsed time for EB-GCL specimens comprising sodium poly(acrylic acid) with low molecular weight (PALW), medium molecular weight (PAMW), and high molecular weight (PAHW) at different polymer mass loadings (5, 8, or 10%) and permeated with 500 mM NaCl and 167 mM $CaCl_2$ solutions: (a,b) dry-sprinkled specimens; (c,d) dry-mixed specimens; (e,f) wet-mixed specimens. Standardized hydraulic conductivity (k_{6766}) values for the conventional GCL specimens comprising unenhanced sodium bentonite (NaB) permeated with 500 mM NaCl and 167 mM $CaCl_2$ also are indicated.

An additional test for a specimen prepared by dry mixing with 8% of PAMW, i.e., PAMW8DM, and permeated with 167 mM $CaCl_2$ is in progress (Figure 1.6c,d). The initial behavior is similar to that for specimen PAMW8DS. However, unlike the results for specimen PAMW8DS, the hydraulic conductivity of specimen PAMW8DM increased after approximately 2.4 *PVF* and has plateaued at approximately 2.3×10^{-10} m/s, which is 21 times greater than the hydraulic conductivity of 1.1×10^{-11} m/s for the PAMW8DS specimen to the same solution (Table 1.4). This difference in behavior likely reflects the difference in specimen preparation method (dry mixing vs. dry sprinkling).

For tests conducted with specimens prepared using the wet mixing method (Figure 1.6e,f), specimens PALW5WM, PAMW5WM, and PAHW5WM were permeated with 500 mM NaCl (Table 1.3), whereas specimens PALW5WM, PAMW8WM, and PAHW5WM were permeated with 167 mM $CaCl_2$ (Table 1.4). Note that the test involving specimen PAMW8WM is still ongoing such that the results of this test are not discussed. Thus, comparisons of the results for the three specimens permeated with 500 mM NaCl and the two specimens with 5% polymer mass loading and permeated with 167 mM $CaCl_2$ provide a direct assessment of the effect of the polymer molecular weight on the hydraulic conductivity with respect to each permeant solution. Also, comparison of the results for specimen PALW5WM and specimen PAHW5WM based on permeation with 500 mM NaCl versus those based on permeation with 167 mM $CaCl_2$ provides a direct assessment of the effect of type of permeant solution.

All the wet-mixed EB-GCL specimens permeated with 500 mM NaCl resulted in significantly lower and similar k_{6766} values relative to that for the conventional GCL, i.e., $0.17 \leq k_{EB\text{-}GCL}/k_{GCL} \leq 0.28$, whereas the k_{6766} values for the two specimens with 5% polymer mass loading (PALW5WM and PAHW5WM) permeated with 167 mM $CaCl_2$ also were similar and lower than that for the conventional GCL, i.e., $0.56 \leq k_{EB\text{-}GCL}/k_{GCL} \leq 0.60$. Thus, for the wet-mixed EB-GCL specimens, the molecular weight of the polymer had little effect on the improvement in hydraulic performance of the EB-GCLs relative to that for the conventional GCL, although the improvement was less significant in the case of permeation with 167 mM $CaCl_2$ versus 500 mM NaCl. Also, for specimen PALW5WM, permeation with 500 mM NaCl resulted in $k_{EB\text{-}GCL}/k_{GCL} = 0.28$ whereas permeation with 167 mM $CaCl_2$ resulted in $k_{EB\text{-}GCL}/k_{GCL} =$

0.60. Similarly, for specimen PAHW5WM, permeation with 500 mM NaCl resulted in $k_{EB\text{-}GCL}/k_{GCL}$ = 0.19 whereas permeation with 167 mM $CaCl_2$ resulted in $k_{EB\text{-}GCL}/k_{GCL}$ = 0.56. Thus, the wet-mixed EB-GCL specimens were less effective based on permeation with 167 mM $CaCl_2$ relative to 500 mM NaCl. Nonetheless, all the wet-mixed EB-GCL specimens resulted in improved hydraulic performance relative to that for the conventional GCL. Also, an initial decreasing temporal trend in hydraulic conductivity occurred for several of the wet-mixed EB-GCL specimens (e.g., Figures 1.5e,f and1.6e,f). These decreasing trends in hydraulic conductivity are similar to those exhibited by EB-GCLs comprising HYPER clay, which is a CMC-enhanced bentonite prepared via a more advanced wet-mixing method (e.g., Di Emidio et al. 2015).

Tests conducted with the wet-mixed EB-GCLs enhanced with PA (Figure 1.6e,f) behaved differently than those conducted with the dry-sprinkled EB-GCLs enhanced with PA. For example, for permeation with 167 mM $CaCl_2$, the hydraulic conductivity of 3.1×10^{-10} m/s for specimen PAHW5WM is approximately 7.8 times higher than that of 4.0×10^{-11} m/s for specimen PAHW5DS, whereas the hydraulic conductivity of 8.2×10^{-11} m/s for specimen PAMW8WM is approximately 7.5 times higher than that of 1.1×10^{-11} m/s for specimen PAMW8DS, although the test with PAMW8WM is still ongoing. Also, for permeation with 500 mM NaCl, the hydraulic conductivity of 4.8×10^{-11} m/s for specimen PAMW5WM is 1.8 times higher than that of 2.6×10^{-11} m/s for specimen PAMW5DS, whereas the hydraulic conductivity of 5.2×10^{-11} m/s for specimen PAHW5WM is 4.0 times higher than that of 1.3×10^{-11} m/s for specimen PAHW5DS. In contrast, the hydraulic conductivity to 500 mM NaCl of 7.8×10^{-11} m/s for specimen PALW5WM is 3.1 times lower than that of 2.4×10^{-10} m/s for specimen PALW5DS. Thus, in general, the hydraulic conductivity of the wet-mixed specimens was higher than that of the dry sprinkled specimens, with the lone exception occurring for the lowest molecular weight PA at the lowest polymer mass loading (i.e., PALW5). These results indicate that the method of specimen preparation, i.e., dry versus wet, can affect the hydraulic conductivity of PA-enhanced EB-GCLs. The mechanisms underlying the greater relative effectiveness of the dry-sprinkled EB-GCLs versus wet-mixed EB-GCLs enhanced with the same polymer and polymer content are further advanced in Chapter 4.

1.4.2.4 EB-GCLs enhanced with PAx

The results of the hydraulic conductivity tests for EB-GCLs enhanced with PAx are summarized in Tables 1.3 and 1.4 and shown in Figure 1.7a,b. These specimens, designated as PAx5DS, were prepared by dry sprinkling the NaB with 5% PAx by mass (Fig. 1.2). The hydraulic conductivity of the PAx5DS specimen permeated with 500 mM NaCl was 2.5×10^{-11} m/s (Table 1.3), which is about an order-of-magnitude lower than the value of 2.8×10^{-10} m/s for the conventional GCL specimen (i.e., $k_{EB\text{-}GCL}/k_{GCL}$ = 0.089). The test with the PAx5DS specimen permeated with 167 mM $CaCl_2$ is still ongoing, but the current hydraulic conductivity is approximately 2.3×10^{-10} m/s (Table 1.4), which is about 2.3 times lower than the value of 5.5×10^{-10} m/s for the conventional GCL specimen (i.e., $k_{EB\text{-}GCL}/k_{GCL}$ = 0.38). In comparison, the values of $k_{EB\text{-}GCL}/k_{GCL}$ for specimens PAMW5DS and PAHW5DS based on permeation with 500 mM NaCl are 0.093 and 0.046, respectively, whereas those for specimens PALW5DS, PAMW5DS, and PAHW5DS based on permeation with 167 mM $CaCl_2$ are 1.0, 0.85, and 0.073, respectively. Thus, the use of the covalently crosslinked PA does not appear to be as effective as the linear PA with respect to the 500 mM NaCl solution, whereas the PAx appears to be more effective than the PALW or PAMW, and similar in effectiveness to PAHW, with respect to the 167 mM $CaCl_2$ solution.

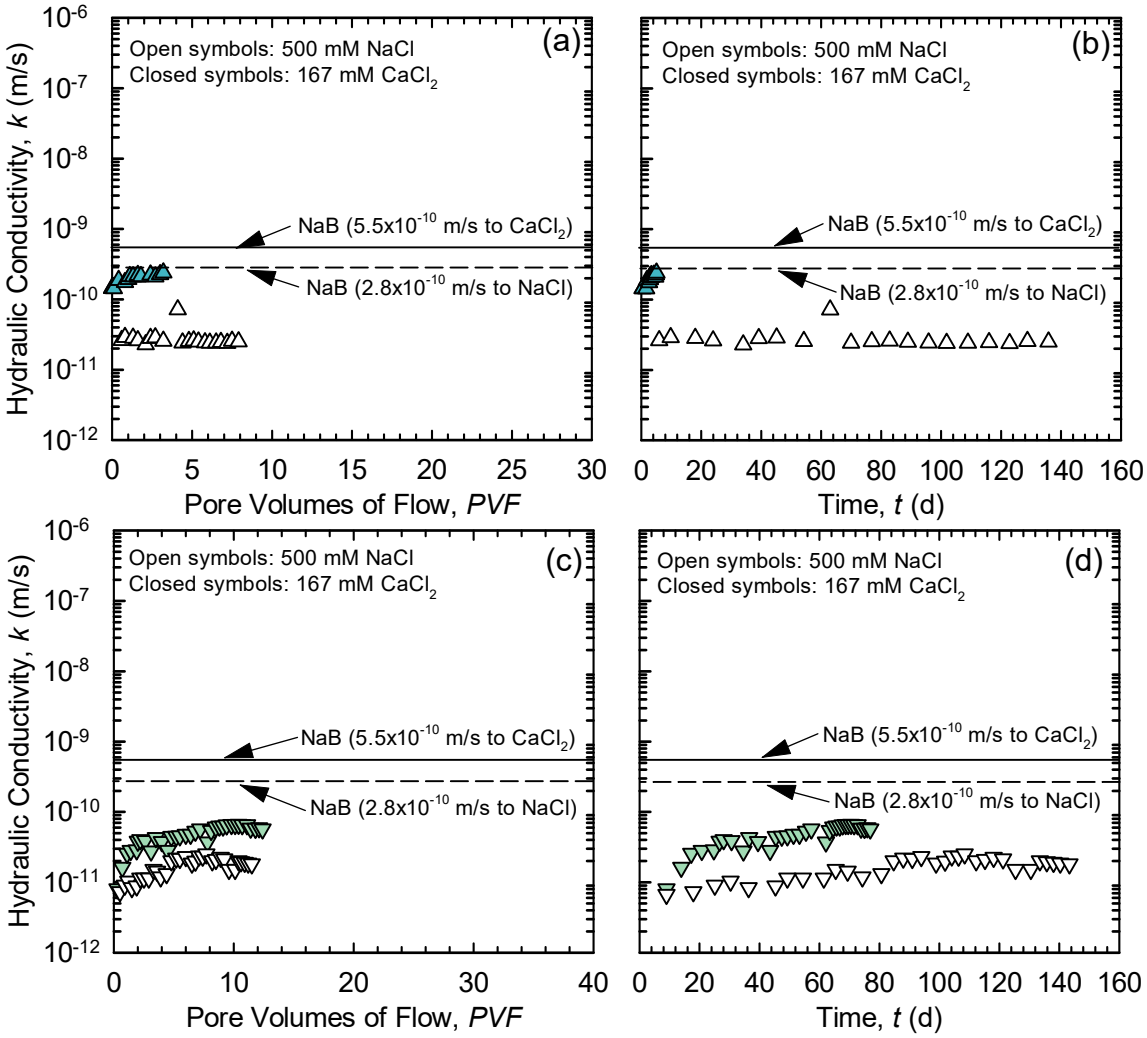

Figure 1.7: Hydraulic conductivity test results as a function of pore volumes of flow and elapsed time for EB-GCL specimens comprising bentonite polymer composite (BPC) at 5% polymer mass loading and permeated with 500 mM NaCl and 167 mM $CaCl_2$ solutions: (a,b) dry-sprinkled specimens; (c,d) dry-mixed specimens; (e,f) wet-mixed specimens. Standardized hydraulic conductivity (k_{6766}) values for the conventional GCL specimens comprising unenhanced sodium bentonite (NaB) permeated with 500 mM NaCl and 167 mM $CaCl_2$ also are indicated.

1.4.2.5 EB-GCLs enhanced with BPC

The results of the hydraulic conductivity tests for EB-GCLs enhanced with BPC are summarized in Tables 1.3 and 1.4 and shown in Figure 1.7c,d. The specimens, designated as BPC5DM, were prepared by dry mixing the BPC with the NaB to result in a polymer mass loading of 5%. The k_{6766} values of the specimens to both 500 mM NaCl and 167 mM $CaCl_2$ were 1.1×10^{-11} m/s and 3.2×10^{-11} m/s, respectively, which reflect

a significantly better hydraulic performance for the EB-GCL relative to that of the conventional GCL (i.e., $k_{EB\text{-}GCL}/k_{GCL}$ = 0.039 and $k_{EB\text{-}GCL}/k_{GCL}$ = 0.058, respectively). By comparison, the $k_{EB\text{-}GCL}/k_{GCL}$ values for the best performing EB-GCLs comprising 5% of PA were 0.093 and 0.046 for PAMW5DS and PAHW5DS, respectively, based on permeation with 500 mM NaCl, and 0.073 for PAHW5DS based on permeation with 167 mM $CaCl_2$. Thus, the hydraulic performance of the specimen based on in-situ polymerization to produce the BPC was not better than that of the best performing EB-GCLs comprising 5% of PA.

1.4.3 Polymer retention and elution

All EB-GCLs permeated in this research eluted a fraction of polymer during permeation, indicating that complete polymer retention was not achieved regardless of the preparation method, polymer type, or polymer mass loading. The PA and CMC polymers are water soluble and can increase solution viscosity with increasing polymer concentration. However, as shown in Figure 1.8, the cross-linking and formation of visible polymer strands, or hydrogel, was evident in the effluent samples of the EB-GCLs prepared with PA and CMC. Hydrogel has been hypothesized to form primarily due to divalent cations (predominantly Ca^{2+}) available in the permeant solution that ionically bond and cross-link multiple anionic polymer chains (Scalia et al. 2014, 2018; Tian 2019). The soluble Ca^{2+} and, to a lesser extent, Mg^{2+} within the base NaB as well as the Ca^{2+} in the $CaCl_2$ permeant solution (Figures 1.8a,b) provide cations for ionic cross-linking. Due to the presence of multivalent cations in the soluble salts and on the exchange complex of the NaB, principally Ca^{2+} (Table 1.1), cross-linking also can occur in the EB-GCLs permeated with 500 mM NaCl (Figure 1.8c,d). However, cross-linking via cations creates a transient network that can be altered due to changes in solution pH, cation concentrations, or application of shear forces (Buchholz and Graham 1998), such as by varying the hydraulic gradient applied during hydraulic conductivity testing.

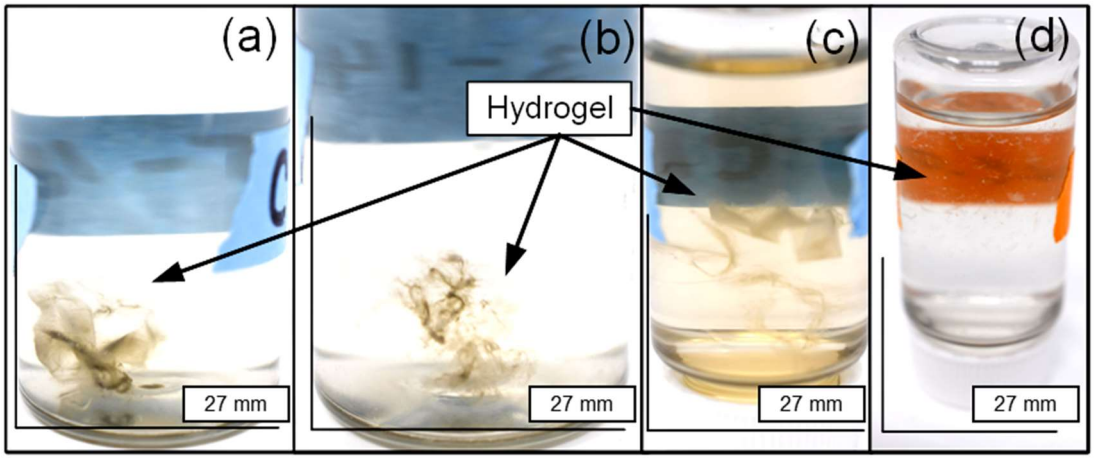

Figure 1.8: Hydrogel strands within effluent sample bottles from the PALW5DS specimens permeated with (a,b) 167 mM $CaCl_2$ and (c) 500 mM NaCl, and (d) the CMCHV5DM specimen permeated with 500 mM NaCl.

The existence of hydrogel in the effluent does not necessarily confirm that the same hydrogel existed within the interparticle, intra-aggregate, and/or interaggregate pores of the EB-GCL specimens during permeation. However, as shown in Figures 1.9a-c, hydrogel also was present on the inflow sides of the nonwoven geotextile and base plate of the permeameter. Polymer migration towards the inflow side likely began during hydration as a result of a combination of a dissolved polymer concentration gradient moving in the path of least resistance, especially in the case of EB-GCLs prepared via dry-sprinkling where the polymer is placed on the inflow side of the GCL. Specimens that exhibited hydrogel formation on the nonwoven geotextiles or within the permeameter are indicated with respect to the final hydraulic conductivity values in Tables 1.3 and 1.4. The presence of hydrogel within the permeameter (e.g., on the base plate and geotextiles) as well as in the effluent implies that hydrogel also was present within the interparticle, intra-aggregate, and/or interaggregate pores of the EB-GCL specimens. These observations support the hypothesis previously postulated by Scalia et al. (2014, 2018) and Tian et al. (2016a,b, 2017, 2019) that clogging of pores with polymer hydrogel is the primary mechanism reducing the hydraulic conductivity of EB-GCLs relative to the conventional GCL comprising unenhanced NaB. Further discussion of the role of hydrogel formation in hydraulic conductivity of EB-GCLs is provided in Chapter 4.

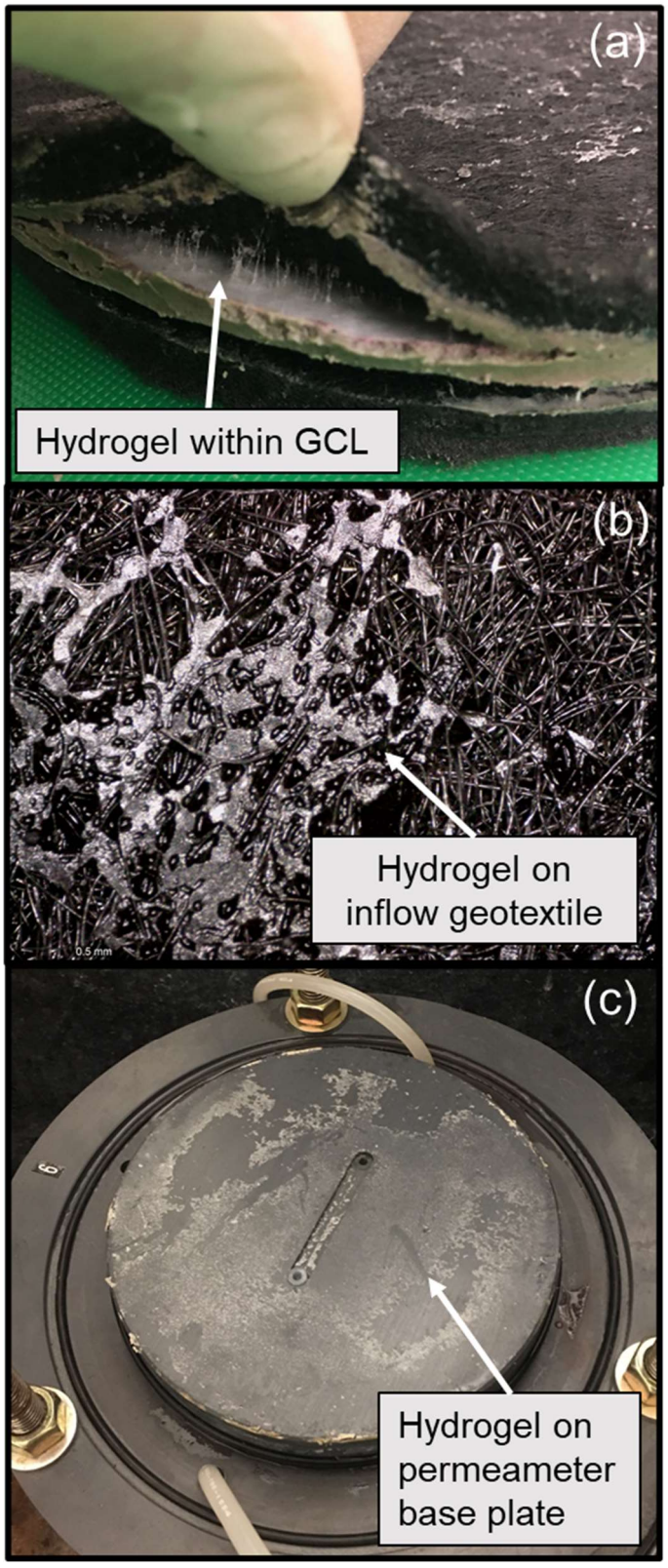

Figure 1.9: Visible crosslinked polymer in hydraulic conductivity testing of EB-GCL specimens: (a,b) PAHW5DS permeated with 167 mM $CaCl_2$; (c) PAMW8DS permeated with 167 mM $CaCl_2$.

1.4.3 Preferential flow

Tests where preferential flow was indicated by the presence of concentrated rhodamine dye on the outflow side of the specimen are indicated with respect to the final hydraulic conductivity values in Tables 1.3 and 1.4. Preferential flow was evident under two conditions. First, when the hydraulic conductivity of the EB-GCL was unexpectedly higher than that for the conventional GCL with the same permeant solution, the tests were dyed as previously described, and the specimen was inspected for evidence of preferential flow paths upon termination of the test. If preferential flow was observed to be the result of setup error, such as being caused by geotextiles pinching together during setup due to uneven bentonite loading, then the test was considered unacceptable and repeated. Data from tests that were deemed unacceptable are not reported herein.

Second, preferential flow also was manifested by a steadily increasing temporal trend in hydraulic conductivity, resulting in a final hydraulic conductivity higher than the baseline hydraulic conductivity of the conventional GCL. This preferential flow behavior was evident for specimens CMCLV5DM and CMCHV5DM permeated with 167 mM $CaCl_2$, where the dye revealed a preferential flow path in the center of these specimens. Both EB-GCLs were prepared by the dry-mixing method, resulting in a mixture of polymer granules within the base NaB (Figure 1.2). The increasing trend in hydraulic conductivity observed for these specimens (Figures 1.5c,d) is believed to be due to polymer elution. In the dyed portion of the specimen, the polymer network likely created an interconnected path from the inflow to the outflow side of the specimens. As the polymer was eluted, the flow likely occurred through the pathway opened by the loss of polymer. Although the initial results at ~2 *PVF* for the PAMW8DM specimen being permeated with 167 mM $CaCl_2$ exhibited an increasing trend in hydraulic conductivity, the current results have since plateaued and do not exhibit an increasing trend. Additional hydraulic conductivity testing of EB-GCLs prepared by dry mixing with CMC and PA at higher polymer contents is required to verify the role of the dry mixing method or polymer type on preferential flow.

1.5 DISCUSSION

1.5.1 Effects of polymer properties and specimen preparation methods

Summary plots of the hydraulic conductivity (k_{6766}) for all the EB-GCL specimens are shown in Figure 1.10 as a function of polymer type and mixing method. Overall, the hydraulic performance of the EB-GCLs to the NaCl solution was better than that to the $CaCl_2$ solution (Figure 1.10a). Unexpectedly, increasing PA molecular weight did not correlate necessarily with decreasing hydraulic conductivity, since the lowest hydraulic conductivity of the EB-GCLs with PA occurred for the PAMW8DS specimen. In contrast, the PALW was not effective in reducing hydraulic conductivity relative to the that of unenhanced NaB, even at the highest polymer mass loading of 10%. As previously mentioned, considerations need to be given to the final polymer content of the specimen after permeation as well as the effective initial distribution of polymer across specimen during preparation. Either polymer elution and/or a thin layered section or gap in polymer placement in an EB-GCL may result in a higher hydraulic conductivity.

As shown in Figure 1.10a, the viscosity of the CMC did not impact the hydraulic conductivity. The decrease in hydraulic conductivity of the CMC-enhanced GCLs relative to that for the conventional GCL, which was approximately one order of magnitude or less, was not as significant as that for the other EB-GCLs, which was greater than one order of magnitude.

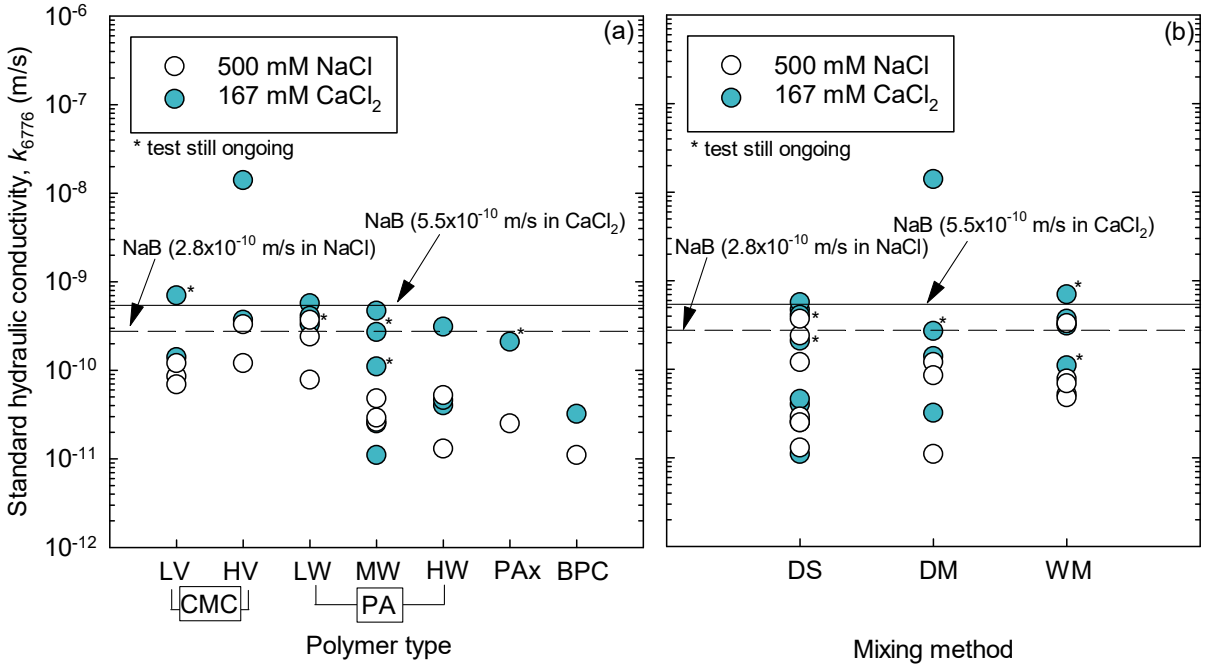

Figure 1.10: Standard hydraulic conductivity (k_{6776}) as a function of (a) polymer type (i.e. sodium carboxymethylcellulose (CMC) with low viscosity (LV) or high viscosity (HV) and poly(acrylic acid) (PA) with low, medium, or high molecular weight (LW, MW, HW, respectively), covalently crosslinked sodium polyacrylate (PAx), and bentonite polymer composite (BPC)), and (b) method of specimen preparation (dry-sprinkle (DS), dry-mixing (DM), and wet-mixing (WM)). Standardized hydraulic conductivity (k_{6766}) values for the conventional GCL comprising unenhanced sodium bentonite (NaB) permeated with 500 mM NaCl and 167 mM $CaCl_2$ also are indicated. The hydraulic conductivities of ongoing tests as well as the BPC5DM permeated with 500 mM NaCl indicate the last measured hydraulic conductivity.

The structural differences between PA and CMC may be a controlling factor in the differences in behavior. The crosslinking potential for the CMC may be lower than that for the PAs due to a fewer the number of carboxyl groups, which depends on the DoS. In this case, CMC bridging to bound cations within the interparticle, intra-aggregate, and/or interaggregate pore matrix of the EB-GCLs would be lessened, resulting in less retention of the CMC and a higher hydraulic conductivity.

As shown in Figure 1.10b, the dry-mixed EB-GCL comprising 5% of BPC (BPC5DM) resulted in the lowest hydraulic conductivity to 500 mM NaCl of 1.1×10^{-11} m/s, with the dry-sprinkled EB-GCL comprising 5% of covalently crosslinked PAx (PAx5DS) resulting in a hydraulic conductivity only 2.3 times greater (2.5×10^{-11} m/s). The hydraulic conductivity of specimen PAx5DS permeated with 167 mM $CaCl_2$ solution is still ongoing, but the initial hydraulic conductivity is higher than those achieved using

PAMW and PAHW. Based on the results of this study, the PAx may provide a suitably low hydraulic conductivity when permeated with a concentrated NaCl solution but does not appear to offer any advantage relative to PAMW and PAHW when permeated with a concentrated $CaCl_2$ solution.

As shown in Figure 1.10b, all the hydraulic conductivity values for the dry-sprinkled EB-GCLs except for one were lower than those for the conventional GCL, with the lone exception being for specimen PALW5DS with a hydraulic conductivity to 167 mM $CaCl_2$ that was essentially the same as that for the conventional GCL specimen (Table 1.4). As a result of the location of the polymer at the inflow side of the dry-sprinkled specimens (Figure 1.2), if the polymer fails to mobilize and clog the pores of the adjacent NaB, then the hydraulic conductivity is governed solely by the NaB. In contrast, dry or wet mixing the polymer with the NaB leads to the potential for incomplete distribution of the polymer throughout the specimen during preparation, especially with a lower polymer mass loading. In this case, elution of the polymer may lead to a preferential flow path resulting in a hydraulic conductivity that is higher than that of the conventional GCL, due to flow occurring through larger, interaggregate pores created by the polymer elution.

1.5.2 Effect of polymer mass loading

The effect of polymer mass loading on the hydraulic conductivity (k_{6766}) of all the EB-GCL specimens is illustrated in Figure 1.11 based on permeation with 500 mM NaCl (Fig. 1.11a,c,e) and 167 mM $CaCl_2$ (Fig. 1.11b,d,f). For the dry-sprinkled prepared specimens (Figure 1.11a,b), the lowest hydraulic conductivity to both permeant solutions for specimens at 5% polymer mass loading occurred for the EB-GCL specimens with PAHW, whereas the lowest hydraulic conductivity for either 8% or 10% polymer mass loadings to both permeant solutions occurred for the EB-GCL specimens with PAMW. The overall lowest hydraulic conductivity based on permeation with 500 mM NaCl of 1.3×10^{-11} m/s occurred for the specimen with 5% of PAHW (Figure 1.11a), whereas the overall lowest hydraulic conductivity based on permeation with 167 mM $CaCl_2$ of 1.1×10^{-11} m/s occurred for the specimen with 8% of PAMW (Figure 1.11b), which also was the overall lowest hydraulic conductivity to either permeant solution. The dry-sprinkling method used in this study was implemented by hand such that the results may highlight variations in the distribution of

polymer for a given specimen. Replicate tests are required to confirm whether these results reflect a limitation to the reduction of hydraulic conductivity with increasing polymer loading or are an artifact of the variation of polymer distribution resulting from the dry sprinkling method.

As shown in Figures 1.11c,e, no conclusions can be drawn with respect to the effect of polymer mass loading on the hydraulic conductivity of the dry-mixed or wet-mixed EB-GCL specimens permeated with 500 mM NaCl, since only the 5% polymer mass loading was evaluated for these specimens. The data also are limited with respect to the dry-mixed and wet-mixed EB-GCL specimens permeated with 167 mM $CaCl_2$ (Fig. 1.11d,f), with all but one of the specimens comprising 5% polymer mass loading. In terms of the results for the dry-mixed specimens (Figure 1.11c,d), the EB-GCL enhanced with 5% BPC resulted in the overall lowest hydraulic conductivity to either permeant liquid of 1.1×10^{-11} m/s based on permeation with 500 mM NaCl (Table 1.3). An interesting observation is that this hydraulic conductivity value is essentially the same as the aforementioned lowest values to either permeant solution for specimens dry-sprinkled with 5% of PAHW (500 mM NaCl) or 8% of PAMW (167 mM $CaCl_2$). For the wet-mixed specimens enhanced with 5% polymer mass loading and permeated with 500 mM NaCl (Figure 1.11e), all the measured hydraulic conductivity values are similar (4.8×10^{-11} m/s $\leq k_{6766} \leq$ 7.8×10^{-11} m/s) and are similarly lower than that of 2.8×10^{-10} m/s for conventional GCL, except for the specimen enhanced with CMCHV with a hydraulic conductivity of 3.3×10^{-10} m/s (Table 1.3). In contrast, none of the wet-mixed specimens enhanced with 5% polymer and permeated with 167 mM $CaCl_2$ resulted in hydraulic conductivity values that were appreciably different than that of 5.5×10^{-10} m/s for the conventional GCL, where the preliminary results for the specimen enhanced with 8% PAMW indicate a somewhat lower hydraulic conductivity. Overall, simply increasing the polymer mass loading does not necessarily result in lower hydraulic conductivity, as other factors such as type of polymer and method of specimen preparation may control the hydraulic behavior.

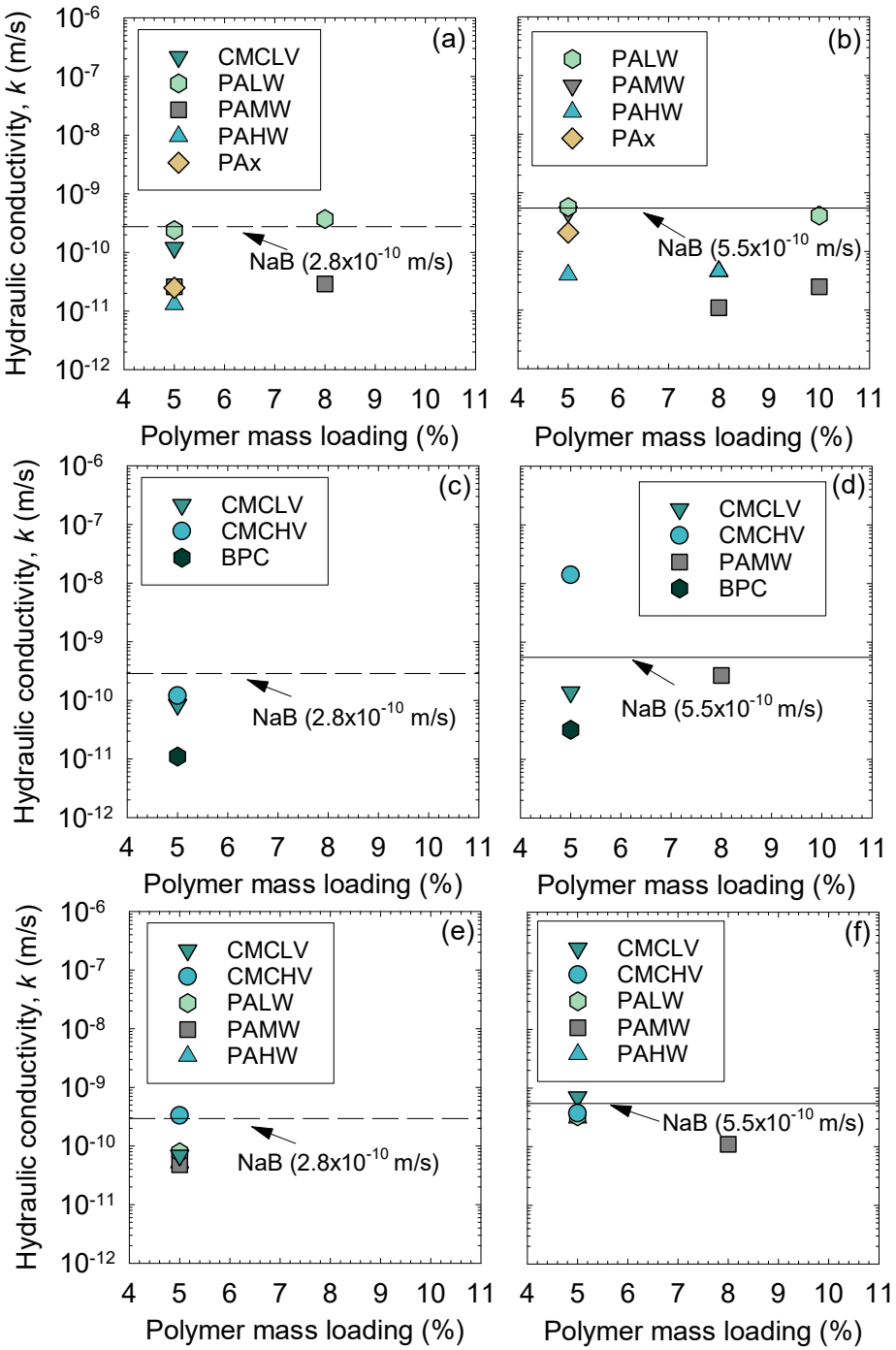

Figure 1.11: Effect of polymer mass loading on hydraulic conductivity (k_{6766}) of EB-GCL specimens prepared by (a,b) dry sprinkling, (c,d) dry mixing, and (e,f) wet mixing of sodium carboxymethylcellulose with high viscosity (CMCHV) and low viscosity (CMCLV), sodium poly(acrylic acid) with low molecular weight (PALW), medium molecular weight (PAMW), and high molecular weight (PAHW), covalently crosslinked sodium polyacrylate (PAx), and bentonite polymer composite (BPC) and permeated with (a,c,e) 500 mM NaCl and (b,d,f) 167 mM $CaCl_2$. Standardized hydraulic conductivity (k_{6766}) values for the conventional GCL comprising unenhanced sodium bentonite (NaB) permeated with 500 mM NaCl and 167 mM $CaCl_2$ also are indicated.

1.6 CONCLUSIONS

Hydraulic conductivity tests were conducted in accordance with ASTM D6766 on specimens of a conventional GCL comprising a natural (unenhanced), powdered NaB and EB-GCLs comprising the NaB enhanced with one of several anionic polymers at mass loadings of 5%, 8%, and/or 10%. Three methods were used to prepare the EB-GCL specimens, dry sprinkling (DS), dry mixing (DM), and/or wet mixing (WM). The polymers included CMC with low and high viscosity (CMCLV and CMCHV), liner PA with low, medium, and high molecular weights (PALW, PAMW, PAHW) of approximately 5000, 50000, and 345000 g/mol, respectively, and a covalently crosslinked PA (PAx). An EB previously produced by in-situ polymerization to include 28.5% by mass of polyacrylate known as bentonite polymer composite (BPC) also was used to prepare dry-mixed EB-GCL specimens at a polymer mass loading of 5% (i.e., an EB with 17.3% of BPC). The hydraulic conductivity tests were conducted at low effective stress (27 kPa) using concentrated electrolyte solutions (500 mM NaCl and 167 mM $CaCl_2$) with high ionic strength (I = 500 mM) to represent aggressive chemical conditions. Qualitative polymer elution analysis was performed based on observations of hydrogel formation and linear polymer crosslinking. The following conclusions are based on the findings of this study.

- EB-GCLs comprising anionic polymers at low polymer mass loadings (≤ 10%) and prepared using different mixing methods have the potential to improve chemical incompatibility relative to conventional GCLs with natural (unenhanced) NaB based on permeation with high ionic strength (500 mM) electrolyte solutions.
- The measured hydraulic conductivity of EB-GCLs prepared with anionic polymers is affected by the type and properties (molecular weight and viscosity) of the polymer, the polymer mass loading (i.e., 5, 8, and 10%), and the method of specimen preparation (i.e., DS, DM, WM). However, the benefits of an increase in molecular weight or percentage enhancement in resisting hydraulic incompatibility and resulting in a lower hydraulic conductivity relative to that for the conventional GCL comprising the unenhanced NaB are limited. Thus, limitlessly increasing either or both of these parameters will not necessarily continuously decrease the hydraulic conductivity.

- The overall best hydraulic performance for the EB-GCLs prepared with linear anionic polymers evaluated in this study occurred for those prepared by dry sprinkling with 5% of PAHW and 8% of PAMW, with a hydraulic conductivity of 1.3×10^{-11} m/s to 500 mM NaCl and 4.0×10^{-11} m/s to 167 mM $CaCl_2$ for the specimen with PAHW, and 2.9×10^{-11} m/s to 500 mM NaCl and 1.1×10^{-11} m/s to 167 mM $CaCl_2$ for the specimen with PAHW. The EB-GCL enhanced with 5% of BPC by dry mixing resulted in similarly good performance with a hydraulic conductivity of 1.1×10^{-11} m/s to 500 mM NaCl and 3.2×10^{-11} m/s to 167 mM $CaCl_2$. Thus, low hydraulic conductivity ($\leq 4.0\times10^{-11}$ m/s) of EB-GCLs to aggressive inorganic chemical solutions can be achieved with low mass percentage polymer enhancement.
- The dry mixing method of specimen preparation provided the best hydraulic performance for the EB-GCLs with the least amount of required effort of the mixing methods tested. The dry and wet mixing methods result in the polymer being dispersed within the matrix of particles and aggregates of particles such that, if the polymer is eluted upon permeation, a preferential flow path through the EB-GCL can be created resulting in an increase in hydraulic conductivity.
- All EB-GCLs tested in this study eluted a fraction polymer during permeation. Observations of hydrogel in multiple effluent samples and on post-permeated EB-GCLs specimens support pore clogging by the hydrogel within the pore network of EB-GCLs as the primary mechanism for low hydraulic conductivity to the aggressive permeant solutions used in this study. However, preferential, interaggregate flow paths that correlated with polymer elution and higher hydraulic conductivity also were identified in multiple EB-GCL specimens, emphasizing the importance of polymer retention for maintaining the low hydraulic conductivity of the EB-GCLs.
- The ASTM D6766 termination criteria are sufficient for generally, but insufficient for universally, predicting the hydraulic conductivity of the permeated EB-GCLs with lower percent (5-10%) of anionic polymer enhancements. These criteria do not consider the long-term impact of polymer

elution. Further research is necessary to determine the long-term effect of polymer elution on the hydraulic conductivity of EB-GCLs.

- More research is necessary to determine the mechanisms controlling EB-GCL behavior. The potential pore clogging occurring by the hydrogel formed within the pore network of the specimen cannot be proven without more quantitative results related to polymer retention and elution behavior of EB-GCLs and the potential for hydrogel formation. This topic is the subject of the following chapters.

REFERENCES

Ashmawy, A., Darwish, E., Sotelo, N. and Muhammad, N. 2002. Hydraulic performance of untreated and polymer-treated bentonite in inorganic landfill leachates. *Clays and Clay Minerals*, 50(5), 546-552.

ASTM. 2006. Standard test method for swell index of clay mineral component of geosynthetic clay liners. D5890, West Conshohocken, Pennsylvania, USA.

ASTM. 2010. Standard test methods for liquid limit, plastic limit, and plasticity index of soils. D4318, West Conshohocken, Pennsylvania, USA.

ASTM. 2011. Standard practice for classification of soils for engineering purposes (Unified Soil Classification System). D2487, West Conshohocken, Pennsylvania, USA.

ASTM. 2014. Standard test method for rapid determination of carbonate content of soils. D4373, West Conshohocken, Pennsylvania, USA.

ASTM. 2018. Standard test method for evaluation properties of geosynthetic clay liners permeated with potentially incompatible liquids. D6766, West Conshohocken, Pennsylvania, USA.

ASTM. 2018. Standard test method for measuring the exchange complex and cation exchange capacity of inorganic fine-grained soils. D7503, West Conshohocken, Pennsylvania, USA.

Benson, C., Oren, A., and Gates, W. 2010. Hydraulic conductivity of two geosynthetic clay liners permeated with a hyperalkaline solution. *Geotextiles and Geomembranes*, 28(2), 206-218.

Bohnhoff, G. 2012. Membrane behavior, diffusion, and compatibility of a polymerized bentonite for containment barrier applications, Ph.D. dissertation, Colorado State University, Fort Collins, Colorado, USA.

Bohnhoff, G., and Shackelford, C. 2013. Improving membrane performance via bentonite polymer nanocomposite. *Applied Clay Science*, 86, 83-98.

Bohnhoff, G., Shackelford, C., and Sample-Lord, K. 2014. Calcium resistant membrane behavior of a polymerized bentonite. *Journal of Geotechnical and Geoenvironmental Engineering*, 140(3), 04013029.

Bohnhoff, G., Shackelford, C., Malusis, M., Scalia, J., Benson, C., Edil, T., Di Emidio, G., Katsumi. T., and Mazzieri, F. 2013. Novel bentonites for containment barrier applications, Proceedings, 18th International Soil Mechanics and Geotechnical Engineering-Challenges and Innovations in Geotechnics Conference, P. Delage, J. Desrues, R. Frank, A. Puech, F. Schlosser, Eds., Presses des Ponts, Paris, 4, 2997-3000.

Bouazza, A., and Gates, W. 2014. Overview of performance compatibility issues of GCLs with respect to leachates of extreme chemistry. *Geosynthetics International*, 21(2), 151-167.

Bradshaw, S., Benson, C., and Scalia, J. 2013. Hydration and cation exchange during subgrade hydration and effect on hydraulic conductivity of geosynthetic clay liners. *Journal of Geotechnical and Geoenvironmental Engineering*, 139(4), 526-538.

Buchholz, F. and Graham, A. 1998. Modern superabsorbent polymer technology, Wiley-VCH, New York.

Chai, J., and Prongmanee, N. 2020. Barrier properties of a geosynthetic clay liner using polymerized sodium bentonite. *Geotextiles and Geomembranes*, 48, 392-399.

Chen, J., Salihoglu, H., Benson, C., Likos, W., and Edil, T. 2019. Hydraulic conductivity of bentonite-polymer composite geosynthetic clay liners permeated with coal combustion product leachates. *Journal of Geotechnical and Geoenvironmental Engineering*, 145(9), 04019038.

Di Emidio, G., Van Impe, W., and Mazzieri, F. 2010. A polymer enhanced clay for impermeable geosynthetic clay liners. Proceedings. Sixth International Environmental Geotechnics Conference, International Society for Soil Mechanics and Geotechnical Engineers, New Delhi, India.

Di Emidio, G., Van Impe, W., and Verástegui Flores, R. 2011. Advances in geosynthetic clay liners: Polymer enhanced clays. Proceedings, Geo-Frontiers 2011 Conference, ASCE, Reston, Virginia, USA.

Di Emidio, G., Mazzieri, F., Verastegui-Flores, R., Van Impe, W. and Bezuijen, A. 2015. Polymer-treated bentonite clay for chemical resistant geosynthetic clay liners. *Geosynthetics International*, 22(1), 125-137.

Guyonnet, D., Cazaux, D., Vigier-Gailhanou, H., and Chevrier, B. 2009. Effect of cation exchange on hydraulic conductivity in a sand-bentonite-polymer-mixture. Proceedings, 12th International Waste Management and Landfill Symposium, CISA, Cagliari, Italy.

Katsumi, T., Onikata, M., Hasegawa, S., Lin, L., Kondo, M., and Kamon, M. 2001. Chemical compatibility of modified bentonite permeated with inorganic chemical solutions. *Geoenvironmental Impact Management*, Thomas Telford, London, 419-424.

Katsumi, T., Ishimori, H., Onikata, M., and Fukagawa, R. 2008. Longterm barrier performance of modified bentonite materials against sodium and calcium permeant solutions. *Geotextiles and Geomembranes*, 26(1), 14-30.

Koerner, R. 2005. Designing with geosynthetics, 5th edition, Pearson Prentice Hall, Upper Saddle River, New Jersey, USA, 635.

Kolstad, D., Benson, C., Edil, T. and Jo, H. 2004. Hydraulic conductivity of dense prehydrated GCL permeated with aggressive inorganic solutions. *Geosynthetics International*, 11(3), 233-241.

Lee, J., and Shackelford, C. 2005. Impact of bentonite quality on hydraulic conductivity of geosynthetic clay liners. *Journal of Geotechnical and Geoenvironmental Engineering*, 131(1), 64-77.

Malusis, M. and Scalia, J. 2007. Hydraulic conductivity of an activated carbon-amended geosynthetic clay liner. GeoDenver 2007. New Peaks in Geotechnics, ASCE, Reston, Virginia, USA, 1-13.

Markovitz H, and Kimball, G.E. 1949. The effect of salts on the viscosity of solutions of polyacrylic acid. *Journal of Colloid Science*, 5, 115-139.

Mazzieri, F., Di Emidio, G. and Van Impe, P. 2010. Diffusion of calcium chloride in a modified bentonite: impact on osmotic efficiency and hydraulic conductivity. *Clays and Clay Minerals*, 58(3), 351-363.

Meer, S., and Benson, C. 2007. Hydraulic conductivity of geosynthetic clay liners exhumed from landfill final covers. *Journal of Geotechnical and Geoenvironmental Engineering*. 133(5), 550-563.

Onikata, M., Kondo, M., Hayashi, N., and Yamanaka, S. 1996. Development and characterization of multiswellable bentonite, 2nd International Congress on Environmental Geotechnics, IS-Osaka '96, M. Kamon, Ed., Nov. 5-8, 1996, Osaka, Japan, Balkema, Rotterdam, 1, 587-590.

Onikata, M., Kondo, M., Hayashi, N., and Yamanaka, S. 1999. Complex formation of cation-exchanged montmorillonites with propylene carbonate: Osmotic swelling in aqueous electrolyte solutions. *Clays and Clay Minerals*, 47(5), 672-677.

Petrov, R., Rowe, R., and Quigley, R., 1997. Selected factors influencing GCL hydraulic conductivity. *Journal of Geotechnical and Geoenvironmental Engineering*, 123(8), 683-695.

Rad, N., Jacobson, B., and Bachus, R. 1994. Compatibility of geosynthetic clay liners with organic and inorganic permeants, Proceedings, Fifth International Conference on Geotextiles, Geomembranes and Related Products, Singapore, 1165-1168.

Reddy, K. El-Zein, A. Airey, D. Alonso-Marroquin, F. Schubel, P., and Manalo, A. 2020. Self-healing polymers: synthesis methods and applications. *Nano-Structures & Nano-Objects*, 23, 100500.

Scalia, J. and Benson, C. 2011. Hydraulic conductivity of geosynthetic clay liners exhumed from landfill final covers with composite barriers. *Journal of Geotechnical and Geoenvironmental Engineering*, 137(1), 1-13.

Scalia, J., Benson, C., Bohnhoff, G., Edil, T., and Shackelford, C. 2014. Long-term hydraulic conductivity of a bentonite-polymer composite permeated with aggressive inorganic solutions. *Journal of Geotechnical and Geoenvironmental Engineering*, 140(3), 04013025.

Scalia, J., Benson, C., Edil, T., Bohnhoff, G., and Shackelford, C. 2011. Geosynthetic clay liners containing bentonite polymer nanocomposite. GeoFrontiers 2011 Advances in Geotechnical Engineering, J. Han and D. Alazamora, Eds., ASCE, Reston, Virginia, USA, 2001-2009.

Scalia, J., Bohnhoff, G., Shackelford, C., Benson, C., Sample-Lord, K., Malusis, M., and Likos, W. 2018. Enhanced bentonites for containment of inorganic wastes by GCLs. *Geosynthetics International*, 25(4), 392-411.

Schroeder, C., Monjoie, A., Illing, P., Dosquet, D. and Thorez, J. 2001. Testing a factory-prehydrated GCL under several conditions. Proceedings, Sardinia 2001, 8th International Waste Management and Landfill Symposium, Pula, Italy, CISA Environmental Sanitary Engineering Centre, Cagliari, Italy, 187-196.

Shackelford, C. 1994. Waste-soil interactions that alter hydraulic conductivity, Hydraulic Conductivity and Waste Contaminant Transport in Soil, D. Daniel and S. Trautwein, Eds., STP 1142, ASTM, West Conshohoken, Pennsylvania, USA, 111-168.

Shackelford, C., Benson, C., Katsumi, T., Edil, T., and Lin, L. 2000. Evaluating the hydraulic conductivity of GCLs permeated with non-standard liquids. *Geotextiles and Geomembranes*, 18(2-4), 133-161.

Tian, K., Benson, C. and Likos, W. 2016a. Hydraulic conductivity of geosynthetic clay liners to low-level radioactive waste leachate. *Journal of Geotechnical and Geoenvironmental Engineering*, 142(8), 1-12.

Tian, K., Likos, W., and Benson, C. 2016b. Pore-scale imaging of polymer-modified bentonite in saline solutions, Proceedings, Geo-Chicago 2016, GSP No. 271, ASCE, Reston, Virginia, USA, 468-477.

Tian, K., Benson, C. and Likos, W. 2017. Effect of anion ratio on the hydraulic conductivity of a bentonite-polymer geosynthetic clay liner. Proceedings, Geo-Frontiers 2017, Orlando, Florida, USA, GSP No. 276, ASCE, Reston, VA, USA, 180-189.

Tian, K., Likos, W., and Benson, C. 2019. Polymer elution and hydraulic conductivity of bentonite-polymer composite geosynthetic clay liners. *Journal of Geotechnical and Geoenvironmental Engineering*, 145(10), 04019071.

Trauger, R. and Darlington, J. 2000. Next-Generation Geosynthetic Clay Liners for Improved Durability and Performance. TR-220. Colloid Environmental Technologies Company, Arlington Heights, Illinois, USA.

Van Krevelen, D. 1990. *Properties of polymers*., 1st edition, Elsevier, New York.

Chapter 2

Adsorption of poly(acrylic) acid by sodium bentonite, pyrophyllite, and sodium homo-ionized bentonite

SUMMARY

Identifying the potential for adsorption between anionic polymer enhancements and the base sodium bentonite (NaB) in bentonites enhanced with polymers is critical to understanding the mechanisms controlling the hydraulic conductivity of these enhanced bentonites (EBs) when used in geosynthetic clay liners (EB-GCLs). In this study, batch equilibrium adsorption tests were conducted with poly(acrylic acid) (PA) of a high molecular weight (345000 g/mol) as the adsorbate and NaB comprising 85-91% sodium montmorillonite (MMT) as the adsorbent in various inorganic salt solutions (500 mM NaCl, 167 mM Na_2SO_4, 16.67 $CaCl_2$, 167 mM $CaCl_2$, and 12.25 mM $CaSO_4$) to determine the adsorption capacity of NaB for PA and the role of the cationic or anionic species of the solutions. Pyrophyllite, a charge neutral phyllosilicate mineral with the same crystalline structure as MMT, also was used as an adsorbent to determine the effect of the net negative surface charge of the MMT on polymer retention, and a homo-ionized sodium bentonite (HI-NaB) was evaluated as an adsorbent to determine the potential for edge bonding. The results of this study were consistent with those of previous studies pertaining to anionic polymer adsorption onto negatively charged particles/surfaces at more dilute solid:solution ratios than the 1:40 ratio used in this study (i.e., 25 g of bentonite per liter of solution). The adsorption capacity of NaB for PA was limited for systems dominated by Na^+, but more significant in systems dominated by $Ca^{2+}$and adsorption of PA onto NaB increased with increasing Ca^{2+} concentration. Adsorption capacity of NaB for PA was found to reduce at a solution dependent maximum PA concentration, where preferred PA inter-chain interaction occurred. The preference of PA for inter-chain interaction appeared to increase in the presence of SO_4^{2-} (compared to Cl^-) in solution. Adsorption of PA was limited with pyrophyllite in both Na^+- and Ca^{2+}-dominated systems, and with HI-NaB in Na^+-dominated systems, indicating the minimal role of mineral edge charges in PA adsorption. The results of this study indicate that cation bridging is likely

the primary mechanism for adsorption of PA onto NaB in EBs. An observed reduction in adsorption capacity of the NaB for a pH greater than the pKa of ~4.5 for the PA may have resulted from an increase in the degree of ionization of the PA chain, increasing the repulsion between the negatively charged surfaces of the PA and MMT. Further research is required to evaluate the impact of solution pH on the adsorption mechanism of cation bridging.

2.1 INTRODUCTION

Conventional geosynthetic clay liners (GCLs) are thin (5-10 mm), manufactured hydraulic and chemical containment barriers comprising a layer of sodium bentonite (NaB) sandwiched between two geotextiles and held together by needle punching, stitching, or an adhesive. The hydraulic resistance of GCLs is due to the NaB, which swells upon hydration with water or dilute chemical solutions to form a tight, low hydraulic conductivity (< ~5.0×10^{-11} m/s) sealing layer. However, in applications involving containment of liquids with aggressive chemistries, such as hypersaline solutions or solutions with low or high pH, the NaB in GCLs does not swell sufficiently, such that the hydraulic conductivity can be several orders-of-magnitude higher, resulting in ineffective containment (e.g., Shackelford et al. 2000; Lee and Shackelford 2005; Benson et al. 2010; Bouazza and Gates 2014; Chen et al. 2019).

Enhanced-bentonite geosynthetic clay liners (EB-GCLs) are GCLs that incorporate a chemically enhanced bentonite (EB) for the purpose of improving hydraulic compatibility and performance in cases where conventional GCLs are deemed to be hydraulically incompatible (Scalia et al. 2018). For example, anionic polymer-enhanced bentonites (EBs) are produced by combining natural (unenhanced) NaB with anionic polymers such as sodium carboxymethylcellulose (CMC) and poly(acrylic acid) (PA). Although EB-GCLs have been shown to result in improved hydraulic compatibility and lower hydraulic conductivity relative to that of conventional GCLs in cases involving containment of liquids with aggressive chemistries, the mechanisms controlling the hydraulic compatibility of these EB-GCLs are not fully understood (Flynn and Carter 1998; Trauger and Darlington 2000; Katsumi et al. 2001, 2008; Di Emidio 2010; Di Emidio et al. 2010; Scalia et al. 2014; Scalia and Benson 2016; Tian et al. 2016a,b; Scalia and Benson 2017; Tian et

al. 2017; Scalia et al. 2018; Tian et al. 2019; Yu et al. 2019). Thus, an improved understanding of the mechanisms controlling the hydraulic compatibility of EB-GCLs is required in order to predict the long-term behavior of EB-GCLs used as barriers in chemical containment applications.

For EB-GCLs comprising anionic polymer EBs, an important step towards a better understanding of the mechanisms controlling the hydraulic behavior of the EB-GCLs is identifying the potential for adsorption between the anionic polymer enhancement and the base NaB. Anionic polymer adsorption to clay platelets has been hypothesized to occur through at least three potential mechanisms, all of which may occur simultaneously at available bonding sites on the surfaces of the montmorillonite (MMT) platelets within the NaB. These mechanisms include: (i) complexation via anion exchange (Ruhrwein and Ward 1952; Michaels and Morelos 1955; Lee et al. 1991; Rigenbach et al. 1995), (ii) edge bonding via H-bonding or ligand exchange (Emerson 1956; Kohl and Taylor 1961; Laird 1997), and (iii) cation bridging (Theng 1982; Laird 1997; Breen 1999).

The purpose of this study was to determine the degree of adsorption of PA with NaB in concentrated inorganic salt solutions and the effects, if any, of cationic or anionic species on adsorption. Batch equilibrium adsorption tests (BEATs) were conducted with a high molecular weight PA (345,000 g/mol) as the adsorbate dissolved within a solution of 500 mM NaCl, 167 mM Na_2SO_4, 16.67 $CaCl_2$, 167 mM $CaCl_2$, or 12.25 mM $CaSO_4$, and a NaB (85-91% MMT) as the adsorbent. Pyrophyllite, a charge neutral phyllosilicate mineral with the same crystalline structure as MMT but without isomorphic substitution also was tested for adsorption capacity to determine the effect of the net negative surface charge (cation exchange capacity) of the MMT. A homo-ionized sodium bentonite (HI-NaB) also was used as an adsorbent to determine the potential for edge bonding.

The approach used in this study differs in two ways from that of previous studies involving clay suspensions for which extensive clay-anionic-polymer interactions have been studied (Ruhrwein and Ward 1952; Michaels and Morelos 1955; Emerson 1956; Kohl and Taylor 1961; Theng 1982; Lee et al. 1991; Rigenbach et al. 1995; Laird 1997; Breen 1999; Theng 2012). First, the solid:solution ratio of 1:40 by mass

(i.e., 25 g bentonite per liter of solution) used in this study is much higher (less solution per unit mass of NaB) than in the previous studies (e.g., 1 g/L). Second, the inorganic chemical solutions used as the solvent for PA are more concentrated than those used in the previous studies. Both differences were undertaken to better represent the conditions to which EB-GCLs would be expected to encounter in containment applications. The results of this study provide further insight into the mechanisms controlling the hydraulic compatibility and low hydraulic conductivity of EB-GCLs subjected to concentrated inorganic chemical solutions.

2.2 BACKGROUND

2.2.1 Montmorillonite structure

An understanding of the multiple scales of MMT, the primary clay mineral in NaB, is required to understand the potential adsorption interactions between PA and NaB. The crystalline structure of MMT comprises an octahedral sheet (O) sandwiched between two silica tetrahedral sheets (T) (T-O-T). The charge deficiency of MMT due to isomorphic substitution results in a net negative surface charge, which is balanced by an equivalent charge of cations that are electrostatically bound to the surfaces of the MMT platelets (Mitchell and Soga 2005). These bound counter ions and associated water molecules comprise the diffuse double layer (DDL) (Bolt 1956; Mitchell 1993; Van Olphen 1963). The dominant bound cation is referred to as the primary exchangeable cation, and the MMT is designated based on this cation. If the dominant exchangeable cation is sodium (Na^+), then the montmorillonite is referred to as sodium montmorillonite or Na-MMT (Tessier, 1990).

Montmorillonite behavior generally is described with respect to microscopic, mesoscopic, and macroscopic scales (Tessier 1984; Van Damme 1995; Jullien et al. 2005; Salles et al. 2008). At the microscopic scale, MMT exists as single T-O-T clay platelets (lamellae), approximately 0.96 nm thick (Norrish 1954; Bergaya et al. 2006b). Between these platelets exists the interlayer or interlamellar space in which cations, anions, and polar water molecules (when the clay is hydrated) can exist.

Scales larger than microscopic are more difficult to define, as their existence depends on the hydration and pore chemistry of the MMT. At the mesoscopic scale (2-50 nm) and the macroscopic scale (> 50 nm), MMT particles are formed by stacks of parallel platelets. Montmorillonite particles have been referred to by many terms, including tactoids (Quirk and Aylmore 1971; Shomer and Mingelgrin 1978), colloids (Derjaguin and Landau 1941; Verwey and Overbeek 1948; Salles et al. 2009), crystallites (Likos et al. 2010), and quasi-crystals (Quirk and Aylmore 1971; Laird 2006; Likos and Wayllace 2010). The platelets forming a particle are bonded together by Van der Waals forces and cations in the clay micropores (Laird 2006). These bonds are weak and can be cleaved easily by polar water molecules during hydration. Within the meso-pores, Van der Waals forces and cations act to adhere adjacent particles (Marshall 1964). Polar water molecules and liquids also can act to cleave these bonds (Van Olphen 1977). Particles also can adhere to adjacent particles forming increasingly larger aggregates. Each level of porosity and structure plays a role in the hydration and crystalline and osmotic swelling of MMT (Hendricks et al. 1940; Mooney et al. 1952; Norrish and Quirk 1954; Van Olphen 1977).

Clay platelets and particles can be categorized into one of four basic fabrics, as illustrated schematically in Figure 1 (Van Olphen 1977; Mitchell and Soga 2005). Platelets can be dispersed without face-to-face or edge-to-face interactions (Figure 1a), dispersed with face-to-face interactions (Figure 1b), flocculated with edge-to-face interactions (Figure 1(c)), or flocculated and aggregated where MMT platelets are oriented face-to-face to form clay particles and the particles are oriented edge-to-face (Figure 1d).

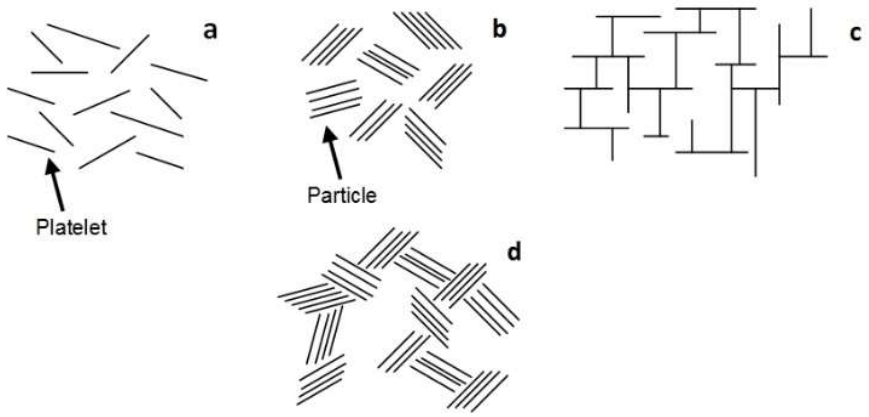

Figure 2.1: Clay fabrics: (a) dispersed; (b) aggregated and dispersed; (c) flocculated; (d) aggregated and flocculated (adapted from van Olphen, 1977).

2.2.2 Montmorillonite-anionic polymer adsorption

Clay-anionic polymer interactions are controlled by multiple variables including the types of clay mineral and anionic polymer, and the ionic strength and pH of the hydrating solution. Anionic polymer adsorption to clay platelets has been hypothesized to occur via three mechanisms, all of which may occur simultaneously at available bonding sites on the clay particle surfaces or edges. These hypothesized bonding mechanisms include (i) cation bridging (Theng 1982; Laird 1997; Breen 1999; Theng 2012), (ii) complexation via anion exchange (Ruhrwein and Ward 1952; Michaels and Morelos 1955; Lee et al. 1991; Rigenbach et al. 1995; Theng 2012), and (iii) edge bonding, i.e., H-bonding or ligand exchange at clay platelet edges (Emerson 1956; Kohl and Taylor 1961; Laird 1997; Theng 2012). The cross-linking behavior of polymer chains also is governed by edge bonding and cation bridging, which leads to competition between polymer-polymer interactions and clay-surface interactions with water (Theng 2012).

Cation-bridging has been proposed as the primary interaction mechanism between an anionic polymer and any available basal surface in a clay mineral (Theng 1976; Theng and Scharpenseel 1976; Laird 1997; Deng et al. 2006b). Cation bridging can occur directly between a polyanion-cation-clay surface or through a water molecule (hydrated cation). Higher cation valence and conditions resulting in a lower zeta potential are hypothesized to allow anionic polymer chains to approach the clay surface, giving rise to greater adsorption potential (Mortensen 1962). In a typical clay-water system, metal hydroxides (e.g., iron,

silicon, magnesium, and calcium) and other ligands (e.g., OH^-, SO_4^{2-}, Cl^-) compete for the Lewis acid (electron receiving) site of the central ion (Al^{3+}) of the aluminum hydroxide ($Al(OH)_3$). The net charge associated with terminal hydroxyl groups on clay mineral surfaces can be either positive (+) or negative (-) depending on the external solution (pore water) pH, with a net positive charge at low pH (high H^+ concentration) and a net negative charge a high pH (low H^+ concentration). When the net charge of an edge surface is positive due to protonation of the aluminum hydroxide, complexation can occur. In this case, the anionic polymer can adsorb through electrostatic attraction to the positive edge charge, known as anion exchange. The capacity of this interaction to occur in a clay-polymer system relies on the anion exchange capacity of the clay, which is a function of pH (Ruehrwein and Ward 1952; Mortensen 1962; Bidwell et al. 1970; Stiffert and Epinasse 1980; Sastry et al. 1995; Blockhaus et al. 1997). Anion adsorption in the hydrated clay system is favored by a lower pH, which is coupled with a release of hydroxides and a general affinity of surface sites for metal cations or ligands (Stumm and Morgan 1996). Hydrogen bonding or ligand exchange also can occur between anionic polymer functional groups such as the carboxyl group (COO^-) and the edge surface hydroxyls (Michaels and Morelos 1955; Emerson 1956; Kohl and Taylor 1961; Laird 1997). Adsorption capacity via edge surfaces correlates to the amount of available edge surface area (Warkentein and Miller 1958; Lee et al. 1991), which is relatively low in MMT (Grimm 1968).

Black et al. (1965) found that anionic polymer-clay adsorption in dilute clay suspensions could be affected by Ca^{2+}. The results of the study indicated that anionic polyacrylamide adsorption increased with increasing $CaCl_2$ concentration. This correlation was attributed to compression of the DDL due to Ca^{2+}, resulting in the reduction of interparticle repulsive forces and encouraging interparticle bridging of bonded polymer, and charge screening by Ca^{2+} that reduces the apparent negative charge on the polymer.

Interparticle bridging occurs when a polymer chain bonds to more than one surface of different clay particles. The flocculating behavior of a polymer in polymer-clay suspensions has been credited to interparticle bridging on multiple clay surfaces but not proven to be attributable to a single bonding mechanism (Michaels 1964; Rauselt et al. 1964; Black et al. 1965).

2.2.3 Poly(acrylic) acid

A polymer is a macromolecule or a compound with a relatively high molecular weight that comprises repeating smaller units called monomers covalently bonded together. Anionic polymers require cations for electrical neutrality, which are strongly solvated during polymer hydration. Poly(acrylic acid) ([-$CH_2CH(CO_2H)$-]$_n$) is a high molecular-weight, synthetic polymer of acrylic acid. The negatively charged carboxyl group (COO^-) on the polymer repeating unit is satisfied by protons (H^+) (Buchholz and Graham 1998).

The degree of ionization of PA is a representation of the fraction of COO^- interaction. The pH of the solution and the pKa for PA of approximately 4.5 (e.g., Michaels and Morelos 1955; Das and Somasundaran 2001) will determine the degree of ionization (DOI) of the PA in a specific solution. At low pH, the PA will have a lower ratio of COO^-/COOH (lower ionization), and as pH increases, the ionization of PA will also increase. The DOI also depends on cations present in solution, which can form ion pairs with available COO^- or screen the negative charge (Michaels and Morelos 1955; Cabaness et al. 1971).

For mixtures of NaB and PA in solution, a reduction in DOI can reduce NaB and PA repulsion, bringing surfaces in closer proximity which promotes adsorption of PA. Michaels and Morelos (1955) found that polyacrylate adsorption to kaolinite was greater at a lower pH, where the polyacrylate charge density was reduced. A lesser ionized polyacrylate chain could approach the kaolinite surface and adsorb via hypothesized H-bonding. However, adsorption still occurred when the polyacrylate chain was expected to be almost fully ionized (pH > 6). This adsorption was attributed to a pH that was approximately 2.2 units lower at the surface of the kaolinite, within the double layer, compared to that of the ambient solution, which resulted in a polyacrylate chain with a lesser DOI than would be expected in the ambient solution.

Adsorption of anionic polymers on MMT also depends on the degree of interaction between anionic polymer chains in solution. Intermolecular bonding between polymers reduces the bonding sites available for possible adsorption. Ionization of the anionic polymer chain acts to extend the chain and repulse neighboring chains. As the ionization is reduced, sites on the same chain or between chains can be in closer

proximity and ultimately fold or crosslink via H-bonding or multivalent cations. Michaels and Morelos (1955) hypothesized that intramolecular coiling of polyacrylate in a NaOH solution was brought about by reduction in ionization and strong hydrogen bonding that could occur between carboxyl groups.

2.3 MATERIALS

2.3.1 Sodium bentonite

The powdered NaB used in this study was obtained from Colloid Environmental Technologies Company (CETCO, Hoffman Estates, Illinois, USA), and is the same NaB used in Bentomat® GCLs as well as other studies on GCL behavior (Bohnhoff 2012; Bohnhoff and Shackelford 2013; Bohnhoff et al. 2014; Scalia et al. 2014), although these studies used a granular form of the same NaB. The particle-size distribution of the powdered NaB used is shown in Figure 2.2. As summarized in Table 2.1, the swell index of the NaB in deionized water (DIW) is 31.4 mL/2 g, and the cation exchange capacity (CEC) is 78 $cmol^+/kg$. The exchange sites are occupied by approximately 44% Na, 36% Ca, 17% Mg, and 2% K.

Table 2.1: Selected properties of the sodium bentonite (NaB) tested in this study (Scalia et al. (2014)).

Property	Method	NaB
Swell index with deionized water (mL/ 2g)	ASTM D5890-06	31.4
Carbonate content (%)	ASTM D4373-10	1.3
Na-montmorillonite content (%)	x-ray diffraction (10 samples)	85-91
Cation exchange capacity, *CEC* ($cmol^+/kg$)	ASTM D7503-18	78.0
Soluble metals: ($cmol^+/kg$):	ASTM D7503-18	
Ca		0.2
Mg		0.1
Na		18.1
K		0.4
Bound/exchangeable metals (mole fraction):	ASTM D7503-18	
Ca		0.36
Mg		0.17
Na		0.44
K		0.02

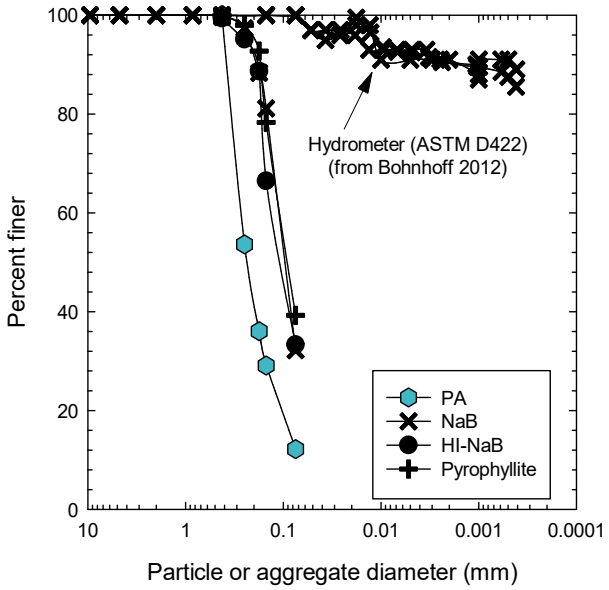

Figure 2.2: Particle-size distributions of ground poly(acrylic acid) (PA) (adsorbate) and clay minerals (adsorbents) including powdered sodium bentonite (NaB), homoionized sodium bentonite (HI-NaB), and pyrophyllite based on mechanical sieve analysis of the dry materials unless otherwise indicated.

2.3.2 Poly(acrylic acid)

The PA (molecular weight ~345000 g/mol) was contained at 25% solids in water. The PA in water was air dried at 20°C until solidified and then ground and screened. Grinding of the PA was completed using a rotary blade grinder (KitchenAid BCG211OB; Benton Harbor, Michigan, USA).

2.3.3 Sodium homo-ionized bentonite

To investigate the importance of multivalent cations (e.g., Ca^{2+}) on PA adsorption, BEATs were conducted with a sodium homo-ionized bentonite (HI-NaB) in 500 mM NaCl. The HI-NaB was prepared using the dialysis method described by Sample-Lord and Shackelford (2016). Although preparation of homo-ionized clays with 100% of the exchange positions occupied by a single cation species is difficult to achieve (van Olphen 1963; Sample-Lord and Shackelford 2016), homo-ionization is practically achieved when > 95% of the exchange sites are occupied by a single cation species (e.g., Olson and Mesri 1970). Twenty-five grams of NaB were placed into a dialysis bag comprising regenerated cellulose membrane tubing (width = 100 mm, Spectra/Por 1, MWCO: 6000-8000 Da, Spectrum Chemical Mfg. Corp., New Brunswick, New

Jersey, USA), followed by 300 mL of 2 M NaCl solution. The dialysis membrane restricts movement of the NaB particles, while allowing H_2O and ions in solution to pass freely through. The dialysis bag was sealed with nylon closures and placed into a 7.6 L glass jar filled with 7 L of the 2 M NaCl solution. The glass jar was placed on a magnetic stirrer and covered to minimize evaporation. The 2 M NaCl solution in the jar was replaced at 2 h increments the first day over the first 8 h to expedite cation exchange, and then daily for 2 weeks. After dialysis was complete, the same procedure was completed with the HI-NaB using DIW (instead of 2 M NaCl) to remove freely mobile excess soluble salts from the HI-NaB. The replacement of DIW was continued until the change in the *EC* of the liquid in the jar over a 24-h period was negligible ($\Delta EC \leq 0.03$ mS/m). The HI-NaB then was dried in an oven at 110 °C and ground and sieved to achieve a similar particle-size distribution as the original NaB (see Figure 2.2).

2.3.4 Pyrophyllite

To investigate the effect of surface charge, BEATs were conducted with pyrophyllite, a neutral mineral with the same T-O-T crystalline structure as MMT. The lack of isomorphic substitution in pyrophyllite results in no net layer surface charge and, thus, no exchangeable interlayer cations. The BEATs with pyrophyllite were used to determine if adsorption is possible without a net-negative structural charge and without resultant cations retained within a DDL, like available for the MMT. The particle-size distribution of the pyrophyllite was similar to the NaB (see Figure 2.2). More details regarding the structure and particle-size distribution of the pyrophyllite are provided in Appendix C.

2.3.5 Inorganic salt solutions

A summary of the inorganic solutions used in this study and the properties of these solutions (concentration, ionic strength, electrical conductivity, and pH) are provided in Table 2.2. The inorganic salt solutions were prepared using deionized water (DIW) as the solvent and were stored in collapsible carboys with no headspace to prevent interaction with the atmosphere. The $CaCl_2$ solutions were prepared with $CaCl_2$ di-hydrate, $CaCl_2 \cdot 2H_2O$ (Alfa Aesar; Ward Hill, Massachusetts, USA) and DIW. The NaCl, Na_2SO_4 (Fisher Chemical; Hampton, New Hampshire, USA) and $CaSO_4$ (EM Science; Cherry Hill, New Jersey, USA)

solutions was prepared with the anhydrous salt and DIW. The prepared solutions were stored in collapsible carboys with no headspace to limit interaction with the atmosphere.

Table 2.2: Summary of solutions used as hydrating liquids and permeant solutions in this study.

Solution	Concentration (mM)	Ionic strength, I (mM)	Electrical conductivity, EC (mS/m)	pH (-)
NaCl	500	500	4850	6.17
$CaCl_2$	167	500	3170	5.81
$CaCl_2$	16.67	50	384	4.75
$CaSO_4$	12.5	50	194	5.04
Na_2SO_4	167	500	2590	5.91

2.4 METHODS

2.4.1 Batch equilibrium adsorption tests

The BEATs were conducted using PA as the adsorbate and NaB as the adsorbent following a method similar to batch adsorption experiments previously reported in literature (e.g., Roy et al. 1992; Lam et al. 2014; Sparks et al. 2015). Polymer stock solutions were prepared by mixing the dried and ground PA into inorganic salt solutions in a sealed beaker for at least 2 h with a magnetic mixer. Then, 40 mL of polymer stock solution was extracted from the beaker and added to 50 mL centrifuge tubes containing 0.95 g of NaB, which correlates with a 1:40 solid:solution ratio by mass after the polymer, which represented 5% by mass of the NaB, was added. The determination of the solid:solution ratio is discussed further in Appendix B. The tubes were mixed end-over-end at 30 rpm for 24 h in a tumbler. After mixing, the tubes were centrifuged at 2500 rpm (IEC Centra CL2 Benchtop Centrifuge, Thermo Electron Corporation, Madison, Wisconsin, USA) for 10 min and then rested for 2 h. The supernatant was extracted via decanting and tested to determine polymer content. Two methods, viz., total organic carbon (TOC) analysis of the decanted supernatant, and absorbance of the decanted supernatant via UV-spectroscopy, were compared for determining the adsorbed and non-adsorbed polymer factions of each batch adsorption test. A description and comparison of the methods is provided in Appendix B. UV-spectroscopy was determined to produce the most accurate polymer concentration and was used to analyze the collected supernatants. Prior to

selection of the final method for conducting the BEATs, a sensitivity analysis was completed to determine the impacts of (i) soil:solution ratio, (ii) mixing time, (iii) centrifuge rate and (iv) time, and (v) effective soil:solution separation (decanting/washing), on PA adsorption. The sensitivity analysis is presented in Appendix B.

2.4.2 UV Spectroscopy

Polymer concentration in the supernatant was measured using UV spectroscopy (Genesys 10UVv scanning spectrophotometer, Thermo Electron Corporation, Madison, Wisconsin, USA). UV spectroscopy is used to measure polymer contents in solution, most commonly in wastewater and water treatment applications (e.g., Gramain and Mayard 1981; Gibbons and Ormeci 2013; Momani and Ormeci 2014). UV spectroscopy obtains the absorbance spectra of a compound (including polymer) in solution and then the absorbance (A) measured at each wavelength is converted by a polymer-specific proportionality constant to the concentration (C) of a specific polymer in a specific solution following Beer-Lambert's law, or:

$$A = \varepsilon b C \tag{2.1}$$

where ε equals the molar absorptivity of the compound in solution ($M^{-1}m^{-1}$) and b is the path length which is equivalent to the internal width of the cuvette (sample holder) (typically 0.01 m).

Due to the unique nature of the mixtures used in this study (NaB and concentrated salt solutions), additional considerations were made in the development of the calibration of absorbance to polymer concentration at each wavelength. The Cl^- present in both the NaCl and $CaCl_2$ solutions absorbs strongly at wavelengths less than 195 nm. As shown in Figure 2.3, polymer solutions prepared at PA concentrations ranging from 0 to 500 mg/L in the 500 mM NaCl presented the same measure of absorbance (A), regardless of polymer concentration. The strong absorbance of the Cl^- in the 500 mM NaCl obscured the change in absorbance with change in polymer concentration at a wavelength of 190 nm. To find the wavelengths at which the Cl^- would not obscure the change in polymer concentration, solutions of NaCl and $CaCl_2$ were prepared with a range of concentrations (0.5 mM- 500 mM) and used to determine the "zero wavelength"

(λ_o) of the solutions, where the chloride containing salt solutions no longer registered a measurable absorbance ($A \leq 0$). As shown in Figure 2.4a, the λ_o varied with type and concentration of salt solution (NaCl vs. $CaCl_2$). However, as shown in Figure 2.4b, the λ_o generally was proportional to the solution ionic strength. A wavelength range of 215-220 nm was chosen for further UV spectroscopy testing to ensure that the highest ionic strength of the solutions tested in this study (500 mM) did not interfere with absorbance measurements.

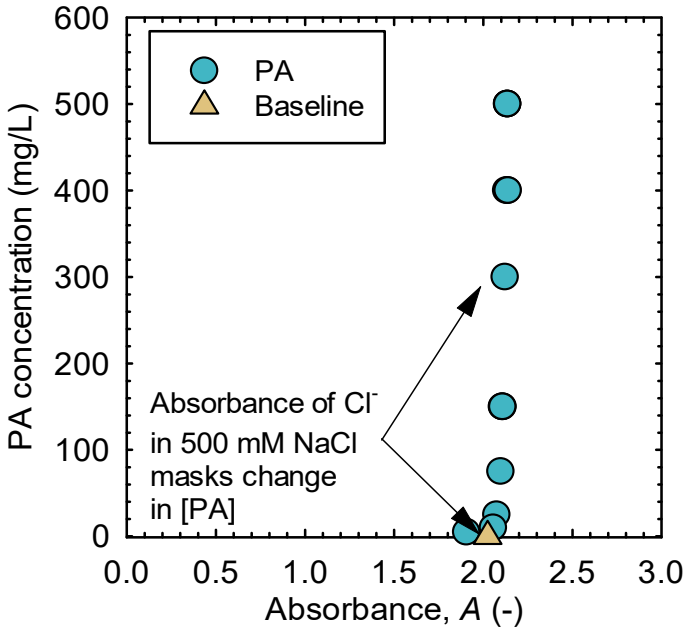

Figure 2.3: Poly(acrylic) acid (PA) concentration versus absorbance measured at 190 nm in 500 mM NaCl.

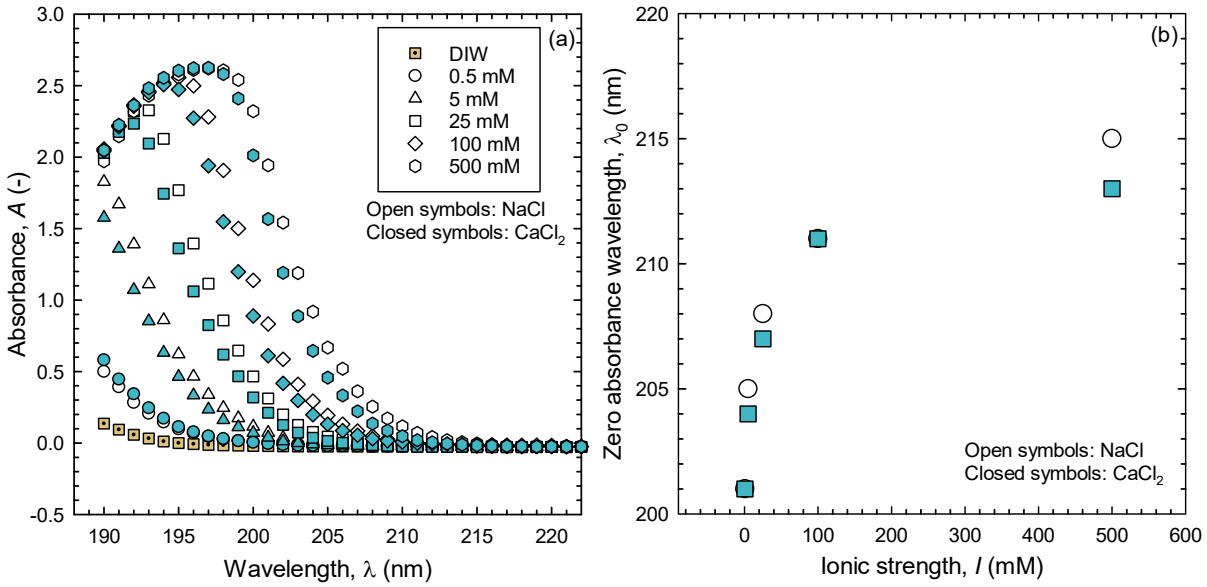

Figure 2.4: (a) Absorbance versus wavelength for de-ionized water (DIW) and sodium chloride (NaCl) and calcium chloride ($CaCl_2$) solutions at various ionic strengths; (b) zero absorbance wavelength versus ionic strength of NaCl and $CaCl_2$ solutions.

The BEATs with NaB (1:40 soil:solution ratio) also produced a change in measured absorbance of the supernatant in the centrifuged samples of the prepared suspensions. The potential for the soluble metals within the NaB to exchange with the initially bound cations results in a higher measured absorbance than that for the base 167 mM $CaCl_2$ solution and a positive, non-zero absorbance for solutions decanted from NaB with 167 mM $CaCl_2$. Therefore, the decanted supernatant of the NaB (baseline supernatant) and 167 mM $CaCl_2$ solutions was diluted at ratios of 1:2, 1:5, and 1:10 by volume to determine if diluting the baseline supernatant would reduce the measured absorbance to zero. As shown in Figure 2.5, the 1:5 and 1:10 dilutions resulted in reducing the increase in absorbance due to the NaB soluble salts back to zero absorbance. A 1:10 dilution was chosen for the polymer concentration calibration and batch adsorption testing for simplicity.

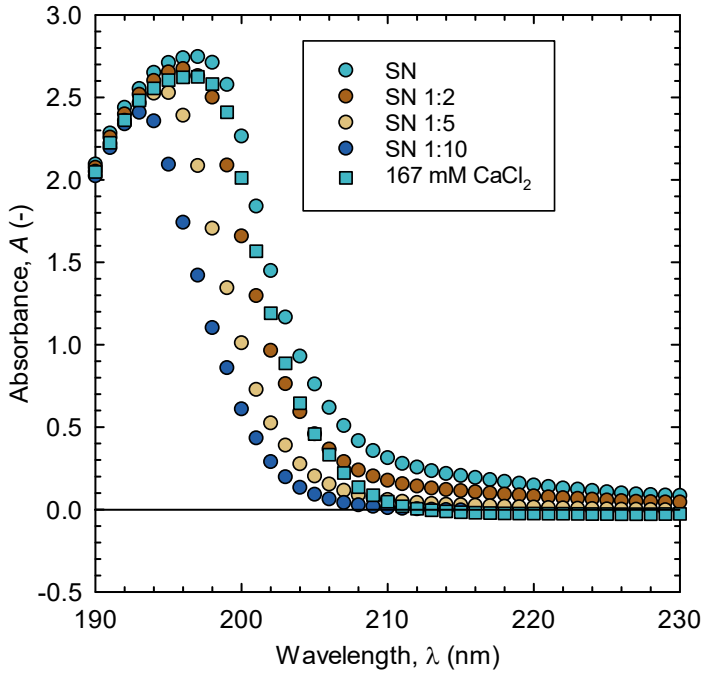

Figure 2.5: Comparison of the measured absorbance versus wavelength for a 167 mM $CaCl_2$ solution versus that for the supernatant (SN) and 1:2, 1:5, and 1:10 (by volume) dilutions of the SN resulting from the batch equilibrium adsorption tests.

To account for the presence of soluble salts in NaB, calibration curves were prepared by adding PA to representative extracted supernatant. A solution of interest (e.g., 167 mM $CaCl_2$) was combined with the base NaB but without polymer (0.95 g NaB with 40 mL of solution) following the same mixing and subsequent centrifugation procedure as that for the BEATs. The resulting NaB supernatant was collected and combined to produce a bulk volume of representative extracted supernatant. This supernatant then was used as the solvent to prepare polymer stock solutions by adding a known mass of polymer to produce a known polymer concentration. The polymer stock solutions were mixed at 600 rpm for at least 4 h. Samples of the polymer stock solution then were pipetted into a quartz cuvette and analyzed using UV spectroscopy for absorbance at wavelengths ranging from 215 to 220 nm. Samples both without dilution and with a 1:10 dilution by volume with DIW were analyzed to allow for measurement across a wide range of polymer concentrations. Samples with higher polymer concentrations (> 5000 mg/L) often exceeded the maximum

measurable absorbance of the spectrophotometer ($A = 3$). In this case, only diluted samples were measured. At least three replicates were collected for each dilution at each polymer concentration.

Calibration curves over the 215-220 nm wavelength range resulted in similar linear trends (Figure 2.6) with similar values of the coefficient of determination, R^2 (~0.99), and a low standard deviation, regardless of dilution. The 215 nm wavelength was selected to measure absorbance and determine polymer concentration because this wavelength resulted in a low standard deviation (≤ 0.014) and a R^2 close to unity (0.99) for both solutions, both undiluted and with 1:10 dilution concentration ranges

For each solution, the ranges of detectable polymer contents and the accuracy of the linear trend varied. Calibration curves for calculating polymer concentration from measured absorbance were prepared based on both diluted (1:10) and undiluted samples of the extracted supernatant generated with each salt solution, providing a wide range of detectable polymer concentrations, as shown in Figure 2.7. Diluted samples resulted in a similar linear trend of polymer concentration versus absorbance for all solutions (Figure 2.7a), whereas bi-linear trends resulted from the undiluted samples (Figure 2.7b). To ensure accurate polymer quantification, separate linear calibration curves were generated for each solution for diluted and undiluted samples. The absorbance ranges and calibration variables for each solution and absorbent based on diluted and undiluted samples are presented in Table 2.3. Pyrophyllite and HI-NaB do not contain soluble salts, so the calibration curves used for the BEATs involving these absorbents were prepared with stock solution (viz. not extracted supernatant).

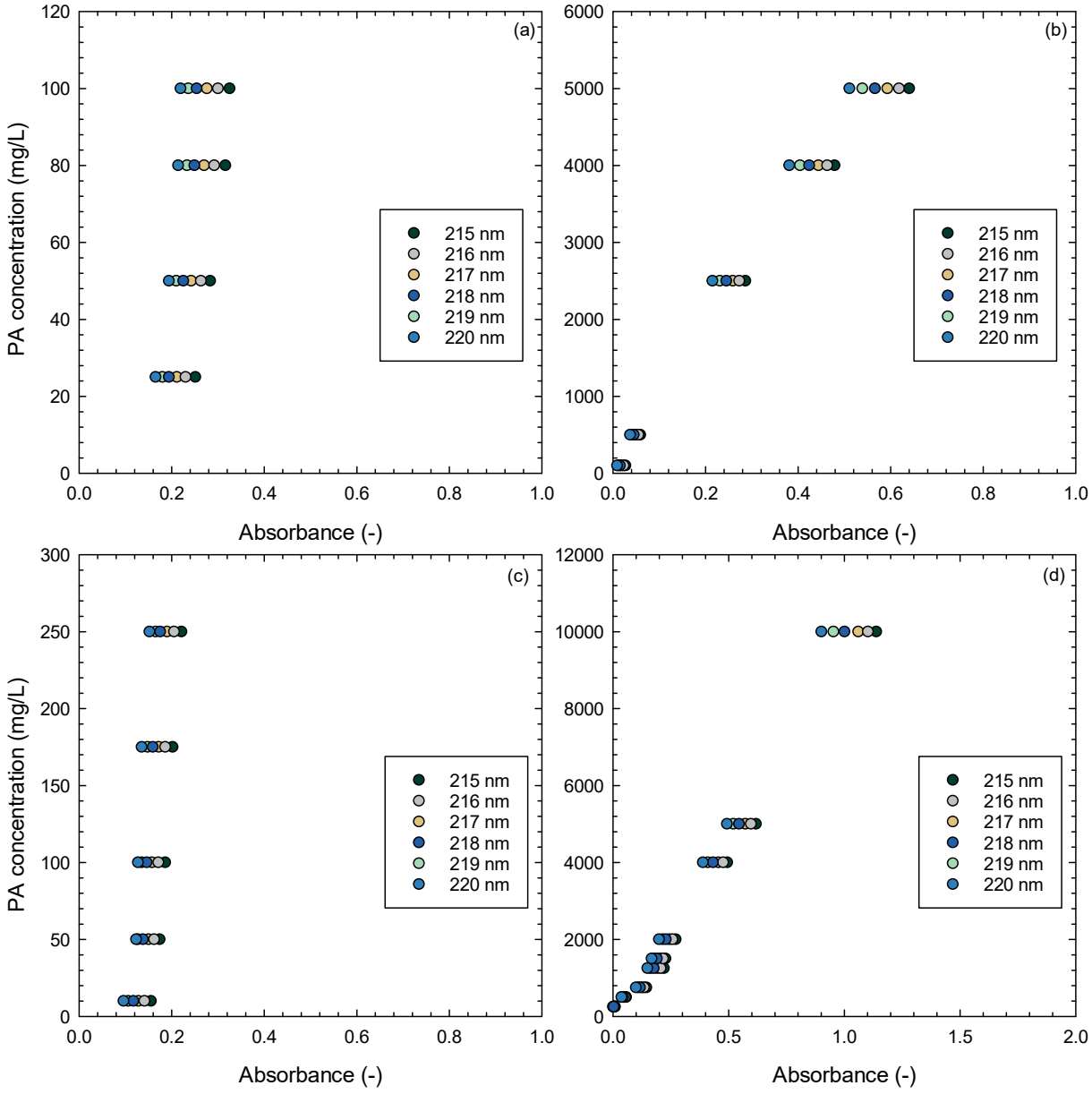

Figure 2.6: Poly(acrylic acid) (PA) concentration as a function of absorbance measured at different wavelengths for supernatants of batch equilibrium adsorption tests using 500 mM NaCl (a) without dilution and (b) with 1:10 (by volume) dilution, and 167 mM $CaCl_2$ (c) without dilution and (d) at 1:10 (by volume) dilution.

Table 2.3: Calibration equations for poly(acrylic acid) concentration (C) as a function of absorbance (A) for adsorbent and solution tested.

Adsorbent	Solution	C (mg/L)	A (-)	Regression Equation	R^2
Sample Dilution (by volume) 1:10					
Sodium bentonite (NaB)	167 mM $CaCl_2$	250-10000	0.009-1.138	8216A+159.8	0.9918
	500 mM NaCl	100-5000	0.027-0.640	8045A+20.35	0.9949
	16.67 mM $CaCl_2$	600-4550	0.055-0.553	7994A+118.5	0.9993
	12.5 mM $CaSO_4$	90-2050	0.004-0.234	8230A+104.5	0.9974
Pyrophyllite	167 mM $CaCl_2$	500-10000	0.049-1.199	8216A+159.8	0.9997
	500 mM NaCl	500-2500	0.046-0.289	8861A-322.1	0.9763
Homo-ionized NaB (HI-NaB)	500 mM NaCl	500-2500	0.046-0.289	8861A-322.1	0.9763
No Sample Dilution					
NaB	167 mM $CaCl_2$	10-250	0.155-0.221	3769A-589.3	0.9810
	500 mM NaCl	25-100	0.251-0.325	959.4A-218.1	0.9756
	16.67 mM $CaCl_2$	100-1075	0.240-1.416	8861A-322.1	0.9915
	12.5 mM $CaSO_4$	20-700	0.180-1.049	970.3A-122.7	0.9960
Pyrophyllite	167 mM $CaCl_2$	100-2500	0.056-2.647	921.0A+4.906	0.9985
	500 mM NaCl	25-2000	0.003-2.239	8861A-322.1	0.9980
HI-NaB	500 mM NaCl	25-2000	0.003-2.239	8861A-322.1	0.9980

Note: R^2 = coefficient of determination

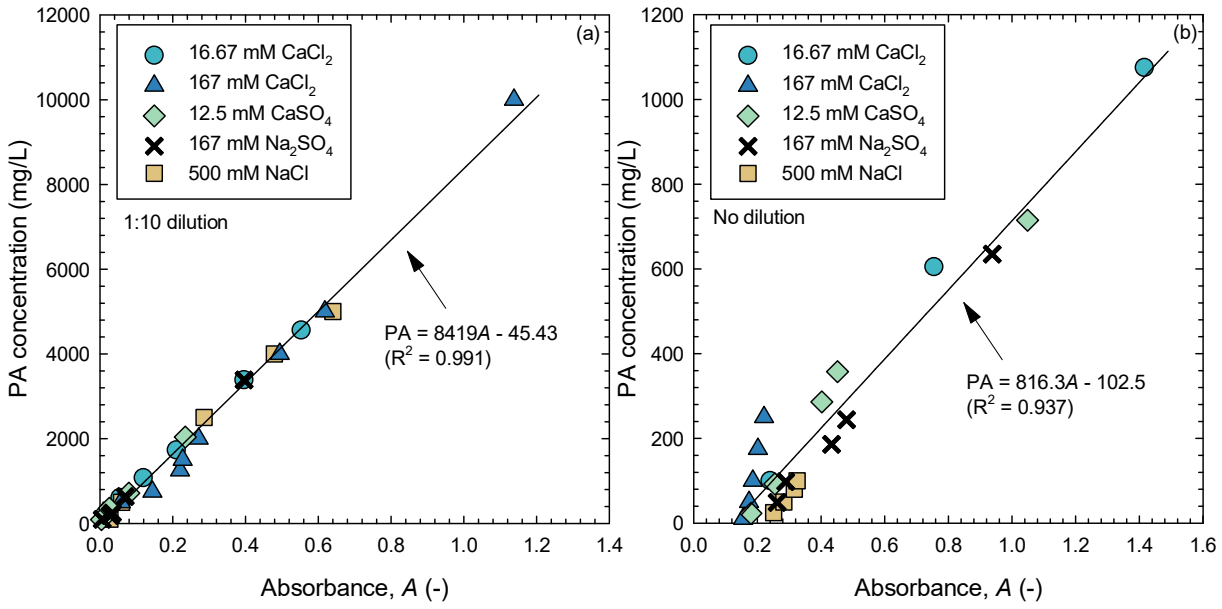

Figure 2.7: Poly(acrylic acid) (PA) calibration curves for supernatants (mixed with NaB then centrifuged and decanted) with five salt solutions: (a) 1:10 (by volume) dilution; (b) undiluted.

2.4.3 Other applications of UV-Vis Spectroscopy

The UV-Vis spectroscopy methods used in this study also can be applied to measure polymer contents in the effluent samples of hydraulic conductivity tests conducted with EB-GCLs. However, the effluent concentration must represent a non-hydrogel forming concentration of the polymer tested. Solid hydrogel polymer in the effluent sample will result in a heterogenous sample that cannot be measured accurately. Care should also be taken to consider the concentration of ions in the effluent, as this concentration is complex and varies over the duration of permeation.

2.4.4 Adsorption isotherms

The BEATs conducted in this are summarized in Table 2.4. An adsorption isotherm was developed for each adsorbent with the PA as the adsorbate in each solution tested. The amount of PA adsorbed at equilibrium, q_e (mg PA/g NaB), was determined as follows:

$$q_e = \frac{(C_o - C_e) \times V}{m} \tag{2.2}$$

where C_o and C_e (mg/L) are the initial and equilibrium PA concentrations, respectively, V is the volume of the solution (40 mL), and m is the mass of adsorbent (0.95 g). The use of 0.95 g of adsorbent was chosen such that a 1250 mg/L polymer concentration represented a 5% polymer addition by mass, reflecting the most commonly added polymer enhancement fraction for the EB-GCLs prepared in Chapter 1.

Table 2.4: Summary of batch equilibrium adsorption tests for adsorption of poly(acrylic acid) dissolved within different salt solutions to different adsorbents.

Adsorbent	Solutions	Purpose
Sodium bentonite (NaB)	500 mM NaCl, 167 mM $CaCl_2$	To investigate cation bridging via Ca^{2+}
	16.67 mM $CaCl_2$, 12.5 mM $CaSO_4$, 167 mM Na_2SO_4	To investigate effect of anion Cl^- vs. SO_4^{2-}
Pyrophyllite	500 mM NaCl, 167 mM $CaCl_2$	To investigate effect of edge versus surface charge
Homo-ionized NaB	500 mM NaCl	To investigate edge bonding potential

2.5 RESULTS

2.5.1 Experimental adsorption data

The BEAT results with NaB in the five different solutions are summarized in Tables 2.5 and 2.6, and with pyrophyllite in 167 mM $CaCl_2$ and 500 mM NaCl and HI-NaB in 500 mM NaCl are summarized in Table 2.7, and all of the results are shown in Fig. 2.8. Values of C_e and q_e in Tables 2.5-2.7 represent averages from three replicate BEATs. Negative values of q_e (< 0 mg/g) shown in Tables 2.5 and 2.7 result from inaccuracy from the calibration curves.

Table 2.5: Average batch adsorption data for adsorption of poly(acrylic acid) (PA) to sodium bentonite (NaB) in salt solutions with an ionic strength of 500 mM [C_o = source PA concentration; C_e = equilibrium (final) PA concentration; q_e = equilibrium adsorbed mass of PA per gram of NaB].

167 mM $CaCl_2$			500 mM NaCl			167 mM Na_2SO_4		
C_o (mg/L)	C_e (mg/L)	q_e (mg/g)	C_o (mg/L)	C_e (mg/L)	q_e (mg/g)	C_o (mg/L)	C_e (mg/L)	q_e (mg/g)
56	1.00[a]	2.34	109	60.8	2.04	500	416.3	3.52
555	3.3	23.2	533	322.4	7.76	1250	1462.7	-8.95
1316	25.9	54.3	633	438.3	8.18	2500	2897	-16.7
4991	278.4	198.4	1250	1172	3.28	-	-	-
7020	3413	151.9	2028	2014	0.55	-	-	-
10010	7079	123.4	2517	2215	12.7	-	-	-

[a] below detection limit (< 10 mg/L)

Table 2.6: Average batch adsorption data for adsorption of poly(acrylic acid) (PA) to sodium bentonite (NaB) in salt solutions with an ionic strength of 50 mM [C_o = source PA concentration; C_e = equilibrium (final) PA concentration; q_e = equilibrium adsorbed mass of PA per gram of NaB].

16.67 mM $CaCl_2$			12.5 mM $CaSO_4$		
C_o (mg/L)	C_e (mg/L)	q_e (mg/g)	C_o (mg/L)	C_e (mg/L)	q_e (mg/g)
500	52.7	18.8	500	33.9	19.6
1250	77.9	49.3	1250	174.7	45.3
2500	1423	45.3	2500	2356	6.07

Table 2.7: Batch adsorption data for adsorption of poly(acrylic acid) (PA) to pyrophyllite and homo-ionized sodium bentonite (HI-NaB) in 500 mM NaCl and 167 mM $CaCl_2$ (pyrophyllite only) [C_o = source PA concentration; C_e = equilibrium (final) PA concentration; q_e = equilibrium adsorbed mass of PA per gram of adsorbent].

Pyrophyllite						HI-NaB		
167 mM $CaCl_2$			500 mM NaCl			500 mM NaCl		
C_o (mg/L)	C_e (mg/L)	q_e (mg/g)	C_o (mg/L)	C_e (mg/L)	q_e (mg/g)	C_o (mg/L)	C_e (mg/L)	q_e (mg/g)
2518	2044	20.0	109	119.6	-0.44	109	189.7	-3.39
4991	4500	20.7	533	488.5	1.89	533	549.3	-0.67
10010	9322	29.0	1310	1149	6.76	1253	884.8	15.5
-	-	-	-	-	-	1310	1201	4.57
-	-	-	-	-	-	5000	4356	27.2

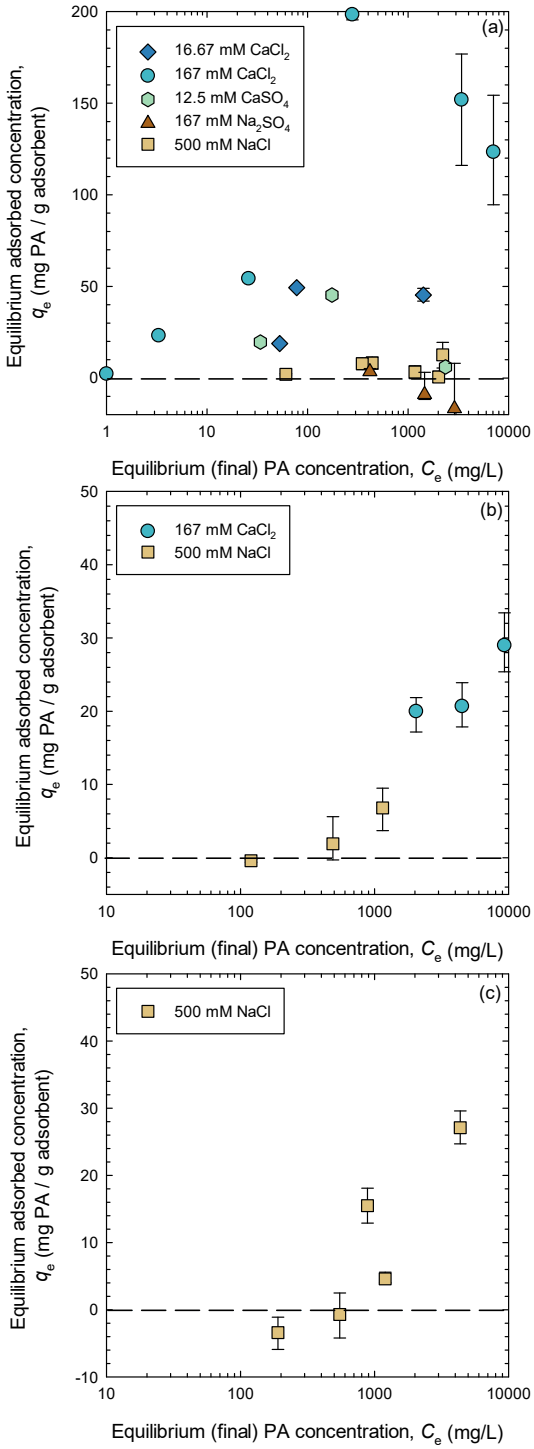

Figure 2.8: Batch equilibrium adsorption test data for adsorption of poly(acrylic acid) (PA) in different salt solutions to different adsorbents: (a) sodium bentonite (NaB); (b) pyrophyllite; (c) homo-ionized NaB (HI-NaB). Each data point represents the averages of three replicate tests. Error bars calculated based on standard deviation of calibrated absorbance measurements in each solution.

2.6 Linear fitting of isotherms

Linear fitting of the PA adsorption data was conducted for each adsorbent based on the following equation:

$$q_e = K_d C_e \tag{2.3}$$

where K_d is the portioning coefficient for linear adsorption known as the distribution coefficient (L/g) (Freeze and Cherry 1979). The results of the linear fittings are shown in Fig. 2.9.

Due to the mineral properties of pyrophyllite, cation adsorption can occur only via edge bonding. Although the results in Figure 2.9a,d for pyrophyllite suggest a small amount of PA adsorption, the measured q_e values are likely the result of polymer entrapment during centrifuging and not adsorption. For pyrophyllite, maximum measured q_e for 500 mM NaCl and 167 mM $CaCl_2$ were only 7.3 mg/g and 29 mg/g, respectively, relative to the respective C_e of 1148 mg/L and 9322 mg/L. Measured adsorption is believed to be the result of polymer trapped within the NaB pores during centrifuging. As shown in Figure 2.9c,d and Table 2.8, low K_d (3.7 L/g $\leq K_d \leq$ 6.3 L/g) indicate that adsorption of PA onto NaB and HI-NaB in 500 mM NaCl likely did not occur, as the values are similar to those measured for the pyrophyllite.

The BEATs conducted with 167 mM Na_2SO_4 with an ionic strength equivalent to that for 500 mM NaCl were unsuccessful. Using the developed calibration curves, the measured C_e was greater than the C_o, resulting in a negative average q_e. However, based on the error bars in Figure 2.9c, maximum values of q_e were likely 0 mg/L. The overestimation of C_e may have occurred due to the simultaneous presence of the NaB, the anionic polymer, and the high concentration of SO_4^{2-}, all of which are negatively charged, limiting successful separation of the NaB (with adsorbed PA) from supernatant during centrifuging. Further study is needed to better document and understand the adsorption behavior PA on NaB in strong Na_2SO_4 solutions.

The adsorbed fraction of PA onto NaB and, thus, K_d, generally increases with increasing Ca^{2+} concentration (Figure 2.9a,b and Table 2.8). Linear fitting was completed for only the increasing (upward) portion of the data, as shown in Figure 2.9a,b. The inverted V-shape of the adsorption isotherms with solutions containing Ca^{2+} in this study indicate that polymer concentration as well as Ca^{2+} concentration

affected the adsorption of PA onto NaB. The results of this study indicate that for each solution containing Ca^{2+}, there is a maximum C_o of PA that produces a maximum q_e. If C_o increases beyond the C_o corresponding with maximum q_e, the PA inter-chain interaction increases and reduces q_e. The preference of PA for inter-chain interaction appears to increase in the presence of SO_4^{2-} (compared to Cl^-) in solution, as exhibited by the drastic decrease of q_e from 45.3 mg/g to 6.7 mg/g in 12.5 mM $CaSO_4$ when increasing C_o from 1250 mg/L to 2500 mg/L, respectively. The highest K_d (713 L/g) resulted with the 167 mM $CaCl_2$ solution, which contained the highest concentration of Ca^{2+}.

Results of BEATs in solutions containing Na^+ resulted in K_d values close to zero ($-5.66\ L/g \leq K_d \leq 6.3\ L/g$) and poor R^2 values ($-0.495 \leq R^2 \leq 0.832$), indicating that little to no adsorption of PA occurred onto the adsorbents in the Na solutions tested. The highest R^2 of 0.832 occurred for the BEATs with NaB in 167 mM Na_2SO_4, where the resulting K_d from the linear fitting was negative.

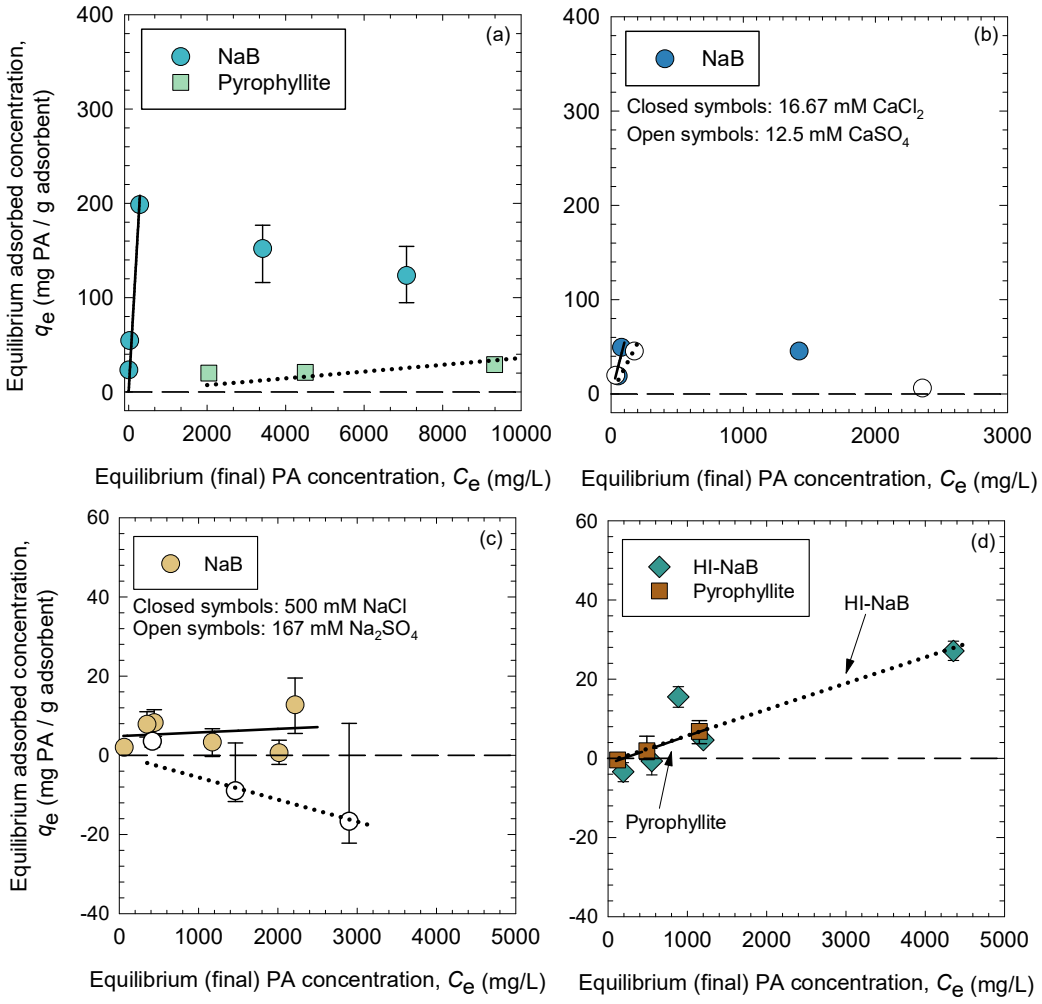

Figure 2.9: Linear fitting of measured batch adsorption test data for adsorption of poly(acrylic acid) (PA) to different adsorbents (NaB = sodium bentonite; HI-NaB = homo-ionized NaB) in different salt solutions: (a) 167 mM $CaCl_2$; (b) 16.67 mM $CaCl_2$ and 12.5 mM $CaSO_4$; (c) 500 mM NaCl and 167 mM Na_2SO_4; (d) 500 mM NaCl.

Table 2.8: Linear distribution coefficient, K_d, values for each salt solution and adsorbent (NaB = sodium bentonite; HI-NaB = homo-ionized NaB).

Solution	NaB		Pyrophyllite		HI-NaB	
	K_d (L/g)	R^2	K_d (L/g)	R^2	K_d (L/g)	R^2
500 mM NaCl	3.7	-0.495	5.5	0.927	6.3	0.771
167 mM $CaCl_2$	713[a]	0.942	3.6	-3.01	N/A	
167 mM Na_2SO_4	-5.66	0.832	N/A		N/A	
12.5 mM $CaSO_4$	270[a]	0.952	N/A		N/A	
16.67 mM $CaCl_2$	545[a]	0.946	N/A		N/A	

[a] Linear fitting through increasing linear trend
N/A = not analyzed
R^2 = coefficient of determination

2.7 Langmuir isotherm

The BEAT data were fit using the Langmuir adsorption isotherm equation to evaluate the potential for nonlinear adsorption of PA. The Langmuir adsorption isotherm equation can be written as follows:

$$q_e = \frac{Q_L K_L C_e}{1+K_L C_e} \tag{2.4}$$

where Q_L is the maximum adsorbed concentration (mg PA/g adsorbent) or adsorption capacity, and K_L (L/g) is the Langmuir constant, related to the affinity or net enthalpy of adsorption. The results of the non-linear fitting of the batch tests are summarized in Table 2.9 and Figure 2.10. The data plotted in Figure 2.10a,b is also provided in Figure 2.11a,b using a log scale for clarity.

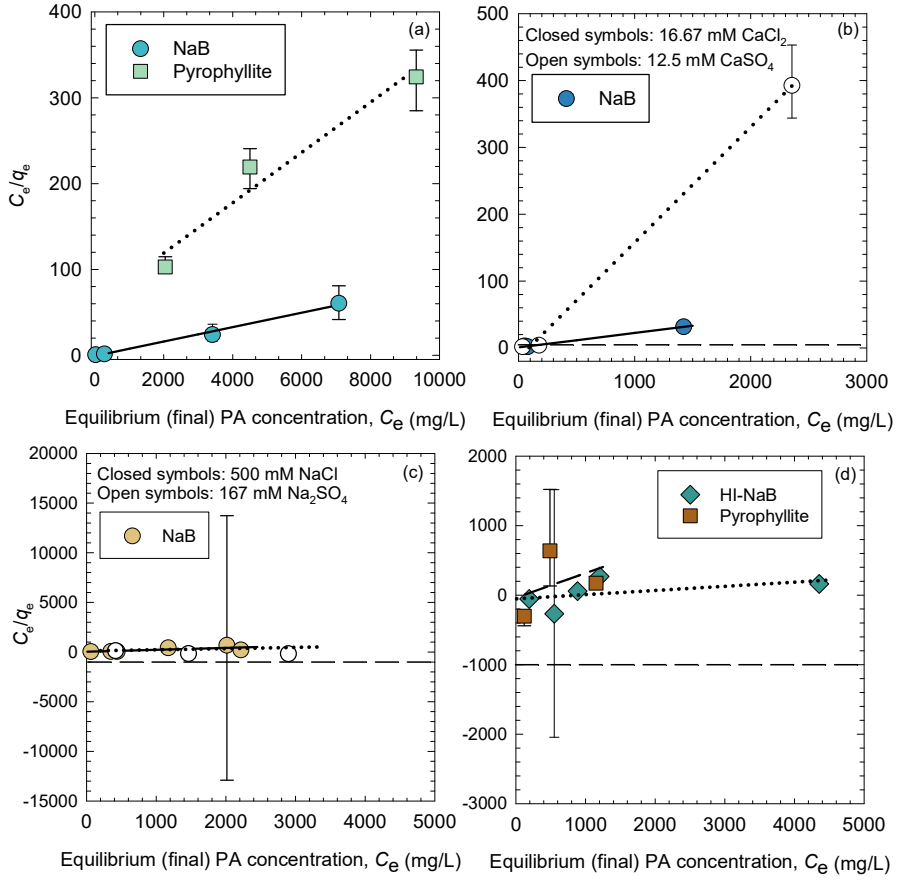

Figure 2.10: Langmuir isotherm of measured batch adsorption test data for adsorption of poly(acrylic acid) (PA) to different adsorbents (NaB = sodium bentonite; HI-NaB = homo-ionized NaB) in different salt solutions: (a) 167 mM $CaCl_2$; (b) 16.67 mM $CaCl_2$ and 12.5 mM $CaSO_4$; (c) 500 mM NaCl and 167 mM Na_2SO_4; (d) 500 mM NaCl.

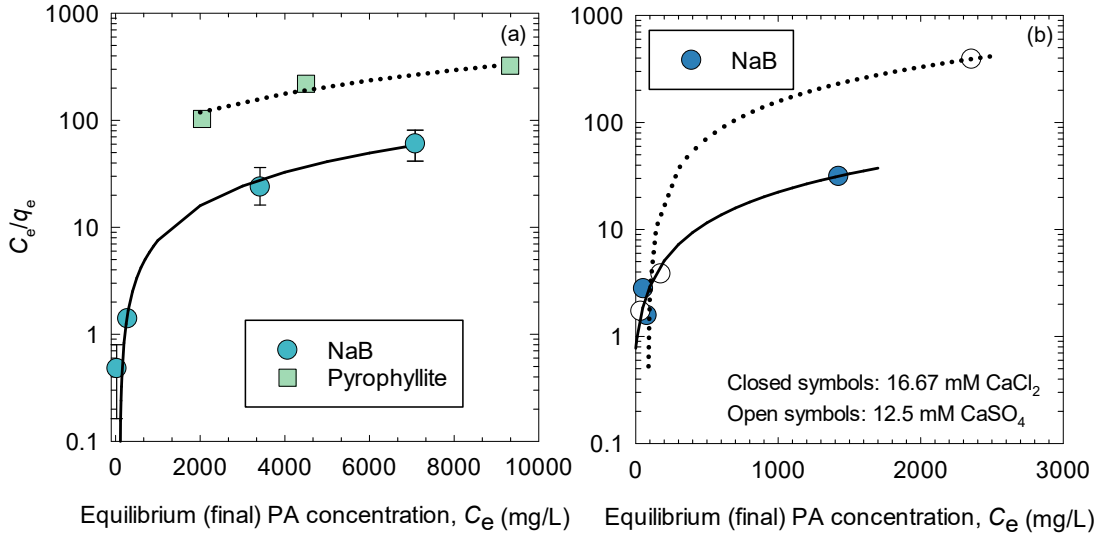

Figure 2.11: Langmuir isotherm of measured batch adsorption test data for adsorption of poly(acrylic acid) (PA) to different adsorbents (NaB = sodium bentonite; HI-NaB = homo-ionized NaB) in different salt solutions: (a) 167 mM $CaCl_2$; (b) 16.67 mM $CaCl_2$ and 12.5 mM $CaSO_4$.

Table 2.9: Langmuir fitting parameters obtained by linear fitting for each salt solution and adsorbent (NaB = sodium bentonite; HI-NaB = homo-ionized NaB).

Solution	NaB			Pyrophyllite			HI-NaB		
	Q_L (mg/g)	K_L (L/g)	R^2	Q_L (mg/g)	K_L (L/g)	R^2	Q_L (mg/g)	K_L (L/g)	R^2
500 mM NaCl	5.08	0.006	0.001	2.89	-0.008	0.081	16.4	-0.001	0.018
167 mM $CaCl_2$	238	0.017	0.993	34.1	$4.0x10^{-4}$	0.912		N/A	
167 mM Na_2SO_4	-8.63	-0.001	0.642		N/A			N/A	
12.5 mM $CaSO_4$	5.78	-0.012	0.980		N/A			N/A	
16.67 mM $CaCl_2$	46.3	0.028	0.995		N/A			N/A	

N/A = not analyzed
R^2 = coefficient of determination

As shown in Figure 2.10a,b, the Langmuir isotherm fits the BEAT data collected for the adsorption of PA onto NaB in the Ca containing solutions ($0.980 \geq R^2 \leq 0.995$). Unlike the linear fitting, the Langmuir isotherm in the Ca^{2+} solutions models the adsorption behavior past the maximum C_o, where inter-chain interaction was hypothesized to reduce adsorption (as seen for the linear fitting). Relatively high R^2 values ($R^2 > 0.980$) could suggest nonlinear sorption behavior for the adsorption of PA onto NaB in Ca^{2+} solutions. As shown in Table 2.9, the maximum adsorbed concentration (Q_L) for the adsorption of PA onto NaB

increases (5.78, 46.3, 238 mg PA/g NaB) with increasing Ca^{2+} concentration (12.5mM $CaSO_4$, 16.67 mM $CaCl_2$, 167 mM $CaCl_2$). The Langmuir isotherm also fits the BEAT data collected for PA adsorbed onto the pyrophyllite in the 167 mM $CaCl_2$ (R^2 = 0.912) with an estimated Q_L of 34.1 mg PA/g pyrophyllite. As shown in Figure 2.10c,d and Table 2.9, the Langmuir isotherm does not fit the BEAT data collected for the adsorption of PA onto NaB, pyrophyllite, or HI-NaB in the tested Na solutions ($0.001 \geq R^2 \leq 0.642$).

2.8 pH behavior

The measured PA concentrations are plotted versus the measured pH in Figure 2.12. The data are separated by blank solutions, representing PA mixed in the indicated solution (e.g., 500 mg/L PA in 500 mM NaCl), PA in NaB supernatant solutions, and batch solutions representing the supernatant analyzed from the BEATs.

As shown in Figure 2.12, pH is strongly correlated to polymer concentration. Poly(acrylic acid) contains carboxyl groups (-COOH) that will exchange H^+ cations for the Na^+ or Ca^{2+} available in solution. As H^+ is released into solution, the solution becomes more acidic. This behavior is reflected in all sampled solutions. Blank and supernatant solutions tested for each solution resulted in similar values of pH at each polymer concentration. Although the supernatant solution contains a wider variety of ions than the blank solution, PA underwent similar cation exchange behavior in both the supernatant and blank solutions.

For the BEATs with pyrophyllite, the pH trends were similar to the trend measured for the blank and supernatant in the same solution. Since pyrophyllite has no cation exchange capacity, the behavior for pyrophyllite was the same as that for the blank and supernatant solutions, as expected.

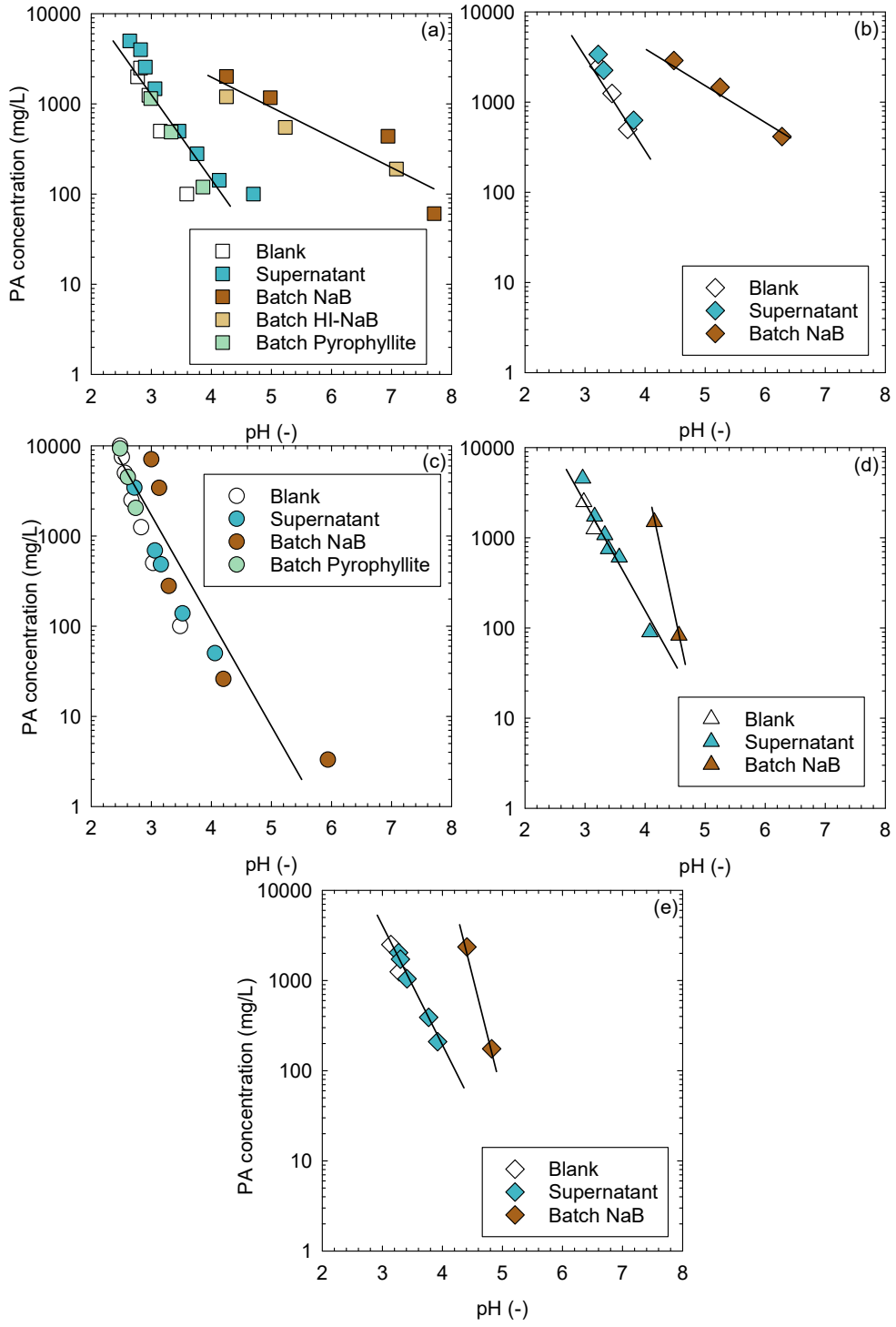

Figure 2.12: Poly(acrylic acid) (PA) concentration as a function of supernatant pH measured in either blank (polymer only), sodium bentonite (NaB) supernatant-polymer stock solutions, or batch adsorption collected supernatant with a clay mineral adsorbent (NaB) pyrophyllite, or homo-ionized NaB prepared with various salt solutions: (a) 500 mM NaCl; (b) 167 mM Na_2SO_4; (c) 167 mM $CaCl_2$; (d) 16.67 mM $CaCl_2$; (e) 12.5 mM $CaSO_4$.

The maximum adsorbed concentration is plotted as a function of the supernatant pH in Figure 2.13. For the tests with NaB in 167 mM $CaCl_2$, the pH did not shift at PA concentrations less than 300 mg/L (C_o < 500 mg/L). In solutions containing Ca^{2+}, PA adsorption occurred. When PA adsorption occurs, the polymer exists as loops with tails moving away from the montmorillonite basal surface (e.g., Theng 1982). The extended portions of the PA chain likely blocked the edge sites of the montmorillonite, preventing the buffering of the solution pH.

Samples with a pH > 4 resulted in less adsorption (lower q_e) than the samples with a pH < 4. The highest q_e values for NaB occurred with pH > 4 were achieved with solutions containing Ca^{2+}. All of the sample with pH < 4 occurred for all tests conducted with 167 mM $CaCl_2$ at PA concentrations (C_o) less than 5000 mg/L. At greater polymer concentrations, the pH of the supernatant with NaB in 167 mM $CaCl_2$ were slightly greater than 4 and the q_e were lower (less adsorption) than those for pH lower than 4.

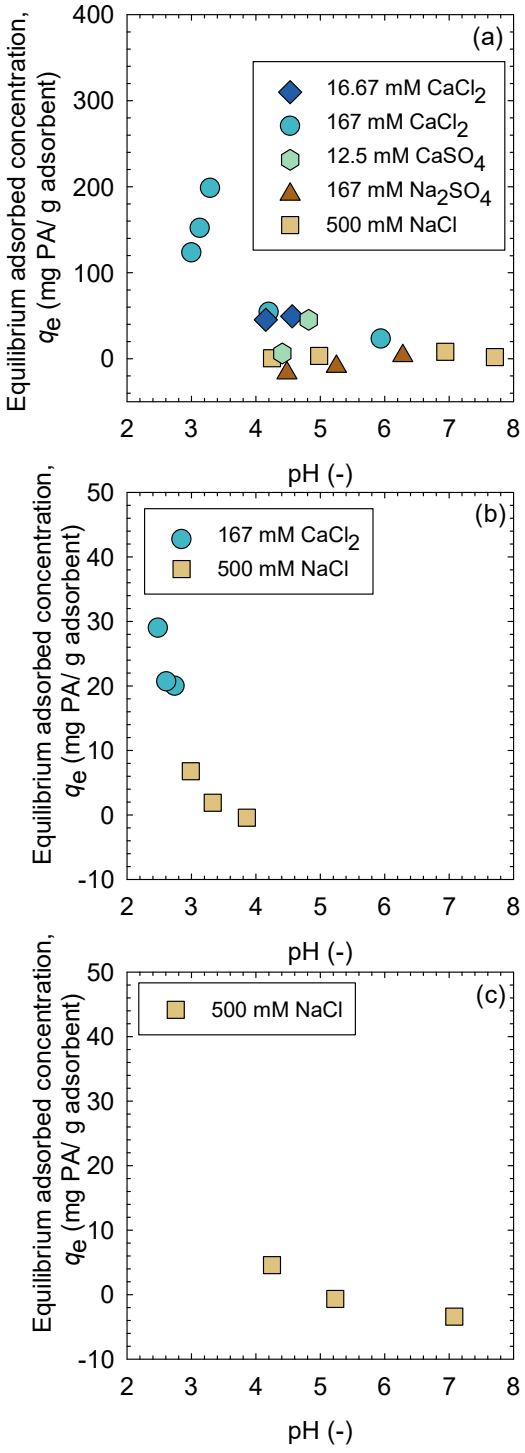

Figure 2.13: Measured equilibrium adsorbed concentration, q_e, of poly(acrylic acid) (PA) in different salt solutions versus supernatant pH from batch adsorption testing conducted with different adsorbents: (a) sodium bentonite (NaB), (b) pyrophyllite, and (c) homo-ionized NaB.

2.9 DISCUSSION

2.9.1 Cation-bridging

The results of this study are consistent with those from previous studies for anionic polymer adsorption onto negatively charged particles/surfaces, although previous studies were at lower concentrations and lower (more dilute) solid:solution ratios (e.g., Theng 1976; Theng and Scharpenseel 1976; Laird 1997; Deng et al. 2006). For NaB, PA adsorption increased with increasing Ca^{2+} concentration in the order 12.5 mM $CaSO_4$ < 16.67 mM $CaCl_2$ < 167 mM $CaCl_2$, resulting in increasing K_d in the respective order 270 < 545 < 713 L/g. As previously noted, Black et al. (1965) found that anionic polyacrylamide adsorption increased with $CaCl_2$ concentration, which was attributed to the compression of the DDL and reduction of repulsive, negative surface charge, charge screening of the anionic polymers, and flocculation of platelets encouraging interparticle bridging of bonded polymer. Similarly, cation bridging also is postulated to be the primary mechanism for adsorption of anionic PA by NaB used in, as illustrated schematically Figure 2.14. As mentioned previously, the inverted V-shape of the adsorption isotherms with solutions containing Ca^{2+} in this study indicate that both polymer concentration and Ca^{2+} concentration affected the adsorption of PA with NaB. Cation bridging (crosslinking) also can occur between polymer chains in the presence of Ca^{2+}. If the PA concentration increases beyond the that corresponding with maximum q_e, the PA inter-chain interaction increases which reduces q_e. The preference of PA for inter-chain interaction appears to increase in the presence of SO_4^{2-} (compared to Cl^-) in solution, exhibited by the drastic decrease of q_e from 45.3 mg/g to 6.7 mg/g in 12.5 mM $CaSO_4$ when increasing C_o from 1250 mg/L to 2500 mg/L, respectively.

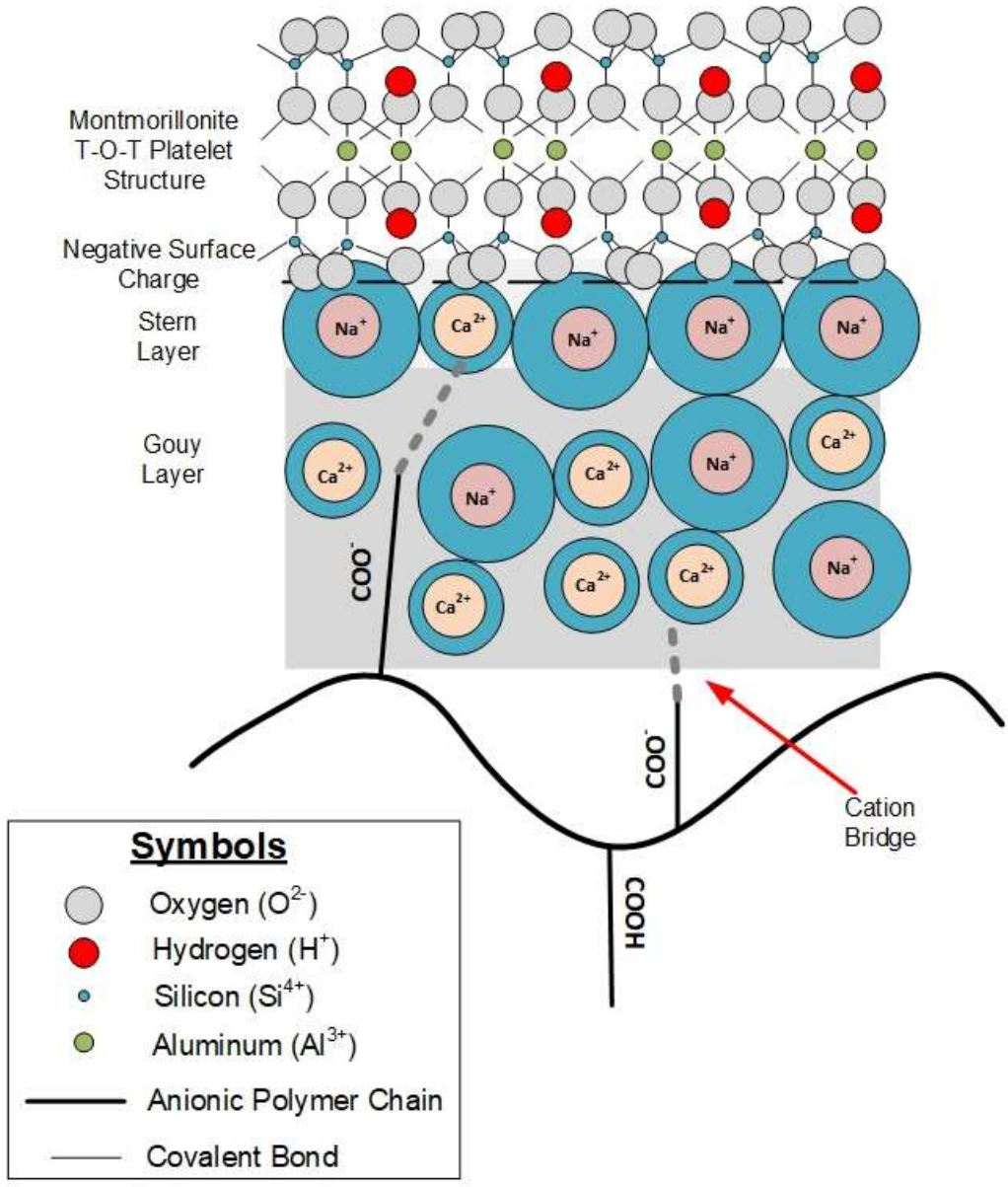

Figure 2.14: Schematic of hydrated cation bridging mechanism for adsorption of poly(acrylic acid) onto the basal surface of montmorillonite mineral (MMT) component of sodium bentonite.

The limited adsorption of PA by NaB in the 500 mM NaCl compared to the greater adsorption in 167 mM $CaCl_2$ suggests that other adsorption mechanisms, such as complexation or edge bonding (H-bonding or ligand exchange), are insignificant for PA adsorption relative to cation-bridging at high salt concentrations. However, because only a single high concentration NaCl solution was evaluated, further research is required to determine whether the limited adsorption is a function of the high concentration of NaCl.

2.9.2 pH behavior

In BEATs conducted with NaB, the shift in pH is a result of solution interaction with the PA, solution interaction with the NaB, and PA interaction with NaB. Ion exchange can occur between PA or NaB. As shown in Figure 2.12, the pH of the supernatant for 500 mM NaCl with NaB and HI-NaB and 167 mM Na_2SO_4 with NaB are different than those for the blank and NaB baseline supernatants with the same solutions, increasing to more neutral and alkaline pH values. This behavior is consistent with buffering capacity of the hydroxyl groups (-OH) at the edge sites of montmorillonite (Yong et al. 1990). Although a similar shift was exhibited by batch tests in 16.67 mM $CaCl_2$ and 12.5 mM $CaSO_4$, the pH remained lower than 5.

For pH at the pKa of approximately 4.5 for PA, the number of COOH and COO^- groups on the PA chain are approximately equal. For pH < pKa, the carboxyl groups on the PA chain are primarily undissociated (i.e., COOH). As the pH increases to values greater than the pKa, PA disassociation increases (Wisniewska and Chibowski 2005). As illustrated in Figure 2.13, the reduction in adsorption capacity of the NaB for pH > pKa of the PA may have been the result of an increase in the DOI of the PA chain. Increasing the DOI of the PA chain can reduce the charge screening effect of the cations in solution, increasing the repulsion between the negatively charged surfaces of the PA and MMT. Further study is required to understand the effect of pH on the adsorption of PA onto NaB via cation bridging, and if pH can be used to engineer polymer adsorption in EB-GCLs.

2.10 CONCLUSIONS

In this study, a series of batch equilibrium adsorption tests (BEATs) was conducted with a high molecular weight (345000 g/mol) poly(acrylic acid) (PA) as the absorbate and a sodium bentonite (NaB) with 85-91% montmorillonite (MMT)] as the adsorbent. The BEATS were conducted in 16.67 and 167 mM $CaCl_2$, 500 mM NaCl, 12.25 mM $CaSO_4$, and/or 167 mM Na_2SO_4 solutions to determine the adsorption capacity of NaB for anionic polymers in EB-GCLs and determine the effects of cationic or anionic chemical species of the hydrating solutions. Pyrophyllite, a charge neutral phyllosilicate mineral with the same crystalline

structure of MMT, also was evaluated as an absorbent to determine the effect of the net negative surface charge of the MMT on behavior. Finally, a homo-ionized sodium bentonite (HI-NaB) also was used as an adsorbent to determine the potential for edge bonding. The following conclusions are drawn from the results of this study.

- The results of this study are consistent with those from previous studies involving anionic polymer adsorption onto negatively charged particles/surfaces despite that these previous studies were conducted at lower (more dilute) solid:solution ratios and at lower concentrations than used in this study. Adsorption of PA by NaB increased with increasing Ca^{2+} concentration (12.5 mM $CaSO_4$ < 16.67 mM $CaCl_2$ < 167 mM $CaCl_2$), resulting in increasing K_d (270 < 545 < 713 L/g).
- A threshold PA concentration was apparent such that the amount of PA adsorbed decreased for concentrations greater than this threshold (maximum) concentration. The results of this study indicated that for each Ca^{2+}containing solution, there is a maximum source concentration (C_o) of PA that that corresponds to a maximum q_e. For C_o greater than this maximum or threshold concentration, PA inter-chain interaction increases such that the magnitude of q_e decreases. For example, q_e decreased from 198.4 mg/g to 151.9 mg/g in 167 mM $CaCl_2$ as the C_o for PA increased from 4991 mg/L to 7020 mg/L, respectively. The preference of PA for inter-chain interaction appears to increase in the presence of SO_4^{2-} (compared to Cl^-) in solution, such that q_e decrease from 45.3 mg/g to 6.7 mg/g in 12.5 mM $CaSO_4$ when as C_o increased from 1250 mg/L to 2500 mg/L, respectively.
- In soil-solution systems dominated by Na^+, the adsorption capacity for PA with NaB was limited ($K_d \leq 3.7$ L/g), while in systems dominated by Ca^{2+}, NaB exhibited a much higher adsorption capacity ($K_d \geq 270$ L/g). Limited adsorption ($K_d \leq 6.3$ L/g) also occurred for both pyrophyllite and HI-NaB, indicating limited contributions of MMT particle edge sites and edge bonding to PA adsorption. These results support the hypothesis that cation bridging is likely to be the dominant

adsorption mechanism for anionic polymers at high concentrations (> mg/L) in EBs amended with anionic polymers for use in EB-GCLs for containment of aggressive solutions.

- For the BEATs conducted with NaB in the Ca^{2+} solutions, better fits to the data were obtained with the nonlinear, Langmuir adsorption isotherm equation ($0.980 \geq R^2 \leq 0.995$) relative to those based on linear adsorption ($0.942 \geq R^2 \leq 0.946$). However, for the BEATs conducted with NaB, pyrophyllite, or HI-NaB in the Na^{+} solutions, the nonlinear fits with the Langmuir equation were as poor ($0.001 \geq R^2 \leq 0.642$) as those for the linear fits ($-0.450 \geq R^2 \leq 0.832$). These results suggest that adsorption occurs in polymer-NaB in systems containing sufficient calcium via cation bridging. If sufficient calcium (Na dominated) is not available, little to no adsorption occurs.
- The more neutral (alkaline) pH values of the supernatant in 500 mM NaCl with NaB and HI-NaB and 167 mM Na_2SO_4 in NaB are consistent with buffering capacity of the hydroxyl groups (-OH) at the edge sites of MMT. Although a similar shift to a more alkaline pH was exhibited by batch tests in 16.67 mM $CaCl_2$ and 12.5 mM $CaSO_4$, pH values remained lower than 5 (pKa ~4.5). Further research is required to understand the impacts of PA adsorption on the buffering capacity of MMT.
- The adsorption of PA onto NaB was correlated with pH. With NaB, for pH greater than the pKa of ~4.5 for the PA, a reduction in adsorption capacity of the PA may have been due to increase in the DOI of the PA chain, increasing the repulsion between the negatively charged surfaces of the PA and MMT. Further research is required to evaluate the impact of solution pH on the adsorption mechanism of cation bridging.
- UV-Vis spectroscopy was shown to be an accurate method to measure polymer concentrations in concentrated inorganic solutions. This method should be applicable for measuring PA concentrations in effluent samples collected from EB-GCL hydraulic conductivity tests insofar as the polymer enhancement is non-hydrogel forming in solution. However, care should be taken to consider the polymer type (e.g., non-dissolved polymers will not work) and effluent ion concentration.

REFERENCES

ASTM. 2006. Standard test method for swell index of clay mineral component of geosynthetic clay liners. D5890, West Conshohocken, Pennsylvania, USA.

ASTM. 2014. Standard test method for rapid determination of carbonate content of soils. D4373, West Conshohocken, Pennsylvania, USA.

ASTM. 2018. Standard test method for measuring the exchange complex and cation exchange capacity of inorganic fine-grained soils. D7503, West Conshohocken, Pennsylvania, USA.

Benson, C., Oren, A., and Gates, W. 2010. Hydraulic conductivity of two geosynthetic clay liners permeated with a hyperalkaline solution. *Geotextiles and Geomembranes*, 28(2), 206-218.

Bergaya, F., Lagaly, G., Faïza, Bergaya, B., and Gerhard, L. 2006b. General introduction: clays, clay minerals, and clay science, Chapter 1, Developments in Clay Science, Elsevier, 1-18.

Bidwell, J., Jepson, W., Toms, G. 1970. The interaction of kaolinite with polyphosphate and polyacrylate in aqueous solutions- some preliminary results. *Clay Minerals*, 8, 445-459.

Black. A., Birkner, F., Morgan, J. 1965. Destabilization of dilute clay suspensions with labelled polymers. *Journal of American Water Works Association*, 57, 1547-1560.

Blockhaus, F., Sequaris, J., Narres, H., Schwuger, M. 1996. Interactions of a water soluble polymeric detergent additive (polycarboxylate) with clay minerals from soil. *Progress of Colloid and Polymer Science*, 101, 23-29.

Bohnhoff, G. 2012. Membrane behavior, diffusion, and compatibility of a polymerized bentonite for containment barrier applications, Ph.D. dissertation, Colorado State University, Fort Collins, Colorado, USA.

Bohnhoff, G., and Shackelford, C. 2013. Improving membrane performance via bentonite polymer nanocomposite. *Applied Clay Science*, 86, 83-98.

Bohnhoff, G., Shackelford, C., and Sample-Lord, K. 2014. Calcium resistant membrane behavior of a polymerized bentonite. *Journal of Geotechnical and Geoenvironmental Engineering,* 140(3), 04013029.

Bolt, G. 1956. Physico-chemical analysis of the compressibility of pure clays. *Geotechnique*, 6(2), 86-93.

Bouazza, A. and Gates, W. 2014. Overview of performance compatibility issues of GCLs with respect to leachates of extreme chemistry. *Geosynthetics International*, 21(2), 151-167.

Breen, C. 1999. The characterization and use of polycation-exchanged bentonites. *Applied Clay Science,* 15, 187-219.

Buchholz, F. and Graham, A. 1998. *Modern Superabsorbent Polymer Technology*. John Wiley and Sons, New York, New York, USA.

Cabaness, W., Yen-Chin Lin, T., and Parkanyi, C. 1971. Effect of pH on the reactivity ratios in the copolymerization of acrylic acid and acrylamide. *Journal of Polymer Science*, Part A-1, 9, 2155-2170.

Chen, J., Salihoglu, H., Benson, C., Likos, W., and Edil, T. 2019. Hydraulic conductivity of bentonite-polymer composite geosynthetic clay liners permeated with coal combustion product leachates. Journal of Geotechnical and Geoenvironmental Engineering, 145(9), 04019038.

Das, K. and Somasundaran, P. 2001. Ultra-low dosage flocculation of alumina using polyacrylic acid. *Colloids and Surfaces A: Physicochemical and Engineering Aspects*,182, 1-3, 25-33.

Deng, Y., Dixon, J., and White, G. 2006. Adsorption of polyacrylamide on smectite, illite, and kaolinite. *Soil Science Society of America Journal*, 70, 297-304.

Derjaguin, B. and Landau, L. 1941. Theory of the stability of strongly charged lyophobic sols and of the adhesion of strongly charged particles in solutions of electrolytes. *Actual Physical Chemistry*, 14, 633-662.

Di Emidio, G. 2010. Hydraulic conductivity and chemico-osmotic performance of polymer treated clays, Ph.D. dissertation, University of Ghent, Ghent, Belgium.

Di Emidio, G., Van Impe, W., and Mazzieri, F. 2010. A polymer enhanced clay for impermeable geosynthetic clay liners. Proceedings. Sixth International Environmental Geotechnics Conference, International Society for Soil Mechanics and Geotechnical Engineers, New Delhi, India.

Emerson, W. 1956. Synthetic soil conditioners. *Journal of Agricultural Science*, Cambridge, 47, 117-121.

Flynn, B. and Carter, G. 1998. Waterproofing material and method of fabrication thereof. US Patent Number: 6,537,676 B1.

Freeze, R. and Cherry, J. 1979. *Groundwater*, Prentice-Hall, Inc., Englewood Cliffs, New Jersey, USA.

Gibbons, M. and Ormeci, B. 2013. Quantification of polymer concentration in water using UV-Vis spectroscopy. *Journal of Water Supply: Research and Technology-Aqua*, 62(4), 205-213.

Gramain, P. and Mayard, P. 1981. Elongational deformation by shear flow of flexible polymers adsorbed in porous media. *Macromolecules*, 14, 180-184.

Grimm, R. 1968. *Clay mineralogy,* McGraw-Hill, New York, New York, USA.

Hendricks, S., Nelson, R., and Alexander, L. 1940. Hydration mechanism of the clay Na-montmorillonite with various cations. *Journal of American Chemistry Society*, 62, 1457-1464.

Jo, H., Katsumi, T., Benson, C. H. and Edil, T. B. (2001). Hydraulic conductivity and swelling of non-prehydrated GCLs permeated with single species salt solutions, *Journal of Geotechnical and Geoenvironmental Engineering*, ASCE 127(7): 557–567.

Jullien, M., Raynal, J., Kohler, E., and Bildstein, O. 2005. Physicochemical reactivity in clay rich materials: tools for safety assessment. *Oil and Gas Science Technology*, 60(1), 107-120.

Katsumi, T., Onikata, M., Hasegawa, S., Lin, L., Kondo, M., and Kamon, M. 2001. Chemical compatibility of modified bentonite permeated with inorganic chemical solutions. *Geoenvironmental Impact Management*, 419-424.

Katsumi, T., Ishimori, H., Onikata, M., and Fukagawa, R. 2008. Long term barrier performance of modified bentonite materials against sodium and calcium permeant solutions. *Geotextiles and Geomembranes*, 26(1), 14–30.

Kohl, R. and Taylor, S. 1961. Hydrogen bonding between the carbonyl group and Wyoming bentonite. *Soil Science,* 91, 223-227.

Laird, D. 1997. Model for crystalline swelling of 2:1 phyllosilicates. *Clays and Clay Minerals*, 44, 553-559.

Laird, D. 2006. Influence of layer charge on swelling of smectites. *Applied Clay Science*, 37, 74-87.

Lam, C., Martin, P., Jefferis, S., and Gifford Goodhue, K. 2014. Determination of residual concentration of active polymer in a polymeric support fluid. *Geotechnical Testing Journal*, 37(1), 1-14.

Lee, L., Rahbari, R., Lecourtier, J., and Chauveteau, G. 1991. Adsorption of polyacrylamides on different faces of kaolinites. *Journal of Colloid Interface Science*, 147, 351-357.

Lee, J., and Shackelford, C. 2005. Impact of bentonite quality on hydraulic conductivity of geosynthetic clay liners. *Journal of Geotechnical and Geoenvironmental Engineering*, 131(1), 64-77.

Likos, W. and Wayllace, A. 2010. Porosity evolution of free and confined bentonites during interlayer hydration. *Clays and Clay Minerals*, 58(3), 399–414.

Likos, W., Bowders, J., and Gates, W. 2010. Geosynthetic clay liners for waste containment facilities. M*ineralogy and engineering properties of bentonite*, CRC Press, Taylor and Francis.

Marshall, C. 1964. *The physical chemistry and mineralogy of soils. Vol. 1: soil materials*. Wiley and Sons, New York, New York, USA.

Michaels, A. 1954. Aggregation of suspensions by polyelectrolytes. *Industrial & Engineering Chemistry Research*, 46, 1485-1490.

Michaels, A. and Morelos, O. 1955. Polyelectrolyte adsorption by kaolinite. *Industrial & Engineering Chemistry Research*, 47, 1801-1809.

Mitchell, J. 1993. *Fundamentals of soil behavior*, John Wiley and Sons, New York.

Mitchell, J. and Soga, K. 2005. *Fundamentals of soil behavior*, 3rd edition, John Wiley and Sons, Hoboken, New Jersey, USA.

Momani, F. and Ormeci, B. 2014. Optimization of polymer dose based on residual polymer concentration in dewatering supernatant. *Water, Air, & Soil Pollution*, Springer, 225, 2154.

Mooney, R., Keenan, A., and Wood, L. 1952. Adsorption of water by montmorillonite. I. Heat of desorption and application of BET theory. *Journal of American Chemical Society*, 74, 1367-1371.

Mortensen, J. 1957. Adsorption of hydrolyzed polyacrylonitrile on kaolinite I. effect of exchange cation and anion. *Soil Science Society of America*, 21, 385-388.

Norrish, K. 1954. The swelling of montmorillonite. Transactions Faraday Society, 18, 120-134.

Norrish, K. and Quirk, J. 1954. Crystalline swelling of montmorillonite, use of electrolytes to control swelling. *Nature*, 173, 255-257.

Olson, R. and Mesri, G. 1970. Mechanisms controlling compressibility of clays. *Journal of Soil Mechanics & Foundations*, 96, 1863-1878.

Quirk, J. and Aylmore, A. 1971. Domains and quasi-crystalline regions in clay systems. Soil Science Society of America Proceedings, 35, 652–654.

Rigenbach, E., Chauveteau, G., and Pefferkorn, E. 1995. Effect of soluble aluminum ions on poly-electrolyte-alumina interaction. Kinetics of polymer adsorption and colloid stabilization. *Colloids Surface and Physicochemical Engineering*, 99, 161-173.

Roy, W., Krapac, I., Chou, S., and Griffin, R. 1992. Batch-type procedures for estimating soil adsorption of chemicals. *EPA Technical Resource Document*, EPA/530-SW-87-006-F, U.S. Environmental Protection Agency, Washington, D.C., 100 p.

Ruhrwein, R. and Ward, D. 1952. Mechanism of clay aggregation by polyelectrolytes. *Soil Science*, 73, 485-492.

Salles, F., Beurroies, I., Bildstein, O., Jullien, M., Raynal, J., Denoyel, R. and Van Damme, H. 2008. A calorimetric study of mesoscopic swelling and hydration sequence in solid Na-montmorillonite. *Applied Clay Science*, 39(3-4), 186-201.

Salles, F., Douillard, J., Denoyel, R., Bildstein, O., Jullien, M., Beurroies, I. and Van Damme, H. 2009. Hydration sequence of swelling clays: evolutions of specific surface area and hydration energy. *Journal of Colloid and Interface Science*, 333, 510-522.

Sample-Lord, K. and Shackelford, C. 2016. Dialysis method to control exchangeable sodium and remove excess salts from bentonite. *Geotechnical Testing Journal*, 39(2), 1-11.

Sastry, N., Sequaris, J., and Schwuger, M. 1995. Adsorption of polyacrylic acid and sodium dodecylbenzenesulfonate on kaolinite. *Journal of Colloid Interface Science*, 171, 224-233.

Scalia, J., and Benson, C. 2016. Evaluation of Na-bentonite-polyacrylate mixtures to enhance the chemical resistance of geosynthetic clay liners, Proceedings, Geo-Chicago 2016, GSP No. 271, ASCE, Reston, Virginia, USA, 388-397.

Scalia, J., and Benson, C. 2017. Polymer fouling and hydraulic conductivity of mixtures of sodium bentonite and a bentonite-polymer composite. *Journal of Geotechnical and Geoenvironmental Engineering*, 143(4), 04016112.

Scalia, J., Benson, C., Bohnhoff, G., Edil, T., and Shackelford, C. 2014. Long-term hydraulic conductivity of a bentonite-polymer composite permeated with aggressive inorganic solutions. *Journal of Geotechnical and Geoenvironmental Engineering,* 140(3), 04013025.

Scalia, J., Bohnhoff, G., Shackelford, C., Benson, C., Sample-Lord, K., Malusis, M., and Likos, W. 2018. Enhanced bentonites for containment of inorganic wastes by GCLs. *Geosynthetics International*, 25(4), 392-411.

Shackelford, C., Benson, C., Katsumi, T., Edil, T., and Lin, L. 2000. Evaluating the hydraulic conductivity of GCLs permeated with non-standard liquids. *Geotextiles and Geomembranes*, 18(2-4), 133-161.

Shomer, I. and Mingelgrin, U. 1978. A direct procedure for determining the number of plates in tactoids of smectites: the Na/Ca-montmorillonite case. *Clays and Clay Minerals*, 26, (2), 135-138.

Sparks, D., Romero-Gonzalez, M., El-Taboni, E., Freeman, C. Hall, S., Kakonyi, G. Swanson, L., Banwart, S. and Harding, J. 2015. Adsorption of poly acrylic acid onto the surface of calcite: an experimental and simulation study. *Physical Chemistry Chemical Physics*, 17, 27357-27365.

Stiffert, B. and Epinasse, P. 1980. Adsorption of organic diacids and sodium polyacrylate onto montmorillonite. *Clays and Clay Minerals*, 28, 381-387.

Stumm, W. and Morgan, J. 1996. Aquatic Chemistry, 3rd edition. Wiley, New York, New York, USA.

Tessier, D. 1984. Etude exp6rimentale de l'organisation des matriaux argileux. Hydratation, gonflement et structuration au cours de la dessication et de la rhumectation. Ph.D. thesis. University of Paris, Paris, France.

Tessier, D. 1990. *Behavior and microstructure of clay minerals,* Plenum Press, Baltimore, MD, USA.

Theng, B. 1976. Interactions between montmorillonite and fulvic acid. *Geoderma*, 15, 243-251.

Theng, B. 1982. Clay-polymer interactions: summary and perspectives. *Clays and Clay Minerals*, 30, 1-9.

Theng, B. 2012. Formation and properties of clay-polymer complexes. Second edition. *Developments in Clay Science*, Vol. 4. Elsevier, Amsterdam, Netherlands.

Theng, B. and Scharpenseel, H. 1976. The adsorption of 14C-labelled humic acid by montmorillonite. Proceedings, International Clay Conference 1975. Applied Publishing Ltd., Wilmette, Illinois, USA.

Tian, K., Benson, C. and Likos, W. 2016a. Hydraulic conductivity of geosynthetic clay liners to low-level radioactive waste leachate. *Journal of Geotechnical and Geoenvironmental Engineering*, 142(8), 1–12.

Tian, K., Likos, W., and Benson, C. 2016b. Pore-scale imaging of polymer-modified bentonite in saline solutions, Proceedings, Geo-Chicago 2016, GSP No. 271, ASCE, Reston, Virginia, USA, 468-477.

Tian, K., Benson, C. and Likos, W. 2017. Effect of anion ratio on the hydraulic conductivity of a bentonite-polymer geosynthetic clay liner. Proceedings, Geo-Frontiers 2017, Orlando, Florida, USA, GSP No. 276, ASCE, Reston, VA, USA, pp. 180–189.

Tian, K., Likos, W., and Benson, C. 2019. Polymer elution and hydraulic conductivity of bentonite-polymer composite geosynthetic clay liners. *Journal of Geotechnical and Geoenvironmental Engineering,* 145(10), 04019071.

Trauger, R. and Darlington, J. 2000. Next-Generation Geosynthetic Clay Liners for Improved Durability and Performance. TR-220. Colloid Environmental Technologies Company, Arlington Heights, Illinois, USA.

Van Damme, H. 1995. Scale invariance and hydric behaviour of soils and clays. Compte-rendu de l'Academie des Sciences de Paris, t.320, serie IIA, 665-681.

Van Olphen, H. 1963. *An introduction to clay colloid chemistry*, Interscience, New York.

Van Olphen, H. 1977. *An introduction to clay colloid chemistry, 2nd Edition*, John Wiley and Sons, New York.

Verwey, E. and Overbeek, J. 1948. *Theory of stability of lyophobic colloids*, Elsevier, Amsterdam, Netherlands.

Warkentein, B. and Miller, R. 1958. Conditions affecting the formation of the montmorillonite polyacrylic acid bond. *Soil Science*, 85, 14-18.

Wiśniewska M, and Chibowski S. 2005. Influences of temperature and purity of polyacrylic acid on its adsorption and surface structures at ZrO_2-polymer solution interface. *Adsorption Science and Technology*, 23, 655–667.

Yong, R., Warkentin, B., Phadungchewit, Y., and Galvez, R. 1990. Buffer capacity and lead retention in some clay minerals. *Water, Air, & Soil Pollution*, 53, 53-67.

Yu, B., El-Zein, A., and Rowe, R. 2020. Effect of added polymer on the desiccation and healing of a geosynthetic clay liner subject to thermal gradients. *Geotextiles and Geomembranes*, 48, 928-939.

Chapter 3

Polymer quantification methods for geosynthetic clay liners enhanced with anionic polymers

SUMMARY

Two methods, total carbon (TC) and loss on ignition (LOI), and several procedures were evaluated for the purpose of quantifying the amount of polymer in anionic polymer enhanced-bentonite geosynthetic clay liners (EB-GCLs). Both methods can be applied either to an enhanced bentonite (EB), comprising the mixture of natural sodium bentonite (NaB) and a polymer, referred to as a composite procedure, or to each component material (viz. polymer and NaB) separately, referred to as a component procedure. Procedures evaluated included component LOI, composite TC, and two component TC procedures, one that measured solely TC (component A TC) and the other that measured both TC and total inorganic carbon (TIC) (component B TC). The EBs evaluated included NaB enhanced with different types of anionic polymers including, poly(acrylic acid) (PA) at low (5000 g/mol), medium (50000 g/mol), and high (345000 g/mol) molecular weights, low and high viscosity sodium carboxymethyl cellulose (CMC), and a covalently crosslinked sodium polyacrylate (PAx). Polymer contents were determined for the EB-GCL specimens after permeation with 500 mM NaCl or 167 mM $CaCl_2$. The EB for component LOI exhibited higher mass loss when ignited individually than when ignited in the EBs, regardless of total specimen mass of the EB or the total specimen masses of the individually measured losses (1 g or 3 g). The composite TC procedure provided an accurate measurement (error $\leq \pm$ 6.0 %) of polymer loading in EB-GCLs that had not been hydrated, corroborating the usefulness of composite TC for characterization of the polymer content in pre-permeated EB-GCLs. The component A TC procedure also provided an accurate option (error $\leq \pm$ 6.4 %) for measuring polymer loading of non-hydrated EB-GCLs. Although the component B TC procedure accounts for changes in the TIC (and potentially the total organic carbon, TOC) in the NaB during permeation, the composite and component A TC procedures resulted in similar final polymer contents

(within 0.4 - 0.8% depending on permeant solution) to the component B TC procedure, indicating that all three TC procedures are viable options for post-permeation polymer quantification of EB-GCLs comprising anionic-polymer EBs. These procedures can be used on post-permeated specimens as an additional tool for quantifying polymer elution.

3.1 INTRODUCTION

Anionic-polymer enhanced bentonites (EBs) refer to natural sodium bentonite (NaB) that has been amended or enhanced with anionic polymers such as sodium carboxymethylcellulose (CMC) and poly(acrylic acid) (PA). These EBs are used in enhanced-bentonite geosynthetic clay liners (EB-GCLs) for chemical containment applications in cases where the use of conventional GCLs comprising unenhanced NaB results in unacceptably high hydraulic conductivity and performance when permeated with liquids with aggressive chemistries that limit bentonite swelling (e.g., Scalia et al. 2014, 2018; Athanassopoulos et al. 2015; Tian et al. 2016a,b; Chen et al. 2019). Polymer quantification of these EB-GCLs is essential for quality assurance and quality control (QA/QC) in terms of ensuring the correct polymer content and the uniform distribution of the polymer across a manufactured roll. The measurement of polymer content before and after permeation of EB-GCLs subjected to different permeant liquids, stresses, and hydraulic gradients also can assist in understanding the polymer retention mechanisms in specific EB-GCLs (Scalia et al. 2014; Tian et al. 2016b; Chen et al. 2019). Currently, polymer quantification commonly is performed using a loss-on-ignition (LOI) method, such as described in ASTM D7348-13 (ASTM 2013).

Traditionally, LOI methods have been used not only to determine the organic content of soils, but also to measure polymer content in EBs by assuming the mass lost during ignition equates to complete degradation of the polymer. However, the NaB present in the enhanced bentonites (EBs) also experiences a small mass loss due to tightly held water that is not released during oven drying (Grim 1968; Scalia et al. 2014; Williams 2018). Scalia et al. (2014) used LOI to determine the polymer content of 28.5% in an EB referred to as bentonite polymer composite (BPC) by first measuring separately the masses lost on ignition

by the system components, viz., the polymer enhancement (polyacrylate) and bentonite (LOI = 74.7% and 1.6%, respectively).

The other established method used for measuring organic content in soil samples is total carbon (TC) analysis. Gustitus et al. (2021) identified three potential procedures for quantifying polymer in EB-GCLs comprising BPC, a component LOI, a composite LOI, and a composite total carbon (TC) procedure. Component procedures rely on measurements conducted on the bentonite and polymer materials individually whereas the composite procedures represent measurements conducted solely on mixtures of bentonite and polymer (i.e., EBs) with known polymer contents. Both LOI and TC methods are used to develop calibration curves that are then used subsequently to determine the polymer content of specimens.

This study was conducted, in part, to corroborate the recommendations given by Gustitus et al. (2021) for use of TC procedures to quantify polymer content in EB-GCLs comprising BPC, referred to as BPC-GCLs, also apply to other types of EB-GCLs. In this study, the results of the component LOI and composite TC procedures used by Gustitus et al. (2021) to quantify the polymer loading in BPC-GCLs, as well as a component TC procedure, were compared for use in evaluating the polymer content in laboratory prepared EB-GCLs. The comparison is based on EBs containing different anionic polymer types including PA at low, medium, and high molecular weights, CMC with either low viscosity or high viscosity, and a covalently crosslinked sodium polyacrylate (PAx). In addition, the composite and component TC procedures also were evaluated for determining the polymer contents of EB-GCLs that were permeated with either 500 mM NaCl or 167 mM $CaCl_2$.

3.2 BACKGROUND

Gustitus et al. (2021) tested three potential procedures for quantifying the polymer content of BPC-GCLs, viz., the component LOI, composite LOI, and composite TC. They compared the three polymer quantification procedures using three different polymers, two crosslinked polymers and a linear polymer, over a range of polymer mass loadings, prior to hydration and after hydration (but before permeation). The polymer quantification via the component LOI procedure was found to be inaccurate due to changes in the

thermal degradation of the polymers tested in an EB. The accuracy in the determination of the mass of polymer lost using the LOI method based on the component procedure versus the composite procedure was shown to depend on the type of thermal degradation reactions the polymer underwent during ignition (endothermic and/or exothermic) via thermogravimetric analysis (TGA) and differential scanning calorimetry (DSC). Although TGA analysis is not analogous to LOI (e.g., TGA involves ignition under argon, a nonoxidizing environment, whereas LOI involves ignition in a muffle furnace, an oxidizing environment), the difference in masses remaining between polymers heated individually versus polymers heated in bentonite mixtures produced a source of bias that could either over or underestimate the final polymer content in non-hydrated (pre-permeated) BPC. In contrast, the composite LOI procedure was reliable for measuring the polymer contents of the non-hydrated BPC, but inaccurate for BPC specimens that had been hydrated in a cell for 7 days before subsequent drying and LOI measurement. Also, the variation in measured polymer contents was dependent on the type of hydrating liquid, i.e., deionized water (DIW) or 50 mM $CaCl_2$ solution, and the polymer content. The variation in measured polymer content tended to be less for the DIW versus 50 mM $CaCl_2$ and tended to increase with increasing polymer content. Finally, the variation in polymer contents based on the composite LOI method with hydrated specimens was attributed to changes in the conformation of the polymer chains as well as changes to the composition of the exchange complex of the NaB, specifically an increase in Ca^{2+}, caused by hydration with solutions with increasing Ca^{2+} concentrations that may be connected to a reduction of water molecules that are tightly held by the NaB and not lost during ignition.

Gustitus et al. (2021) showed the composite TC procedure was more accurate in determining the polymer content of hydrated BPC specimens, regardless of type of hydrating solution or polymer content. The composite TC procedure was hypothesized to be less sensitive to the material changes due to hydration, because the TC method measures the total amount of carbon released during combustion. Gustitus et al. (2021) recommended the composite LOI method for quantification of initial polymer loading of BPC-GCLs and the composite TC procedure for quantification following BPC hydration. Although not tested by

Gustitus et al. (2021), the composite TC procedure also was recommended for determining polymer contents in post-permeated specimens of the BPC-GCLs based on an extrapolation of the results for the hydrated specimens.

3.3 MATERIALS

The materials used in this study included powdered NaB, CMC with two different viscosities, linear PA with three different molecular weights, and a cross-linked PA (PAx). The CMCs are designated as CMCLV and CMCHV corresponding to CMC with low viscosity and high viscosity, respectively, and the PAs are designated as PALW, PAMW, and PAHW corresponding to PA with low, medium, and high molecular weights, respectively.

3.3.1 Sodium bentonite

The NaB was obtained from Colloid Environmental Technologies Company (CETCO) of Hoffman Estates, Illinois, USA, and is the same NaB used in Bentomat GCLs as well as other studies on GCL behavior (Bohnhoff 2012, Bohnhoff and Shackelford 2013, Bohnhoff et al. 2014, Scalia et al. 2014), except these studies used a granular form of the same NaB. As reported by Scalia et al. (2014), the NaB had a swell index in DIW of 31.4 mL/2 g, and a cation exchange capacity (CEC) of 78 $cmol^{+}/kg$. The exchange sites were occupied by approximately 40% Na, 36% Ca, 17% Mg, and 2% K. The particle-size distribution of the NaB qualifies the material nominally as a powdered bentonite (e.g., Howell et al. 1997).

3.3.2 Sodium carboxymethylcellulose

The CMCHV is produced by MP Biomedical (Irvine, CA, USA), and the CMCLV is produced by Calbiochem® (Millipore Sigma, Burlngton, Massachusetts, USA). The molecular weight of CMCHV, calculated from the degree of substitution (DoS = 0.65-0.85) and degree of polymerization (DP) of 3200 provided by the manufacturer, is 685290-736500 g/mol ($[C_6H_7O_2(OH)_x(OCH_2COONa)_y]_n$, where n is the DP, $x + y = 3$, and y is the DoS). The average molecular weight and DoS of the CMCLV were not provided by the manufacturer. The particle sizes of the CMCs were not altered from the manufacturer provided

material and included 97.6 % finer than 0.15 mm and 78.3 % finer than 0.075 mm for the CMCHV, and 97.0 % finer than 0.15 mm and 64.9 % finer than 0.075 mm for the CMCLV.

3.3.3 Poly(acrylic acid)

The PA ([-$CH_2CH(CO_2H)$-]$_n$) used in this study is a synthetic polymer of acrylic acid, polymerized to achieve a range of molecular weights. The negatively charged carboxylic moiety (COO^-) on the polymer repeating unit (R) is satisfied by a proton (H^+). Commercial PA is primarily differentiated by a weighted average molecular weight, which describes the average chain DP (Buchholz and Graham 1998). Poly(acrylic acid) that is covalently crosslinked is known as crosslinked PA (PAx).

The three linear anionic PAs used in this study, none of which are covalently crosslinked, were obtained from Polysciences Inc. (Warrington, Pennsylvania, USA). The molecular weights of the PALW, PAMW, and PAHW as provided by the manufacturer were approximately 5000, 50000, and 345000 g/mol, respectively. When needed for dry mixtures, the PA in solution was air dried until solidified and then ground and screened. Grinding of the polymer was completed using a rotary blade grinder (KitchenAid BCG211OB blade grinder; Benton Harbor, Michigan, USA). The PA was ground to achieve a similar particle-size distribution as the base NaB to allow for homogeneous mixing (Shackelford et al. 2000; Malusis and Scalia 2007).

A covalently crosslinked PAx also was used in this study for comparison with the linear PAs. The PAx was a partial, sodium salt-graft-poly(ethylene oxide) (Aldrich Chemistry, St. Louis, Missouri, USA). The average molecular weight was not provided by the manufacturer.

3.3.4 Electrolyte solutions

Two concentrated inorganic solutions with ionic strength, I (= $\frac{1}{2}\Sigma c_i z_i^2$, where c_i = molar concentration of ionic species i, and z_i = charge of ionic species i), of 500 mM, viz., 167 mM $CaCl_2$ and 500 mM NaCl, were used as hydrating and permeant liquids to evaluate the effect of permeation on polymer quantification of EB-GCLs. The electrical conductivity (EC) and pH of the 167 mM $CaCl_2$ solution were 3280 mS/m and 5.8, respectively, whereas the respective EC and pH of the 500 mM NaCl were 4850 mS/m and 6.2. The

$CaCl_2$ solution was prepared by dissolving di-hydrate $CaCl_2$, $CaCl_2 \cdot 2H_2O$ (Alfa Aesar, Ward Hill, Massachusetts, USA) in DIW, and the NaCl solution was prepared by dissolving anhydrous NaCl (Fisher Chemical, Hampton, New Hampshire, USA) in DIW. The prepared solutions were stored in collapsible carboys with no headspace to limit interaction with the atmosphere.

3.4 METHODS

3.4.1 Component loss on ignition

Scalia et al. (2014) and Gustitus et al. (2021) used variations of the LOI method described as Method A in ASTM D7348 to quantify polymer contents in EBs and EB-GCLs. The component LOI procedure used in this study is the same as that used by Scalia et al. (2014) and Gustitus et al. (2021) except: (i) smaller sample masses of 1 g and 3 g were used compared to the 5 g samples used by both Scalia et al. (2014) and Gustitus et al. (2021); (ii) ignition was completed by ramping to a maximum temperature of 550 °C, which is the same as Scalia et al. (2014) but different than the 750 °C used by Gustitus et al. (2021); and (iii) the mass loss of the crucible during ignition was considered negligible. The maximum temperature of 550 °C exceeds the decomposition temperature of ~200 °C for both PA and CMC (McGaugh and Kottle 1967), but is lower than the decomposition temperatures of 600 to 800 °C for both $CaCO_3$ and CaO (Kasozi et al. 2009), two accessory minerals typically present in NaB at low percentages (< 3% by mass). Empty, clean crucibles were ignited at 550 °C for 1 h and stored in a desiccator before testing to ensure crucible mass loss during sample ignition was negligible.

Polymer quantification using the component LOI procedure was evaluated using known quantities of the linear anionic polymers (CMCLV, CMCHV, PALW, PAMW, PAHW), but was not evaluated for the BPC. Component LOI analysis was not completed for the BPC because the polymer used to enhance the BPC was not available for individual (component) testing, as noted by Scalia et al. (2014) and Gustitus et al. (2021). No grinding was required for the tested specimens as all materials passed a US No. 60 sieve (0.25 mm opening) per Method A in ASTM D7348.

A known mass of 1 g of a wet specimen of an EB or the NaB with initial gravimetric water contents (w_i) ranging from 5.2 to 13.7 %, was oven-dried in a ceramic crucible at 110 ºC until no further mass loss was measured. Masses were measured using an analytical balance (Genesys 10S UV-Vis Spectrophotometer, Thermo Fisher Scientific, Waltham, Massachusetts, USA). Specimens then were ignited at 550 ºC using a muffle furnace (Thermolyne™ Benchtop 1100 °C Muffle Furnace, Thermo Fisher Scientific, Waltham, Massachusetts, USA). After ignition, the specimens were cooled in a desiccator and the final mass of the specimen and crucible after ignition (m_f) was measured. Then, the component or composite LOI values were calculated as follows:

$$\text{LOI} = \frac{m_i - m_f}{m_i - m_c} \tag{3.1}$$

where m_i = initial specimen and crucible mass after drying, and m_c = initial crucible mass. With the measured component and composite LOI values, the mass fraction of the polymer (m_p) was determined from the following relationships:

$$\text{LOI}_p m_p + \text{LOI}_b m_b = \text{LOI}_{eb} \tag{3.2}$$

and

$$m_p + m_b = 1 \tag{3.3}$$

where LOI_p = fraction mass loss after ignition of the polymer component, LOI_b = fraction mass loss after ignition of the bentonite component, LOI_{eb} = fraction mass loss after ignition of the EB, and m_b = fraction of total mass represented by the bentonite. Finally, based on Eqs. 3.2 and 3.3, the expression for m_p is as follows:

$$m_p = \frac{\text{LOI}_{eb} - \text{LOI}_b}{\text{LOI}_p - \text{LOI}_b} \tag{3.4}$$

As shown in Table 3.1 and Figure 3.1a, the LOI for the NaB and polymers were affected by a range of material dependent differences when using a total specimen mass of 1 g. Variance in the LOI

measurement of NaB can be attributed to varying amounts of clay mineral structural water that are removed by dehydration due to exposure to air before ignition (e.g., Sun et al. 2009; Hoogsteen et al. 2015). Hoogsteen et al. (2015) reduced LOI variance in soil specimens by increasing specimen mass from 1 to 2 g or more and by rotating the specimens midway through ignition to overcome temperature variations in the muffle furnace. Thus, the LOI tests were repeated using a specimen mass of 3 g and rotating the specimen in the muffle furnace after 2 h of ignition. The resulting component LOI values are shown in Table 3.1 and Figure 3.1b. Increasing the total specimen mass to 3 g successfully reduced the variance and standard deviation of all material LOIs except for that of PAHW, which exhibited lower variance and standard deviation than the other polymers based on the 1 g specimens.

Table 3.1: Loss on ignition (LOI) of 1 g and 3 g specimens of sodium bentonite (NaB), low and high viscosity carboxymethylcellulose (CMCLV, CMCHV), and low, medium, and high molecular weight poly(acrylic acid) (PALW, PAMW, PAHW).

Material	1 g				3 g			
	LOI (%)	***n***	**Variance**	**Standard Deviation**	**LOI (%)**	***n***	**Variance**	**Standard Deviation**
NaB	1.3	9	0.26	0.51	1.7	3	2.0×10^{-4}	0.012
CMCLV	80.1	9	3.32	1.82	79.0	3	3.5×10^{-5}	0.006
CMCHV	79.6	9	0.08	0.28	79.7	3	4.5×10^{-3}	0.067
PALW	95.4	9	11.60	3.41	98.3	3	4.0×10^{-3}	0.063
PAMW	100.1	6	0.06	0.24	99.8	3	1.0×10^{-4}	0.010
PAHW	97.8	6	$4.8\text{x}10^{-3}$	0.07	97.7	3	6.0×10^{-3}	0.077

Note: *n* = number of specimens

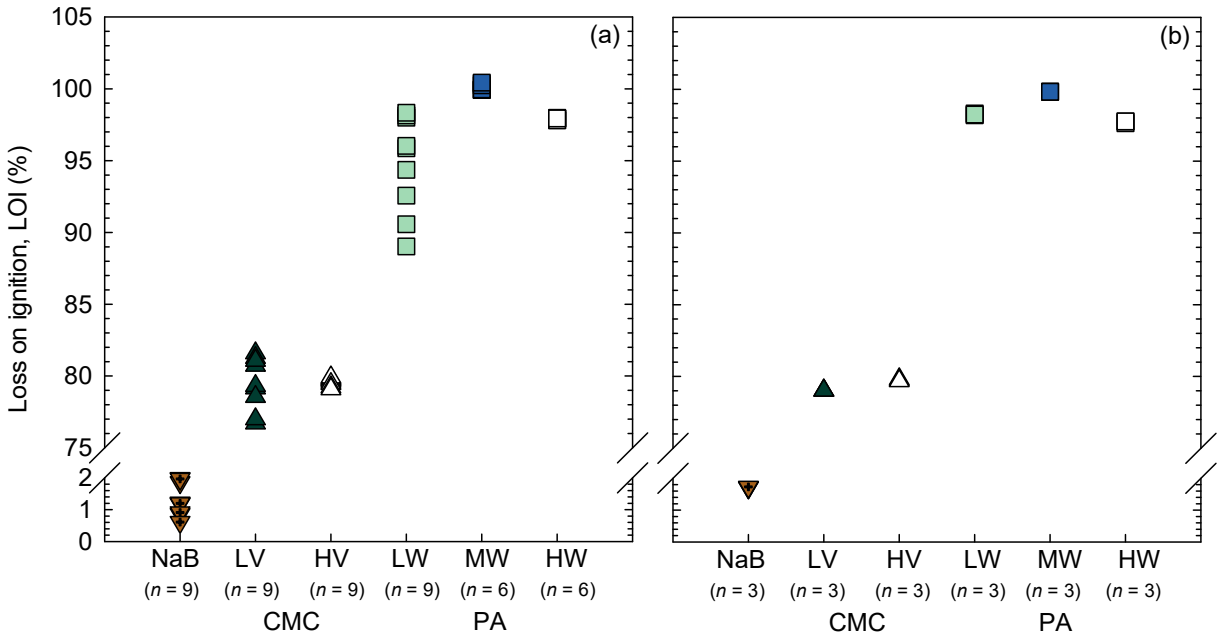

Figure 3.1: Loss on ignition (LOI) of 1 g and 3 g specimens of sodium bentonite (NaB), sodium carboxymethylcellulose (CMC) with low viscosity (LV) and high viscosity (HV), and poly(acrylic acid) (PA) with low, medium, and high molecular weight (LW, MW, HW): (a) 1 g; (b) 3 g. (Note: *n* = number of specimens)

3.4.2 Total carbon analysis

Three procedures of TC analysis, viz., the component A and component B TC procedures and a composite TC procedure, were evaluated for quantifying the polymer content in EBs. Detailed descriptions of each method follow.

3.4.2.1 Component A TC procedure

Solid TC analysis was completed in triplicate on oven-dried (110 °C) specimens by combustion in an induction furnace using a LECO TrueSpec CN analyzer (LECO Corporation, St. Joseph, Michigan, USA). Blank calibration and carbon standard (drift) calibration were completed before each analysis. Blank and carbon standard specimens also were analyzed after every 10 specimens. For specimens containing less than 5 % total carbon (TC), a soil standard was used, whereas for specimens containing ≥ 5 % TC, a plant standard was used. The results of the TC analyses for the NaB and polymers used to prepare the EBs, which represent the average values of three specimens, are shown in Table 3.2.

Table 3.2: Average of three replicated measurements of total carbon (TC) for sodium bentonite (NaB), low and high viscosity carboxymethylcellulose (CMCLV, CMCHV), low, medium, and high molecular weight poly(acrylic acid) (PALW, PAMW, PAHW), and cross-linked poly(acrylic acid) (PAx).

Material	TC (%)	Standard deviation (%)
NaB	0.3677	0.0034
CMCLV	47.31	0.4507
CMCHV	47.29	0.2839
PALW	49.72	0.1282
PAMW	35.88	0.0739
PAHW	36.52	0.0707
PAx	37.04	0.5120

The total carbon content of an EB, TC_{eb}, is given as follows:

$$TC_b m_b + TC_p m_p = TC_{eb} \tag{3.5}$$

where TC_b = measured TC for NaB, and TC_p = measured TC for polymer. The combination of Eq. 3.3 with Eq. 3.5 results in the following expression for the polymer content of the EB:

$$m_p = \frac{TC_{eb} - TC_b}{TC_p - TC_b} \tag{3.6}$$

3.4.2.2 Component B TC procedure

Since TC analysis does not differentiate between total inorganic carbon (TIC) and total organic carbon (TOC), changes in the TOC and/or TIC contents of bentonites that occur during permeation may cause discrepancies in the determination of the polymer contents of EB-GCLs. For example, permeation of bentonites can result in dissolution of calcium carbonate ($CaCO_3$) in the bentonite (e.g., Freeze and Cherry 1979; Shackelford 1994; Guyonnet et al. 2005), which in turn will reduce the TIC and, therefore, the TC of the bentonite, i.e., since TC = TIC + TOC. The carbonate (CO_3^{2-}) content inherent in sodium bentonites will translate to a value of TIC that comprises a fraction of the initially measured TC, and the initial CO_3^{2-} content of the NaB tested in this study is 1.3% (Scalia et al. 2014). A reduction in the TC of the NaB due to permeation would not be represented by the measured TC in the aforementioned component A TC

procedure or the subsequent composite TC procedure. Thus, the component B TC procedure was used in this study to determine if factoring in the potential changes in the TOC and/or TIC of the NaB during permeation impacted the final measured polymer content.

To investigate the impact of potential changes in TOC and TIC in the pre- and post-permeated NaB and EB-GCLs, TC and TIC analyses were conducted to determine the TOC content from the following relationship:

$$\text{TOC} = \text{TC} - \text{TIC} \tag{3.7}$$

Then, the total organic carbon content of a EBs, TOC_{eb}, is given as follows:

$$\text{TOC}_b m_b + \text{TOC}_p m_p = \text{TOC}_{eb} \tag{3.8}$$

where TOC_b = total organic carbon for NaB, and TOC_p = total organic carbon for polymer. Finally, the combination of Eqs. 3.3 and 3.8 results in the following expression for the polymer content:

$$m_p = \frac{\text{TOC}_{eb} - \text{TOC}_b}{\text{TOC}_p - \text{TOC}_b} \tag{3.9}$$

The TIC in the EB and NaB specimens was presumed to be equivalent to the total soil $CaCO_3$, which was measured using the modified pressure-calcimeter method (Sherrod et al. 2002). The TIC was measured for pre-permeated specimens of the NaB and EBs and post-permeated specimens of each unenhanced GCL and EB-GCL. The initial TC, TIC, and TOC contents of the NaB and each wet-mixed EB are shown in Table 3.3. The measured TC and TIC represent an average from three specimens.

Table 3.3: Measured (initial, pre-permeation) total carbon (TC) and total inorganic (TIC) and calculated total organic carbon (TOC) for sodium bentonite (NaB) and wet-mixed enhanced bentonites comprising 5% of low or high viscosity carboxymethylcellulose (CMCLV, CMCHV) or low, medium, and high molecular weight poly(acrylic acid) (PALW, PAMW, PAHW).

Material	TC (%)			TIC (%)			TOC (%)	Polymer Content (%)
	Average value	Standard deviation	*n*	Average value	Standard deviation	*n*		
NaB	0.368	0.003	3	0.215	0.011	3	0.153	0.0
CMCLV	2.289	0.016	3	0.009	NA	1	2.280	5.041
CMCHV	2.232	0.017	3	0.278	NA	1	1.954	5.848
PALW	2.197	0.030	3	0.186	NA	1	2.011	3.750
PAMW	2.724	0.002	3	0.083	NA	1	2.641	5.277
PAHW	2.599	0.015	3	0.109	NA	1	2.490	4.958

Notes: *n* = number of specimens; NA = not applicable (insufficient number of specimens for calculation)

3.4.2.3 Composite total carbon analysis

The composite TC procedure refers to the use of calibration curves based on the measured TC of EBs (TC_{eb}) with different known polymer loadings. The calibration curves, shown in Figure 3.2, were developed by measuring the TC_{eb} of mixtures with known polymer contents ranging from 1.0 to 5.6 % of polymer (by mass). Similar to the component A TC procedure, all the measurements for the composite TC procedure were performed on specimens that had not been exposed to a hydrating or permeant solution.

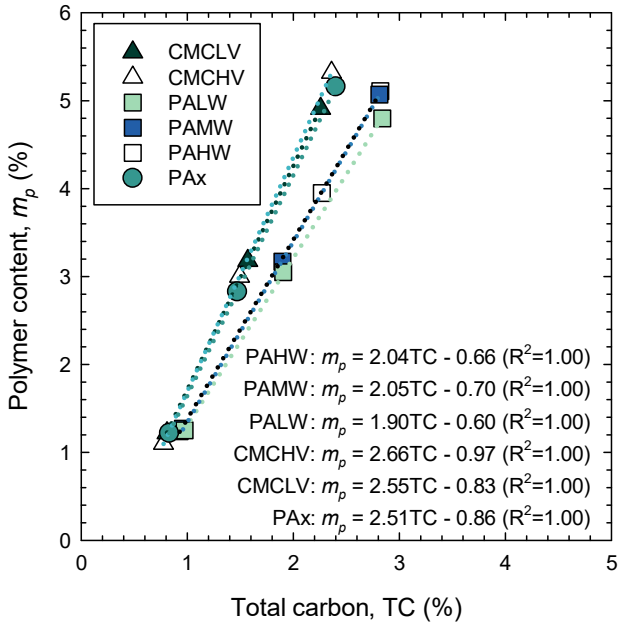

Figure 3.2: Calibration curves of polymer content as a function of total carbon for specimens of EBs with low and high viscosity carboxymethylcellulose (CMCLV. CMCHV), low, medium, and high molecular weight poly(acrylic acid) (PALW, PAMW, PAHW), and crosslinked poly(acrylic acid) (PAx) polymers at known polymer mass loadings.

3.4.3 EB-GCL specimen preparation and hydraulic conductivity measurement

Enhanced bentonites were prepared using the wet mixing method described in Chapter 1 and were tested for hydraulic conductivity in the form of unreinforced GCL specimens. The layers of a typical GCL were reproduced with each EB following the method described in Scalia et al. (2014). A non-woven, calendared geotextile (PolySpun heavy-duty landscape fabric) was placed below and then above a layer of EB. An additional non-woven geotextile with a mass per area of 1 kg/m^2 was placed below and above the GCL to serve as the bounding drainage layers in place of porous stones and filter paper as per Scalia et al. (2014). Specimens were prepared in flexible-wall permeameters with a 152.4 mm diameter in an even layer at 4.5 kg/m^2. This bentonite mass per area is similar to that for commercial GCLs (e.g., Koerner 2005).

Hydraulic conductivity tests were performed following the method described in Chapter 1 using flexible-wall permeameters following ASTM D6766-18 (ASTM 2018). Upon termination of the hydraulic conductivity tests, the post-permeated specimens were divided in half, and from a single half, divided again

into thirds to produce three samples for TC and TIC analysis. The samples were oven dried at 110 ºC, ground using a mortar and pestle, and passed in entirety through a No. 80 sieve (0.177 mm) prior to TC and TIC analyses.

3.5 RESULTS AND DISCUSSION

3.5.1 Initial polymer quantification

3.5.1.1 Component LOI

The component LOI analysis was evaluated for accuracy in predicting the polymer contents of EBs based on Eq. 4 to corroborate the findings of Gustitus et al. (2021). Both 1 g and 3 g specimens of EBs with known contents of the CMCHV were prepared. The resulting measured polymer contents are shown versus the actual polymer contents in Figure 3.3. The measured polymer contents for the 1 g specimens were determined based on the average LOI measured for both the 1 g and 3 g specimens as summarized in Table 3.1, with the former indicated as CMCHV 1 g A in Figure 3.3 and the latter indicated as CMCHV 1 g B in Figure 3.3. These different calculations were undertaken to determine if using mass loss from a 3 g specimen to calculate polymer content in a 1 g specimen increased the accuracy of the measured polymer contents for the 1 g specimen. Polymer contents of 3 g specimens were calculated using only the 3 g values (Table 3.1). The 3 g specimens with PAHW also were tested to determine any effect due to polymer type.

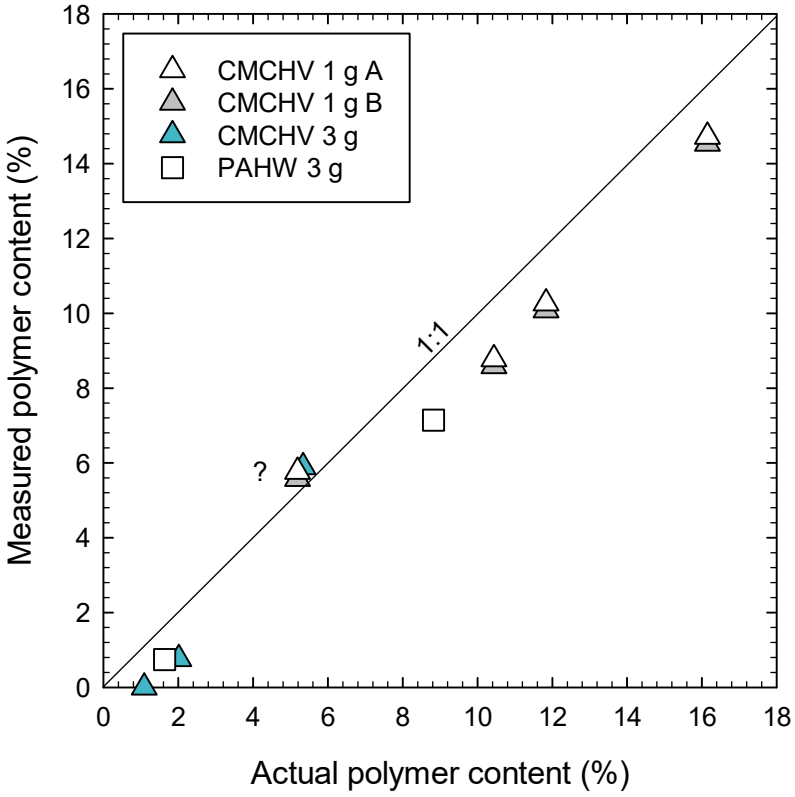

Figure 3.3: Actual versus measured polymer contents from component loss-on-ignition testing of 1 g and 3 g specimens of EBs comprising high viscosity carboxymethylcellulose (CMCHV) and high molecular weight poly(acrylic acid) (PAHW) polymers.

The results of the component LOI procedure are consistent with the observations of Gustitus et al. (2021). As seen in Figure 3.3, the component LOI testing of EBs containing CMCHV and PAHW consistently underestimated the actual polymer content by 0.89-2.6 %, regardless of specimen mass, polymer type, or the total specimen mass for the losses. An outlier occurred for both 1 g and 3 g mixtures containing CMCHV at an actual polymer content of 5.2-5.9 %, where the component LOI procedure overestimated the actual polymer content by 0.4-0.5 %. The reason for this deviation is unknown. The mass loss from component LOI analysis was higher when ignited individually than when ignited in the EBs, regardless of specimen mass or the specimen masses of the individually measured losses. These results corroborate the conclusions made by Gustitus et al. (2021) for BPC-GCLs regarding the component LOI procedure and the differences in loss in mass of polymers individually versus in EBs. As shown by Gustitus

et al. (2021), the EB mass losses using component LOI analysis also may differ depending on permeant solution chemistries such that a correction factor to account for under-prediction is unlikely to be effective. For this reason, no other polymer mixtures were tested using the component LOI procedure.

3.5.1.2 Evaluation of component A TC analysis

The results of the component A TC analysis for specimens of EBs prepared at known polymer contents ranging from 1.0 to 5.5 % with the linear anionic polymers (CMCLV, CMCHV, PALW, PAMW, PAHW) and covalently crosslinked PAx are shown in Figure 3.4. The average deviation (measured % – actual %) and error [(measured – actual) /actual × 100%] in polymer content are summarized in Table 3.4 for each polymer and polymer content using the component A TC analysis. There was good agreement (error ≤ ± 4.0 %) between the measured and actual polymer contents for the EBs for all linear polymers with 1 to 2 % polymer contents. The agreement was poorer ($2.1 \leq \left|\text{error}\right| \leq 6.4$ %) for polymer contents ranging from 3.0 to 5.5%. Overall, the worst agreement ($3.1 \leq \left|\text{error}\right| \leq 13.6$ %) was observed for the EBs with the PAx polymer. The greatest standard deviation in the measured TC also occurred with for the PAx mixtures (Table 3.3).

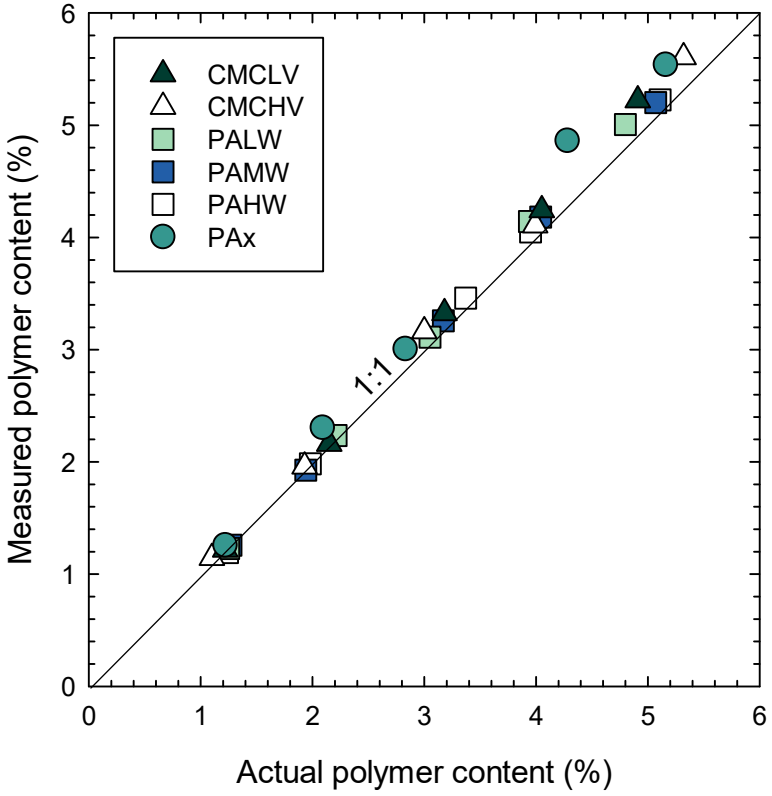

Figure 3.4: Actual versus measured polymer contents from component A total carbon testing of specimens of EBs with low or high viscosity carboxymethylcellulose (CMCLV, CMCHV), low, medium, or high molecular weight poly(acrylic acid) (PALW, PAMW, PAHW), and crosslinked poly(acrylic acid) (PAx) polymers.

Table 3.4: Actual versus measured polymer contents of specimens of EBs with low or high viscosity carboxymethylcellulose (CMCLV, CMCHV), low, medium, or high molecular weight poly(acrylic acid) (PALW, PAMW, PAHW), and crosslinked poly(acrylic acid) (PAx) polymers using component A total carbon analysis.

Polymer	Actual (%)	Measured (%)	Deviation (%)	Error (%)
CMCLV	1.22	1.22	0.000	-0.16
	2.15	2.16	0.010	0.51
	3.18	3.33	0.145	4.59
	4.05	4.24	0.191	4.79
	4.91	5.22	0.316	6.37
CMCHV	1.10	1.14	0.043	4.00
	1.93	1.96	0.030	1.45
	3.00	3.17	0.166	5.53
	3.99	4.11	0.117	2.98
	5.32	5.61	0.289	5.39
PALW	1.25	1.23	-0.020	-1.68
	2.21	2.23	0.027	1.09
	3.05	3.11	0.066	2.07
	3.94	4.14	0.207	5.13
	4.80	5.01	0.210	4.29
PAMW	1.27	1.26	-0.012	-1.02
	1.94	1.93	-0.013	-0.72
	3.17	3.26	0.091	2.78
	4.04	4.18	0.145	3.51
	5.07	5.20	0.128	2.60
PAHW	1.24	1.19	-0.053	-4.03
	1.98	1.98	0.000	0.00
	3.37	3.46	0.093	2.67
	3.95	4.05	0.095	2.53
	5.11	5.23	0.114	2.35
PAx	1.22	1.26	0.037	3.11
	2.09	2.30	0.214	10.29
	2.83	3.01	0.175	6.29
	4.28	4.86	0.584	13.60
	5.16	5.54	0.376	7.34

3.5.1.3 Evaluation of the composite TC procedure

The results of the composite TC procedure for specimens of the EBs prepared at known polymer contents ranging from 1.0 to 5.6 % with the linear anionic polymers (CMCLV, CMCHV, PALW, PAMW, PAHW) and covalently crosslinked PAx are shown in Figure 3.5. The deviations and errors between the measured and actual polymer contents are summarized in Table 3.5. The results indicate good agreement between the measured and actual polymer contents ($\left|\text{error}\right| \leq 6.0$ %) for all polymers at approximately 2% polymer

content and for all linear polymers at 3 to 4% polymer content. Similar to the results of the component A TC analysis, the greatest error (6.0 %) occurred for the PAx mixture at 4.3% actual polymer content.

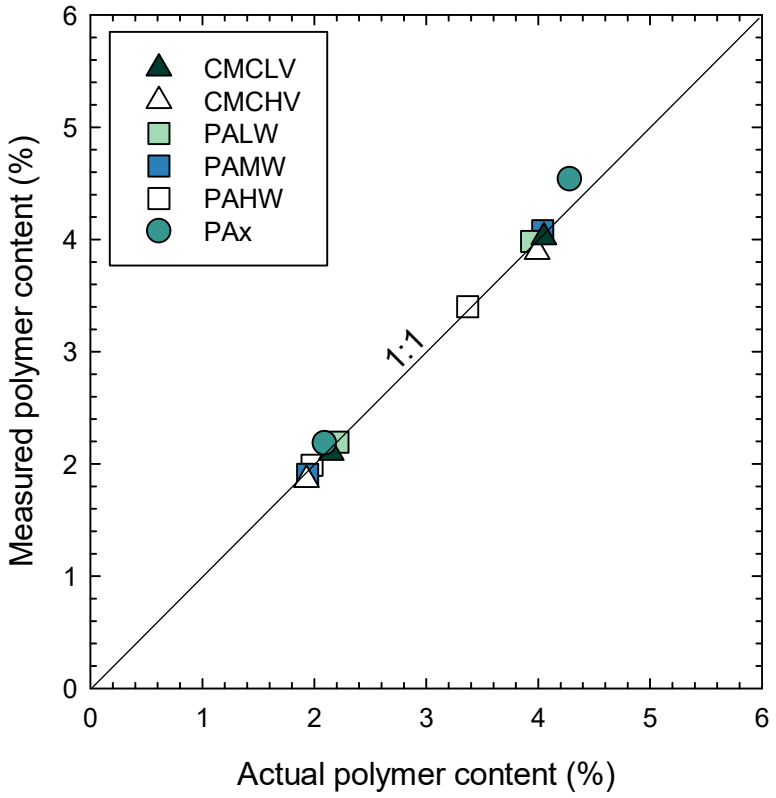

Figure 3.5: Actual versus measured polymer contents from composite total carbon testing of specimens of EBs with low or high viscosity carboxymethylcellulose (CMCLV, CMCHV), low, medium, or high molecular weight poly(acrylic acid) (PALW, PAMW, PAHW), and crosslinked poly(acrylic acid) (PAx) polymers.

Table 3.5: Actual versus measured polymer contents of specimens of EBs with low or high viscosity carboxymethylcellulose (CMCLV, CMCHV), low, medium, or high molecular weight poly(acrylic acid) (PALW, PAMW, PAHW), and crosslinked poly(acrylic acid) (PAx) polymers using composite total carbon analysis.

Polymer	Actual (%)	Measured (%)	Deviation (%)	Error (%)
CMCLV	2.15	2.10	-0.050	-2.33
	4.05	4.02	-0.030	-0.74
CMCHV	1.93	1.86	-0.072	-3.75
	3.99	3.89	-0.100	-2.51
PALW	2.21	2.19	-0.017	-0.77
	3.94	3.98	0.043	1.09
PAMW	1.94	1.91	-0.032	-1.67
	4.04	4.08	0.039	0.95
PAHW	1.98	1.99	0.008	0.40
	3.37	3.40	0.032	0.94
PAx	2.09	2.18	0.094	4.53
	4.28	4.54	0.259	6.05

The agreement between the measured and actual polymer contents for both the component A and composite procedures for TC analysis illustrates that both procedures are sufficient to measure the initial polymer content of an EB-GCL with the polymer types and mass loadings evaluated. The results based on the composite A TC analysis also are consistent with those of Gustitus et al. (2021), who found that the composite TC procedure was accurate for measuring the polymer contents of non-hydrated BPC-GCLs for contents 2.0 – 10 % (20-100 g polymer/ kg bentonite). Finally, the results indicate that this method also is accurate for other EB-GCLs, such that this method likely can be used for QA/QC purposes to measure the polymer contents of commercially produced EB-GCL products, although only a range of 1.9 – 4.3 % was tested in this study. However, to calibrate the composite TC procedure, at least three EB-GCLs with the same EB but different, known polymer mass loadings are required. Component A TC analysis also provides another option for accurate measurement of polymer loading of commercial EB-GCL products if a range of polymer loaded EB-GCLs is not available, or if the TC of the pure polymer is known (e.g., provided by the manufacturer) or can be measured.

3.5.2 Post-permeation polymer quantification

The results of the composite TC analyses of the EB-GCL samples both prior to and after permeation with 500 mM NaCl or 167 mM $CaCl_2$ are summarized in Figure 3.6. Because there was no polymer in the unenhanced GCL, the TC was expected to decrease from pre- to post permeation due to the dissolution of $CaCO_3$ ($CaCO_3 \rightarrow CaO + CO_2$ and/or $CaCO_3 \rightarrow Ca^{2+} + CO_3^{2-}$) and subsequent flushing of CO_2 and/or CO_3^{2-} from the specimen resulting in a reduction in TIC content. As expected, the TIC content of the unenhanced GCL decreased post permeation (Figure 3.6b). However, the TC content and, therefore, calculated TOC content, increased during permeation by a factor of 2.0 when permeated with the 167 mM $CaCl_2$ and a factor of 2.8 when permeated with the 500 mM NaCl. The initial TOC of the unenhanced GCL (i.e., TOC of the NaB) can be explained by a small fraction of organic matter that is present in the NaB. However, the additional TOC of the NaB gained during permeation, if unaccounted for, would result in an overprediction of the polymer content by approximately 0.3%. An increase of TOC in the NaB during permeation can result from inorganic carbon assimilation (e.g., conversion of dissolved CO_2 to organic matter) by microbes within the GCLs during long-duration permeation (53 to 308 d in this study) of unenhanced GCLs (Shackelford 1994). When disassembled post-permeation, all GCLs produced a strong organic odor, and some degree of black or orange discoloration was visible, which is indicative of biological activity within the GCL specimen (e.g., Tong and Shackelford 2016). As seen in Figure 3.6a, the increase in TC of NaB appears to be dependent on the permeant solution, with a slightly higher increase for the specimen permeated with 500 mM NaCl versus with 167 mM $CaCl_2$ (increase in TC of 0.14 - 0.28 % and 0.07 - 0.09 %, respectively). The reason for the difference in increase of TC is unknown.

The TC content in all EB-GCLs decreased from pre- to post permeation, regardless of permeant solution. As shown in Figure 3.6b, a small fraction of the decrease in TC can be attributed to the reduction in TIC content. Analysis of the pre-permeated EB produced with CMCLV resulted in a lower TIC relative to that for the post-permeated specimen, which cannot be explained. This value will be measured again for confirmation. However, most of the decrease in TC is attributed to the decrease in TOC (Figure 3.6c) due

to polymer elution during permeation. The TOC content for the EB-GCLs permeated with 167 mM $CaCl_2$ was higher than that for those permeated with 500 mM NaCl, likely due to increased hydrogel formation via cross-linking with Ca^{2+} or increased polymer adsorption (see Chapter 2), resulting in increased retention (Scalia et al. 2018; Tian et al. 2019). Changes in TOC also varied with polymer type. Polymer elution has been identified as a possibility for EBs modified with sodium polyacrylate such as bentonite polymer composite (Scalia et al. 2018; Tian et al. 2019). Although the mechanisms behind polymer elution behavior are still uncertain (e.g., see Chapter 4), differences in post-permeation polymer content due to polymer type or solution may be important for analysis of long-term EB-GCL hydraulic behavior. In addition, given the small post-permeated increase in TOC measured for the conventional GCL specimens by the same method, the post-permeated polymer contents of the EB-GCL specimens may slightly over predict ($\leq$ 0.3%) the actual polymer retention.

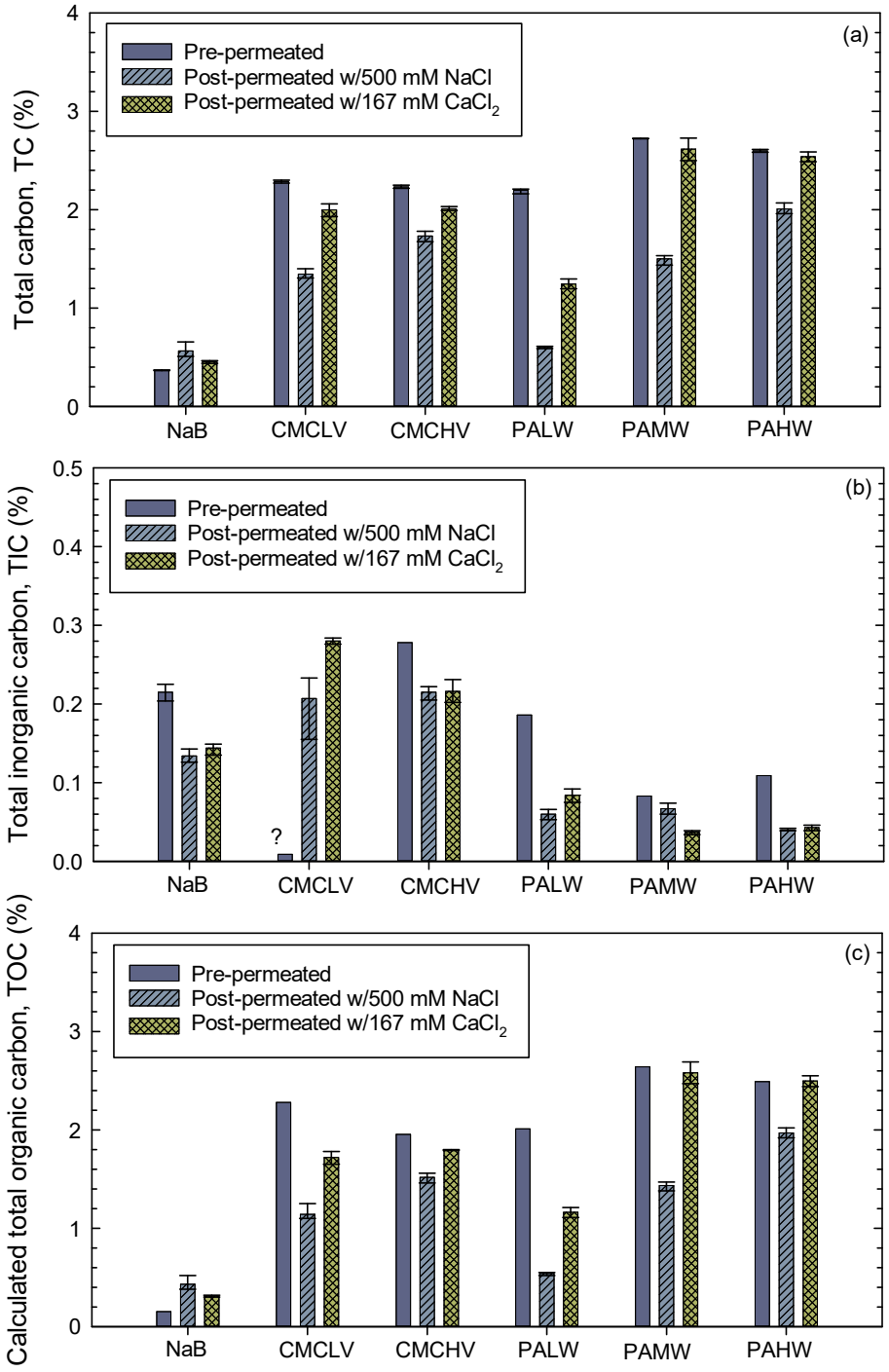

Figure 3.6: Pre-permeated and post-permeated carbon contents for sodium bentonite (NaB) and wet-mixed enhanced-bentonite geosynthetic clay liners (EB-GCLs) prepared with low or high viscosity carboxymethylcellulose (CMCLV, CMCHV) and low, medium, or high molecular weight poly(acrylic acid) (PALW, PAMW, PAHW): (a) measured total carbon; (b) inorganic carbon; (c) calculated total organic carbon.

To investigate whether the changes in TIC and TOC of NaB affect the accuracy of the component A or composite TC procedures, all three TC procedures were used to estimate the final polymer contents of the post-permeated conventional GCL and EB-GCL specimens. The previously noted increase in TOC of conventional GCL specimen during permeation due to microbial activity was accounted for in the TOC_b used in the calculation of the polymer content. The TOC_b content from the component B TC procedure reflects the post-permeated, measured value of TOC, instead of the initial TOC, for the conventional GCL in the respective permeant solution.

The resulting polymer contents are shown in Figure 3.7 for permeation of the EB-GCL specimens comprising each type of polymer with either 167 mM $CaCl_2$ or 500 mM NaCl. As expected, polymer contents calculated using the component B TC procedure are consistently lower than those calculated using the component A TC procedure. This difference can be attributed to the higher TOC content for the NaB in the component B TC procedure, due to the use of the post-permeated value of TOC_b to calculate polymer content with Eq. 3.9. The polymer contents from the composite TC procedure were consistently lower than those from the component A TC procedure. However, unlike the component B TC procedure, which incorporates correcting for carbonate minerals, the polymer contents based on the composite TC procedure varied with polymer type and permeant solution. Overall, the maximum deviation in polymer content resulting among the three TC procedures was approximately 0.4 % for permeation with 167 mM $CaCl_2$ and 0.8 % for permeation with 500 mM NaCl. Note that this analysis is intended to compare methods to measure polymer content, such that a discussion of polymer retention mechanisms between different EB-GCLs is warranted herein but can be found in Chapter 4.

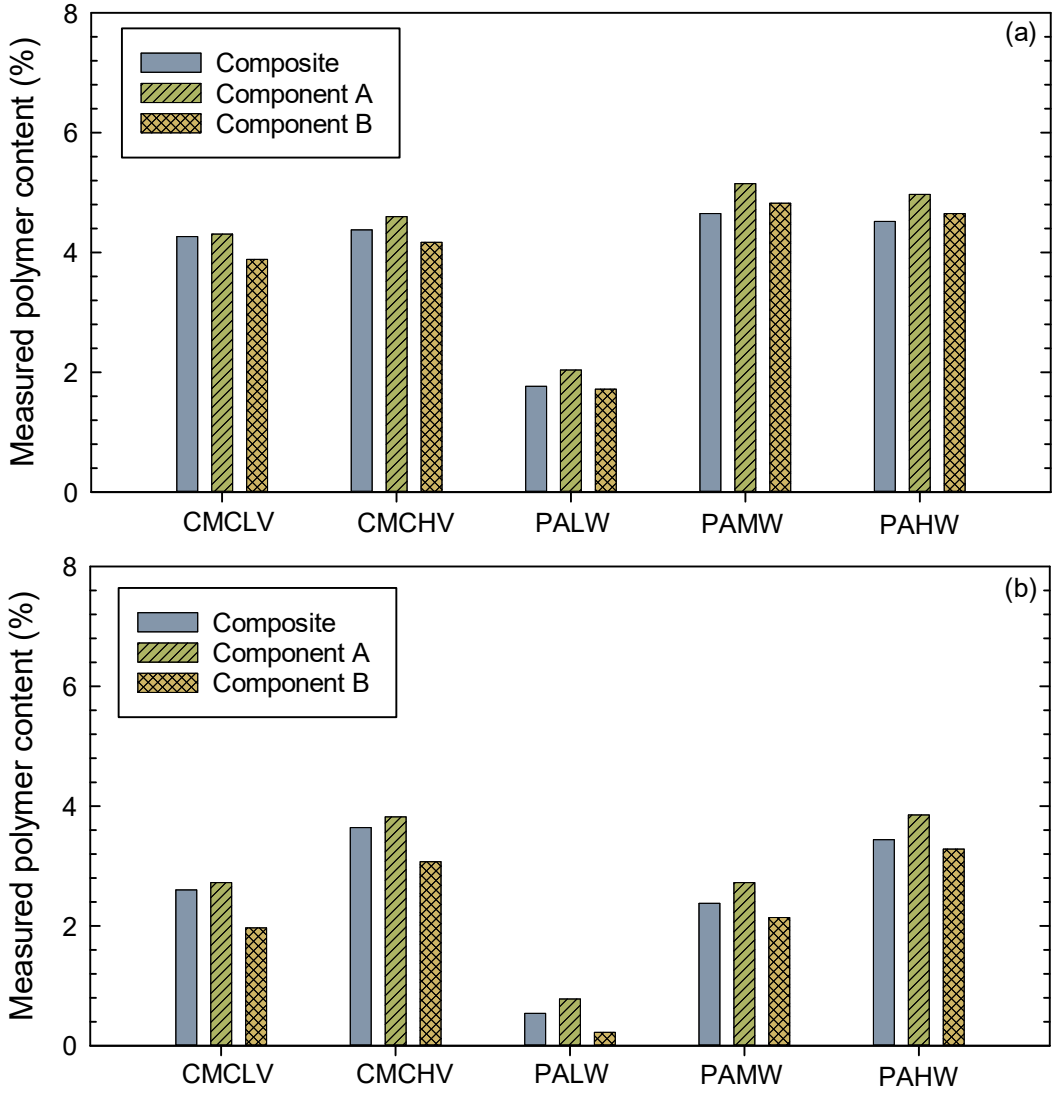

Figure 3.7: Measured polymer contents based on the composite, component A, and component B total carbon procedures for wet-mixed enhanced-bentonite geosynthetic clay liners (EB-GCLs) prepared with low or high viscosity carboxymethylcellulose (CMCLV, CMCHV) and low, medium, or high molecular weight poly(acrylic acid) (PALW, PAMW, PAHW) : (a) 167 mM $CaCl_2$; (b) 500 mM NaCl.

3.6 RECOMMENDATIONS

Accurate measurement of polymer contents in EB-GCLs is necessary to conduct proper QA/QC and to evaluate EB-GCL long-term hydraulic and polymer retention behavior. However, due to material variability or testing limitations, the specific TC method that is most appropriate for quantifying the polymer content

of any given EB-GCL also may vary. The following recommendations are made based on the results of this study.

- For polymer quantification of "new" EB-GCLs:
    - the composite TC procedure can be used if at least three specimens of the same EB-GCL but with a known range of different polymer contents are available, or solely for QA/QC based on a product-specified TC threshold or matching an as-tested product; and
    - the component A TC procedure can be used if separate specimens of the polymer and sodium bentonite components are available, or if the TC of these components is available in product specifications.
- For post-permeated EB-GCLs, the component B TC procedure can be used, which includes measurement of TIC on samples of post-permeated specimens, if separate specimens of the polymer and sodium bentonite are available. However, if potential changes in the TOC of the sodium bentonite during permeation are desired using the component B TC procedure, an unenhanced GCL comprising the same sodium bentonite as used to produce the enhanced bentonite for an EB-GCL also must be permeated under the same testing conditions.

3.7 CONCLUSIONS

Two methods and several procedures to determine polymer content in EB-GCLs were evaluated, including the component LOI procedure and the composite TC procedure used by Gustitus et al. (2021), and two component TC procedures, one that measured solely TC (component A TC) and the other that measured both TC and TIC (component B TC). Different EBs were tested containing different anionic polymer types including, poly(acrylic acid) (PA) at low (5000 g/mol), medium (50000 g/mol), and high (345000 g/mol) molecular weights, a low and high viscosity grade of sodium carboxymethyl cellulose (CMC), and a covalently crosslinked sodium polyacrylate (PAx). The differences in measured polymer content using the composite and component TC procedures for wet-mixed EB-GCLs specimens after permeation with either 500 mM NaCl or 167 mM $CaCl_2$ also were evaluated. This study corroborates the findings and

recommendations of Gustitus et al. (2021) for BPC-GCLs but is applied to other types of EB-GCLs. The following conclusions are drawn from the findings of this study.

- The bias in the measurement of the LOIs of the component LOI procedure, described by Gustitus et al. (2021), was confirmed. The linear anionic polymers (CMCHV and PAHW) used to produce the EBs for component LOI exhibited higher mass loss when ignited individually than when ignited in the EBs, regardless of total specimen mass of the EB or the total specimen masses of the individually measured losses (1 g or 3 g).
- The composite TC procedure provides an accurate measurement ($\left|\text{error}\right| \leq \pm 6.0$ %) of polymer loading in anionic polymer based EB-GCLs that have not been hydrated, which agrees with the recommendation by Gustitus et al. (2021) for use of the composite TC procedure for measurement of the as-manufactured polymer loading of commercial EB-GCL products.
- Component A TC analysis provides an accurate option for measuring polymer loading of non-hydrated, commercial EB-GCL products if a sufficient range of polymer mass loading (e.g., 2.0, 4.0, and 5.0 %) is not available.
- The composite and component A TC procedures for non-hydrated or pre-permeated specimens were verified as suitable for verifying manufacturer stated polymer mass loadings or, when not specified, determining the polymer mass loading (relative to a value) and variability of the loading.
- Although the component B TC procedure accounts for changes in the TIC (and potentially the TOC) in the NaB during permeation, the composite and component A TC procedures resulted in final polymer contents that were similar to those of the component B TC procedure (within 0.4-0.8% depending on permeant solution), indicating that all three TC analysis procedures are viable options for post-permeation polymer quantification to better understand EB-GCL issues such as polymer elution.

REFERENCES

Athanassopoulos, C., Benson, C., Donovan, M. and Chen, J. 2015. Hydraulic conductivity of a polymer-modified GCL permeated with high-pH solutions. Proceedings, Geosynthetics Conference 2015, Portland, Oregon, USA, Industrial Fabrics Association International, Roseville, MN, USA, 181–186.

ASTM. 2013. Standard test methods for loss on ignition (LOI) of solid combustion residues. D7348, West Conshohocken, Pennsylvania, USA.

ASTM. 2018. Standard test method for evaluation properties of geosynthetic clay liners permeated with potentially incompatible liquids. D6766, West Conshohocken, Pennsylvania, USA.

Bohnhoff, G. 2012. Membrane behavior, diffusion, and compatibility of a polymerized bentonite for containment barrier applications, Ph.D. dissertation, Colorado State University, Fort Collins, Colorado, USA.

Bohnhoff, G., and Shackelford, C. 2013. Improving membrane performance via bentonite polymer nanocomposite. *Applied Clay Science*, 86, 83-98.

Bohnhoff, G., Shackelford, C., and Sample-Lord, K. 2014. Calcium resistant membrane behavior of a polymerized bentonite. *Journal of Geotechnical and Geoenvironmental Engineering*, 140(3), 04013029.

Chen, J., Salihoglu, H., Benson, C., Likos, W., and Edil, T. 2019. Hydraulic conductivity of polymer-bentonite composite geosynthetic clay liners permeated with coal combustion product leachates. *Journal of Geotechnical and Geoenvironmental Engineering*, 145(9), 04019038.

Grim, R. 1968. *Clay Mineralogy*, 2nd edition. McGraw-Hill, New York, New York, USA.

Gustitus, S., Nguyen, D., Chen, J., and Benson, C. 2021. Quantifying polymer loading in polymer-bentonite composites using loss on ignition and total carbon analyses. *Geotechnical Testing Journal*, 44.

Guyonnet, D., Gaucher, E., Gaboriau, H., Pons, C.-H., Clinard, C., Norotte, V., and Didier, G. 2005. Geosynthetic clay liner interaction with leachate: correlation between permeability, microstructure, and surface chemistry. *Journal of Geotechnical and Geoenvironmental Engineering*, 131(6), 740-749.

Hoogsteen, M., Lantinga, E., Bakker, E., Groot, J., and Tittonell, P. 2015. Estimating soil organic carbon through loss on ignition: effects of ignition conditions and structural water loss. *European Journal of Soil Science*, 66, 320-328.

Howell, J., Shackelford, C., Amer, N., and Stern, R. 1997. Compaction of sand-processed clay soil mixtures. *Geotechnical Testing Journal*, 20(4), 443-458.

Kasozi, G., Nkedi-Kizza, P., and Harris, W. 2009. Varied carbon content of organic matter in histosols, spodosols, and carbonatic soils. *Soil Science Society of America Journal*, 73, 1313-1318.

Malusis, M. and Scalia, J. 2007. Hydraulic conductivity of an activated carbon-amended geosynthetic clay liner. GeoDenver 2007. New Peaks in Geotechnics, American Society of Civil Engineers, Reston, VA, 1-13.

McGaugh, M. and Kottle, S. 1967. The thermal degradation of poly(acrylic acid). *Journal of Polymer Science*, 5(9), 817-820.

Scalia, J., Benson, C., Bohnhoff, G., Edil, T., and Shackelford, C. 2014. Long-term hydraulic conductivity of a polymer-bentonite composite permeated with aggressive inorganic solutions. *Journal of Geotechnical and Geoenvironmental Engineering,* 140(3), 04013025.

Scalia, J., Bohnhoff, G., Shackelford, C., Benson, C., Sample-Lord, K., Malusis, M., and Likos, W. 2018. Enhanced bentonites for containment of inorganic wastes by GCLs. *Geosynthetics International*, 25(4), 392-411.

Shackelford, C. 1994. Waste-soil interaction that alter hydraulic conductivity. Hydraulic Conductivity and Waste Containment Transport in Soil, D. Daniel and S. Trautwein, Eds., STP 1142, ASTM, West Conshohoken, PA, 111-168.

Shackelford, C., Benson, C., Katsumi, T., Edil, T., and Lin, L. 2000. Evaluating the hydraulic conductivity of GCLs permeated with non-standard liquids. *Geotextiles and Geomembranes*, 18(2-4), 133-161.

Sherrod, L., Dunn, G., Peterson, G. and Kolberg, R. 2002. Inorganic carbon analysis by modified pressure-calcimeter method. *Soil Science Society of America Journal,* 66, 299-305.

Sun, H., Nelson, M., Chen, F., and Husch, J. 2009. Soil mineral structural water loss during loss on ignition analyses. *Canadian Journal of Soil Science*, 89, 603-610.

Tian, K., Benson, C. and Likos, W. 2016a. Hydraulic conductivity of geosynthetic clay liners to low-level radioactive waste leachate. *Journal of Geotechnical and Geoenvironmental Engineering*, 142(8), 1-12.

Tian, K., Likos, W., and Benson, C. 2016b. Pore-scale imaging of polymer-modified bentonite in saline solutions, Proceedings, Geo-Chicago 2016, GSP No. 271, ASCE, Reston, Virginia, USA, 468-477.

Tian, K., Likos, W., and Benson, C. 2019. Polymer elution and hydraulic conductivity of polymer-bentonite composite geosynthetic clay liners. *Journal of Geotechnical and Geoenvironmental Engineering* 145(10), 04019071.

Tong, S. and Shackelford, C. 2016. Standardized hydraulic conductivity testing of compacted sand-bentonite mixtures. *Geotechnical Testing Journal*, 39(6), GTJ20150204.

Williams, T. 2018. Hydraulic properties of geosynthetic clay liners. Master's thesis, University of Virginia, Charlottesville, Virginia, USA.

Chapter 4

Mechanisms controlling the hydraulic conductivity of anionic polymer-enhanced geosynthetic clay liners

SUMMARY

Understanding the mechanisms controlling the hydraulic conductivity of polymer-enhanced bentonites (EB) used in geosynthetic clay liners (GCLs) to aggressive chemical solutions is critical to forecasting long-term hydraulic performance of these EB-GCLs used as barriers in chemical containment applications. Accordingly, the results of hydraulic conductivity (k) tests performed on specimens of EB-GCLs using concentrated inorganic solutions, i.e., 500 mM NaCl and 167 mM $CaCl_2$, as the permeant liquids were conducted to determine the effects of polymer properties and specimen preparation method on the k and the associated roles of polymer retention and elution in dictating the measured k. The EB-GCL specimens were prepared by mixing a powdered sodium bentonite (PNaB) with the linear, anionic polymers, including poly(acrylic acid) (PA), sodium carboxymethylcellulose (CMC), or a covalently cross-linked, sodium polyacrylate (PAx), via three different preparation methods, viz., dry sprinkling (DS), dry mixing (DM), or wet mixing (WM). A bentonite polymer composite (BPC) also was tested. Physical (pore-clogging) and chemical (adsorption) polymer retention mechanisms were considered. The effects of kinetics, solution chemistry, and polymer type on hydrogel development were qualitatively evaluated by hydrogel formation tests. A granular NaB (GNaB) and pyrophyllite also were tested to determine the effect of interaggregate pore size and surface charge, respectively. Hydraulic conductivity tests at a low hydraulic gradient also were conducted to determine the effect of seepage forces. The results of the hydrogel formation tests illustrated that PA hydrogel was formed in solutions tested during EB-GCL hydration. The EB-GCL specimen preparation method influenced the polymer retention behavior as well as the k. The DS method resulted in low k ($\leq 5.5\times10^{-11}$ m/s) in multiple EB-GCLs, with a low fraction (≤ 2.5 %) of retained polymer. In contrast, polymer elution from EB-GCLs prepared using the DM method resulted in interaggregate flow and an increase in k. Higher polymer retention occurred for the WM EB-GCLs but did not directly correlate

to a low *k*. The BPC GCL tested effectively reduced the hydraulic conductivity compared to the conventional GCL even after eluting a significant fraction of polymer during permeation (~74 %). However, the BPC GCL did not out-perform the other tested EB-GCLs. The mechanisms controlling the *k* of EB-GCLs were understood by idealizing the system as a filtration zone. As flow occurs, the polymer hydrogel (filtrate) migrated into and through the NaB filter. The effective "filtration" of the polymer hydrogel and ultimately the long-term *k* was dependent on: (1) the formation of hydrogel, (2) the insertion of the hydrogels into and blocking of the most conductive pores, (3) a balance of seepage forces and hydrogel crosslink bond strength, (4) the kinetics of hydrogel formation, and (5) adsorption of polymer to the surfaces of the bentonite particles or aggregates of particles.

4.1 INTRODUCTION

Conventional geosynthetic clay liners (GCLs) comprising natural sodium bentonite (NaB) used as engineered barriers in chemical containment applications (e.g., coal combustion residual landfills, brine impoundments, tailings storage facilities, etc.) have been shown to be hydraulically incompatible to aggressive inorganic solutions, such as brines (high salt concentration) or extremely acidic or basic leachates, especially under low confining stresses (Shackelford et al. 2000; Benson et al. 2010; Bouazza and Gates 2014; Chen et al. 2019). Hydraulic incompatibility with a permeant liquid results in a high hydraulic conductivity of the GCL, which is unacceptable for engineered barrier systems. As a result of this compatibility issue between natural NaB and liquids with aggressive chemistry, a plethora of chemically-enhanced bentonites (EBs) that are intended to improve the hydraulic compatibility of GCLs have been developed. The chemical enhancements have included organic compounds such as propylene and glycerol carbonate, linear anionic polymers such as sodium carboxymethylcellulose (CMC) and poly(acrylic acid) (PA), and a host of proprietary (unknown) commercial products (Donovan et al. 2016a,b; Scalia et al. 2018; Donovan et al. 2020; Yu et al. 2020). The resulting EBs are used in place of NaB in conventional GCLs to form enhanced-bentonite GCLs (EB-GCLs). However, the mechanisms responsible for the improved hydraulic compatibility of EB-GCLs modified with anionic polymers are not well understood (Flynn and

Carter 1998; Trauger and Darlington 2000; Katsumi et al. 2008; Di Emidio 2010; Di Emidio et al. 2010; Scalia et al. 2014; Scalia and Benson 2016; Tian et al. 2016a,b; Scalia and Benson 2017; Tian et al. 2017; Scalia et al. 2018; Tian et al. 2019; Yu et al. 2020). Thus, an improved understanding of the mechanisms controlling the hydraulic compatibility of EB-GCLs produced with anionic polymers is needed to better understand of the long-term hydraulic performance of these EB-GCLs.

The purpose of this study was to investigate the mechanisms underlying improved hydraulic compatibility of EB-GCLs produced with anionic polymers. Physical (pore-clogging) and chemical (adsorption) polymer retention mechanisms are explored. Enhanced-bentonite GCLs prepared using EBs enhanced with the PA or CMC, or a covalently cross-linked, sodium polyacrylate (PAx), via dry sprinkling, dry mixing, or wet mixing methods were evaluated. An in-situ polymerized bentonite polymer composite (BPC) studied by others (e.g., Scalia et al. (2011), Scalia et al. (2014), Bohnhoff and Shackelford (2013), and Bohnhoff et al. (2013)) also was evaluated. Finally, a granular NaB (GNaB) and pyrophyllite were tested to determine the effect of interaggregate pore size and surface charge, respectively. Hydraulic conductivity tests at a low hydraulic gradient (i.e., 30 vs. 300) also were conducted to determine the effect of seepage forces and polymer retention or elution. Hydrogel formation tests, x-ray diffraction (XRD) analysis, and swell index (SI) tests were conducted to clarify the mechanisms controlling EB-GCL hydraulic compatibility. The results of this study further elucidate the understanding of the complex mechanisms underlying the improved hydraulic compatibility and performance of anionic-polymer EB-GCLs.

4.2 BACKGROUND

Understanding the behavior of anionic polymers in inorganic solutions provides a basis for an improved understanding of the role of anionic polymer-enhanced EB-GCLs. Anionic polymer behavior is affected by several factors that are variable in EB-GCLs applications. For example, the types and concentrations of dissolved ions present in hydrating and permeant solutions and the hydraulic shear applied within pores via applied hydraulic gradients will change the polymer configuration and distribution in the EB-GCL. Further

background on the primary factors governing the behavior of anionic polymers in inorganic solutions follows.

4.2.1 Anionic polymer properties and cross-linking

The architectures for the polymers used in this study are linear or cross-linked. A linear polymer comprises a single line of monomers and dissolves in aqueous solution. Cross-linked polymers contain branches that are linked to other polymer chains and can absorb water (swell) to form a hydrogel, which is an insoluble, three-dimensional network of cross-linked polymer chains (Buchholz and Graham 1998; Teraoka 2002).

The water solubility or degree of swelling of a polymer or a polymer network is controlled by the ionic groups along the polymer chains [e.g., negative carboxylate (COO^-)]. These ionic groups require ions of the opposite charge to satisfy electroneutrality. Anionic polymers require cations, and these cations are strongly solvated during hydration (Buchholz and Graham 1998).

Polymers can be cross-linked via covalent or physical (ionic or hydrogen bonding) cross-linking. If an anionic polymer does not contain cross-linked networks, the polymer is water soluble (Buchholz and Graham 1998; Teraoka 2002). Covalent cross-linking is permanent and occurs when two polymer chains are covalently bonded together. Covalent cross-linking can occur either from the copolymerization of a primary monomer with a di-, tri-, or tetra monomer in a free-radical initiated addition polymerization or through a polymer chain reaction with a di- or tri-functional reagent, i.e., esterification of poly(acrylic acid (Buchholz and Graham 1998; Plischke et al. 1999). Poly(acrylic acid) that is covalently cross-linked is known as cross-linked polyacrylate (PAx).

Physical (ionic) cross-linking occurs when a polyvalent ion, with a charge opposite to that of the polymer, bonds with two polymer chains (Jackson and Matthews 1994). Physical cross-linking also occurs when two polymer chains are connected via a hydrogen bond between branches or chains (Faulks and Schlinz 1994). The potential for crosslinking of water-solvated linear polymers is a function the presence of reactive groups attached to the polymer chain. The solubility of the linear polymer is a function of the

polymer's polar groups, such as the carboxyl group on the PA, which are available for many different chemical reactions, such as physical crosslinking (e.g., Finch 1983).

4.2.2 Polymer viscosity

Linear anionic polymers tend to behave as Newtonian viscosity (η_o) fluids at low shear rates representing entangled polymer chains. The viscosity decreases with increasing shear rate (shear thinning) until reaching a second, limiting Newtonian viscosity (η_∞), which represents entirely untangled chains (Van Krevelen 1990). High molecular-weight polymers reflect non-Newtonian behavior due to the disentanglement and reorientation of polymer chains in the direction of flow (Markovitz and Kimball 1949).

The conformation of anionic polymers in solution dictates the viscosity of the solution and depends on the polymer molecular weight or chain length and the degree of ionization (DOI). The DOI is determined by the proportion of neutral particles that are ionized into charged particles. For PA, the DOI is equivalent to the ratio of deprotonated to protonated carboxyl groups (i.e., COO^-/COOH). As the DOI increases resulting in an increase in the proportion of COO^-, repulsion of COO^- groups extends the polymer chains which increases the stiffness of the hydrated polymer (Buchholz and Graham 1998).

Anionic polymer DOI also is dependent on the ionic strength, I (= $\frac{1}{2}\Sigma c_i z_i^2$, where c_i = molar concentration of ionic species i, and z_i = charge of ionic species i), of the solution in which the polymer is dissolved. Polymer chains can take various shapes in solution (e.g., extended chain, folded chain, swarm) in both interface and bulk regions. At low salt concentrations (low I), anionic polymer chains are highly extended, but the chains coil at high concentrations (high I) as the negatively charged sites are screened by cations, lowering the DOI and allowing for closer proximity between chains (e.g., Van Krevelen 1990).

Covalently cross-linked polymer rheology is dependent on the degree of swelling and the shear modulus of the swollen polymer gel, both of which are governed by the elastic gel structure (Buchholz and Graham, 1998). In contrast, the rheology of physically cross-linked polymers has not been defined extensively due to the temporary nature of the cross-linking, although the shear modulus has been shown

to relate to crosslink bond strength (Henderson et al. 2010). However, the effect of cross-linked polymer on solution viscosity is limited to the solution that takes part in hydrogel swelling and does not extend to the viscosity of the bulk solution.

4.2.3 Hypothesized mechanisms of EB-GCLs

Mechanisms underlying the low hydraulic conductivity of EBs to aggressive inorganic solutions differ from those of traditional NaB (Onikata et al. 1996, 1999; Trauger and Darlington 2000; Katsumi et al. 2001; 2008; Schroeder et al. 2001; Ashmawy et al. 2002; Kolstad et al. 2004; Guyonnet et al. 2009; Di Emidio et al. 2010, 2011; Mazzieri et al. 2010; Naismith et al. 2011; Scalia et al. 2011; Bohnhoff et al. 2013; Scalia et al. 2014; Tian et al. 2016a,b; Tian et al. 2017; Scalia et al. 2018; Tian et al. 2019; Chai and Prongmanee 2020; Reddy et al. 2020). Current hypotheses for the mechanisms controlling the enhanced hydraulic compatibility of anionic polymer EB-GCLs include: (1) pore-clogging occurring in bentonite polymer composite (BPC), HYPER clay (HC), and densely pre-hydrated (DPH)-GCL (Scalia et al. 2014; Tian et al. 2016a,b; Tian et al. 2017; Scalia et al. 2018; Tian et al. 2019), and (2) enhanced osmotic swell through chemical intercalation occurring in HC (Di Emidio 2010; Di Emidio et al. 2010).

In HC and DPH-GCLs, both of which comprise EBs modified with CMC, XRD analysis has been used to support the hypothesis that CMC intercalates between sodium montmorillonite (MMT) platelets within NaB (Schroeder et al. 2001; Kolstad et al. 2004; Katsumi et al. 2008; Di Emidio et al. 2010). In contrast, other studies indicate that intercalation generally does not occur for anionic polymers (Ruhrwein and Ward 1952; Hagin and Bodman 1954; Emerson 1955; Theng 1970; Gunger and Karaoglan 2001; Deng et al. 2006; Lagaly et al. 2006; Scalia et al. 2014), except for some humic substances (acting as natural polyanions) and polyacrylate when the pH of the mixing solution is less than four (Theng et al. 1986; Satoh and Yamane 1971; Billingham et al. 1997).

Scalia et al. (2014) postulated that the mechanism controlling the low measured hydraulic conductivity of EB-GCLs comprising EBs enhanced with BPC upon permeation with concentrated ($\geq$ 50 mM) $CaCl_2$ solutions was clogging of pores by cross-linked polyacrylate. Tian et al. (2016a,b; 2019) also

noted the lack of a correlation between the swell index and hydraulic conductivity for BPC and commercially produced EB-GCLs comprising proprietary polymer-enhanced bentonites, which suggested that, unlike conventional GCLs, swelling was not the primary mechanism governing the low hydraulic conductivity of the EB-GCLs.

Tian et al. (2019) used scanning electron microscopy (SEM) on specimens of EB-GCL enhanced with BPC that had been permeated with 20 mM or 200 mM $CaCl_2$ and then freeze-dried to illustrate the segregation of the bentonite and polymer in pores of the EB-GCL. Dehydrated polymer hydrogel strands were visible in the pores of the specimen permeated with 20 mM $CaCl_2$, but almost nonexistent in the specimen permeated with 200 mM $CaCl_2$. The difference in the presence of hydrogel in the pores was consistent with the low hydraulic conductivity to the 20 mM $CaCl_2$ (1.2×10^{-11} m/s) and high hydraulic conductivity to the 200 mM $CaCl_2$ (2.9×10^{-8} m/s). These results support the hypothesis that the polymer can effectively clog or block pores within the EB-GCL to produce a low hydraulic conductivity.

4.3 MATERIALS

Several materials were used in this study, including both powdered and granular NaB, CMC with two different viscosities, non-crosslinked linear PA with three different molecular weights, a cross-linked PA (PAx), the aforementioned BPC, and pyrophyllite. The CMCs are designated as CMCLV and CMCHV corresponding to CMC with low viscosity and high viscosity, respectively, and the PAs are designated as PALW, PAMW, and PAHW corresponding to PA with low, medium, and high molecular weights, respectively. The polymer mass loadings that were evaluated included 5, 8, and/or 10 %, and the number appended to the aforementioned designations represents the mass percentage of the polymer added to the NaB to comprise the EB. For example, PALW5 indicates that 5% of the PALW by mass was added to 95% of the NaB by mass. Finally, the EBs are designated as DS, DM, and WM to indicate the method of preparation as dry sprinkling, dry mixing, and wet mixing, respectively. In addition to these solid materials, different chemical solutions were used as hydrating and permeating liquids. Further details on these materials follow.

4.3.1 Sodium bentonite

The NaB used in this study was obtained from Colloid Environmental Technologies Company (CETCO, Hoffman Estates, IL, USA), and is the same NaB used in Bentomat® GCLs as well as other studies on GCL behavior (Scalia et al. 2011; Bohnhoff 2012; Bohnhoff and Shackelford 2013; Bohnhoff et al. 2014; Scalia et al. 2014). The NaB was evaluated in both powdered form (PNaB) and granular (GNaB) form. The PNaB was generated by grinding the GNaB to pass a No. 200 sieve (0.075 mm). The particle-size distributions (PSDs) for both the PNaB and the GNaB are shown in Figure 4.1a, where the PSD for the GNaB is based on a dry analysis by passing the NaB through a stack of sieves in accordance with the procedure for coarse-grained materials (e.g., see Howell et al. 1997; Shackelford et al. 2000, data taken from Scalia et al. 2011), and the PSD for the PNaB is based on both the dry sieve analysis and the results of a hydrometer analysis (ASTM D422 (ASTM 2007) taken from Bohnhoff (2012). The resulting PSDs based on the mechanical sieve analyses for both the GNaB and PNaB resembles that of a clayey sand (SC) based on the Unified Soil Classification System (ASTM D2487 (ASTM 2010) whereas the PSD for the PNaB based on the hydrometer analysis is consistent with that for a high plasticity clay (CH). As shown in Table 4.1, the NaB exhibited a swell index in deionized water (DIW) of 31.4 mL/2 g, and a cation exchange capacity (CEC) of 78 $cmol^{+}/kg$. The exchange sites were occupied by approximately 44% Na, 36% Ca, 17% Mg, and 2% K.

4.3.2 Pyrophyllite

Pyrophyllite also was tested to investigate the effect of clay mineral surface charge. Pyrophyllite is a layered aluminosilicate clay mineral with the same 2:1 crystalline structure as montmorillonite, the primary mineral in NaB (Table 4.1), but is neutral due to a lack of isomorphic substitution which results in zero net layer charge. As a result, there are no exchangeable interlayer cations and no CEC for pyrophyllite. The PSD of the pyrophyllite based on the mechanical sieve analysis is provided in Figure 4.1and is essentially identical to that for the PNaB. More information on the pyrophyllite structure is provided in Appendix C.

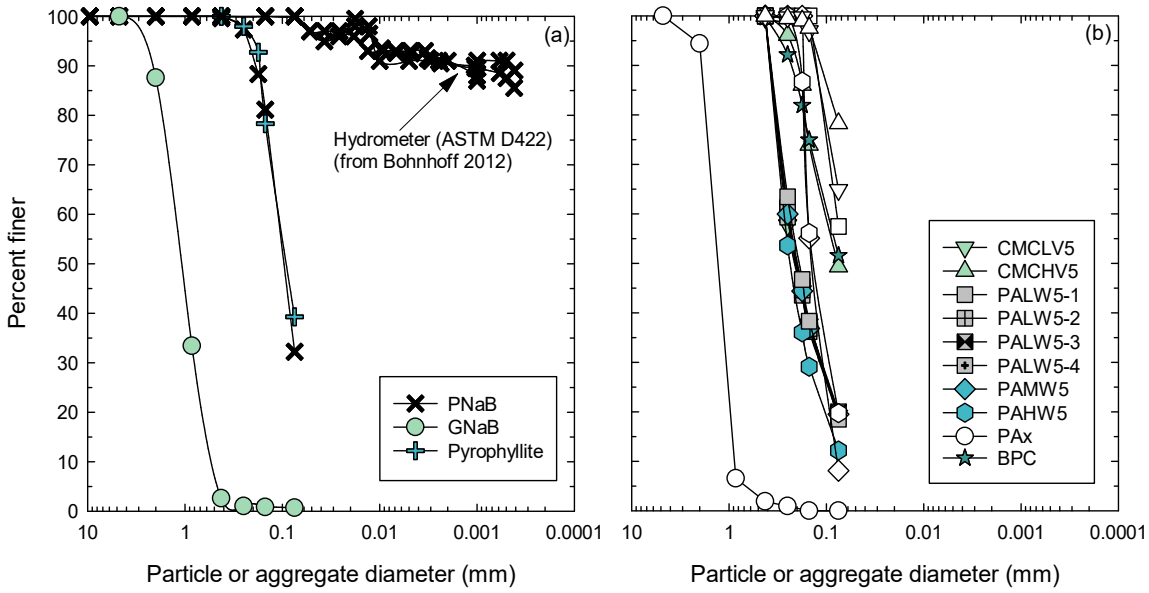

Figure 4.1: Particle-size distributions of materials based on mechanical dry-sieve analysis unless otherwise indicated: (a) base materials including powdered sodium bentonite (PNaB), granular sodium bentonite (GNaB) from Scalia et al. (2011), and pyrophyllite; (b) dry-sieved raw polymers (open symbols) and wet-mixed (WM) enhanced bentonites at 5% polymer mass loading (closed symbols) produced using PNaB, including sodium carboxymethylcellulose with low viscosity (CMCLV) and high viscosity (CMCHV), and poly(acrylic acid) with low, medium and high molecular weight (PALW, PAMW, PAHW), and covalently crosslinked PA (PAx), and bentonite polymer composite (BPC).

Table 4.1: Selected properties of the sodium bentonite (NaB) used in this study as compared with those for the bentonite polymer composite (BPC) (adapted from Scalia et al. 2014).

Property	Standard/Method	NaB	BPC
Swell index (mL/2 g)	ASTM D5890-06	31.4	72.7
Atterberg limits [a]:	ASTM D4318-10		
Liquid limit, *LL*		420	255
Plasticity index, *PI*		381	ND [b]
Unified Soil Classification	ASTM D2487-11	CH	CH
Carbonate content (%)	ASTM D4373-14	1.3	0.0
Montmorillonite content (%)	X-ray diffraction (10 samples)	85-91	73-77
Cation exchange capacity, CEC ($cmol^+/kg$)	ASTM D7503-18	78.0	142.6
Soluble metals ($cmol^+/kg$):	ASTM D7503-18		
Ca		0.2	9.5
Mg		0.1	1.6
Na		18.1	118
K		0.4	0.4
Bound/exchangeable metals (mole fraction):	ASTM D7503-18		
Ca		0.36	0.06
Mg		0.17	0.02
Na		0.44	0.90
K		0.02	0.02

[a] Taken from Bohnhoff 2012. [b] Plastic limit (and thus *PI*) for BPC could not be determined.

4.3.3 Bentonite polymer composite

The BPC used in this study was prepared by the polymerization of acrylic acid within a bentonite slurry, and is the same BPC used in previous studies by Scalia et al. (2011), Bohnhoff and Shackelford (2013), Bohnhoff et al. (2013), and Scalia et al. (2014). The BPC was prepared using the same GNaB as used in this study. As indicated in Table 4.1, the swell index and CEC of the BPC are high (72.7 mL/2 g, and 142.6 $cmol^+/kg$), with Na occupying approximately 90% of the exchange sites. For use in this study, the BPC was ground to a powdered form by mortar and pestle with 51.6% of the particles < 0.075 mm (see Figure 4.1b).

The BPC was tested as intact (i.e., pure BPC), which contained 28.5% polymer by mass, and as a dry-mixed enhancement of the PNaB at 5% polymer by mass (i.e., 17.3% BPC by mass).

4.3.4 Sodium carboxymethylcellulose

Two types of CMC were used in this study, viz., the CMCLV produced by Calbiochem® (Millipore Sigma, Burlngton, MA, USA) and the CMCHV produced by MP Biomedical (Irvine, CA, USA). The molecular weight of CMCHV, calculated from the degree of substitution (DoS = 0.65-0.85) and average chain degree of polymerization (DP) of 3200 provided by the manufacturer, was 685290-736500 g/mol (i.e., $[C_6H_7O_2(OH)_x(OCH_2COONa)_y]_n$, where n is the DP, x + y =3, and y is the DoS). The average molecular weight and DoS of the CMCLV were not provided by the manufacturer. The PSDs for the two CMCs shown in Figure 4.1b were based on the unaltered material provided directly from the manufacturer.

4.3.5 Poly(acrylic acid)

The three different linear, anionic PAs used in this study were all produced by Polysciences Inc. (Warrington, PA, USA). The molecular weights of the PALW, PAMW, and PAHW as provided by the manufacturer were approximately 5000, 50000, and 345000 g/mol, respectively. None of these PAs were covalently crosslinked.

When needed for preparation of EB-GCLs as dry mixtures (described subsequently in Methods), the PA in solution was air dried until solidified and then ground and screened. Grinding of the polymer was completed using a rotary blade grinder (KitchenAid BCG211OB Blade Grinder; Benton Harbor, MI, USA). The PA was ground to achieve a similar PSD as the base PNaB to allow for homogeneous mixing (Shackelford et al. 2000; Malusis and Scalia 2007). The PSDs of each dried PA, based on dry sieving, are shown in Figure 4.1b.

A crosslinked PAx also was used in this study for comparison with the linear, non-crosslinked PAs. The PAx was a partial sodium salt-graft-poly(ethylene oxide) (sodium salt) from Aldrich Chemistry (St. Louis, MO, USA). The average molecular weight of the PAx was not provided by the manufacturer. The PSD of PAx, based on dry sieving, is shown in Figure 4.1b.

4.3.6 Hydrating and permeant solutions

Concentrated inorganic solutions, i.e., 167 mM $CaCl_2$ and 500 mM NaCl, with I = 500 mM were used as hydrating and permeant solutions to evaluate the hydraulic conductivity of the prepared EB-GCLs. The electrical conductivity (*EC*) and pH of the 167 mM $CaCl_2$ solution were 3280 mS/m and 5.8, respectively, whereas the respective *EC* and pH of the 500 mM NaCl were 4850 mS/m and 6.2, respectively. The $CaCl_2$ solution was prepared with $CaCl_2$ di-hydrate, $CaCl_2 \bullet 2H_2O$ (Alfa Aesar; Ward Hill, MA, USA) and DIW. The NaCl solution was prepared with anhydrous NaCl (Fisher Chemical; Hampton, NH, USA) and DIW. The prepared solutions were stored in collapsible carboys with no headspace to limit interaction with the atmosphere.

4.4 METHODS

4.4.1 Bentonite modification

The EBs were prepared using three mixing methods: dry sprinkling (DS), dry mixing (DM), and wet mixing (WM). Dry-sprinkled EBs were prepared by sprinkling a known percentage (by mass) of air-dried polymer evenly as a layer at the inflow side (bottom) of the GCL specimen before placing the air-dried NaB on top (EBs were prepared with PNaB unless otherwise indicated).

Dry-mixed EBs were prepared by adding a percentage (by mass) of air-dried polymer to air-dried NaB. The masses were not corrected for the gravimetric, air-dried (hygroscopic) water content of the NaB of 8.0%. The mixture was rotated end-over-end in a sealed container at 30 rpm for 1 min.

Wet-mixed (WM) EBs were created by first adding a known, target percentage of 5% of air-dry polymer by mass of air-dry NaB into 350 mL of DIW. For wet-mixed EBs prepared with both CMCLV and CMCHV, the air-dried CMC was added to 350 mL of DIW in a mechanical stirrer (Hamilton Beach Single Spindle Drink Mixer, Glen Allen, VA, USA) set to the highest operating speed (18,000 rpm). The CMCs and DIW were mixed for 5 min to allow for the dispersion and hydration of the dried polymer. After 5 min, 50 g air-dried NaB was added in the mechanical stirrer cup with another 150 mL of DIW and mixed at 18,000 rpm for 10 min. Resulting in a total of 500 mL of DIW added and a total mixing time of 15 min.

The EBs wet-mixed with PA were prepared in a similar manner to those wet-mixed with CMC, except the total volumes of DIW for the mixtures containing PALW and PAMW were reduced due to the excessive foam produced by the high shear mixing of PA and DIW. First, the PA was added to the 350 mL of DIW in the hydrated form provided by the manufacturer with a target polymer content of 5 or 8% by mass. After 1 min of mixing (shortened from 5 min due to foaming), 50 g of air-dried NaB was added to the mechanical stirrer. Finally, an additional 75 mL or 150 mL of DIW was added for the mixtures containing PAMW or PAHW, respectively, and mixing continued for an additional 14 min for a total period of 15 min, which was the same as that for the EBs wet-mixed with CMC. The total volumes of DIW, i.e., 350, 425, and 500 mL for the PALW, PAMW, and PAHW mixtures, respectively, reflected the maximum amount of DIW that could be added to the mixture to fill the cup without losing slurry while mixing. The wet-mixed EBs then were oven dried at 105 ºC for 24 h and ground using the rotary blade grinder until 100% passed the U.S. No. 40 sieve (0.420 mm). The particle-size distributions of the wet-mixed EBs are shown in Figure 4.1b. All wet-mixed materials had similar particle-size distributions. The PSDs for four batches of the wet-mixed PALW5 (labelled PALW5-1 to PALW5-4 in Figure 4.1b) were measured to evaluate the grinding consistency of the rotary grinder. As shown in Figure 4.1b, the rotary grinder produced similar PSDs for all replicates.

4.4.2 Geosynthetic clay liner specimens

The hydraulic conductivity of the tested specimens (i.e., unenhanced bentonites (PNaB and GNaB), pyrophyllite and enhanced pyrophyllite, and enhanced bentonites prepared using the dry and wet mixing methods) was measured in the form of unreinforced GCL specimens. The layers of a typical GCL were reproduced with each EB following the method described in Scalia et al. (2014). A non-woven, calendared geotextile (PolySpun heavy-duty landscape fabric) with a mass/area of 0.08 kg/m^2 was placed below and then above a layer of EB. An additional non-woven geotextile with a mass per area of 1 kg/m^2 was placed below and above the GCL to serve as the bounding drainage layers in place of porous stones and filter paper as per Scalia et al. (2014). Specimens were prepared in flexible-wall permeameters with a 152.4 mm

diameter in an even layer at 4.5 kg/m^2. This bentonite mass per area is similar to that for commercial GCLs (e.g., Koerner 2005). The resulting GCL specimen compositions and designations are given in Table 4.2.

Table 4.2 GCL specimen compositions and designations.

Base clay	Polymer type	Polymer molecular weight or viscosity	Target polymer content (%)	Mixing method	GCL designation
PNaB	NA	NA	NA	NA	PNaB
GNaB	NA	NA	NA	NA	GNaB
Pyrophyllite	NA	NA	NA	NA	Pyrophyllite
BPC	PA	Unknown	28.5	ISP	BPC
PNaB	PA	Unknown	5	DM	BPC5DM
PNaB	CMC	LV	5	DM	CMCLV5DM
PNaB	CMC	HV	5	DM	CMCHV5DM
PNaB	CMC	HV	5	WM	CMCHV5WM
PNaB	PA	LW	5	DS	PALW5DS
PNaB	PA	LW	5	WM	PALW5WM
PNaB	PA	MW	5	DS	PAMW5DS
PNaB	PA	MW	8	DS	PAMW8DS
Pyrophyllite	PA	MW	8	DS	PAMW8DS
PNaB	PA	HW	5	DS	PAHW5DS
GNaB	PA	HW	5	DS	PAHW5DS
Pyrophyllite	PA	HW	5	DS	PAHW5DS
Pyrophyllite	PA	HW	32	DS	PAHW32DS
PNaB	PA	MW	5	WM	PAHW5WM
PNaB	PAx	Unknown	5	DS	PAx5DS

Notes: NA = not applicable; PNaB = powdered sodium bentonite; GNaB = granular sodium bentonite; BPC = bentonite polymer composite; CMC = carboxymethylcellulose; PA = poly(acrylic acid); PAx = covalently cross-linked polyacrylate; LV = low viscosity; HV = high viscosity; LW = low molecular weight; MW = medium molecular weight; HW = high molecular weight; ISP = in-situ polymerization; DS = dry sprinkle; DM = dry mixed; WM = wet mixed.

4.4.3 Hydraulic conductivity

Hydraulic conductivity tests were performed using flexible-wall permeameters following ASTM D6766-18 (ASTM 2018) and the falling headwater, constant tailwater method, except backpressure was not applied (e.g., Kolstad et al. 2004; Lee and Shackelford 2005; Meer and Benson 2007; Bradshaw and Benson 2013; Scalia et al. 2014; Tian et al. 2016). Prior to permeation, each specimen was hydrated for 48 h in the permeant solution under an average effective confining stress of 27 kPa. The total confining stress of 34.3 kPa was applied during hydration and throughout the hydraulic conductivity testing via gravity head applied by an elevated water tank. Flushing of the primary inflow circuit was initially performed to introduce

hydrating liquid to the lower GCL boundary and promote hydration, but other lines were not flushed to reduce a possible loss of polymer from the system prior to permeation. As per Jo et al. (2005), 6.4-mm (0.25-in)-diameter tubing was used to prevent clogging of the tubing during permeation. For most tests, a target average hydraulic gradient (i) of 200 was applied via gravity head using glass burettes (falling headwater). The target hydraulic gradient was based on an assumed typical hydrated GCL thickness of 7.5 mm. A hydraulic gradient of 200 to 300 is typical for hydraulic conductivity testing of GCLs due to the typically low k (Shackelford et al. 2000; Scalia et al. 2014). However, the final average hydraulic gradients for the permeated specimens ranged from 122 to 473 due to thinner-than-expected final thicknesses (i.e., 3.01 to 7.00 mm) resulting from a significant reduction in swelling of the NaB in the aggressive inorganic solutions as well as material loss via polymer elution.

Each specimen was permeated from bottom (inflow) to top (outflow) at least until the ASTM D6766 termination criteria were achieved. The primary termination criteria include: (1) a ratio of outflow to inflow within 1.00±0.25; (2) at least two pore volumes of flow (PVF) passed through the specimen; and (3) establishment of chemical equilibrium between the outflow and the inflow based on a ratio of outflow-to-inflow electrical conductivity (EC) within 1.0±0.1. Other requirements include: (i) at least three values of flow rate; (ii) flux and hydraulic conductivity determined over a minimum time period of 8 h; (iii) no significant upward or downward trend in the hydraulic conductivity for the last three measurements; (iv) none of the last three flow rate values less than 0.75 times nor greater than 1.25 times the average flow rate; and (v) flux and hydraulic conductivity based on the average of the last three consecutive measured values. However, since the potential impact of polymer elution is not considered by the ASTM D6766 termination criteria, permeation was continued beyond the duration required by ASTM D6766 for all but one specimen to evaluate the applicability of the ASTM D6766 termination criteria for EB-GCLs.

However, since the ASTM D6766 termination criteria do not consider the behavior of the enhancement during permeation, such as the potential impact of polymer elution, permeation was continued beyond the duration required by ASTM D6766 for all but two specimens to evaluate the applicability of

the ASTM D6766 termination criteria for EB-GCLs. The potential for preferential flow also was evaluated by adding 5 mg/L Rhodamine WT dye to the influent as described in Scalia and Benson (2011).

As indicated by the PSDs in Fig. 4.1, air-dried GNaB is expected to have larger interaggregate pore sizes than PNaB. Thus, hydraulic conductivity tests on specimens of GNaB and EB-GCLs prepared with GNaB and with 5% of PAHW by dry sprinkling also were conducted for comparison with those based on PNaB and the same EB-GCLs except prepared with GNaB to investigate the effect of interaggregate pore size. Also, to evaluate the effect of clay mineral surface charge, hydraulic conductivity tests were conducted using specimens of pyrophyllite and EB-GCLs prepared by dry sprinkling of PAMW at 8% polymer mass loading and PAHW at 5% and 32% polymer mass loadings. with pyrophyllite and DS PAHW at 5% loading, DS PAMW at 8% polymer loading, and DS PAHW at 32% polymer loading. The 32% PAHW polymer loading was evaluated to determine the potential of significant polymer loading to block the pores of an EB-GCL specimen without a potential for polymer adsorption via cation bridging (see Chapter 2). Finally, to evaluate the effect of the applied hydraulic gradient on the measured hydraulic conductivity of the EB-GCLs, hydraulic conductivity tests were reproduced at a lower target gradient of 30 for EB-GCL specimens enhanced by dry sprinkling with 5% PAHW and 5% PALW and permeated with 167 mM $CaCl_2$.

4.4.4 Post-permeation polymer quantification

Total organic carbon (TOC) was used to quantify polymer remaining in an EB-GCL specimen at termination of permeation. Solid total carbon (TC) analysis (per the Component B total carbon (TC) analysis method from Chapter 3) was completed in triplicate on oven-dried (110 ^{o}C) samples by combustion in an induction furnace using a LECO TrueSpec CN analyzer (LECO Corporation, St. Joseph, MI, USA). The baseline TC for the NaB (valid for both GNaB and PNaB) and polymers used to prepare the EBs are reported in Table 4.3.

Table 4.3: Baseline total carbon (TC) contents for sodium bentonite (NaB) and polymers used as enhancements (CMCHV, CMCLV, PAHW, PAMW, PALW, PAx).

Material	TC (%)	Standard deviation (%)
NaB	0.3677	0.0034
CMCHV	47.29	0.2839
CMCLV	47.31	0.4507
PALW	49.72	0.1282
PAMW	35.88	0.0739
PAHW	36.52	0.0707
PAx	37.04	0.5120

As discussed in Chapter 3, TC analysis does not differentiate between total inorganic carbon (TIC) and total organic carbon (TOC). Studies have shown that permeation of bentonites can result in dissolution of calcium carbonate ($CaCO_3$) inherent in the bentonite (e.g., Freeze and Cherry 1979; Shackelford 1994; Guyonnet et al. 2005), resulting in a reduction in the TIC and, therefore, TC of the bentonite. However, because TC is the sum of TIC and TOC (TC = TIC + TOC), TC also can decrease due to a reduction in TOC, for example, by elution in organic matter in traditional NaB and/or polymer in an EB. For this reason, TOC was calculated in the pre- and post-permeated conventional GCL and EB-GCL specimens (see Chapter 3).

To investigate the impact of potential changes in TOC and TIC in the pre- and post-permeated conventional GCLs and EB-GCLs, both TC and TIC were measured to determine the TOC content as follows:

$$\text{TOC} = \text{TC} - \text{TIC} \tag{4.1}$$

With the measured TC and TIC values, and calculated TOC values, the mass fraction of the polymer (m_p) was determined from the following relationships:

$$m_p + m_b = 1 \tag{4.2}$$

and

$$TOC_b m_b + TOC_p m_p = TOC_{eb} \quad (4.3)$$

Where TOC_{eb} is the total organic carbon content of the EB, TOC_b and TOC_p are the respective individual TOC for the bentonite and the polymer components of the EB, and m_b is the fraction of total mass represented by the bentonite in the EB-GCL. Finally, the combination of Eqs. 4.2 and 4.3 results in the following expression for the polymer content:

$$m_p = \frac{TOC_{eb} - TOC_b}{TOC_p - TOC_b} \quad (4.4)$$

The TIC in the EB and NaB specimens was presumed to be equivalent to the total soil $CaCO_3$, which was measured using the modified pressure-calcimeter method (Sherrod et al. 2002). The TIC was measured for pre-permeated specimens of the unenhanced materials (GNaB, PNaB, and pyrophyllite) and the EBs and post-permeated specimens of each unenhanced GCL and EB-GCL. The initial TC, TIC, and TOC contents of the NaB and each wet-mixed EB are given in Table 4.4. The measured TC and TIC represent an average value based on measurements of three specimens.

Values of measured TOC presented in Table 4.4 represent the presence of organic carbon in the tested material. For NaB and pyrophyllite, the initial TOC is representative of a small fraction of initial organic matter present in the soil. For BPC and the wet-mixed EBs, the TOC represents the combination of the initial organic content of the PNaB and the polymer content. As mentioned, the base polymer should be tested for TOC separately to form a baseline and to accurately calculate the mass fractions of bentonite and polymer in the EB. The base polymer for the BPC was not available so calculations of polymer content for the BPC were completed using the baseline TOC of PAHW. Due to this assumption, the initial polymer content of BPC of 22.78 % is less than the reported polymer content of BPC of 28.5 % from Scalia et al. (2014). For this reason, the initial and final polymer contents of the BPC should not be considered precise, but instead, illustrate the change in polymer content from pre- to post-permeation.

The target polymer content for the wet-mixed EBs was 5 %. As seen in Table 4.4, PAHW5WM was closest to this target, while PALW5WM fell 15 % lesser than the target polymer content and CMCHV5WM fell more than 20 % greater than the target polymer content. The variation in the initial polymer contents of the wet-mixed EBs from the target 5 % is expected to be an artifact of the preparation method which may lose polymer during mixing or transfer or unevenly distribute polymer throughout the EB.

Table 4.4: Initial, pre-permeation polymer contents determined from measured total carbon (TC), total inorganic carbon (TIC), and total organic carbon (TOC) contents for sodium bentonite (NaB), pyrophyllite, and enhanced bentonites including bentonite polymer composite (BPC) and anionic polymers (CMCHV, PALW, and PAHW) wet mixed (WM) with PNaB at a target polymer mass content of 5%.

Material	TC (%)		TIC (%)		Average TOC (%)	Polymer Content (%)
	Average value	Standard deviation	Average value	Standard deviation		
NaB	0.3677	0.003	0.215	0.011	0.153	0.0
Pyrophyllite	0.0908	0.002	0.008	0.004	0.082	0.0
BPC	11.12	0.107	0.013	0.002	11.11	22.79[a]
CMCHV5WM	2.232	0.017	0.278	NA	1.954	5.848
PALW5WM	2.197	0.030	0.186	NA	2.011	3.750
PAHW5WM	2.599	0.015	0.109	NA	2.490	4.958

NA = not applicable due to insufficient number of samples for determination
[a] Calculated assuming baseline polymer loss equivalent to PAHW

4.4.4 X-ray diffraction

Polymer intercalation was evaluated via powder XRD measurements using a Bruker D-8 Discover DaVinci X-ray diffractometer (Billerica, MA, USA) with Cu-Kα X-ray source, line focus. A 0.6-mm divergent slit was placed on the primary beam side and a high-resolution energy-dispersive LYNXEYE-XE-T detector (Bruker, Billerica, MA, USA) was placed on the diffracted beam side during the XRD measurements. Measurements were performed with soller slits on the primary and diffracted beam side (2.5° separation). The instrument alignment was verified per NIST 1976b SRM. Samples of NaB and wet-mixed EBs were dried at 110 ºC and manually ground to pass the No. 200 sieve (0.075 mm). Powder samples were placed and lightly compacted in a sample holder with a circular depression for measurement.

4.4.5 Swell index

Swell index was measured to observe the effects of polymer modification on the free swelling of the mixture. Tests were conducted with tap water (pH = 6.38, EC = 9.56 mS/m) and the two salt solutions following ASTM D5890-11 (ASTM 2011). The base NaB and wet-mixed EB were ground using a mortar and pestle until 100% passed the No. 200 sieve. To avoid possible polymer mass loss due to sieving (Christian et al. 2020), the dry-mixed EBs were not ground but instead were prepared by mixing the dry polymers with the NaB that passed the No. 200 sieve.

4.4.6 Hydrogel formation

Four types of hydrogel-formation tests were conducted to evaluate hydrogel development upon exposure to the hydrating and permeant solutions. Each test was designed to allow interpretation of factors such as kinetics, solution chemistry, and polymer type that can affect hydrogel formation.

The first test method was used to observe the potential hydrogel formation (cross-linking potential) of PAHW in solutions over a range of NaCl and $CaCl_2$ concentrations. One gram of dry PAHW was placed into the bottom of a 50-mL centrifuge tube and then 25 mL of a salt solution, including 1.67, 33.33, or 167 mM $CaCl_2$ or 5, 100, or 500 mM NaCl, was added to the tube. After initial observations, the tubes were left at rest for three months to observe any changes in hydrogel formation over time.

A second test method was used to determine if hydrogel had the potential to form during the 48-h hydration period prior to permeation of an EB-GCL. Dry PAx or PAHW polymer was layered between two non-woven geotextiles and hydrated with 80 mL of 500 mM NaCl or 167 mM $CaCl_2$ for 48 h inside a beaker sealed with parafilm. After the 48-h period, the tests were disassembled and inspected for hydrogel formation.

A third test method was adopted as a variant of the second test method to determine the impact of bentonite on hydrogel formation in the 48-h hydration period and mimic the hydration of an EB-GCL without applied cell pressure or effective stress. The procedure was the same as that for the second test

method except an additional layer of PNaB was included above the PAHW layer at 5% mass loading, i.e., the PAHW represented 5% of the total PNAB plus PAHW mass (similar to the dry-sprinkle preparation method of the EB-GCL). After 48 h, the tests were disassembled and inspected for hydrogel formation.

Finally, the purpose of the fourth test method was to provide clarity on the hydrogel formation in EB-GCLs hydrated with 500 mM NaCl. An EB-GCL enhanced by dry sprinkling 5% by mass of PAHW was hydrated in a permeameter with 500 mM NaCl for 48 h following the same method of GCL hydration prior to permeation. After 48 h, the test was disassembled and the EB-GCL was inspected for hydrogel formation.

4.5 RESULTS

4.5.1 Hydraulic conductivity and polymer retention

The testing durations and final physical properties of the conventional GCL and EB-GCL specimens are summarized in Table 4.5, and the hydraulic conductivity and polymer content results are summarized in Table 4.6. Two values of hydraulic conductivity values are shown in Table 4.6, i.e., those based on ASTM D6766 termination criteria (k_{6766}) and those corresponding to the end of permeation (k_f). These values for the specimens prepared with PNaB were previously summarized in Tables 1.3 and 1.4 (Chapter 1). However, the final polymer contents for these specimens were not presented or discussed in Chapter 1. Unless otherwise noted, all hydraulic conductivity values referred to subsequently are the standardized values, i.e., k_{6766}.

Table 4.5: Final properties of conventional and EB GCL specimens.

GCL designation	Base clay	Permeant solution	Elapsed time, t (d)		Pore volumes of flow, PVF		Final specimen properties		
			t_{6766}	t_f	PVF_{6766}	PVF_f	d_f (mm)	L_f (mm)	w_f
PNaB	NA	167 mM $CaCl_2$	1.6	5.6	3.0	9.2	150.3	6.80	0.80
		500 mM NaCl	1.7	4.8	2.6	5.9	152.4	6.10	0.86
GNaB	NA	167 mM $CaCl_2$	<1	<1	2.2	4.9	150.3	6.40	0.84
		500 mM NaCl	<1	<1	2.2	9.1	147.0	6.40	0.74
Pyrophyllite	NA	167 mM $CaCl_2$	<1	<1	5.6	10.4	146.0	4.40	0.57
		500 mM NaCl	<1	<1	6.0	11.4	147.2	4.30	0.58
BPC	BPC	167 mM $CaCl_2$	267	267	29.2	36.8	147.6	5.23	0.87
		500 mM NaCl	NA	85.5	NA	0.9	148.7	5.60	1.06
BPC5DM	PNaB	167 mM $CaCl_2$	44.0	77.0	4.1	11.5	148.0	5.90	0.69
		500 mM NaCl	61.5	143	2.9	11.5	149.1	6.20	0.82
CMCLV5DM	PNaB	167 mM $CaCl_2$	3.0	4.4	3.2	16.2	150.3	5.10	0.91
		500 mM NaCl	196	214	14.8	25.8	150.0	5.51	0.91
CMCHV5DM	PNaB	167 mM $CaCl_2$	65.4	65.5	14.2	21.4	149.0	5.60	0.97
		500 mM NaCl	199	216	18.7	31.3	145.9	5.75	0.96
CMCHV5WM	PNaB	167 mM $CaCl_2$	8.4	8.8	5.7	6.2	152.0	6.60	1.06
		500 mM NaCl	30.5	77.3	3.0	6.9	150.1	6.84	1.18
PALW5DS	PNaB	167 mM $CaCl_2$	1.4	3.7	8.2	16.1	150.7	4.30	0.76
		500 mM NaCl	2.7	18.0	6.6	19.1	149.9	5.30	0.94
PALW5WM	PNaB	167 mM $CaCl_2$	2.5	3.3	5.0	7.0	154.0	5.30	0.85
		500 mM NaCl	5.9	21.0	2.4	7.3	154.1	5.50	0.97
PAMW5DS	PNaB	167 mM $CaCl_2$	1.7	2.4	12.4	15.3	150.4	4.67	0.75
		500 mM NaCl	41.4	73.6	5.8	12.5	145.7	5.20	0.79
PAMW8DS	PNaB	167 mM $CaCl_2$	84.9	117	7.1	13.0	150.8	4.91	0.75
		500 mM NaCl	20.9	59.2	6.7	18.1	150.0	4.80	0.80
PAMW8DS	Pyrophyllite	167 mM $CaCl_2$	<1	<1	4.6	13.8	148.7	5.11	0.61
		500 mM NaCl	<1	<1	8.4	14.8	148.5	4.89	0.61
PAHW5DS	PNaB	167 mM $CaCl_2$	50.2	50.2	13.3	13.3	153.3	4.81	0.79
		500 mM NaCl	34.6	66.4	3.3	8.1	150.2	4.60	0.76
PAHW5WM	PNaB	167 mM $CaCl_2$	1.5	3.3	2.6	5.7	151.5	5.25	0.86
		500 mM NaCl	16.4	188	5.3	20.4	152.1	6.34	1.08
PAHW5DS	GNaB	167 mM $CaCl_2$	<1	<1	2.6	11.7	152.7	5.14	0.81
		500 mM NaCl	<1	<1	4.0	11.5	146.9	5.60	0.77
PAHW5DS	Pyrophyllite	167 mM $CaCl_2$	<1	<1	3.2	7.4	147.9	4.00	0.59
		500 mM NaCl	<1	<1	6.6	13.6	150.1	3.40	0.62
PAHW32DS	Pyrophyllite	167 mM $CaCl_2$	<1	<1	NA	11.4	142.9	3.01	0.59
PAx5DS	PNaB	167 mM $CaCl_2$	0.5	1.0	10.7	17.3	147.8	5.29	0.81
		500 mM NaCl	88.9	136	5.4	7.9	149.7	7.00	0.95

Notes: NA = not applicable; PNaB = powdered sodium bentonite; GNaB = granular sodium bentonite; t_{6766}, PVF_{6766}, = values based on ASTM 6766 termination criteria; t_f, PVF_f = final values at the end of testing; d_f = final specimen diameter; L_f = final specimen final thickness; w_f = final gravimetric water content

Table 4.6: Results of hydraulic conductivity tests for conventional and EB GCL specimens.

GCL designation	Base clay	Permeant solution	Hydraulic conductivity, k ($\times 10^{-10}$ m/s)		$k_{EB\text{-}GCL}/k_{PNaB}$	Polymer retention and elution (%)		
			k_{6766}	k_f[a,b,c]		P_i[d]	P_f[e]	P_f/P_i
PNaB	NA	167 mM $CaCl_2$	5.5	4.8	NA	0	0	NA
		500 mM NaCl	2.8	1.6	NA	0	0	NA
GNaB	NA	167 mM $CaCl_2$	2700	2600	NA	0	0	NA
		500 mM NaCl	2700	2300	NA	0	0	NA
Pyrophyllite	NA	167 mM $CaCl_2$	3500	3200	NA	0	0	NA
		500 mM NaCl	2900	2800	NA	0	0	NA
BPC	BPC	167 mM $CaCl_2$	1.6	1.4[a,c]	0.29	28.5[f]	7.39[g]	25.9
		500 mM NaCl	NA	0.023[b,c]	NA	28.5[f]	7.69[g]	27.0
BPC5DM	PNaB	167 mM $CaCl_2$	0.32	0.55	0.058	5	3.66[g]	73.2
		500 mM NaCl	0.11	0.19	0.039	5	1.82[g]	36.4
CMCLV5DM	PNaB	167 mM $CaCl_2$	1.4	31[a]	0.26	5	2.82	56.4
		500 mM NaCl	0.85	1.2	0.30	5	0.64	12.8
CMCHV5DM	PNaB	167 mM $CaCl_2$	140	180[a]	25	5	3.17	63.4
		500 mM NaCl	1.2	1.4	0.43	5	0.47	9.4
CMCHV5WM	PNaB	167 mM $CaCl_2$	3.7	3.8	0.67	5.85	4.17	93.3
		500 mM NaCl	3.3	2.3	1.2	5.85	3.07	61.4
PALW5DS	PNaB	167 mM $CaCl_2$	5.7	3.4[c]	1.0	5	1.42	28.4
		500 mM NaCl	2.4	1.4	0.86	5	0.07	1.4
PALW5WM	PNaB	167 mM $CaCl_2$	3.3	3.8	0.60	3.75	1.72	51.7
		500 mM NaCl	0.78	0.49	0.28	3.75	0.22	4.4
PAMW5DS	PNaB	167 mM $CaCl_2$	4.7	4.1	0.85	5	1.27	35.4
		500 mM NaCl	0.26	0.27	0.093	5	0.72	14.4
PAMW8DS	PNaB	167 mM $CaCl_2$	0.11	0.11[c]	0.020	8	2.54	31.8
		500 mM NaCl	0.29	0.33	0.010	8	1.25	16.0
PAMW8DS	Pyro	167 mM $CaCl_2$	3400	3400	620	8	0.42	5.3
		500 mM NaCl	670	1100	240	8	0.43	5.4
PAHW5DS	PNaB	167 mM $CaCl_2$	0.40	0.40[c]	0.073	5	0.68	12.8
		500 mM NaCl	0.13	0.18	0.046	5	1.20	24.0
PAHW5WM	PNaB	167 mM $CaCl_2$	3.1	2.5	0.56	4.96	4.65	103
		500 mM NaCl	0.52	0.15	0.19	4.96	3.28	65.6
PAHW5DS	GNaB	167 mM $CaCl_2$	5400	3000[c]	980	5	1.12	22.4
		500 mM NaCl	7800	6300	2800	5	0.96	19.2
PAHW5DS	Pyro	167 mM $CaCl_2$	970	1100	180	5	1.84	36.8
		500 mM NaCl	1800	1600	640	5	2.04	40.8
PAHW32DS	Pyro	167 mM $CaCl_2$	NA	3300	NA	32	0.52	1.63
PAx5DS	PNaB	167 mM $CaCl_2$	24	12[a,c]	4.4	5	4.72	94.4
		500 mM NaCl	0.25	0.25[c]	0.089	5	4.88	97.6

Notes: NA = not applicable; PNaB = powdered sodium bentonite; GNaB = granular sodium bentonite; Pyro = pyrophyllite; t_{6766}, PVF_{6766}, k_{6766} = values based on ASTM 6766 termination criteria; t_f, PVF_f, k_f = final values at the end of testing; $k_{GCL} = k_{6766}$ of NaB GCL specimen; $k_{EB\text{-}GCL} = k_{6766}$ of polymer-amended EB-GCL specimen; P_i = initial polymer content; P_f = final polymer content.

[a] Exhibited interaggregate flow; [b] Terminated early due to polymer clogging; [c] Hydrogel formation observed on specimen geotextiles or permeameter components at post permeation; [d] Based on mass of polymer added for dry-mixed or dry-sprinkled specimens and total carbon analysis for wet-mixed specimens; [e] Measured using total carbon analysis; [f] Reported by Scalia et al. (2014); [g] Calculated using baseline total carbon values for NaB and PAHW

Based on the results in Table 4.6, the hydraulic conductivity of several of the dry-sprinkled and dry-mixed EB-GCL specimens was lower than that for the conventional GCL specimen despite the elution of some fraction of polymer during permeation ($P_f/P_i < 1$). In particular, for the EB-GCLs prepared with linear anionic polymers, the best hydraulic performance occurred for the specimens that were dry sprinkled with 8% of PAMW (PAMW8DS) and 5% of PAHW (PAHW5DS). In the case of the PAMW8DS specimen, the hydraulic conductivity values of 1.1×10^{-11} m/s to 167 mM $CaCl_2$ and 2.9×10^{-11} m/s to 500 mM NaCl are 50 and 10 times lower, respectively, than the values of 5.5×10^{-10} m/s and 2.8×10^{-10} m/s for the conventional GCL specimen comprising PNaB (i.e., $k_{EB\text{-}GCL}/k_{PNaB} = 0.020$ and 0.010, respectively). In the case of the PAHW5DS specimen, the hydraulic conductivity values of 4.0×10^{-11} m/s to 167 mM $CaCl_2$ and 1.3×10^{-11} m/s to 500 mM NaCl are 14 and 22 times lower, respectively, relative to the respective values for the conventional GCL specimen (i.e., $k_{EB\text{-}GCL}/k_{PNaB} = 0.073$ and 0.046, respectively). In addition, the low hydraulic conductivity values for these specimens were obtained despite only a fraction of the polymer being retained by the specimen during permeation ($12.8\% \le P_f/P_i \le 31.8\%$).

Among the other EB-GCL specimens, the results for the specimen dry-mixed with 5% of the BPC (BPC5DM) were similar to those for specimens PAMW8DS and PAHW5DS, with $k_{EB\text{-}GCL}/k_{PNaB}$ of 0.058 and 0.039 to 167 mM $CaCl_2$ and 500 mM NaCl, respectively, and $36.4\% \le P_f/P_i \le 73.2\%$. For the EB-GCL with BPC ($P_i = 28.5$ %) permeated with the 167 mM $CaCl_2$, $k_{EB\text{-}GCL}/k_{PNaB} = 0.29$ even though a significant fraction of polymer (~74%) was eluted during permeation. However, permeation of the EB-GCL with BPC with 500 mM NaCl resulted in a substantial polymer clogging on the inflow side of the BPC GCL that continued through the inflow tubing, which is likely the result of the initially high polymer content of the BPC. As a result, the test was terminated before reaching D6766 termination criteria and no replicate test was completed.

Interaggregate flow behavior, which was confirmed through permeation with rhodamine dye (see Chapter 1), occurred for the dry-mixed EG-GCL specimens with 5% CMCLV or 5% CMCHV (i.e., CMCLV5DM and CMCHV5DM) permeated with both salt solutions. For these EB-GCLs, a consistent

trend in hydraulic conductivity from an initially low value to a higher final value can be attributed to polymer elution from the interaggregate pores (see Chapter 1). Although this preferential flow behavior generally did not necessarily result in a hydraulic conductivity that was higher than that for the conventional GCL specimen with PNaB (i.e., $k_{EB\text{-}GCL}/k_{PNaB} < 1$), the hydraulic conductivity for the CMCHV5DM specimen permeated with 167 mM $CaCl_2$ was 25 times greater than that of unenhanced PNaB ($k_{EB\text{-}GCL}/k_{PNaB} = 25$).

In contrast, the dry-sprinkled EB-GCLs comprising polymer-enhanced PNaB did not exhibit interaggregate flow, i.e., except for specimen PAx5DS permeated with 167 mM $CaCl_2$, which resulted in $k_{EB\text{-}GCL}/k_{PNaB} = 4.4$ despite most of the polymer having been retained within this specimen ($P_f/P_i = 94.4\%$). Otherwise, the highest hydraulic conductivity for these dry-sprinkled EB-GCLs was 5.7×10^{-10} m/s for specimen PALW5DS permeated with 167 mM $CaCl_2$, which was essentially equivalent to that of the unenhanced PNaB ($k_{EB\text{-}GCL}/k_{PNaB} = 1.0$). Thus, polymer elution generally did not result in interaggregate flow paths, which is likely due to the layering of the dry-sprinkled EB-GCLs. For specimen PAx5DS permeated with 167 mM $CaCl_2$, the origin of the higher hydraulic conductivity ($k_{EB\text{-}GCL}/k_{PNaB} = 4.4$) is unknown.

Hydrogel formation was visible on permeameter components for several of the dry-sprinkled and dry-mixed EB-GCL specimens, as reflected, in part, by P_f/P_i values less than unity in Table 4.6. In contrast, there was no visible hydrogel in the post-permeated EB-GCL specimens prepared by wet mixing, despite a typically higher polymer retention (i.e., higher P_f/P_i) for these specimens relative to those prepared with either dry sprinkling or dry mixing (i.e., except for specimen PALW5WM permeated with 500 mM NaCl). However, the higher polymer retention of the wet-mixed EB-GCLs did not necessarily correlate with a lower hydraulic conductivity compared to that of the unenhanced PNaB. For example, specimen CMCHV5WM retained (P_f) 3.1% and 4.2% of the initially added 5.85% CMCHV when permeated with 500 mM NaCl and 167 mM $CaCl_2$, respectively, but achieved hydraulic conductivity values that were only

slightly lower or slightly higher than that of the unenhanced PNaB specimen (i.e., $k_{EB\text{-}GCL}/k_{PNaB}$ = 0.67 and $k_{EB\text{-}GCL}/k_{PNaB}$ = 1.2, respectively).

4.5.2 Effects of interaggregate pore size and surface charge on hydraulic conductivity

The hydraulic conductivity data for tests conducted with conventional GCLs comprising GNaB and pyrophyllite are shown in Figure 4.2, and the test results are summarized in Tables 4.5 and 4.6. The baseline hydraulic conductivity of the conventional GCL comprising GNaB (Figure 4.2c,d) permeated with either solution was 2.7×10^{-7} m/s, which is approximately three orders-of-magnitude higher than the hydraulic conductivity of the conventional GCL with PNaB to 500 mM NaCl and 167 mM $CaCl_2$ of 2.8×10^{-10} m/s and 5.5×10^{-10} m/s, respectively (Table 4.6). The significantly higher hydraulic conductivity with the GNaB results from the limited swelling of the bentonite granules in the concentrated Ca^{2+} and Na^{+} solutions, resulting in larger interaggregate pores available for flow (Shackelford et al. 2000).

As shown in Figure 4.2c,d and Table 4.6, the hydraulic conductivity values of the EB-GCL specimens comprising GNaB dry sprinkled with 5% of PAHW (i.e., specimen PAHW5DS with GNaB) to 500 mM NaCl and 167 mM $CaCl_2$ were 7.8×10^{-7} m/s and 5.4×10^{-7} m/s, respectively, which are even higher than the value of 2.7×10^{-7} m/s for the unenhanced GNaB. Although there was visible formation of hydrogel on the inflow side of the specimen of PAHW5DS comprising the enhanced GNaB permeated with 167 mM $CaCl_2$, the PAHW hydrogel was not successful in decreasing the hydraulic conductivity relative to that for unenhanced GNaB. Interaggregate, preferential flow paths in the specimen were identified through permeation with rhodamine dye, and portions of the specimen where flow had occurred as indicated by the dye had lost significant amounts of polymer based on carbon analysis compared to the undyed portions of the specimen. Although the PAHW5DS EB-GCL prepared with GNaB permeated with 500 mM NaCl was not dyed, similar interaggregate flow behavior is believed to have occurred based on the similar hydraulic conductivities.

The final polymer contents for the GNaB-based EB-GCL dry-sprinkled with 5% of PAHW (specimen PAHW5DS) were low (0.96% and 1.12%), but within a similar range as those for the same EB-

GCL except based on the use of the polymer-enhanced PNaB (0.68% and 1.20%). However, the resulting hydraulic conductivity values were much higher for the GNaB-based EB-GCL (5.4×10^{-7} m/s and 7.8×10^{-7} m/s) versus those for the PNaB-based EB-GCL (4.0×10^{-11} m/s and 1.3×10^{-10} m/s). For the PNaB enhanced with PAHW5DS, a final polymer content of 0.68% and 1.2% was sufficient to produce a low hydraulic conductivity (4.0×10^{-11} m/s and 1.3×10^{-11} m/s, respectively).

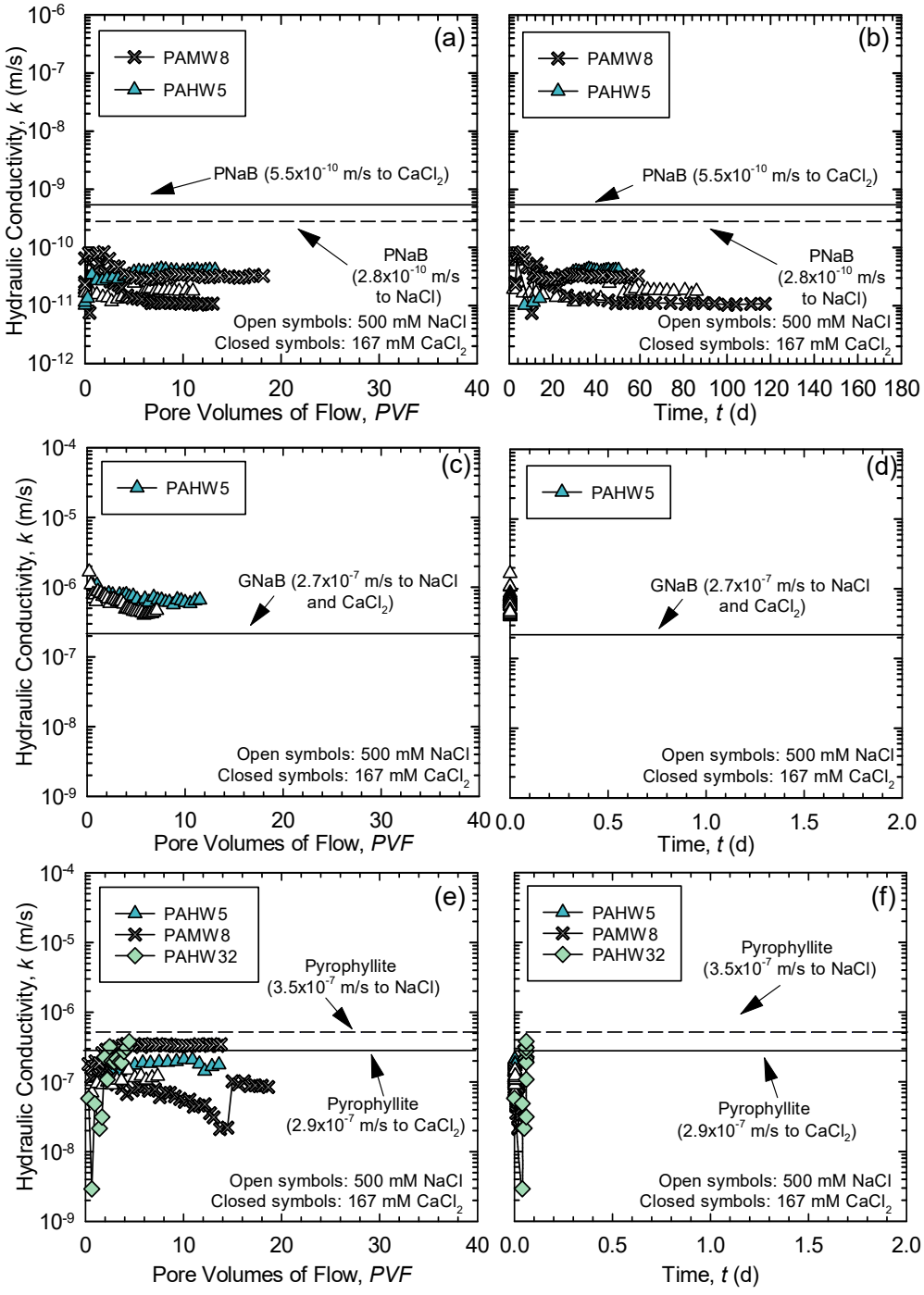

Figure 4.2: Hydraulic conductivity to 500 mM NaCl and 167 mM $CaCl_2$ solutions of EB-GCLs comprising (a,b) powdered sodium bentonite (PNaB), (c,d) granular sodium bentonite (GNaB), and (e,f) pyrophyllite (pyro) enhanced by dry sprinkling with high molecular weight poly(acrylic acid) (PAHW) at 5 or 32% mass loading or medium molecular weight poly(acrylic acid) (PAMW) at 8% mass loading.

The baseline hydraulic conductivity values of the conventional GCL with pyrophyllite to both the 500 mM NaCl and 167 mM $CaCl_2$ of 2.9×10^{-7} m/s and 3.5×10^{-7} m/s, respectively (Table 4.6), also were approximately three orders-of-magnitude higher than those for the previously noted conventional GCL comprising PNaB (i.e., 2.8×10^{-10} m/s and 5.5×10^{-10} m/s, respectively). The higher hydraulic conductivity of pyrophyllite is caused by the lack of mineral swelling. Also, enhancement of pyrophyllite by dry-sprinkling with 5% PAHW (specimen PAHW5DS) or 8% PAMW (specimen PAMW8DS) failed to result in a significantly lower relative to those for the conventional GCL with unenhanced pyrophyllite (Table 4.6). The pyrophyllite EB-GCL with a highest polymer loading of 32% PAHW (specimen PAHW32DS) initially yielded a lower hydraulic conductivity to 167 mM $CaCl_2$ of 2.0×10^{-9} m/s relative to that of 1.8×10^{-7} m/s for the same EB-GCL with 5% polymer loading but after 2 PVF, the hydraulic conductivity was approximately equivalent to that for the baseline pyrophyllite test (3.3×10^{-7} m/s), likely due to polymer elution. This test was not run to ASTM 6766 termination criteria but instead immediately dyed with rhodamine dye to determine if any preferential flow paths had occurred. However, none were identified.

Post-permeation analysis of specimen PAHW32DS indicated an average polymer content of 0.52% versus the final polymer content of 0.68% for specimen PAHW5DS with considerably less initial content of the same polymer (i.e., 5% versus 32%). Although the final polymer content of the EB-GCLs is similar (within a factor of one), the final measured hydraulic conductivity of 3.3×10^{-7} m/s for specimen PAHW32DS permeated with 167 mM $CaCl_2$ is almost four orders-of-magnitude higher than that of 4.0×10^{-11} m/s for specimen PAHW5DS based on enhanced PNaB permeated with the same solution. Further investigation is required to fully understand the explanation for this behavior, but our hypothesis is that the difference in hydraulic performance can be attributed to the bound cations present in the PNaB that are available for polymer cross-linking and chemisorption.

4.5.3 Effect of hydraulic gradient on hydraulic conductivity

Results of the tests performed at a lower hydraulic gradient ($i \approx 30$) based on permeation with 167 mM $CaCl_2$ are shown in Figure 4.8. Although these tests are still ongoing, the initial hydraulic conductivity

trends indicate two distinct behaviors. First, the hydraulic conductivity of the PAHW5DS specimen is about 4.5 times lower at $i \approx 30$ relative to $i \approx 300$, i.e., 8.9×10^{-12} m/s versus 4.0×10^{-11} m/s (Table 4.6). In contrast, the hydraulic conductivity of the PALW5DS specimen at $i \approx 30$ of 1.4×10^{-11} m/s is approximately 1.5 orders of magnitude lower than that of 5.7×10^{-10} m/s at $i \approx 300$ (Table 4.6). Although the lower hydraulic gradient ($i \approx 30$) tests are still ongoing, the decrease in hydraulic conductivity with decrease in hydraulic gradient likely indicates that the polymer is less mobile at a lower hydraulic gradient (i.e., lower seepage force). Nonetheless, polymer hydrogel clogged the outflow end of the test at $i \approx 30$ with the PALW5DS specimen after approximately 135 days of permeation (Figure 4.8b), illustrating that a low hydraulic gradient did not necessarily prevent mobilization of the polymer. This clogging occurred after the test was paused (closed) during lab closure due to restrictions caused by the COVID-19 pandemic. The polymer obstruction was removed from the outflow tubing using pipe cleaners, and the test was resumed, resulting in a re-establishing of the previously measured, higher hydraulic conductivity.

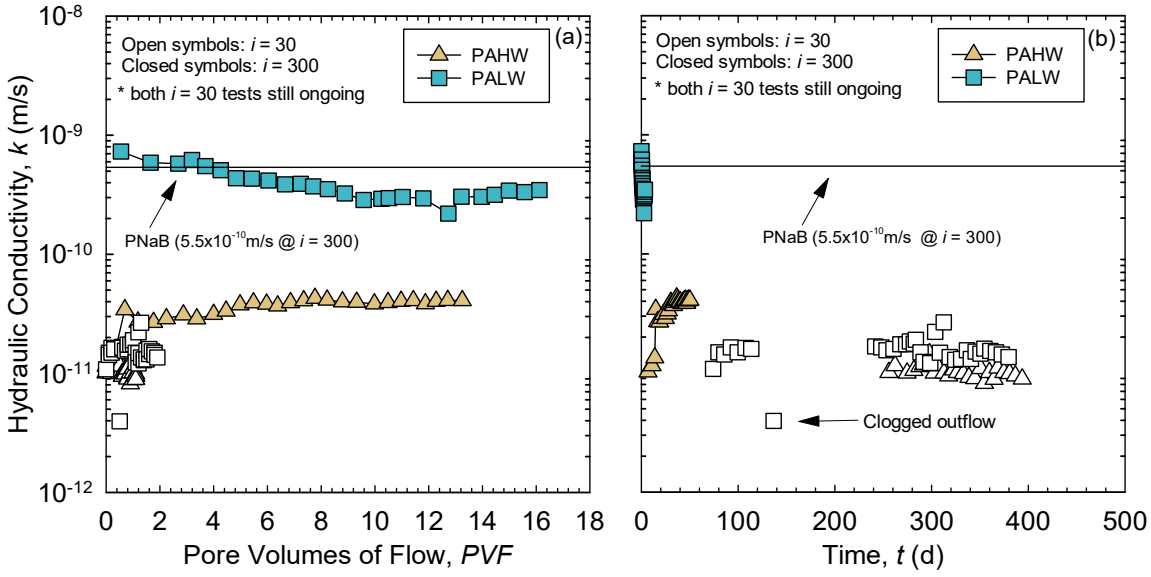

Figure 4.8: Measured hydraulic conductivity of EB-GCL specimens prepared by dry sprinkling of sodium poly(acrylic acid) with low molecular weight (PALW) and high molecular weight (PAHW) at 5% polymer mass loadings and permeated with 167 mM $CaCl_2$ at two different hydraulic gradients (i) as a function of (a) PVF and (b) time. The standardized hydraulic conductivity (k_{6766}) value for the conventional GCL comprising unenhanced sodium bentonite (NaB) permeated with 167 mM $CaCl_2$ also is indicated.

4.5.4 X-ray diffraction

As previously noted, (Section 4.2.3), polymer intercalation between montmorillonite platelets in PNaB has been hypothesized to activate osmotic swelling and prop open the interlayer space when exposed to aggressive liquids and, thereby, increase hydraulic compatibility (e.g., Di Emidio et al. 2010; Scalia et al. 2018). Accordingly, x-ray diffraction (XRD) analysis of the wet-mixed EBs was performed to look for shifts in basal spacing, and the PNaB was analyzed via XRD as a baseline. The resulting diffractograms are shown in Figure 4.4 for 2Θ ranging from 4 to 30°. Dry-mixed EBs were not tested based on the assumption that dry mixing would be less likely than wet mixing to create conditions favorable for intercalation.

As illustrated in Figure 4.4, analysis of the d_{001} peaks does not support CMC or PA intercalation for the wet-mixed EBs. An increase in basal spacing should be identifiable as a shift of the d_{001} peak to a lower 2Θ angle. The d_{001} peaks in Figure 4.4 for the wet-mixed EBs are not shifted leftward. However, the effect of the addition of the anionic polymer does result in a broadening of the sharp d_{001} peak for the base NaB at approximately $2\Theta = 11.5°$. The broadening of the sharp peak for the base NaB indicates an increase in the irregularity of interlayer spaces (addition of amorphous, non-crystalline material) (e.g., Short and Walker 1962; Mitra and Bhattacherjee 1969; Kodama et al. 1971), indicating a potential decrease in the face-to-face structure of montmorillonite platelets in the EB systems. These results suggest that the anionic polymers did not intercalate between the montmorillonite platelets in the wet-mixed EBs but may have affected the fabric of the clay platelets.

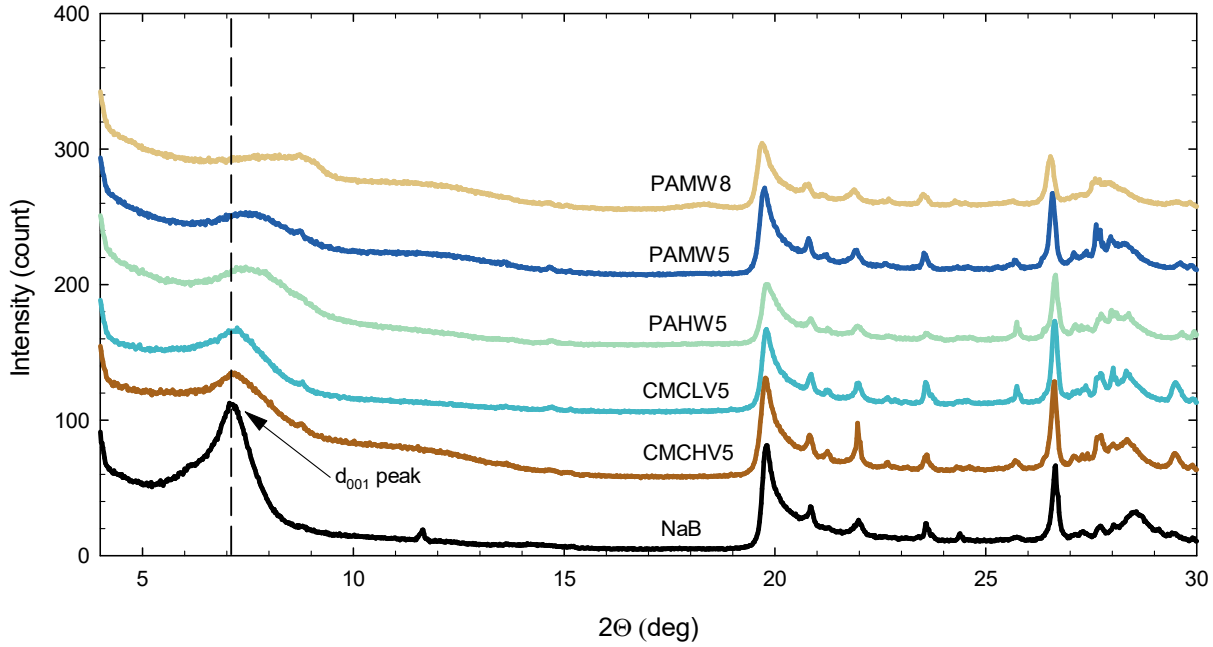

Figure 4.3: X-ray diffraction analysis of powdered sodium bentonite (PNaB) and wet-mixed enhanced bentonites (EBs) prepared with high and low viscosity carboxymethylcellulose (CMCHV, CMCLV) and poly(acrylic acid) with high, medium, and low molecular weights (PAHW, PAMW, PALW) at 5 or 8% polymer mass loading (intensity (count) of each sample shifted by 50 counts for visual separation).

4.5.5 Swell index

The measurement of the swell index of NaB from conventional GCLs is used to determine the prospect of a GCL to achieve a low hydraulic conductivity for a given permeant liquid, i.e., as an indicator parameter for hydraulic conductivity since swelling underlies the hydraulic conductivity of NaB (Shackelford et al. 2000; Jo et al. 2001; Kolstad et al. 2004; Lee et al. 2005; Katsumi et al. 2008). Accordingly, the results of swell index testing of the base PNaB and the EBs comprising PNaB dry mixed or wet mixed with CMC or PA are shown in Figure 4.5 for tap water (Figure 4.5a), 167 mM $CaCl_2$ (Figure 4.5b), and 500 mM NaCl (Figure 4.5c).

The swell index with EBs wet-mixed and dry-mixed with CMC was approximately 30% higher than that of the PNaB in tap water, with the highest swell index occurring for EB wet mixed with CMCHV. The swell index of the EBs wet-mixed and dry-mixed with PA in tap water was consistently lower than that of the PNaB. Relative to tap water, the swell index of all bentonites was lower, as expected, with both the

500 mM NaCl and 167 mM $CaCl_2$, with the lowest swell index occurring with 167 mM $CaCl_2$ solution, as expected based on ionic strength and salt cation charge (Shackelford 1994). However, any increase in swelling of the EBs relative to that of the base NaB was minimal, regardless of dry or wet mixing methods.

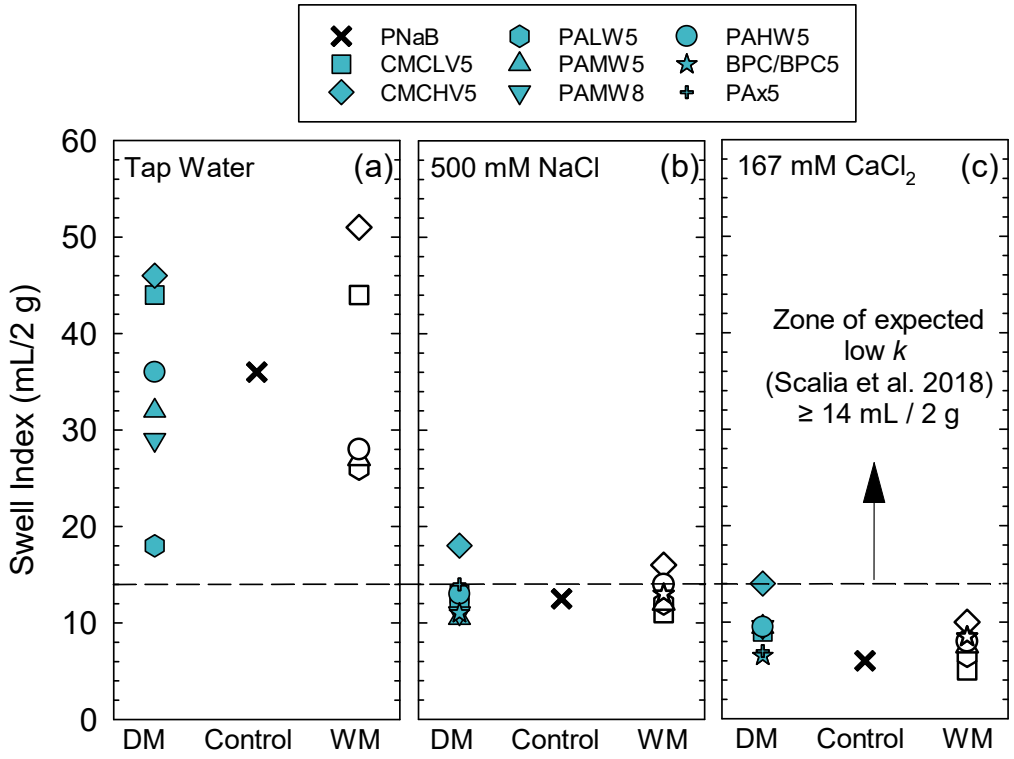

Figure 4.4: Swell indices for powdered sodium bentonite (PNaB), enhanced PNAB prepared with high or low viscosity carboxymethylcellulose (CMCHV, CMCLV) or poly(acrylic acid) with high, medium, or low molecular weights (PAHW, PAMW, PALW), and dry mixed (closed symbols) or wet mixed (open symbols) at 5% or 8% polymer mass loading, and bentonite polymer composite (BPC) in (a) tap water, (b) 500 mM NaCl and (c) 167 mM $CaCl_2$.

4.5.6 Hydrogel formation

Although the measured swell of the EBs evaluated in this study with the aggressive inorganic solutions was not enhanced relative to that for the PNaB, a majority of the hydraulic conductivity values measured (19 out of 22 tests) for the EB-GCLs prepared with PNaB as well as BPC were lower than that for the unenhanced PNaB ($0.020 \leq k_{EB\text{-}GCL}/k_{PNaB} \leq 0.86$). Thus, the likely mechanism controlling the low hydraulic

conductivity of EB-GCLs in this study was pore-blocking or clogging by polymer hydrogels versus swell or intercalation.

To further understand the pore-blocking mechanism, several hydrogel formation tests were conducted. For the first hydrogel formation test involving the observation of the potential for hydrogel formation of PAHW in NaCl and $CaCl_2$ solutions, each polymer loading produced a visible hydrogel in the bottom of the centrifuge tube with both permeant solutions. Upon light shaking/mixing, the PAHW fully dissolved, and the hydrogel was no longer visible. However, after sitting stagnant for three months, the hydrogel again became visible (see Figure 4.6). The initial gel-like appearance of the polymer hydrogel is a result of the solvent diffusing into the polymer prior to dissolution and forming a polymer hydrogel. In contrast, the hydrogel formed over the three months was composed of a visible network of polymer strands, as shown in the magnified image of the hydrogel formed in 33.33 mM $CaCl_2$ solution in Figure 4.6g.

The formation of the hydrogel after three months is likely a result of Brownian motion of the PA chains in solution (e.g., Doi and Edwards 1978; Bijsterbosch et al. 1995). Over time, chains of PA randomly achieve sufficiently low proximity or collide to form cross-links. The formation of the cross-links likely occurs prior to the apparent visibility of the chains in the centrifuge tube, which requires the agglomeration of many such cross-linked chains. The results of this initial hydrogel formation test suggest that hydrogel formation in the 500 mM NaCl or 167 mM $CaCl_2$ solutions is not instantaneous, but rather is based on the formation of cross-links via slow kinetics.

The size and shape of the cross-linked hydrogel formed in the 167 mM $CaCl_2$ are different than those for the hydrogel formed in the 500 mM NaCl and vary with Na^+/Ca^{2+} concentration. As previously noted (Section 4.2.2), the chain configuration of PA will depend on the DOI (ratio of $COO^-/COOH$) of the chain in the hydrating solution (Buccholz and Graham 1998). In $CaCl_2$ solutions, charge screening of the negatively charged carboxyl groups occurs, causing the collapse of the polymer chain into a random coil shape. Calcium (Ca^{2+}) also can participate in ionic cross-linking, resulting in a hydrogel comprising a collapsed, coiled network of interconnected polymer chains, as seen in the hydrogels formed after three

months in the hydrogel formation tests conducted with the 167 mM $CaCl_2$ solution (Figures 4.6a,c,e). The hydrogel formed in the 500 mM NaCl after three months has the appearance of multiple, elongated polymer hydrogels with lower crosslink density (Figures 4.6b,d,f). In the 500 mM NaCl solution, the intermolecular forces causing the cross-linking, hydrogen bonding, and/or dipole-dipole bonding produce hydrogels of different size and density than those in the 167 mM $CaCl_2$ solution. A lower crosslink density in the 500 mM NaCl solution versus that in the 167 mM $CaCl_2$ solution may be a direct result of the reaction kinetics governing the formation of crosslinking with Ca^{2+} in solution. Further study is needed to provide a more direct, quantitative comparison of the size of the hydrogels formed in 167 mM $CaCl_2$ versus 500 mM NaCl.

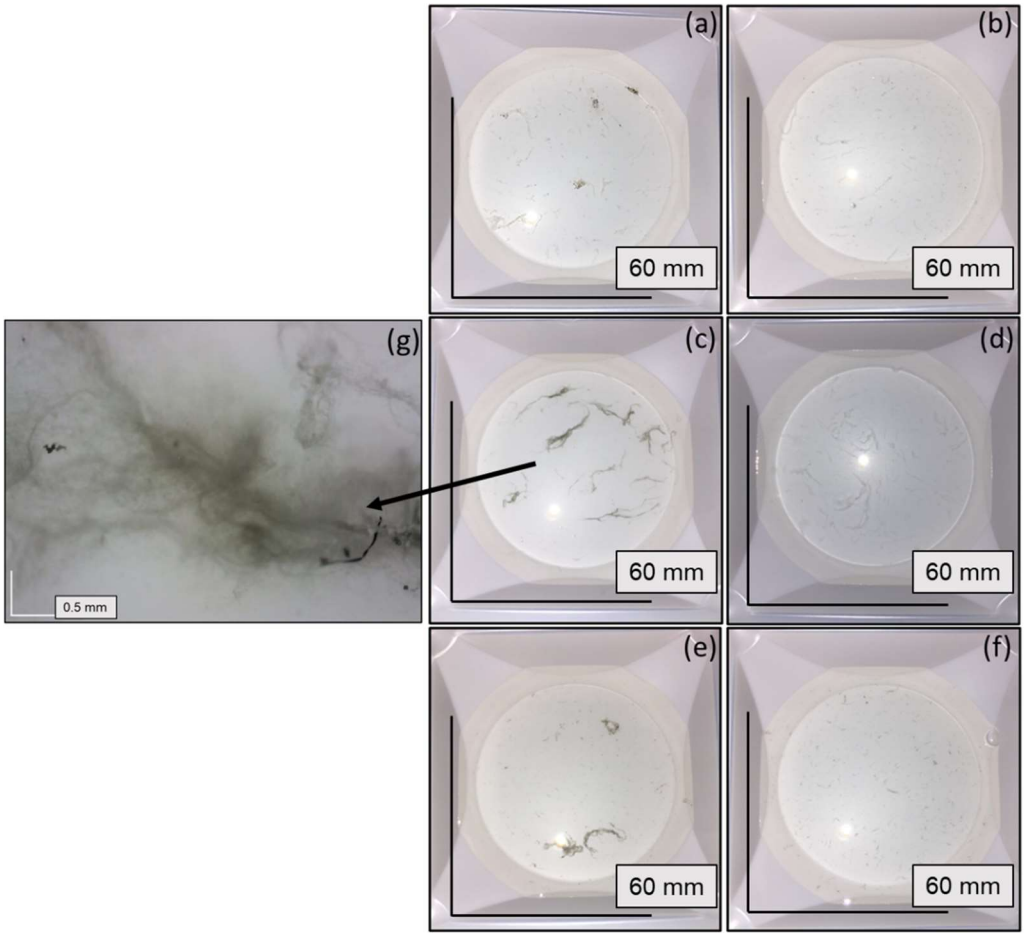

Figure 4.5: Results of hydrogel formation tests after three months: (a) 1.67 mM $CaCl_2$ (ionic strength, I = 5 mM; (b) 5 mM NaCl (I = 5 mM); (c) 33.33 mM $CaCl_2$ (I = 100 mM); (d) 100 mM NaCl (I = 100 mM); (e) 167 mM $CaCl_2$ (I = 500 mM); (f) 500 mM NaCl (I = 500 mM); (g) magnified image of cross-linked strands after three months in 33.33 mM $CaCl_2$.

As expected, in the second hydrogel formation test, the covalently cross-linked PAx swelled and produced hydrogels in both solutions, with the hydrogel formation being much greater (larger degree of visible swelling or volume increase) in the 500 mM NaCl solution relative to the 167 mM $CaCl_2$ solution (e.g., compare Figure 4.7a,b and Figure 4.7c,d, respectively). Covalently cross-linked PAx also resulted in a stable visible hydrogel retained by the PNaB that also was visible on the inflow side of the post-permeated EB-GCL specimen comprising PNaB dry sprinkled with 5% PAx (specimen PAx5DS). In contrast, no hydrogel was formed during the 48-h period for the PAHW in either solution, as previously discussed.

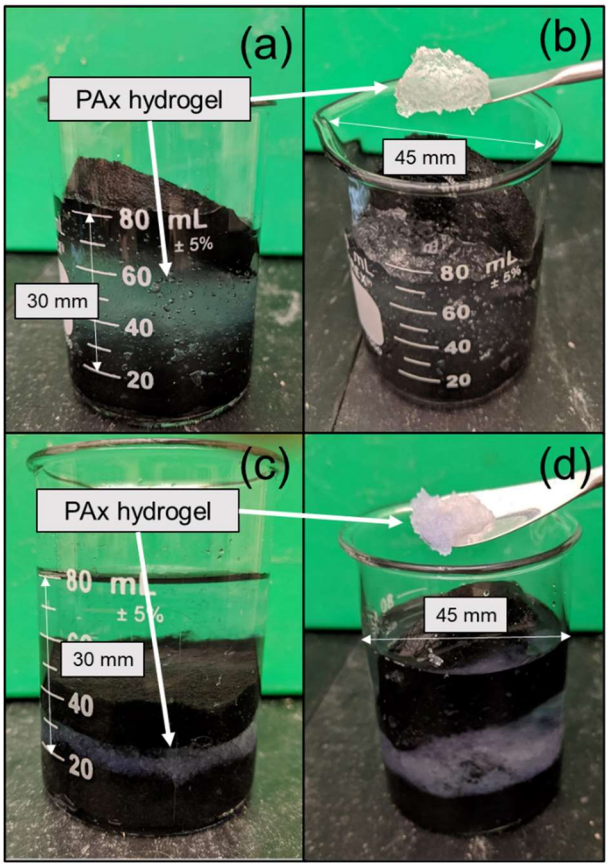

Figure 4.6: PAx hydrogel formation: (a,b) 500 mM NaCl; (c,d) 167 mM $CaCl_2$.

As shown in Figures 4.8a-f, the addition of the PNaB in the third type of hydrogel formation test changed the behavior of the PAHW. For example, in the test with the 167 mM $CaCl_2$ solution, the PAHW in contact with the PNaB coalesced to the PNaB, forming an intact layer of coalesced PAHW and PNaB that could be separated from the non-coalesced PNaB (Figures 4.8c,d). Upon inspection of the coalesced

layer of PAHW and PNaB, hydrogel was visible in the bentonite pores (Figures 4.8e,f). When hydrated with the 500 mM NaCl solution, the PNaB and PAHW also combined into a coalesced layer (Figures 4.8h,i), but the hydrogel formation was not as easily identifiable as in the test with the 167 mM $CaCl_2$ solution, since the layer was fragile and easily broken when stretched such that hydrogel strands could not be photographed.

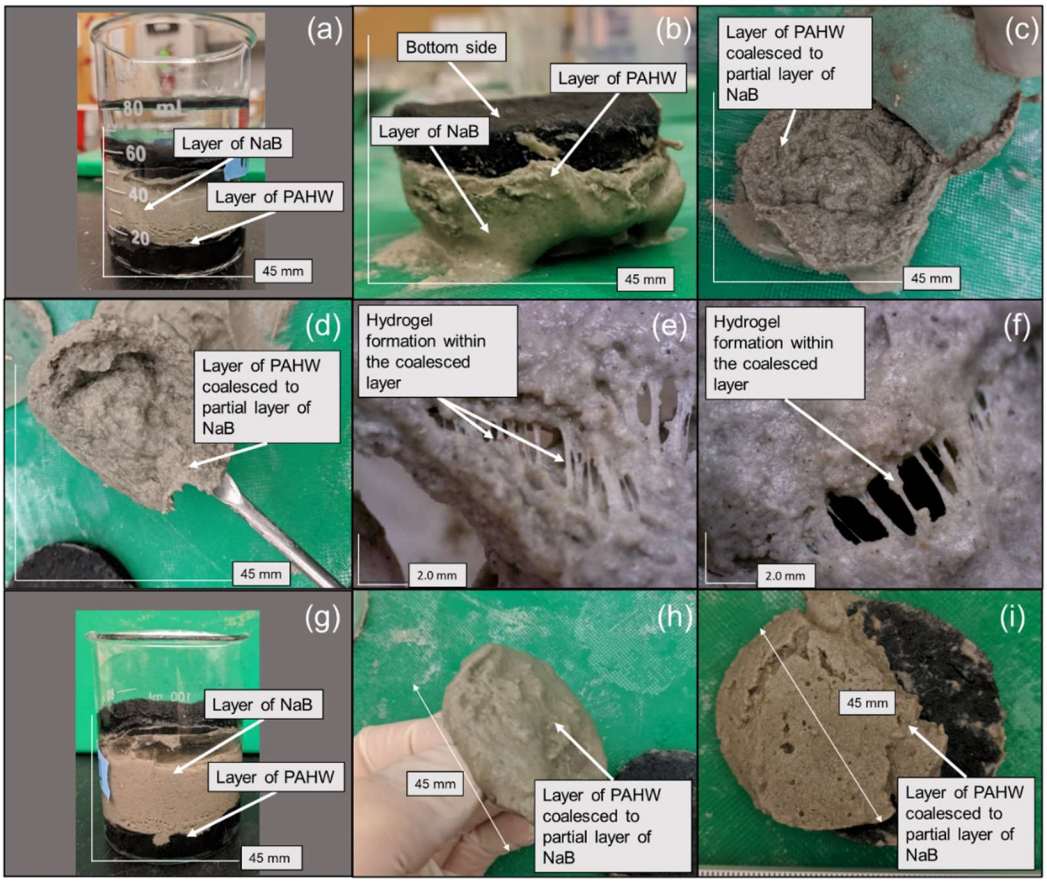

Figure 4.7: Results of hydrogel formation testing involving high molecular weight poly(acrylic acid) (PAHW) with a layer of powdered sodium bentonite (PNaB) and hydrated with (a-d) 167 mM $CaCl_2$ solution and (e-i) 500 mM NaCl solution: (a) test overview; (b) extruded sample; (c,d) PAHW coalesced with PNaB; (e, f) magnified version of PAHW coalesced with NaB; (g) test overview; (h,i) PAHW coalesced with PNaB.

In the fourth type of hydrogel formation test, the formation of hydrogel was confirmed during the hydration of the EB-GCL dry sprinkled with 5% of PAHW (specimen PAHW5DS) with the 500 mM NaCl solution in the permeameter under the 27 kPa effective stress. A visible layer of hydrogel formed on the

inflow side of the specimen and extended from the surface on the inflow side (bottom) of the PNaB through the thin non-woven (carrier) geotextile and onto the outer high-weight non-woven (flow distribution) geotextile.

4.6 DISCUSSION

4.6.1 Swell index and hydraulic conductivity

The swell index of each EB is compared to the final measured hydraulic conductivity *(k_f)* of the EB-GCLs in Figure 4.9. The k_f values instead of k_{D6766} values are reported in Figure 4.9 because these values represent the hydraulic conductivity associated with the final polymer contents determined after testing was completed. Scalia et al. (2018) note that, for NaB, a swell index ≥ 14 mL/2 g generally correlates with a hydraulic conductivity ≤ 3.0×10^{-10} m/s at low effective stress (< 35 kPa). However, as indicated by the results shown in Figure 4.9, a low hydraulic conductivity generally is achieved for the EBs tested in this study without a corresponding swell index ≥ 14 mL/2 g. This lack of correlation between swell index and hydraulic conductivity of the EB-GCLs is consistent with results reported in other studies (Scalia et al. 2014; Tian et al. 2016a,b; Scalia et al. 2018; Tian et al. 2019).

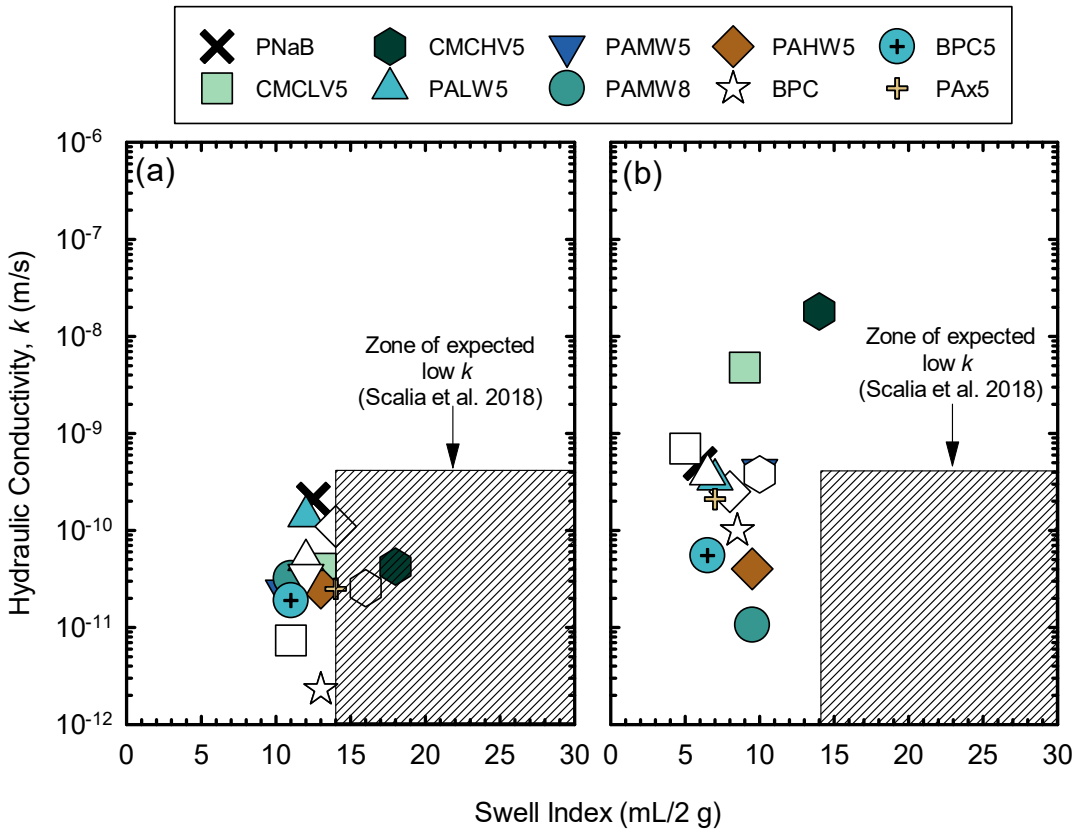

Figure 4.8: Swell indices for powdered sodium bentonite (PNaB) and enhanced bentonites prepared with high and low viscosity carboxymethylcellulose (CMCHV, CMCLV) or poly(acrylic acid) with high, medium, or low molecular weights (PAHW, PAMW, PALW), and dry mixed (closed symbols) or wet mixed (open symbols) at 5% or 8% polymer mass loading versus hydraulic conductivity: (a) 500 mM NaCl permeant solution; (b) 167 mM $CaCl_2$ permeant solution.

4.6.2 Hydraulic conductivity and polymer retention

The hydraulic conductivities and final polymer contents based on permeation with 500 mM NaCl and 167 mM $CaCl_2$ are correlated in Figure 4.10. Note that k_f values instead of k_{D6766} values are reported in Fig. 4.10a because the polymer contents shown in Figure 4.10b were determined after testing was completed. However, based on the hydraulic conductivity values reported in Table 4.4, any differences between the final and standard hydraulic conductivities are minimal.

As shown in Figure 4.10a, EB-GCLs comprising anionic polymers at low mass loadings (≤ 10%) and prepared using different mixing methods have the potential to resist chemical incompatibility upon permeation with high ionic strength inorganic solutions (I = 500 mM). However, all of the k_f values for both the PNaB and the PNaB-based EB-GCLs were < 3.0×10^{-10} m/s when permeated with the 500 mM NaCl

solution, whereas only five of the 12 EB-GCL specimens resulted in a hydraulic conductivity < 1.0×10^{-10} m/s when permeated with the 167 mM $CaCl_2$ solution, indicating that Ca^{2+} containing permeant solution was more detrimental to the hydraulic compatibility of the EB-GCLs.

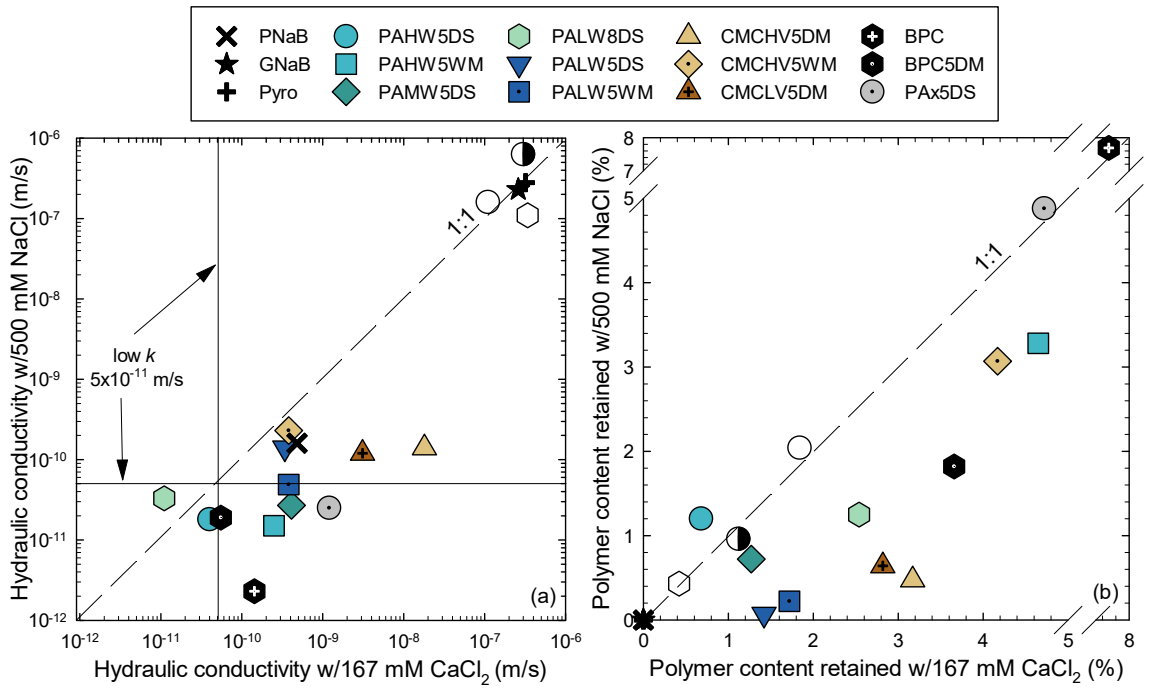

Figure 4.9: Final (after permeation) hydraulic conductivity and polymer content of powdered sodium bentonite (PNaB), pyrophyllite (Pyro), and granular sodium bentonite (GNaB), and EB-GCLs prepared with PNaB (closed symbols), pyrophyllite (open symbols), GNaB (semi-filled symbols), or bentonite polymer composite (BPC) specimens: (a) hydraulic conductivity; (b) polymer content.

In general, the polymer contents shown in Figure 4.10b plot to right of a 1:1 line, indicating higher polymer retention with 167 mM $CaCl_2$ than with 500 mM NaCl, which is consistent with the batch adsorption results in Chapter 2. These results confirm the favorable role of calcium (Ca^{2+}) in increasing polymer retention. Chemisorption of anionic polymers in EB-GCLs will occur primarily through cation bridging for PAHW (Chapter 2). However, the increased retention was not directly correlated with a lower hydraulic conductivity (e.g., CMCHV5WM). The results of batch adsorption tests (Chapter 2) showed that very little polymer was retained with 500 mM NaCl. However, polymer was retained in EB-GCLs permeated with 500 mM NaCl, indicating polymer retention due to some process other than chemisorption (Figure 4.10b). In a system devoid of multivalent cations, retention of polymer in the EB-GCL permeated

with 500 mM NaCl corroborates the role of mechanical entrapment (physical retention) of polymer hydrogel.

4.6.3 Mechanisms controlling the hydraulic conductivity of EB-GCLs

Building on the mechanisms summarized by Scalia et al. (2018), the mechanisms governing the hydraulic conductivity of the EB-GCLs produced in this study are illustrated schematically in Figure 4.11 in terms of the three stages of development and performance, viz., (i) the as-produced, initial dry-state stage, (ii) the subsequent hydration stage when hydrogel is initially allowed to form, and (iii) the permeation stage. A description of these mechanisms follows. The aggregates illustrated in Figure 4.11 could represent PNaB or GNaB and the mechanisms presented can be applied to EB-GCLs prepared with either form of NaB, although the scale of interaggregate pores will be different.

Enhanced bentonite GCLs are considered for use when conventional GCLs result in high hydraulic conductivity (Figure 4.11i) due to limited swelling of the bentonite under the relevant conditions (e.g., effective stress, hydrating/permeating solutions, etc.) and consequent existence of conductive, interaggregate flow paths. As illustrated in Figures 4.11j-l, low hydraulic conductivity is a consequence of effective blocking of the most conductive pores in the NaB, forcing the flow to more tortuous pathways through the NaB and yielding a lower hydraulic conductivity than that for the unenhanced NaB. As illustrated in Figures 4.11m-o, an increase in hydraulic conductivity occurs when the polymer hydrogel is eluted from the pores, resulting in interaggregate flow paths similar to those in the NaB hydrated in the same solution (e.g., Figures 4.11m,n). For the wet-mixed EBs, minimal impact on hydraulic conductivity is observed because the polymer is retained in intra-aggregate pores that do not govern liquid flow. Hydraulic conductivity is not impacted by the wet mixing unless interaggregate pores are blocked, as shown in (Figure 4.11o), due to the movement of polymer hydrogels into the interaggregate pores and consequently, pore blockage to reduce the hydraulic conductivity.

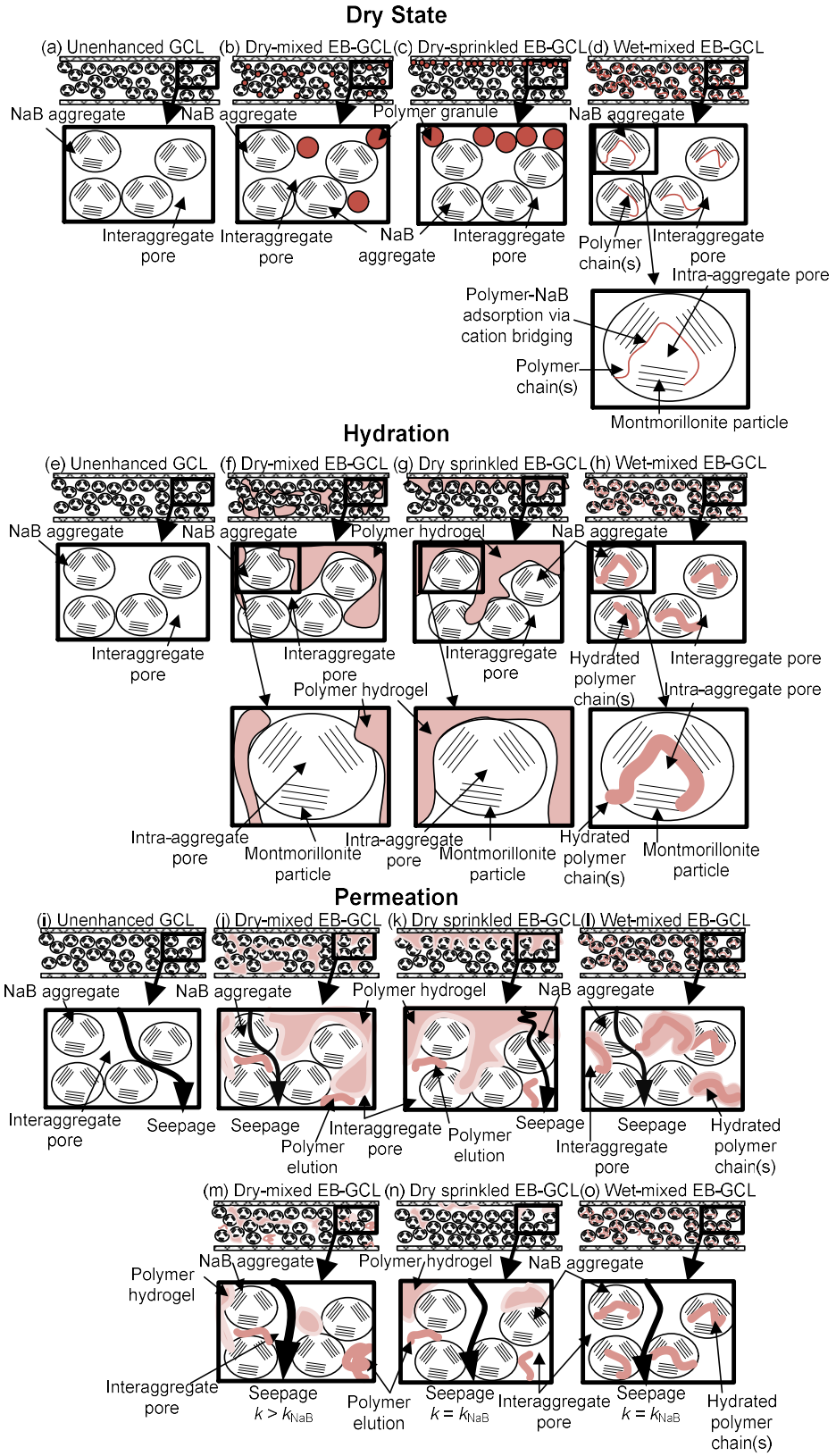

Figure 4.10: Schematic cross-sectional views of the EB-GCLs in the dry state, hydration, and permeation.

4.6.4 Idealization of filtration zone

The mechanisms controlling the hydraulic conductivity of EB-GCLs can be understood by idealizing the system (as illustrated in Figure 4.11) as a filtration zone, where the NaB is the filter (valid for EB-GCLs containing PNaB or GNaB), and the polymer hydrogel is the filtrate. As flow occurs, the polymer hydrogel migrates into and through the NaB filter. The coarsest fractions of the hydrogel are lodged into the conductive pores, decreasing the effective pore size, and ultimately driving further entrapment of smaller hydrogel formations in the next largest pores. However, unlike soil filtration with inert granules, the entrapped hydrogels also have the potential for adsorption to the surfaces of the NaB particles via cation bridging, further cross-linking and bonding with other polymer chains and hydrogels or, if not adsorbed, deforming and flushing if hydraulic gradients are sufficiently high. The effective filtration of the polymer hydrogel and ultimately a low long-term hydraulic conductivity is dependent on (i) the formation of hydrogel, (ii) the random insertion of the hydrogels into the pores such that the largest (most conductive) pores are blocked, (iii) a balance of seepage forces that are sufficient to mobilize the hydrogels into the pores but not so large to cause the hydrogels to untangle due to shear thinning or are dislodged by inertial forces, (iv) the kinetics of hydrogel formation, and (v) adsorption of polymer to the surfaces of the NaB particles.

4.6.5 Factors affecting hydrogel pore clogging

The ability of the polymer hydrogel to block the largest pores and reduce the effective pore sizes is a function of the following factors:

(1) size and shape of the bentonite pores, which are a function of particle-size distribution, swelling, and effective stress;

(2) degree and kinetics of hydrogel formation, which are a function of solution concentration, ion species, pH, polymer molecular weight and concentration, hydration time, and applied hydraulic gradient;

(3) degree of polymer adsorption, which is a function of solution concentration, ion species, pH, and polymer type; and

(4) mixing method of polymer and NaB.

4.6.5.1 Bentonite pore size and shape

The concept of mechanical entrapment (pore blocking) of the hydrogel during permeation is illustrated by the blocking/clogging effect shown in Figure 4.12. Eluted polymer hydrogel from specimen PAHW5DS permeated with 167 mM $CaCl_2$ was tested in a capillary viscometer. The hydrogel present in the effluent effectively clogged the viscometer, altogether preventing flow. Pore sizes in a conventional GCL will vary depending on type of bentonite, degree and type of hydration, and effective stress. However, the clogging of the viscometer tube in Figure 4.12 provides insight into how a cross-linked polymer may become mechanically entrapped within a pore independent of polymer-clay adsorption.

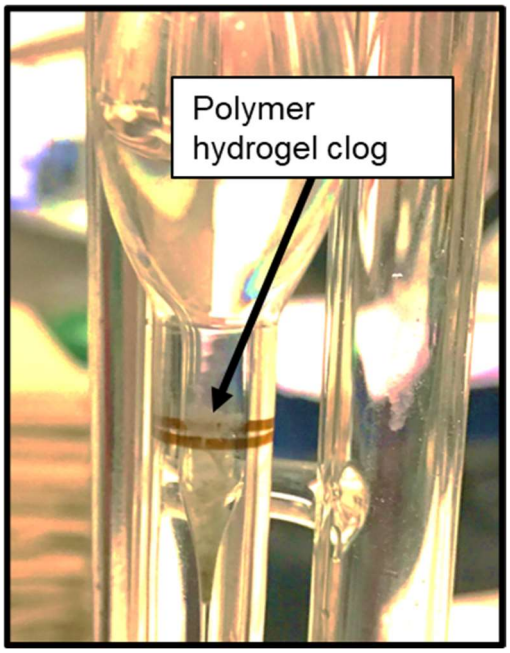

Figure 4.11: Mechanical entrapment of polymer hydrogel in capillary viscometer (Ubbelohde size 0C).

The deviation in hydraulic behavior of EBs produced with GNaB and PNaB illustrates the importance of the interaggregate pore size on the capacity of hydrogel to effectively clog pores and produce a low hydraulic conductivity in an EB-GCL. Similar to the polymer hydrogel clogging shown in the

viscometer (Figure 4.12), the mechanism of mechanical entrapment relies on the interaggregate pores being small enough to retain a fraction of the polymer hydrogel that is sufficient to block the largest pores and reduce hydraulic conductivity, and gradients being sufficiently low so as to not deform, dislodge and flush the hydrogel from the pore throat. The interaggregate pores of the GNaB retained a similar fraction of polymer hydrogel to the pores of the PNaB when enhanced with dry-sprinkled PAHW5, but the hydrogel did not effectively block the largest and most critical pores in the GNaB to result in a low hydraulic conductivity.

4.6.5.2 Hydrogel degree and kinetics

The results of the four hydrogel formation tests confirmed that hydrogel is formed in the presence of NaB by PAHW in both 500 mM NaCl and 167 mM $CaCl_2$ during the 48-h hydration period prior to permeation. However, these results did not clarify what percentage of the polymer had successfully formed hydrogel after 48 h, or what portion of the polymer was influencing hydraulic conductivity. Additional study is needed to determine the effect of hydration time on hydrogel formation and the hydration time impacts on polymer retention and ultimately hydraulic conductivity.

As previously noted, (Section 4.2.2), anionic polymers exhibit non-Newtonian, shear-thinning behavior. The viscosity of anionic polymers depends on the applied shear stress. At lower shear stress, polymers are entangled and remain entangled, yielding high viscosity and hydrogel permanence. As the shear stress increases, the entanglements are broken as the polymer chains reorient in the direction of flow and result in hydrogel shear thinning. The hydrating and permeant solutions will control the initial configuration and size of the polymer chains and the degree of cross-linking that occurs in non-covalently crosslinked polymers. The seepage force in the EB-GCL is controlled by the applied hydraulic gradient (i.e., the fluid velocity), which governs hydraulic forces acting on the intrapore hydrogel. The reduction in hydraulic conductivity of EB-GCL specimen PALW5DS at the lower hydraulic gradient of 30 suggests that the PALW potentially remained more entangled and less mobile, thereby retaining polymer and decreasing flow in the interaggregate pores. These results indicate that hydraulic gradient may impact the hydraulic

conductivity of EB-GCLs in a manner unlike that for conventional GCLs, which remain relatively unimpacted by changes in hydraulic gradient or yield slightly lower hydraulic conductivity at high applied hydraulic gradients due to increased effective stress on the downgradient side of the GCL (Rad et al. 1994; Petrov et al. 1997; Shackelford et al. 2000). Hydraulic gradient also is anticipated to have different effects depending on the types of polymer and permeant solution, and time specific degree of cross-linking and polymer adsorption.

4.6.5.3 Degree of polymer adsorption

The importance of the sodium bentonite component of EB-GCLs was highlighted in the hydraulic conductivity testing of the EB-GCLs produced using pyrophyllite. Although both NaB and pyrophyllite EB-GCLs were hydrated and permeated with the 500 mM $CaCl_2$ solution, with an abundance of Ca^{2+} cations available for polymer cross-linking and hydrogel formation, the hydrogel was not successful in clogging the pyrophyllite pores, resulting in a high hydraulic conductivity ($\geq 6.7\times10^{-8}$ m/s), even at 32% enhancement. The bound cations of the PNaB not only result in greater swelling (bound water) of the PNaB resulting in smaller and more tortuous pores, but also provide cations (exchanged cations and soluble salts) available for polymer cross-linking and polymer-retaining adsorption. Polymer chains slowed by increased tortuosity due to the swelling capacity of PNaB and within a network of pores, in which the largest pores are relatively small, have a greater chance of forming hydrogels and/or adsorbing to the available sites on the mineral surfaces of the NaB.

4.6.5.4 Mixing method

A divergence in hydraulic behavior due to mixing method was evident for the EB-GCLs evaluated in this study. As conceptualized in Figures 4.11j-l, polymer hydrogel retained in the EB-GCLs must block the largest pores to result in a low hydraulic conductivity. Due to the intermixed matrix of the dry-mixed EB-GCLs, polymer elution over multiple pore volumes of flow produced interaggregate flow paths (formerly occupied by dry polymer granules) that resulted in hydraulic conductivity values that were higher than those for the conventional GCL. In contrast, due to the layering of polymer and PNaB in the dry-sprinkled EB-

GCLs, the maximum hydraulic conductivity was equivalent to the baseline hydraulic conductivity for unenhanced PNaB with the same permeant solution. In the case of the wet-mixed EB-GCLs (Figures 4.1lp), polymer was retained within the intra-aggregate pores that do not participate in flow. A resulting low hydraulic conductivity was achieved when the polymer was eluted from the intra-aggregate pores into the interaggregate pores. Polymer migration from the intra-aggregate pores to the interaggregate pores, that results in a low hydraulic conductivity is expected to occur in these cases due to the exchange of Na^+ for multivalent cations (via mass action effects) on the exchange complex of the NaB (McBride 1994). Polymer that was adsorbed via cation bridging is released via cations exchange, allowing the polymer and released cations to migrate to the interaggregate pores. Enhanced bentonite GCLs with higher polymer contents (e.g., BPC with 28.5% polymer) may contain sufficient polymer to overcome this limitation, such that the polymer may readily move into the interaggregate pores. Once a hydrogel is formed in the interaggregate pores, the wet-mixed EB-GCLs are expected to behave similarly to the dry-mixed EB-GCLs. Interestingly, the wet-mixed EB-GCLs may benefit from a higher initial hydraulic gradient that mobilizes polymer hydrogel into to interaggregate pores before the polymer has time to form stable intra-aggregate hydrogel. However, this concept warrants further study.

The results of this study pertaining to the BPC were limited. However, the results collected indicate that the dry and wet mixing methods at lower polymer contents (5, 8, 10%) can result in EB-GCLs that produce similar or even lower hydraulic conductivities than the BPC. More research is necessary to determine the effects of the in-situ polymerization preparation method for EBs and higher polymer contents (> 10 %) on the hydraulic conductivity and polymer retention of EB-GCLs.

4.6.5.5 Influence of magnitude of hydraulic gradient

Hydraulic conductivity testing of conventional GCLs at elevated hydraulic gradients (> 200) is common to reduce the testing duration (e.g., Shackelford et al. 2000). Although an increase in hydraulic gradient typically corresponds to an increase in effective stress in the specimen and a concomitant lower hydraulic conductivity, multiple studies have shown that the magnitude of hydraulic gradient up to values as high as

550 has a relatively minor effect on the measured hydraulic conductivity of conventional GCLs (Rad et al. 1994; Petrov et al. 1997; Shackelford et al. 2000). However, as previously noted, a decrease in the applied hydraulic gradient from approximately 300 to 30 for specimens PALW5DS and PAHW5DS resulted in a decrease in hydraulic conductivity of 1.5 orders of magnitude and approximately three times, respectively. This behavior suggests that the PALW is less mobile at a lower hydraulic gradient and more effective in terms of achieving a low hydraulic conductivity due to a reduction in polymer elution. The lower hydraulic conductivity of the specimens at the lower hydraulic gradient suggests that, unlike conventional GCLs, the magnitude of the hydraulic gradient may affect the measured hydraulic conductivity of EB-GCLs, and the effect may be opposite to that expected based on effective stress considerations. This sensitivity to hydraulic gradient is consistent with the recognized shear thinning of polymers under higher shear stresses, such as under higher hydraulic gradients (e.g., Markovitz and Kimball 1949; Van Krevelen 1990). Nonetheless, since these results are limited, additional study is needed to understand the influence of hydraulic gradient on the measured hydraulic conductivity of EB-GCLs.

4.6.6 Practical implications

Enhanced-bentonite GCLs are used in practice in applications where conventional (unenhanced) GCLs are hydraulically incompatible. An understanding of the pore blocking mechanism controlling the hydraulic conductivity of EB-GCLs provides a path to better design and tailoring of EB-GCLs for specific applications and informs practitioners as to the myriad of interconnected variables that must be considered when designing with EB-GCLs. Geosynthetic clay liners are applied in a variety of engineered systems as barrier systems and each application can vary in applied hydraulic gradient, when the gradient is imposed, effective stress, and permeant chemistry. This study has identified that the hydraulic conductivity of EB-GCLs can be dependent on permeant chemistry, hydraulic gradient, time, polymer type, and mixing method. Considerations for permeant chemistry and applied effective stress have been documented in standard testing methods. However, due to the reported insensitivity of the hydraulic conductivity of conventional GCLs to the applied hydraulic gradient and the low hydraulic conductivity of conventional GCLs, most

laboratory testing of GCLs occurs at hydraulic gradients of 200 or higher to expedite the testing duration (e.g., methods in ASTM D6766). This study suggests that EB-GCLs may be more sensitive to hydraulic gradient and, therefore, the resulting hydraulic conductivity also will be sensitive to the combinations of laboratory testing parameters and EB material properties. The considerations for site-specific variables and representative hydraulic compatibility testing appear to be even more important with EB-GCLs than with conventional GCLs. Additional study is required to better understand how EB-GCLs can be tailored for site-specific applications, such that pore blocking and retention of the polymer amendment is maximized, and polymer elution is minimized. Fortunately, the non-realistic conditions of hydraulic compatibility tests performed in the lab appear to be conservative (yield a higher hydraulic conductivity than may be anticipated in the field), except perhaps in cases of high field gradients such as evaporation ponds.

The polymer hydrogel formed during hydration of the EB-GCL initially must be mobile and evenly distributed to effectively block all highly conductive pores in the base NaB. Upon permeation, mobile hydrogel is propelled into the conductive pores. Uneven distribution of the polymer can result in interaggregate pores that do not contain hydrogel and will control the hydraulic behavior. Although initially mobile, the fraction of hydrogel blocking the pores must be retained to maintain a low, long-term hydraulic conductivity. The elution of polymer amendment from the EB-GCLs still poses implications with respect to the ability to maintain a low hydraulic conductivity for long-term containment. Further testing is necessary to determine the temporal behavior of polymer elution and if the increased cross-linking and adsorption of pore-clogging hydrogel will create permanent pore clogging resulting in low, long-term hydraulic conductivity.

4.7 CONCLUSIONS

Hydraulic conductivity testing was conducted on both conventional GCL specimens comprising PNaB, GNaB, or pyrophyllite and EB-GCL specimens comprising PNaB, GNaB, or pyrophyllite enhanced with anionic linear polymers including high or low viscosity carboxymethylcellulose (CMCHV, CMCLV) or poly(acrylic acid) with high, medium, or low molecular weights (PAHW, PAMW, PALW), and bentonite

polymer composite (BPC), or covalently cross-linked poly(acrylic acid) (PAx) using dry-sprinkling (DS), dry-mixing (DM), and wet-mixing (WM) specimen preparation methods. The tests were conducted in flexible-wall permeameters at low effective stress (27 kPa) at an applied hydraulic gradient (i) of ~300 using 500 mM NaCl and 167 mM $CaCl_2$ as the permeant liquids. An additional test was performed with one of the EB-GCL specimens at a lower gradient of ~30. Polymer retention analysis was completed by measuring initial and final polymer contents of the EB-GCL specimens. Hydrogel formation tests also were conducted to evaluate the potential for hydrogel to form during hydration of the EB-GCLs via polymer cross-linking. The effect of hydraulic conductivity testing variables, including interaggregate pore size, mineral surface charge, and hydraulic gradient also were investigated.

The following conclusions are drawn from the findings of this study.

- Based on multiple lines of evidence, the mechanisms that controlled the hydraulic conductivity of the EB-GCLs evaluated in this study were a combination of mechanical entrapment (physical retention) and adsorption (chemical retention) of polymer hydrogel in the bentonite pores. The ability of an EB-GCL to produce a low hydraulic conductivity to the NaCl or $CaCl_2$ solution was found to be dependent on (i) the formation of hydrogel, (ii) the random insertion of the hydrogels into the pores such that the largest pores are blocked, (iii) a balance of seepage forces, (iv) the kinetics of hydrogel formation, and (v) adsorption of polymer to the surfaces of the NaB particles or aggregates of particles.
- The physical retention of the polymer hydrogel relies on the interaggregate pores being small enough to retain a fraction of the polymer hydrogel that is sufficient to block the largest NaB pores and reduce hydraulic conductivity. For the PNaB-based PAHW5DS specimen, final polymer contents of 0.68% and 1.2% was sufficient to result in a low hydraulic conductivity (4.0×10^{-11} m/s) to both tested solutions. However, the interaggregate pores of the GNaB-based PAHW5DS specimen retained a similar fraction of polymer hydrogel (0.96 % and 1.12%), but the hydrogel did

not effectively block the largest and most critical pores and the resulting hydraulic conductivity was much higher (7.8×10^{-7} and 5.4×10^{-7} m/s).

- The EB-GCL mixing method (i.e., DS, DM, or WM) affected polymer retention as well as hydraulic conductivity. The DS method resulted in in low hydraulic conductivity in multiple EB-GCLs with a low fraction (≤ 2.5 %) of retained polymer. In contrast, polymer elution in EB-GCLs produced using the DM method resulted in interaggregate flow and an increase in hydraulic conductivity. For all but one WM specimen (i.e., specimen PALW5WM), higher polymer retention occurred (≥ 3.0 %). However, the retained polymer was not correlated with a decrease in hydraulic conductivity, leading to the conclusion that the polymer was retained primarily in the intra-aggregate pores and did not actively block the interaggregate pores participating in flow, resulting in high hydraulic conductivities. The WM EB-GCLs that did result in a low, final hydraulic conductivity when permeated with the 500 mM NaCl solution exhibited decreasing trends in hydraulic conductivity, consistent with polymer movement from the intra-aggregate to interaggregate pores.
- The results of this study pertaining to BPC-GCLs were limited. However, the results collected indicated that other EB-GCLs (prepared using simpler methods and at lower polymer contents (5-10%)) can produce similar or even lower hydraulic conductivity than the BPC-GCL.
- The initially bound cations of the base NaB in EBs may provide a source of cations available for polymer cross-linking and potential polymer adsorption. Polymer chains have a greater chance of forming hydrogels and/or adsorbing to the available exchange sites on the NaB mineral surfaces.
- The degree of hydrogel formation in an EB-GCL during hydration as well as the retention of the hydrogel via mechanical entrapment, adsorption, or both during permeation is a complex function of permeant chemistry, hydraulic gradient, time, type of polymer, and the method of mixing the polymer with the base NaB.

- Tests conducted at a lower hydraulic gradient (i), i.e., $i \approx 30$ versus $i \approx 300$, with EB-GCL specimens prepared by dry sprinkling with 5% of PALW and 5% of PAHW and permeated with 167 mM $CaCl_2$ resulted in a lower hydraulic conductivity. For the EB-GCL enhanced with PALW, the hydraulic conductivity at $i \approx 30$ was 1.5 orders-of-magnitude lower than that at $i \approx 300$, whereas for the EB-GCL enhanced with PAHW, the hydraulic conductivity at $i \approx 30$ was approximately three times lower than that at $i \approx 300$. These results suggest that, unlike conventional GCLs, the magnitude of the hydraulic gradient may affect the measured hydraulic conductivity of EB-GCLs, and the effect may be opposite to that expected based on effective stress considerations. This sensitivity to hydraulic gradient is consistent with the recognized shear thinning of polymer hydrogels under higher shear stresses. However, since this conclusion is based on limited results, additional study is needed to understand further the influence of hydraulic gradient on the measured hydraulic conductivity of EB-GCLs.
- The implications of using a hydraulic gradient in laboratory hydraulic conductivity testing that is different than that applied in the field should be considered, especially since hydraulic gradients in field applications often are lower than those used in laboratory hydraulic conductivity testing.
- The complex interplay of the factors affecting the hydraulic conductivity of EB-GCLs, such as polymer type and mixing method, permeant solution, applied hydraulic gradient, degree and kinetics of hydrogel formation, and polymer adsorption, will ultimately dictate the long-term hydraulic compatibility of EB-GCLs. The complexity of these factors should be considered when selecting EB-GCLs for long-term containment applications or designing future generation of these materials.

REFERENCES

Ashmawy, A., Darwish, E., Sotelo, N. and Muhammad, N. 2002. Hydraulic performance of untreated and polymer-treated bentonite in inorganic landfill leachates. *Clays and Clay Minerals*, 50, 5, 546–552.

ASTM. 2006. Standard test method for swell index of clay mineral component of geosynthetic clay liners. D5890, West Conshohocken, Pennsylvania, USA.

ASTM. 2007. Standard Test Method for Particle-Size Analysis of Soils. D422, West Conshohocken, Pennsylvania, USA.

ASTM. 2010. Standard test methods for liquid limit, plastic limit, and plasticity index of soils. D4318, West Conshohocken, Pennsylvania, USA.

ASTM. 2011. Standard practice for classification of soils for engineering purposes (Unified Soil Classification System). ASTM D2487, ASTM International, West Conshohocken, Pennsylvania, USA.

ASTM. 2014. Standard test method for rapid determination of carbonate content of soils. D4373, West Conshohocken, Pennsylvania, USA.

ASTM. 2018. Standard test method for evaluation properties of geosynthetic clay liners permeated with potentially incompatible liquids. D6766, West Conshohocken, Pennsylvania, USA.

ASTM. 2018. Standard test method for measuring the exchange complex and cation exchange capacity of inorganic fine-grained soils. D7503, West Conshohocken, Pennsylvania, USA.

Bijsterboch, B., Bos, M., Dickinson, E., van Opheusden, J., and Walstra, P. 1995. Brownian dynamics simulation of particle gel formation: from argon to yoghurt. Faraday Discussions. 101.

Billingham, J., Breen, C., and Yarwood, J. 1997. Adsorption of polyamine, polyacrylic acid and polyethylene glycol on Na-montmorillonite: an in-situ study using ATR-FTIR. *Vibrational Spectroscopy*, 14, 19-34.

Bohnhoff, G. 2012. Membrane behavior, diffusion, and compatibility of a polymerized bentonite for containment barrier applications, Ph.D. dissertation, Colorado State University, Fort Collins, Colorado, USA.

Bohnhoff, G., and Shackelford, C. 2013. Improving membrane performance via bentonite polymer nanocomposite. *Applied Clay Science,* 86, 83-98.

Bohnhoff, G., Shackelford, C., and Sample-Lord, K. 2014. Calcium resistant membrane behavior of a polymerized bentonite. *Journal of Geotechnical and Geoenvironmental Engineering*, 140(3), 04013029.

Bohnhoff, G., Shackelford, C., Malusis, M., Scalia, J., Benson, C., Edil, T., Di Emidio, G., Katsumi. T., and Mazzieri, F. 2013. Novel bentonites for containment barrier applications, Proceedings, 18th International Soil Mechanics and Geotechnical Engineering-Challenges and Innovations in Geotechnics Conference, P. Delage, J. Desrues, R. Frank, A. Puech, F. Schlosser, Eds., Presses des Ponts, Paris, 4, 2997-3000.

Buchholz, F. and Graham, A. 1998. *Modern superabsorbent polymer technology*, Wiley-VCH, New York.

Chai, J., and Prongmanee, N. 2020. Barrier properties of a geosynthetic clay liner using polymerized sodium bentonite. *Geotextiles and Geomembranes*, 48, 392-399.

Christian, W., Zainab, B., Tian, K., and Abichou, T. 2020. Effect of specimen preparation on the swell index of bentonite-polymer GCLs. *Geotextiles and Geomembranes,* in press.

Deng, Y., Dixon, J., and White, G. 2006. Adsorption of polyacrylamide on smectite, illite, and kaolinite. *Soil Science Society of America Journal*, 70, 297-304.

Di Emidio, G. 2010. Hydraulic conductivity and chemico-osmotic performance of polymer treated clays, Ph.D. Dissertation, University of Ghent, Ghent, Belgium.

Di Emidio, G., Van Impe, W., and Mazzieri, F. 2010. A polymer enhanced clay for impermeable geosynthetic clay liners. Proceedings. Sixth International Environmental Geotechnics Conference, International Society for Soil Mechanics and Geotechnical Engineers, New Delhi, India.

Doi, M. and Edwards, S. 1978. Dynamics of concentrated polymer systems, Part I.-Brownian motion in the equilibrium state. *Journal of the Chemical Society*, 1789-1801.

Donovan, M., Valorio, R., and Gebka, B. 2016a. Polymer enhanced geosynthetic clay liners for extreme leachate chemistries. Proceedings, EuroGeo6 Conference, International Geosynthetics Society, Jupiter, Florida, USA.

Donovan, M., Valorio, R., and Gebka, B. 2016b. Chemical compatibility of polymer modified GCLs in coal combustion residual leachates. Proceedings, Geoamericas 2016 Conference., International Geosynthetics Society, Jupiter, Florida, USA.

Donovan, M., Gebka, B., and Wind, D. 2020. New lighter, longer GCLs for mining applications. Proceedings, Tailings and Mine Waste 2020 Conference, Colorado State University, Fort Collins, Colorado, USA.

Emerson, W. 1955. Complex formation between montmorillonite and high polymers. *Nature (London),* 176, 461.

Faulks, M. and Schlinz, D. 1994. Absorbent structure comprising of a fibrous matrix having dual z-directional gradient. US Patent Number: 5,356,403.

Finch, C. 1983. *Chemistry and technology of water-soluble polymers.* Plenum Press, New York, New York, USA.

Flynn, B. and Carter, G. 1998. Waterproofing material and method of fabrication thereof. US Patent Number: 6,537,676 B1.

Gunger, N. and Karaoglan, S. 2001. Interaction of polyacrylamide polymer bentonite in aqueous system. *Materials Letters*, 48, 168-175.

Guyonnet, D., Cazaux, D., Vigier-Gailhanou, H., and Chevrier, B. 2009. Effect of cation exchange on hydraulic conductivity in a sand-bentonite-polymer-mixture. Proceedings, 12th International Waste Management and Landfill Symposium, CISA, Cagliari, Italy.

Hagin, J. and Bodman, G.B. 1954. Influence of the polyelectrolyte CRD-186 on aggregation and other physical properties of some California and Israeli solids and some clay minerals. *Soil Science*, 78, 367-378.

Henderson, K., Zhou, T., Otim, K., and Shull, K. 2010. Ionically cross-linked triblock copolymer hydrogels with high strength. *Macromolecules*, 43(14), 6193-6201.

Jackson, D. and Matthews, B. 1994. High wicking liquid absorbent composite. US Patent Number: 5,350,370.

Jo, H., Katsumi, T., Benson, C. and Edil, T. 2001. Hydraulic conductivity and swelling of non-prehydrated GCLs permeated with single species salt solutions, *Journal of Geotechnical and Geoenvironmental Engineering*, 127(7), 557–567.

Katsumi, T., Onikata, M., Hasegawa, S., Lin, L., Kondo, M., and Kamon, M. 2001. Chemical compatibility of modified bentonite permeated with inorganic chemical solutions. *Geoenvironmental Impact Management*, Thomas Telford, London, 419-424.

Katsumi, T., Ishimori, H., Onikata, M., and Fukagawa, R. 2008. Long-term barrier performance of modified bentonite materials against sodium and calcium permeant solutions. *Geotextiles and Geomembranes*, 26(1), 14-30.

Kodama, H., Gatineau, L., and Mering, J. 1971. An analysis of x-ray diffraction line profiles of microcrystalline muscovites. *Clays and Clay Minerals*, 19, 405-413.

Kolstad, D., Benson, C., Edil, T. and Jo, H. 2004. Hydraulic conductivity of dense prehydrated GCL permeated with aggressive inorganic solutions. *Geosynthetics International*, 11(3), 233-241.

Lagaly, G., Ogawa, M., Dékány, I., Faïza Bergaya, B. K. G. T., and Gerhard, L. 2006. Chapter 7.3 Clay Mineral Organic Interactions. *Developments in Clay Science*, Elsevier, 309-377.

Lee, J., Shackelford, C., Benson, C., Jo, H., and Edil, T. 2005. Correlating index properties and hydraulic conductivity of geosynthetic clay liners. Journal of Geotechnical and Geoenvironmental Engineering, 131(11), 1319-1329.

Malusis, M. and Scalia, J. 2007. Hydraulic conductivity of an activated carbon-amended geosynthetic clay liner. GeoDenver 2007. New Peaks in Geotechnics, American Society of Civil Engineers, Reston, VA, 1-13.

Markovitz H, and Kimball, G.E. 1949. The effect of salts on the viscosity of solutions of polyacrylic acid. *Journal of Colloid Science*, 5, 115-139.

Mazzieri, F., Di Emidio, G. and Van Impe, P. 2010. Diffusion of calcium chloride in a modified bentonite: impact on osmotic efficiency and hydraulic conductivity. *Clays and Clay Minerals*, 58(3), 351-363.

McBride, M. (1994). *Environmental Chemistry of Soils*. Oxford University Press, New York, NY, USA.

Mitra, G. and Bhattacherjee, S. 1969. X-ray diffraction studies on the transformation of kaolinite into metakaolin: I. Variability of interlayer spacings. *The American Mineralogist.* 54.

Naismith, J., Wammes, J., and Mulleneers, H. 2011. A sustainable mineral barrier option. Proceedings, GeoFrontiers 2011: Advances in geotechnical engineering, ASCE, Reston, VA, USA.

Onikata, M., Kondo, M., Hayashi, N., and Yamanaka, S. 1996. Development and characterization of multiswellable bentonite, 2nd International Congress on Environmental Geotechnics, IS-Osaka '96, M. Kamon, Ed., Nov. 5-8, 1996, Osaka, Japan, Balkema, Rotterdam, 1, 587-590.

Onikata, M., Kondo, M., Hayashi, N., and Yamanaka, S. 1999. Complex formation of cation-exchanged montmorillonites with propylene carbonate: Osmotic swelling in aqueous electrolyte solutions. *Clays and Clay Minerals*, 47(5), 672-677.

Petrov, R., Rowe, R., and Quigley, R., 1997. Selected factors influencing GCL hydraulic conductivity. *Journal of Geotechnical and Geoenvironmental Engineering*, ASCE, Reston, VA 123(8), 683-695.

Plischke, M., Schmidt, M., and Rezai, E. 1999. Adsorbent composite structure formed of a substrate and cross-linkable hydrogel polymer particles. US Patent Number: 5,977,014.

Rad, N., Jacobson, B., and Bachus, R. 1994. Compatibility of geosynthetic clay liners with organic and inorganic permeants, Proceedings, Fifth International Conference on Geotextiles, Geomembranes and Related Products, Singapore, 1165-1168.

Reddy, K. El-Zein, A. Airey, D. Alonso-Marroquin, F. Schubel, P., and Manalo, A. 2020. Self-healing polymers: synthesis methods and applications. *Nano-Structures & Nano-Objects*, 23, 100500.

Ruhrwein, R. and Ward, D.1952. Mechanism of clay aggregation by polyelectrolytes. *Soil Science*, 73, 485-492.

Satoh, T. and Yamane, I. 1971. On the interlamellar complex between Na-montmorillonite and organic substance in certain soil. *Soil Science and Plant Nutrition*, 17, 181-185.

Scalia, J. and Benson, C. 2011. Hydraulic conductivity of geosynthetic clay liners exhumed from landfill final covers with composite barriers. *Journal of Geotechnical and Geoenvironmental Engineering*, 137(1), 1-13.

Scalia, J., and Benson, C. 2016. Evaluation of Na Bentonite-polyacrylate mixtures to enhance the chemical resistance of geosynthetic clay liners, Proceedings, Geo-Chicago 2016, GSP No. 271, ASCE, Reston, Virginia, USA, 388-397.

Scalia, J., and Benson, C. 2017. Polymer fouling and hydraulic conductivity of mixtures of sodium bentonite and a bentonite-polymer composite. *Journal of Geotechnical and Geoenvironmental Engineering*, 143(4), 04016112.

Scalia, J., Benson, C., Bohnhoff, G., Edil, T., and Shackelford, C. 2014. Long-term hydraulic conductivity of a bentonite-polymer composite permeated with aggressive inorganic solutions. *Journal of Geotechnical and Geoenvironmental Engineering,* 140(3), 04013025.

Scalia, J., Benson, C., Edil, T., Bohnhoff, G., and Shackelford, C. 2011. Geosynthetic clay liners containing bentonite polymer nanocomposite. GeoFrontiers 2011 Advances in Geotechnical Engineering, J. Han and D. Alazamora, Eds., ASCE, Reston, Virginia, USA, 2001-2009.

Scalia, J., Bohnhoff, G., Shackelford, C., Benson, C., Sample-Lord, K., Malusis, M., and Likos, W. 2018. Enhanced bentonites for containment of inorganic wastes by GCLs. *Geosynthetics International,* 25(4), 392-411.

Schroeder, C., Monjoie, A., Illing, P., Dosquet, D. and Thorez, J. 2001. Testing a factory-prehydrated GCL under several conditions. Proceedings, Sardinia 2001, 8th International Waste Management and Landfill Symposium, Pula, Italy, CISA Environmental Sanitary Engineering Centre, Cagliari, Italy, 187-196.

Shackelford, C. 1994. Waste-soil interactions that alter hydraulic conductivity. Hydraulic Conductivity and Waste Contaminant Transport in Soil, D. Daniel and S. Trautwein, Eds., STP 1142, ASTM, West Conshohoken, PA, 111-168.

Shackelford, C., Benson, C., Katsumi, T., Edil, T., and Lin, L. 2000. Evaluating the hydraulic conductivity of GCLs permeated with non-standard liquids. *Geotextiles and Geomembranes*, 18(2-4), 133-161.

Short, M. and Walker, P. 1963. Measurement of interlayer spacings and crystal size in turbostatic carbons. *Carbon*, 1, 3-9.

Teraoka, I. 2002. *Polymer solutions: an introduction to physical properties*. Wiley. Hoboken, New Jersey, USA.

Theng, B.K.G. 1970. Interactions of clay minerals with organic polymers. Some practical applications. *Clay and Clay Minerals,* 18, 357-62.

Theng, B., Churchman, G. and Newman, R. 1986. The occurrence of interlayer clay organic complexes in two New Zealand soils. *Soil Science*, 142, 262-266.

Tian, K., Benson, C. and Likos, W. 2016a. Hydraulic conductivity of geosynthetic clay liners to low-level radioactive waste leachate. *Journal of Geotechnical and Geoenvironmental Engineering*, 142(8), 1-12.

Tian, K., Likos, W., and Benson, C. 2016b. Pore-scale imaging of polymer-modified bentonite in saline solutions, Proceedings, Geo-Chicago 2016, GSP No. 271, ASCE, Reston, Virginia, USA, 468-477.

Tian, K., Benson, C. and Likos, W. 2017. Effect of anion ratio on the hydraulic conductivity of a bentonite-polymer geosynthetic clay liner. Proceedings, Geo-Frontiers 2017, Orlando, FL, USA, GSP No. 276, ASCE, Reston, VA, USA, pp. 180–189.

Tian, K., Likos, W., and Benson, C. 2019. Polymer elution and hydraulic conductivity of bentonite-polymer composite geosynthetic clay liners. *Journal of Geotechnical and Geoenvironmental Engineering,* 145(10), 04019071.

Trauger, R. and Darlington, J. 2000. Next-Generation Geosynthetic Clay Liners for Improved Durability and Performance. TR-220. Colloid Environmental Technologies Company, Arlington Heights, Illinois, USA.

Van Krevelen, D. 1990. *Properties of polymers. First Edition*. Elsevier. New York, New York, USA.

Yu, B., El-Zein, A., and Rowe, R. 2020. Effect of added polymer on the desiccation and healing of a geosynthetic clay liner subject to thermal gradients. *Geotextiles and Geomembranes*, in press.

Appendix A: GCL Hydraulic Conductivity Test Summaries

A1. Powdered NaB EB-GCLs

A1.1 Terminated GCL hydraulic conductivity test summaries: permeant 167 mM $CaCl_2$

GCL Hydraulic Conductivity- Gravity Method			
Test ID	**A1**		
GCL type	PAHW5DS	**Terminated test results**	
Polymer type	PAHW	*k* [D6766]	4.0×10^{-11} m/s
Mixing method	DS	PVF [D6766]	13.3
Permeant liquid	167 mM$CaCl_2$	time [D6766]	50.2 d
Permeant liquid EC	31.70 mS/cm	*k* [final]	4.0×10^{-11}m/s
Permeant liquid pH	5.81	PVF [final]	13.3
Specimen diameter	15.3 cm	time [final]	50.2 d
	6.0 in	Avg. EC	32.29 mS/cm
Specimen thickness	0.48 cm	Avg. pH	4.77
		Final sat.	104%
Avg. effective stress	27.2 kPa	Final porosity	0.67
	3.94 psi	Final void ratio	2.04
Avg. gradient	301	Final ρ_d	0.88 Mg/m^3
Avg. polymer content initial (%)	5	Final ω	0.76
Avg. polymer content final (%)	0.68	Hydrogel GCL	yes
Preferential flow (Y/N)	Not Tested	Hydrogel effluent	yes

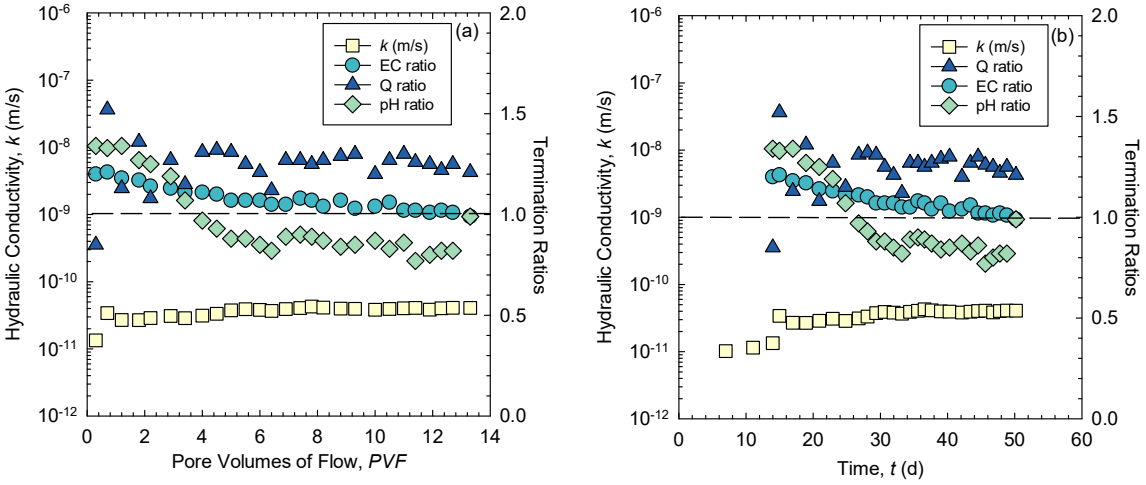

GCL Hydraulic Conductivity- Gravity Method

Test ID	A2		
GCL type	PAHW8DS	**Terminated test results**	
Polymer type	PAHW	*k* [D6766]	5.4×10^{-11} m/s
Mixing method	DS	PVF [D6766]	3.8
Permeant liquid	167 mM$CaCl_2$	time [D6766]	24.6 d
Permeant liquid EC	31.70 mS/cm	*k* [final]	5.4×10^{-11}m/s
Permeant liquid pH	5.81	PVF [final]	3.8
Specimen diameter	14.9 cm	time [final]	24.6 d
	5.8 in	Avg. EC	32.23 mS/cm
Specimen thickness	0.62 cm	Avg. pH	4.42
		Final sat.	74%
Avg. effective stress	26.8 kPa	Final porosity	0.74
	3.9 psi	Final void ratio	2.79
Avg. gradient	246	Final ρ_d	0.70 Mg/m^3
Avg. polymer content initial (%)	8	Final ω	0.79
Avg. polymer content final (%)	0.34	Hydrogel GCL	yes
Preferential flow (Y/N)	Not Tested	Hydrogel effluent	yes

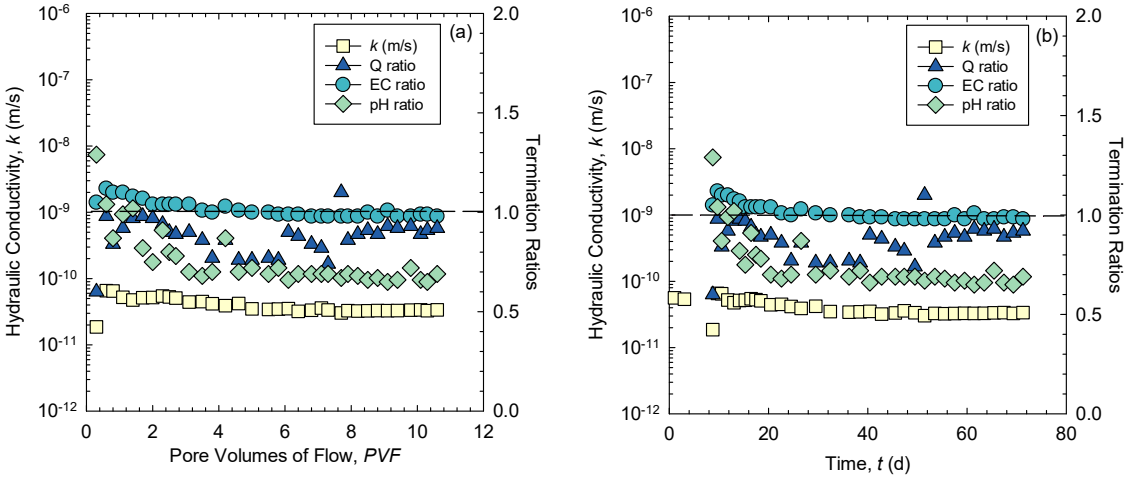

GCL Hydraulic Conductivity- Gravity Method

Test ID	A3		
GCL type	PAHW5WM	**Terminated test results**	
Polymer type	PAHW	*k* [D6766]	3.1×10^{-10} m/s
Mixing method	WM	PVF [D6766]	2.6
Permeant liquid	167 mM$CaCl_2$	time [D6766]	1.5 d
Permeant liquid EC	31.70 mS/cm	*k* [final]	2.5×10^{-10}m/s
Permeant liquid pH	5.81	PVF [final]	5.7
Specimen diameter	14.9 cm	time [final]	3.3 d
	6.0 in	Avg. EC	31.27 mS/cm
Specimen thickness	0.62 cm	Avg. pH	4.73
		Final sat.	102%
Avg. effective stress	27.3 kPa	Final porosity	0.69
	3.96 psi	Final void ratio	2.24
Avg. gradient	272	Final ρ_d	0.83 Mg/m^3
Avg. polymer content initial (%)	4.52	Final ω	0.86
Avg. polymer content final (%)	4.65	Hydrogel GCL	no
Preferential flow (Y/N)	Not Tested	Hydrogel effluent	yes

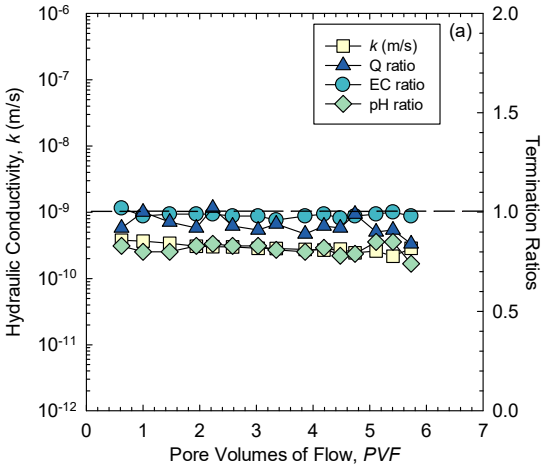

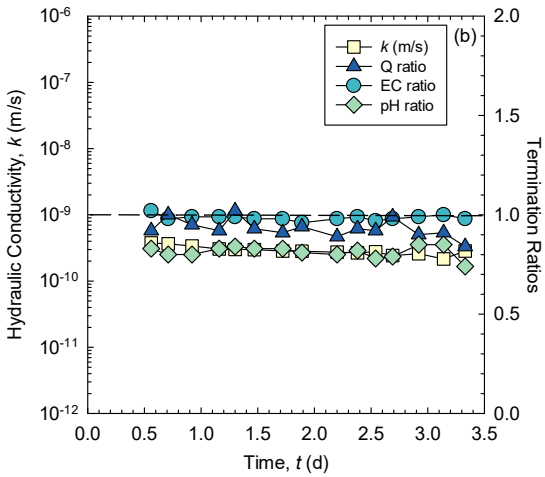

GCL Hydraulic Conductivity- Gravity Method

Test ID	A4		
GCL type	PAMW5DS	**Terminated test results**	
Polymer type	PAHW	*k* [D6766]	4.7×10^{-10} m/s
Mixing method	DS	PVF [D6766]	12.4
Permeant liquid	167 mM$CaCl_2$	time [D6766]	1.7 d
Permeant liquid EC	31.70 mS/cm	*k* [final]	4.2×10^{-10}m/s
Permeant liquid pH	5.81	PVF [final]	15.3
Specimen diameter	15.0 cm	time [final]	2.4 d
	5.9 in	Avg. EC	31.27 mS/cm
Specimen thickness	0.47 cm	Avg. pH	4.73
		Final sat.	110%
Avg. effective stress	27.4 kPa	Final porosity	0.65
	3.98 psi	Final void ratio	1.84
Avg. gradient	300	Final ρ_d	0.94 Mg/m^3
Avg. polymer content initial (%)	5	Final ω	0.75
Avg. polymer content final (%)	1.27	Hydrogel GCL	no
Preferential flow (Y/N)	Not Tested	Hydrogel effluent	yes

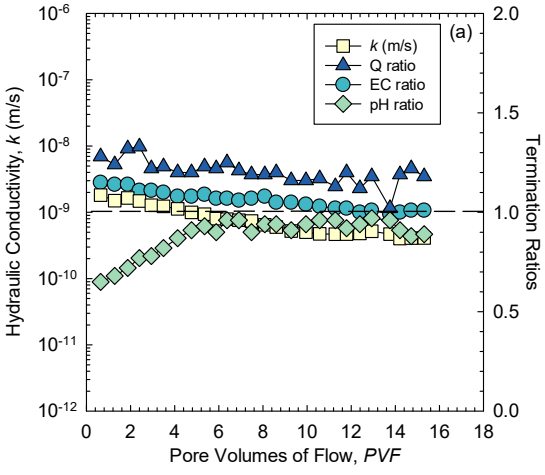

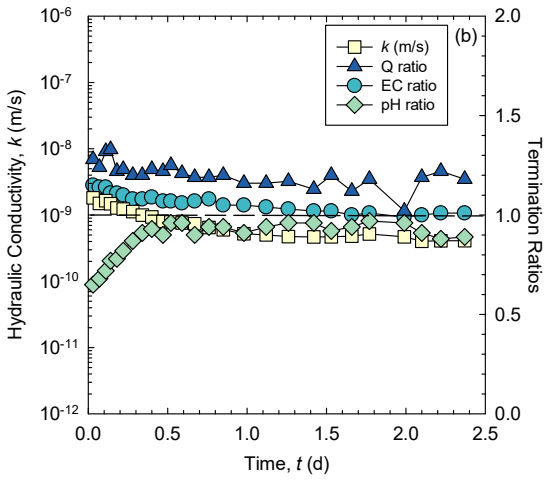

GCL Hydraulic Conductivity- Gravity Method

Test ID	A5		
GCL type	PAMW8DS	**Terminated test results**	
Polymer type	PAMW	*k* [D6766]	1.1×10^{-11} m/s
Mixing method	DS	PVF [D6766]	7.1
Permeant liquid	167 mM$CaCl_2$	time [D6766]	84.9 d
Permeant liquid EC	31.70 mS/cm	*k* [final]	1.1×10^{-11} m/s
Permeant liquid pH	5.81	PVF [final]	13.0
Specimen diameter	15.1 cm	time [final]	117 d
	6.0 in	Avg. EC	35.52 mS/cm
Specimen thickness	0.47 cm	Avg. pH	4.70
		Final sat.	95%
Avg. effective stress	27.2 kPa	Final porosity	0.68
	3.95 psi	Final void ratio	2.10
Avg. gradient	293	Final ρ_d	0.86 Mg/m^3
Avg. polymer content initial (%)	8	Final ω	0.75
Avg. polymer content final (%)	2.54	Hydrogel GCL	yes
Preferential flow (Y/N)	Not Tested	Hydrogel effluent	yes

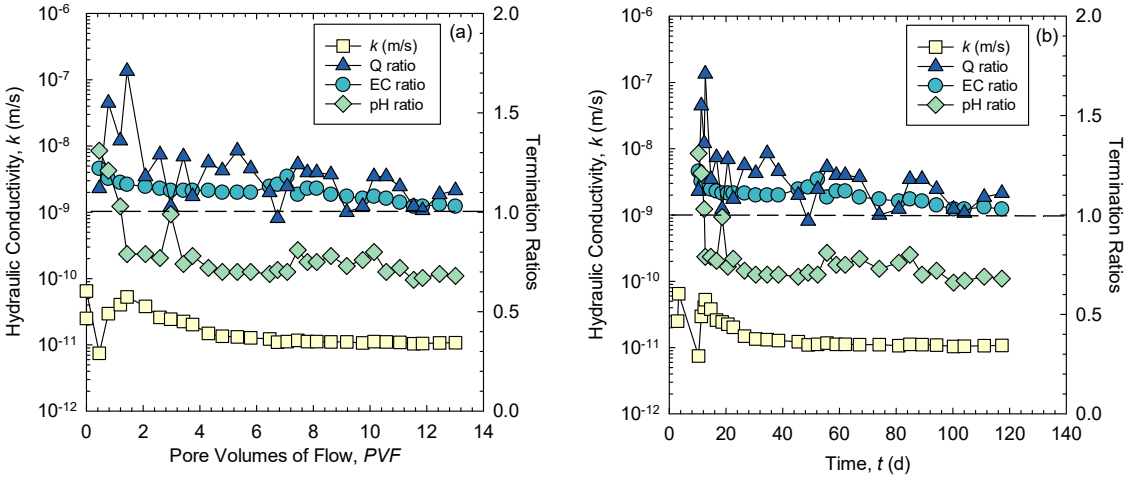

GCL Hydraulic Conductivity- Gravity Method

Test ID	A6		
GCL type	PAMW10DS	**Terminated test results**	
Polymer type	PAMW	*k* [D6766]	2.5×10^{-11} m/s
Mixing method	DS	PVF [D6766]	3.8
Permeant liquid	167 mM$CaCl_2$	time [D6766]	48.7 d
Permeant liquid EC	31.70 mS/cm	*k* [final]	2.7×10^{-11} m/s
Permeant liquid pH	5.81	PVF [final]	10.1
Specimen diameter	14.8 cm	time [final]	112 d
	5.8 in	Avg. EC	31.37 mS/cm
Specimen thickness	0.63 cm	Avg. pH	3.70
		Final sat.	65%
Avg. effective stress	26.8 kPa	Final porosity	0.75
	3.89 psi	Final void ratio	3.06
Avg. gradient	244	Final ρ_d	0.66 Mg/m^3
Avg. polymer content initial (%)	10	Final ω	0.74
Avg. polymer content final (%)	4.28	Hydrogel GCL	no
Preferential flow (Y/N)	Not Tested	Hydrogel effluent	yes

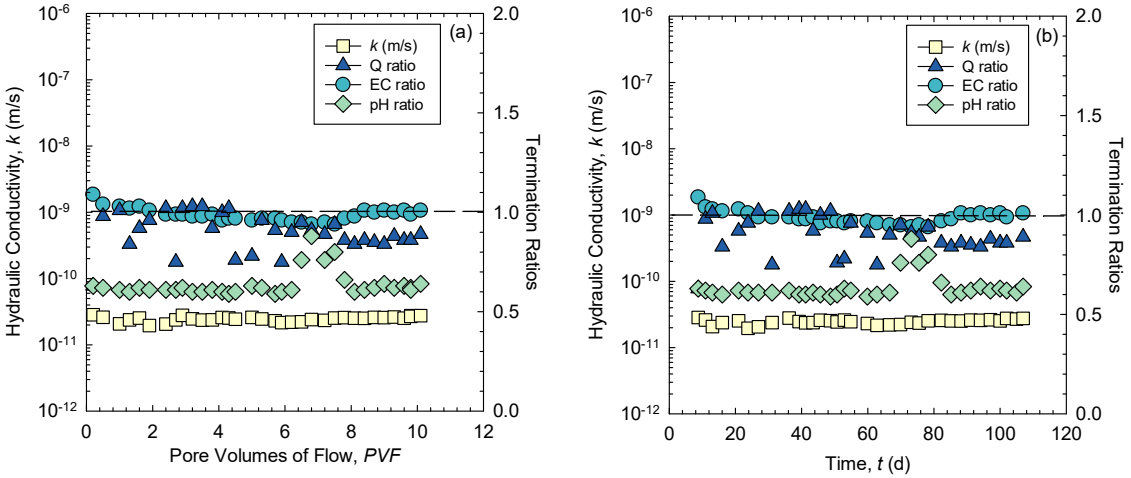

GCL Hydraulic Conductivity- Gravity Method

Test ID	A7		
GCL type	PALW5DS	**Terminated test results**	
Polymer type	PALW	*k* [D6766]	5.7×10^{-10} m/s
Mixing method	DS	PVF [D6766]	8.2
Permeant liquid	167 mM$CaCl_2$	time [D6766]	1.4 d
Permeant liquid EC	31.70 mS/cm	*k* [final]	3.4×10^{-10} m/s
Permeant liquid pH	5.81	PVF [final]	16.1
Specimen diameter	15.1 cm	time [final]	3.7 d
	5.9 in	Avg. EC	33.58 mS/cm
Specimen thickness	0.43 cm	Avg. pH	5.09
		Final sat.	123%
Avg. effective stress	27.3 kPa	Final porosity	0.62
	4.0 psi	Final void ratio	1.65
Avg. gradient	327	Final ρ_d	1.01 Mg/m^3
Avg. polymer content initial (%)	5	Final ω	0.76
Avg. polymer content final (%)	1.42	Hydrogel GCL	yes
Preferential flow (Y/N)	Not Tested	Hydrogel effluent	yes

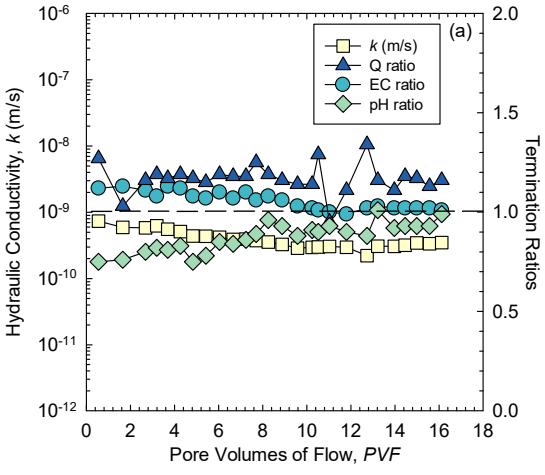

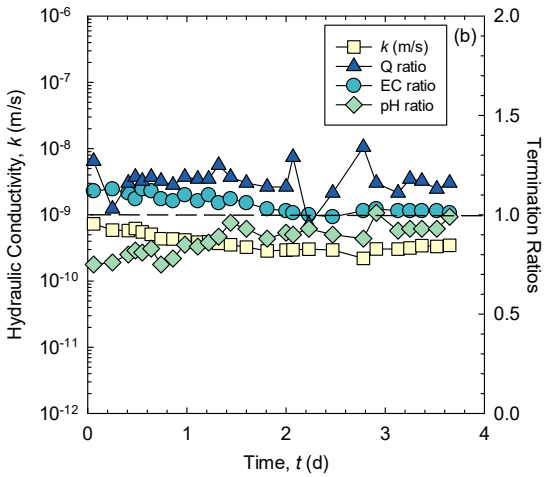

GCL Hydraulic Conductivity- Gravity Method

Test ID	A8		
GCL type	PALW10DS	**Terminated test results**	
Polymer type	PALW	*k* [D6766]	4.1×10^{-10} m/s
Mixing method	DS	PVF [D6766]	3.9
Permeant liquid	167 mM$CaCl_2$	time [D6766]	3.5 d
Permeant liquid EC	31.70 mS/cm	*k* [final]	4.0×10^{-10} m/s
Permeant liquid pH	5.81	PVF [final]	5.5
Specimen diameter	15.0 cm	time [final]	4.3 d
	5.9 in	Avg. EC	32.54 mS/cm
Specimen thickness	0.62 cm	Avg. pH	3.96
		Final sat.	68%
Avg. effective stress	27.3 kPa	Final porosity	0.75
	4.0 psi	Final void ratio	2.97
Avg. gradient	232	Final ρ_d	0.67 Mg/m^3
Avg. polymer content initial (%)	10	Final ω	0.75
Avg. polymer content final (%)	3.1	Hydrogel GCL	yes
Preferential flow (Y/N)	Not Tested	Hydrogel effluent	yes

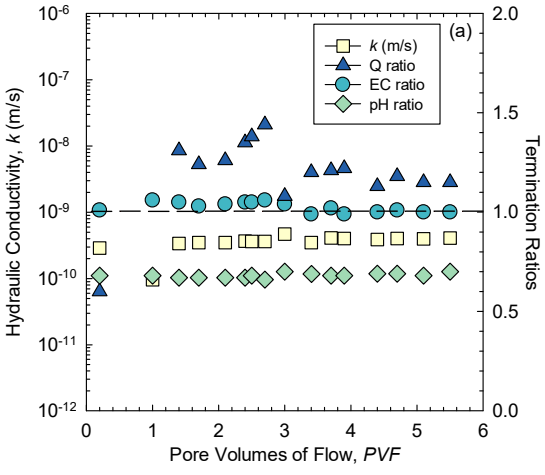

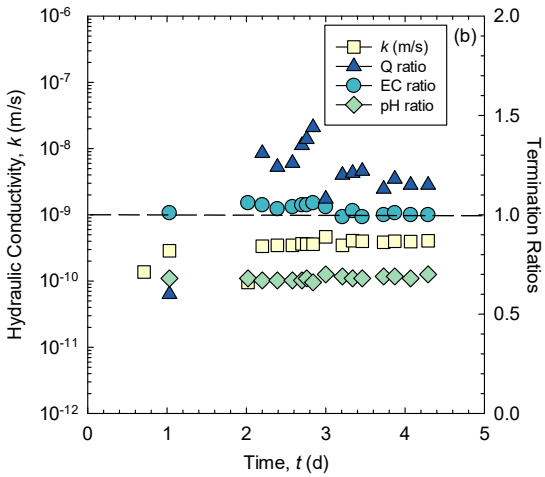

GCL Hydraulic Conductivity- Gravity Method

Test ID	A9		
GCL type	PALW5WM	**Terminated test results**	
Polymer type	PALW	*k* [D6766]	3.3×10^{-10} m/s
Mixing method	WM	PVF [D6766]	5.0
Permeant liquid	167 mM$CaCl_2$	time [D6766]	2.5 d
Permeant liquid EC	31.70 mS/cm	*k* [final]	3.8×10^{-10} m/s
Permeant liquid pH	5.81	PVF [final]	7.0
Specimen diameter	15.4 cm	time [final]	3.3 d
	6.1 in	Avg. EC	28.47 mS/cm
Specimen thickness	0.53 cm	Avg. pH	4.97
		Final sat.	97%
Avg. effective stress	27.3 kPa	Final porosity	0.70
	4.0 psi	Final void ratio	2.36
Avg. gradient	272	Final ρ_d	0.80 Mg/m^3
Avg. polymer content initial (%)	3.33	Final ω	0.85
Avg. polymer content final (%)	1.72	Hydrogel GCL	no
Preferential flow (Y/N)	Not Tested	Hydrogel effluent	yes

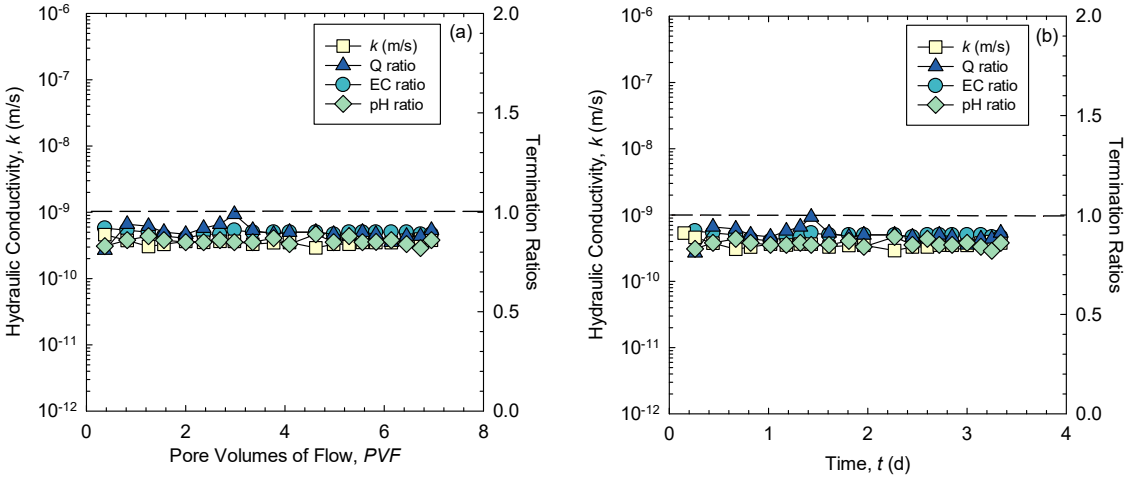

GCL Hydraulic Conductivity- Gravity Method

Test ID	A10		
GCL type	CMCHV5DM	**Terminated test results**	
Polymer type	CMCHV	*k* [D6766]	1.4×10^{-8} m/s
Mixing method	DM	PVF [D6766]	14.2
Permeant liquid	167 mM$CaCl_2$	time [D6766]	65.4 d
Permeant liquid EC	31.70 mS/cm	*k* [final]	1.8×10^{-8} m/s
Permeant liquid pH	5.81	PVF [final]	21.4
Specimen diameter	14.9 cm	time [final]	65.5 d
	5.9 in	Avg. EC	33.01 mS/cm
Specimen thickness	0.76 cm	Avg. pH	6.37
		Final sat.	73%
Avg. effective stress	25.2 kPa	Final porosity	0.78
	3.7 psi	Final void ratio	3.54
Avg. gradient	242	Final ρ_d	0.59 Mg/m^3
Avg. polymer content initial (%)	5	Final ω	0.97
Avg. polymer content final (%)	3.17	Hydrogel GCL	no
Preferential flow (Y/N)	Y	Hydrogel effluent	yes

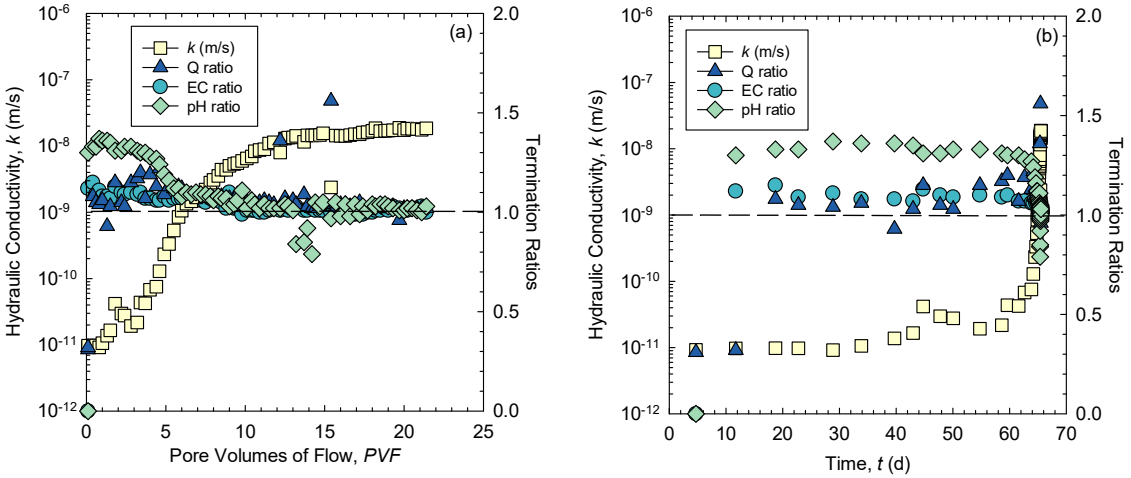

GCL Hydraulic Conductivity- Gravity Method

Test ID	A11		
GCL type	CMCHV5WM	**Terminated test results**	
Polymer type	CMCHV	*k* [D6766]	3.7×10^{-10} m/s
Mixing method	WM	PVF [D6766]	5.7
Permeant liquid	167 mM$CaCl_2$	time [D6766]	8.4 d
Permeant liquid EC	31.70 mS/cm	*k* [final]	3.8×10^{-10} m/s
Permeant liquid pH	5.81	PVF [final]	6.2
Specimen diameter	15.2 cm	time [final]	8.8 d
	6.0 in	Avg. EC	28.43 mS/cm
Specimen thickness	0.66 cm	Avg. pH	7.09
		Final sat.	91%
Avg. effective stress	27.6 kPa	Final porosity	0.76
	4.0 psi	Final void ratio	3.09
Avg. gradient	215	Final ρ_d	0.65 Mg/m^3
Avg. polymer content initial (%)	4.47	Final ω	1.06
Avg. polymer content final (%)	4.17	Hydrogel GCL	no
Preferential flow (Y/N)	Not Tested	Hydrogel effluent	yes

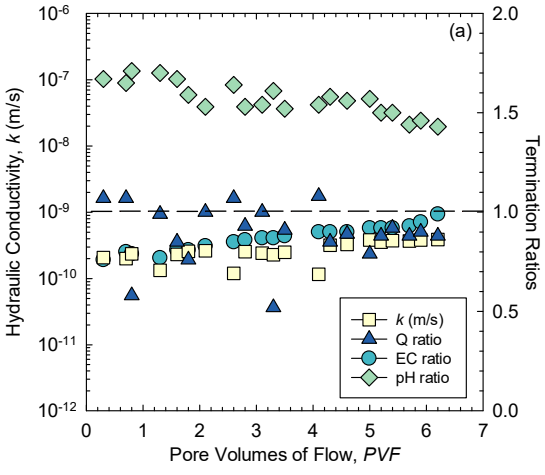

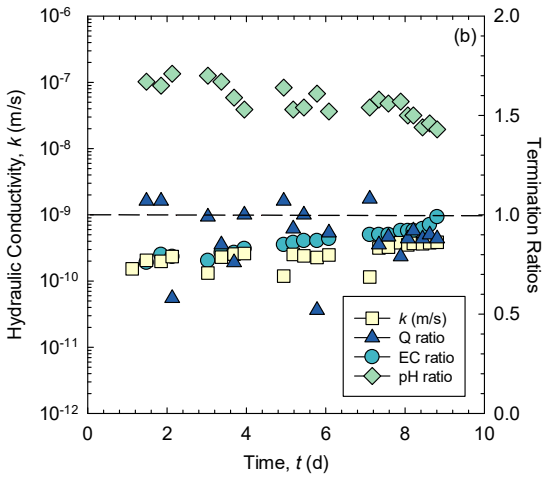

GCL Hydraulic Conductivity- Gravity Method

Test ID	A12		
GCL type	CMCLV5DM	**Terminated test results**	
Polymer type	CMCLV	*k* [D6766]	1.4×10^{-10} m/s
Mixing method	DM	PVF [D6766]	3.2
Permeant liquid	167 mM$CaCl_2$	time [D6766]	3.0 d
Permeant liquid EC	31.70 mS/cm	*k* [final]	3.1×10^{-9} m/s
Permeant liquid pH	5.81	PVF [final]	16.2
Specimen diameter	15.0 cm	time [final]	4.4 d
	5.9 in	Avg. EC	32.68 mS/cm
Specimen thickness	0.51 cm	Avg. pH	6.41
		Final sat.	112%
Avg. effective stress	27.3 kPa	Final porosity	0.68
	4.0 psi	Final void ratio	2.15
Avg. gradient	283	Final ρ_d	0.85 Mg/m^3
Avg. polymer content initial (%)	5	Final ω	0.91
Avg. polymer content final (%)	2.82	Hydrogel GCL	no
Preferential flow (Y/N)	Y	Hydrogel effluent	yes

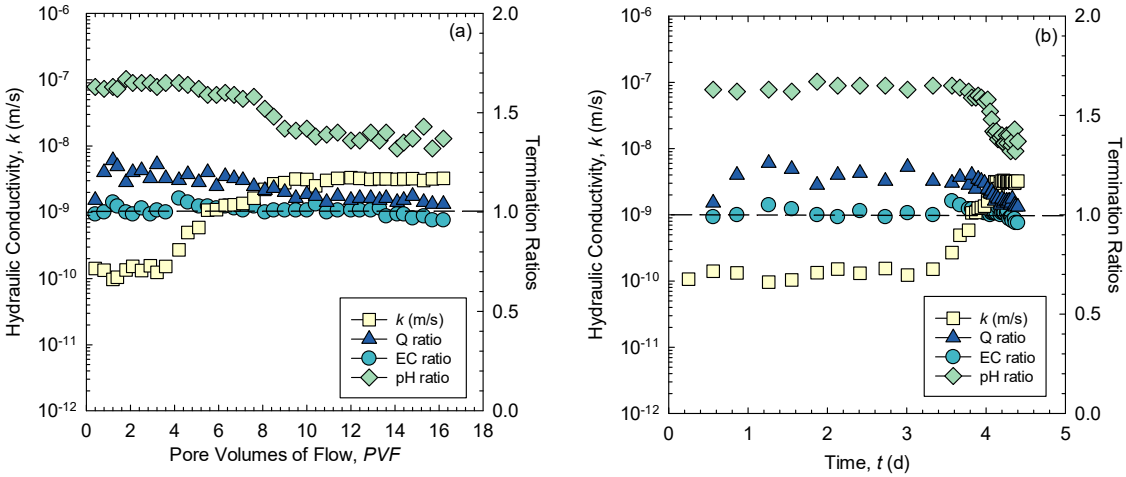

GCL Hydraulic Conductivity- Gravity Method

Test ID	A13		
GCL type	BPC	**Terminated test results**	
Polymer type	BPC	*k* [D6766]	1.6×10^{-10} m/s
Mixing method	none	PVF [D6766]	16.1
Permeant liquid	167 mM$CaCl_2$	time [D6766]	267 d
Permeant liquid EC	31.70 mS/cm	*k* [final]	1.4×10^{-10} m/s
Permeant liquid pH	5.81	PVF [final]	19.3
Specimen diameter	14.8 cm	time [final]	271 d
	5.8 in	Avg. EC	32.81 mS/cm
Specimen thickness	0.52 cm	Avg. pH	5.25
		Final sat.	121%
Avg. effective stress	27.5 kPa	Final porosity	0.66
	4.0 psi	Final void ratio	1.91
Avg. gradient	267	Final ρ_d	0.92 Mg/m^3
Avg. polymer content initial (%)	28.5	Final ω	0.87
Avg. polymer content final (%)	7.39	Hydrogel GCL	yes
Preferential flow (Y/N)	Y	Hydrogel effluent	yes

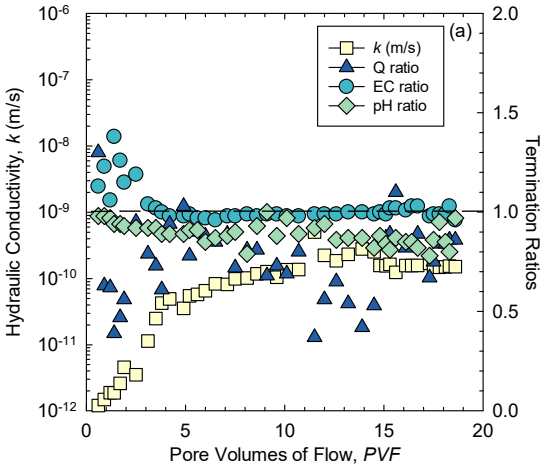

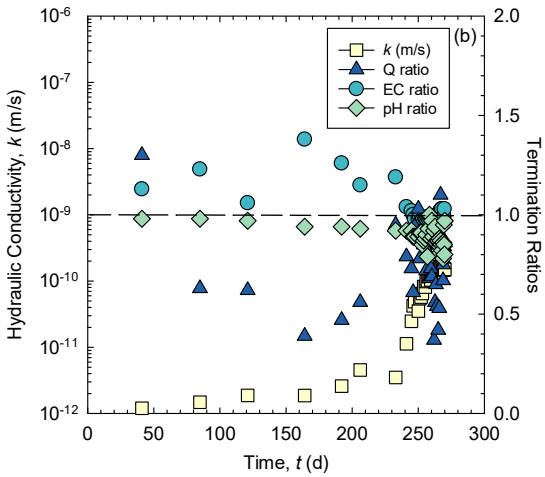

GCL Hydraulic Conductivity- Gravity Method

Test ID	A14		
GCL type	BPC5DM	**Terminated test results**	
Polymer type	BPC	*k* [D6766]	1.6×10^{-10} m/s
Mixing method	DM	PVF [D6766]	16.1
Permeant liquid	167 mM$CaCl_2$	time [D6766]	267 d
Permeant liquid EC	31.70 mS/cm	*k* [final]	1.4×10^{-10} m/s
Permeant liquid pH	5.81	PVF [final]	19.3
Specimen diameter	14.8 cm	time [final]	271 d
	5.8 in	Avg. EC	31.23 mS/cm
Specimen thickness	0.59 cm	Avg. pH	7.32
		Final sat.	75%
Avg. effective stress	27.4 kPa	Final porosity	0.71
	4.0 psi	Final void ratio	2.49
Avg. gradient	237	Final ρ_d	0.77 Mg/m^3
Avg. polymer content initial (%)	5	Final ω	0.69
Avg. polymer content final (%)	3.66	Hydrogel GCL	yes
Preferential flow (Y/N)	Not tested	Hydrogel effluent	yes

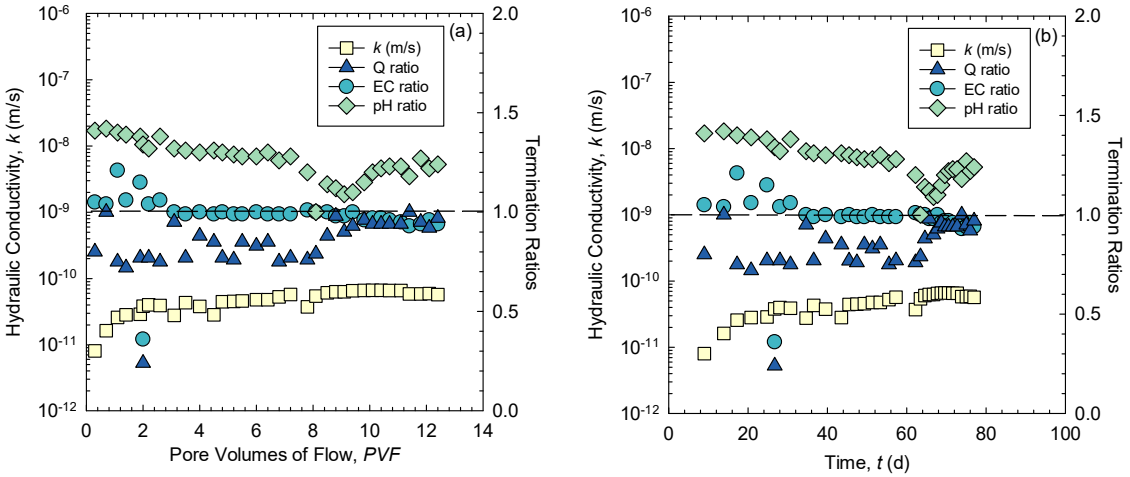

GCL Hydraulic Conductivity- Gravity Method

Test ID	**A15**		
GCL type	PAx5DS	**Terminated test results**	
Polymer type	PAx	*k* [D6766]	2.4×10^{-10} m/s
Mixing method	DS	PVF [D6766]	10.7
Permeant liquid	167 mM$CaCl_2$	time [D6766]	0.5 d
Permeant liquid EC	31.70 mS/cm	*k* [final]	1.2×10^{-9} m/s
Permeant liquid pH	5.81	PVF [final]	17.3
Specimen diameter	15.2 cm	time [final]	1.0 d
	6.0 in	Avg. EC	29.80 mS/cm
Specimen thickness	0.53 cm	Avg. pH	6.26
		Final sat.	103%
Avg. effective stress	27.8 kPa	Final porosity	0.68
	4.1 psi	Final void ratio	2.10
Avg. gradient	251	Final ρ_d	0.86 Mg/m^3
Avg. polymer content initial (%)	5	Final ω	0.81
Avg. polymer content final (%)	4.72	Hydrogel GCL	yes
Preferential flow (Y/N)	Y	Hydrogel effluent	yes

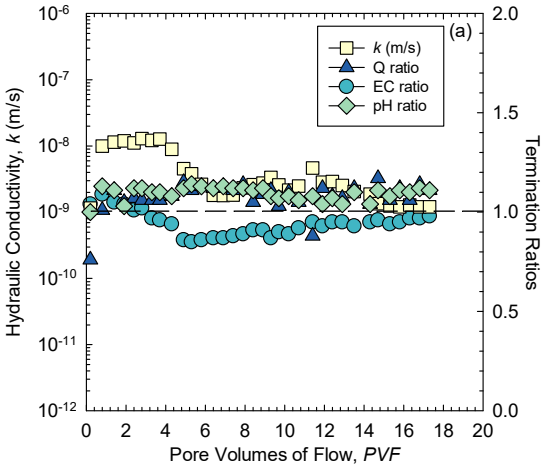

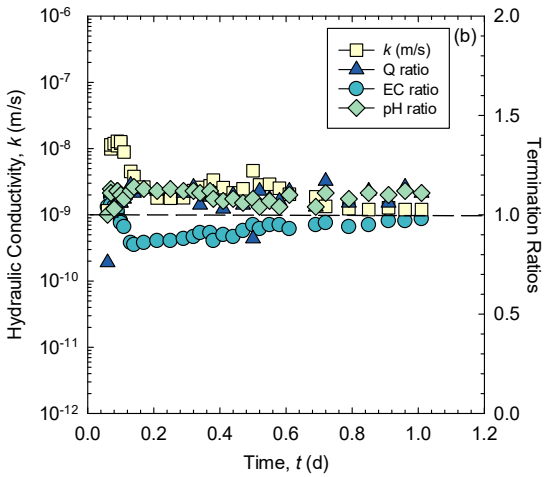

A1.2. Terminated GCL hydraulic conductivity test summaries: permeant 500 mM NaCl

GCL Hydraulic Conductivity- Gravity Method			
Test ID	**B1**		
GCL type	PAHW5DS	**Terminated test results**	
Polymer type	PAHW	*k* [D6766]	1.3×10^{-11} m/s
Mixing method	DS	PVF [D6766]	3.3
Permeant liquid	500 mM NaCl	time [D6766]	34.6 d
Permeant liquid EC	48.53 mS/cm	*k* [final]	1.8×10^{-11}m/s
Permeant liquid pH	6.17	PVF [final]	8.1
Specimen diameter	15.0 cm	time [final]	66.4 d
	5.9 in	Avg. EC	47.44 mS/cm
Specimen thickness	0.46 cm	Avg. pH	6.70
		Final sat.	117%
Avg. effective stress	27.3 kPa	Final porosity	0.64
	3.96 psi	Final void ratio	1.77
Avg. gradient	311	Final ρ_d	0.97 Mg/m^3
Avg. polymer content initial (%)	5	Final ω	0.78
Avg. polymer content final (%)	1.20	Hydrogel GCL	No
Preferential flow (Y/N)	Not Tested	Hydrogel effluent	Yes

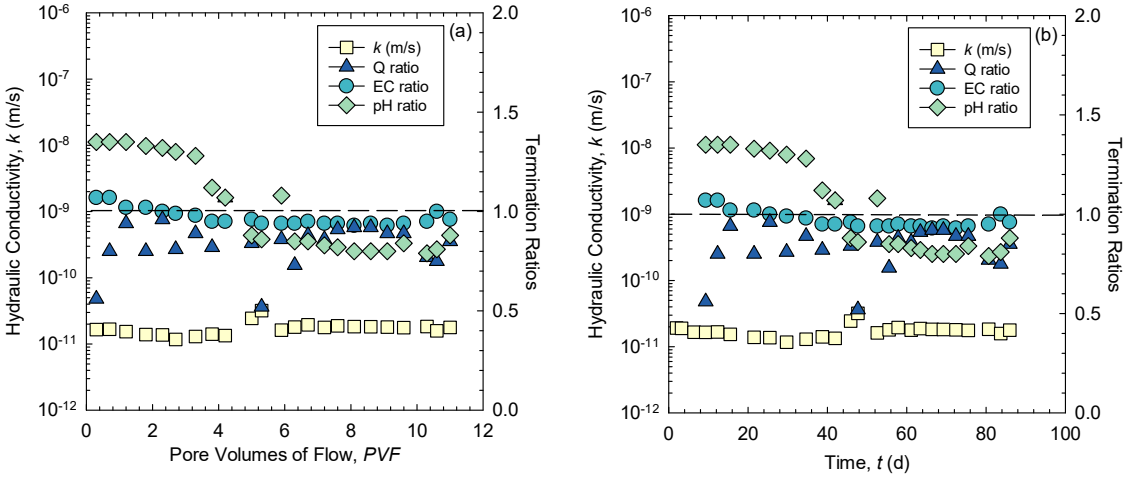

GCL Hydraulic Conductivity- Gravity Method

Test ID	B2		
GCL type	PAHW5WM	**Terminated test results**	
Polymer type	PAHW	*k* [D6766]	5.2×10^{-11} m/s
Mixing method	WM	PVF [D6766]	5.3
Permeant liquid	500 mM NaCl	time [D6766]	16.4 d
Permeant liquid EC	48.53 mS/cm	*k* [final]	1.5×10^{-11}m/s
Permeant liquid pH	6.17	PVF [final]	20.4
Specimen diameter	15.2 cm	time [final]	188 d
	6.0 in	Avg. EC	46.46 mS/cm
Specimen thickness	0.63 cm	Avg. pH	5.19
		Final sat.	98%
Avg. effective stress	27.3 kPa	Final porosity	0.75
	4.0 psi	Final void ratio	2.94
Avg. gradient	225	Final ρ_d	0.68 Mg/m^3
Avg. polymer content initial (%)	4.52	Final ω	1.08
Avg. polymer content final (%)	3.28	Hydrogel GCL	no
Preferential flow (Y/N)	Not Tested	Hydrogel effluent	yes

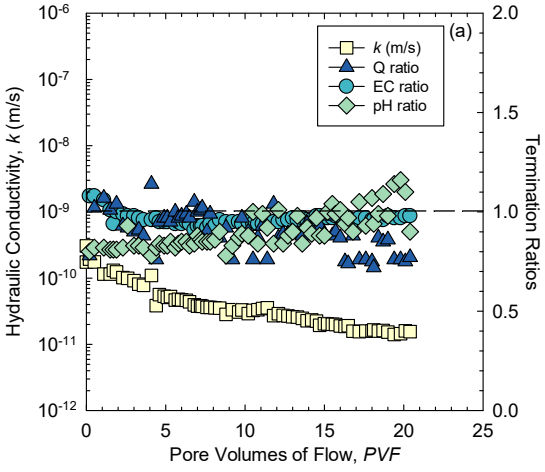

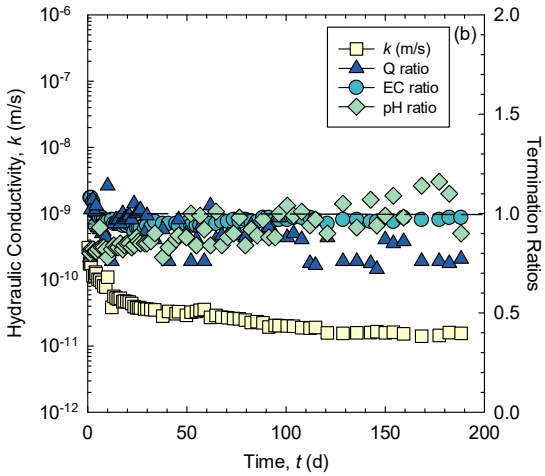

GCL Hydraulic Conductivity- Gravity Method

Test ID	B3		
GCL type	PAMW5DS	**Terminated test results**	
Polymer type	PAMW	*k* [D6766]	2.6×10^{-11} m/s
Mixing method	DS	PVF [D6766]	5.8
Permeant liquid	500 mM NaCl	time [D6766]	41.4 d
Permeant liquid EC	48.53 mS/cm	*k* [final]	2.7×10^{-11}m/s
Permeant liquid pH	6.17	PVF [final]	12.5
Specimen diameter	14.6 cm	time [final]	73.6 d
	5.7 in	Avg. EC	51.02 mS/cm
Specimen thickness	0.52 cm	Avg. pH	5.39
		Final sat.	106%
Avg. effective stress	27.2 kPa	Final porosity	0.66
	3.9 psi	Final void ratio	1.98
Avg. gradient	276	Final ρ_d	0.90 Mg/m^3
Avg. polymer content initial (%)	5	Final ω	0.79
Avg. polymer content final (%)	0.72	Hydrogel GCL	no
Preferential flow (Y/N)	Not Tested	Hydrogel effluent	yes

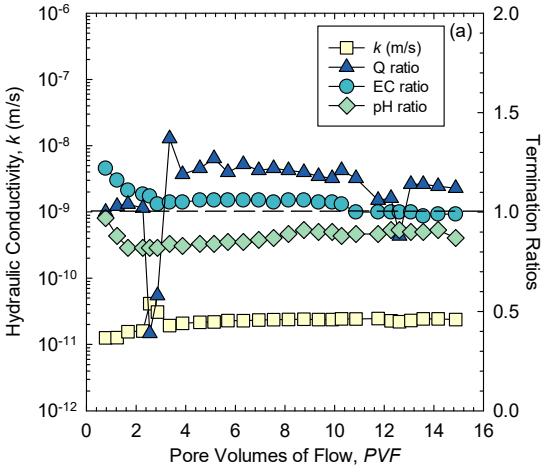

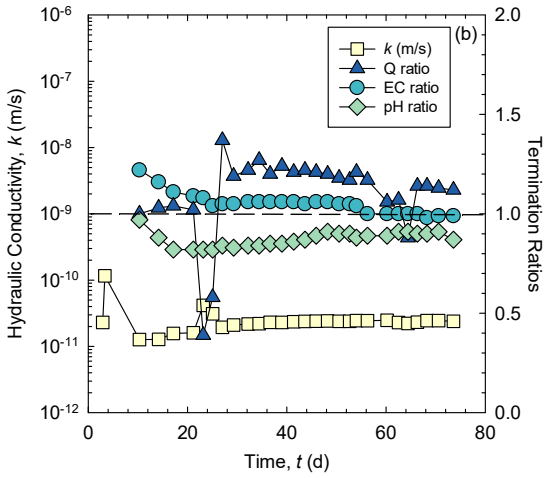

GCL Hydraulic Conductivity- Gravity Method

Test ID	B4		
GCL type	PAMW8DS	**Terminated test results**	
Polymer type	PAMW	*k* [D6766]	2.9×10^{-11} m/s
Mixing method	DS	PVF [D6766]	6.7
Permeant liquid	500 mM NaCl	time [D6766]	20.9 d
Permeant liquid EC	48.53 mS/cm	*k* [final]	3.3×10^{-11}m/s
Permeant liquid pH	6.17	PVF [final]	18.1
Specimen diameter	15.0 cm	time [final]	59.2 d
	5.9 in	Avg. EC	50.69 mS/cm
Specimen thickness	0.48 cm	Avg. pH	4.86
		Final sat.	107%
Avg. effective stress	27.3 kPa	Final porosity	0.67
	4.0 psi	Final void ratio	1.99
Avg. gradient	299	Final ρ_d	0.89 Mg/m^3
Avg. polymer content initial (%)	8	Final ω	0.80
Avg. polymer content final (%)	1.25	Hydrogel GCL	no
Preferential flow (Y/N)	Not Tested	Hydrogel effluent	yes

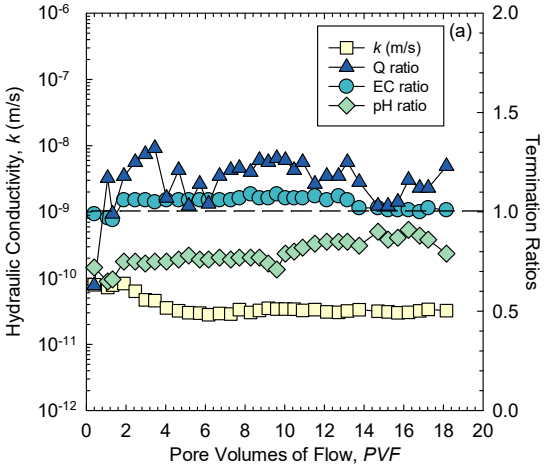

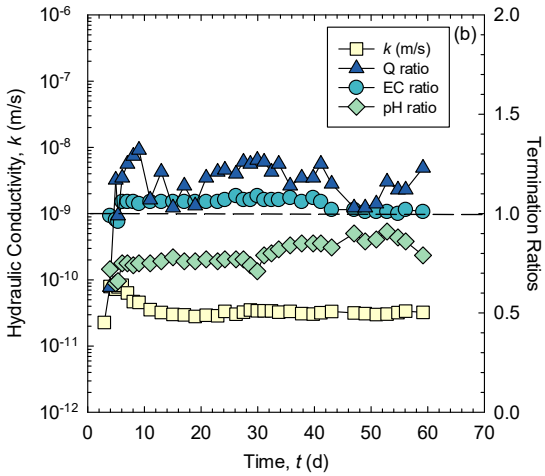

GCL Hydraulic Conductivity- Gravity Method

Test ID	B5		
GCL type	PAMW5WM	**Terminated test results**	
Polymer type	PAMW	*k* [D6766]	4.8×10^{-11} m/s
Mixing method	WM	PVF [D6766]	4.5
Permeant liquid	500 mM NaCl	time [D6766]	22.4 d
Permeant liquid EC	48.53 mS/cm	*k* [final]	3.5×10^{-11}m/s
Permeant liquid pH	6.17	PVF [final]	11.5
Specimen diameter	15.4 cm	time [final]	85 d
	6.1 in	Avg. EC	46.21 mS/cm
Specimen thickness	0.69 cm	Avg. pH	5.05
		Final sat.	84%
Avg. effective stress	27.2 kPa	Final porosity	0.77
	3.9 psi	Final void ratio	3.38
Avg. gradient	209	Final ρ_d	0.61 Mg/m^3
Avg. polymer content initial (%)	4.84	Final ω	1.06
Avg. polymer content final (%)	2.14	Hydrogel GCL	no
Preferential flow (Y/N)	Not Tested	Hydrogel effluent	yes

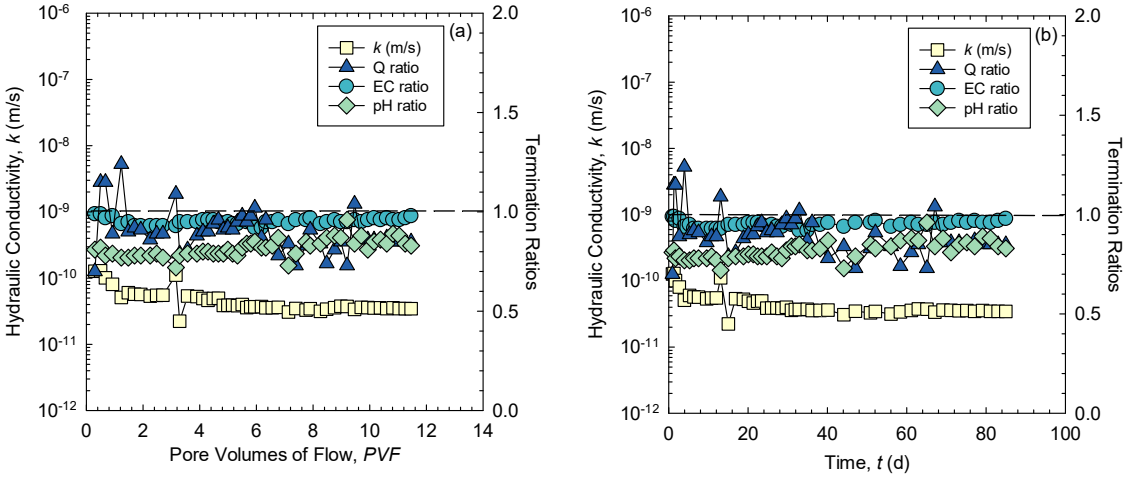

GCL Hydraulic Conductivity- Gravity Method

Test ID	B6		
GCL type	PALW5DS	**Terminated test results**	
Polymer type	PALW	*k* [D6766]	2.4×10^{-10} m/s
Mixing method	DS	PVF [D6766]	6.6
Permeant liquid	500 mM NaCl	time [D6766]	2.7 d
Permeant liquid EC	48.53 mS/cm	*k* [final]	1.4×10^{-11}m/s
Permeant liquid pH	6.17	PVF [final]	19.1
Specimen diameter	15.0 cm	time [final]	18 d
	5.9 in	Avg. EC	50.59 mS/cm
Specimen thickness	0.53 cm	Avg. pH	5.85
		Final sat.	114%
Avg. effective stress	27.3 kPa	Final porosity	0.69
	4.0 psi	Final void ratio	2.20
Avg. gradient	269	Final ρ_d	0.84 Mg/m^3
Avg. polymer content initial (%)	5	Final ω	0.94
Avg. polymer content final (%)	0.07	Hydrogel GCL	no
Preferential flow (Y/N)	Not Tested	Hydrogel effluent	yes

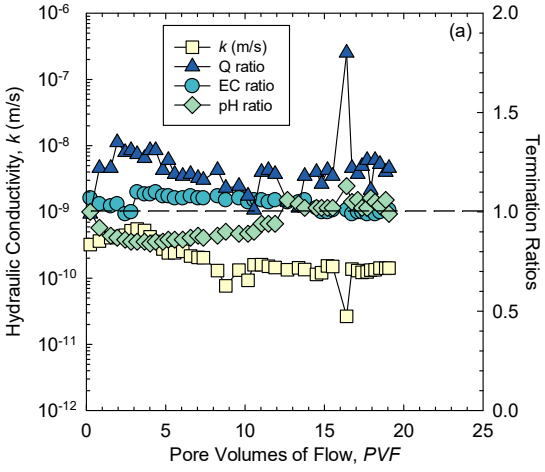

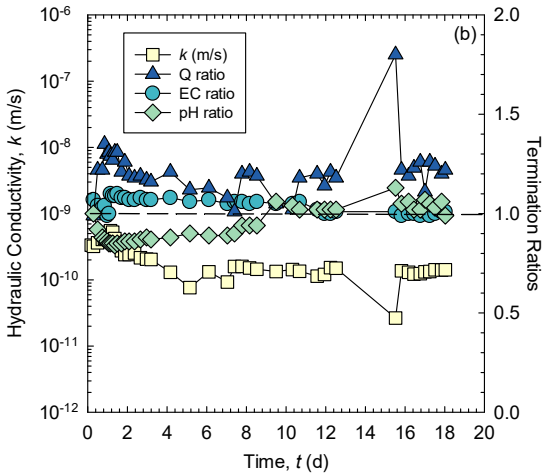

GCL Hydraulic Conductivity- Gravity Method

Test ID	B7		
GCL type	PALW5WM	**Terminated test results**	
Polymer type	PALW	*k* [D6766]	7.8×10^{-11} m/s
Mixing method	WM	PVF [D6766]	2.4
Permeant liquid	500 mM NaCl	time [D6766]	5.9 d
Permeant liquid EC	48.53 mS/cm	*k* [final]	4.9×10^{-11}m/s
Permeant liquid pH	6.17	PVF [final]	7.3
Specimen diameter	15.4 cm	time [final]	21 d
	6.1 in	Avg. EC	45.12 mS/cm
Specimen thickness	0.55 cm	Avg. pH	5.62
		Final sat.	105%
Avg. effective stress	27.4 kPa	Final porosity	0.71
	4.0 psi	Final void ratio	2.48
Avg. gradient	259	Final ρ_d	0.77 Mg/m^3
Avg. polymer content initial (%)	3.33	Final ω	0.97
Avg. polymer content final (%)	0.22	Hydrogel GCL	no
Preferential flow (Y/N)	Not Tested	Hydrogel effluent	yes

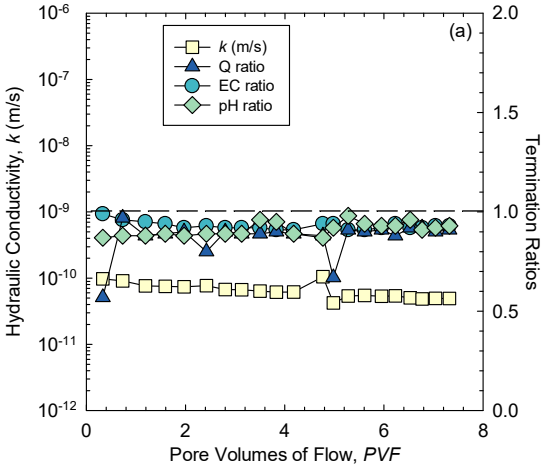

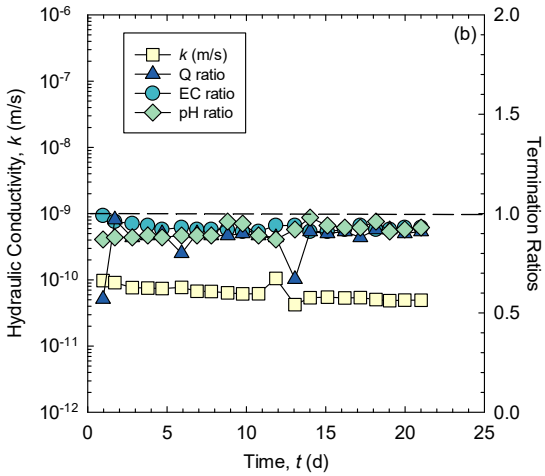

GCL Hydraulic Conductivity- Gravity Method

Test ID	B8		
GCL type	CMCHV5DM	**Terminated test results**	
Polymer type	CMCHV	*k* [D6766]	1.2×10^{-10} m/s
Mixing method	DM	PVF [D6766]	18.7
Permeant liquid	500 mM NaCl	time [D6766]	199 d
Permeant liquid EC	48.53 mS/cm	*k* [final]	1.4×10^{-10} m/s
Permeant liquid pH	6.17	PVF [final]	31.3
Specimen diameter	14.6 cm	time [final]	216 d
	5.7 in	Avg. EC	51.72 mS/cm
Specimen thickness	0.58 cm	Avg. pH	8.16
		Final sat.	112%
Avg. effective stress	27.3 kPa	Final porosity	0.70
	4.0 psi	Final void ratio	2.29
Avg. gradient	247	Final ρ_d	0.81 Mg/m^3
Avg. polymer content initial (%)	5	Final ω	0.96
Avg. polymer content final (%)	0.47	Hydrogel GCL	no
Preferential flow (Y/N)	Not Tested	Hydrogel effluent	yes

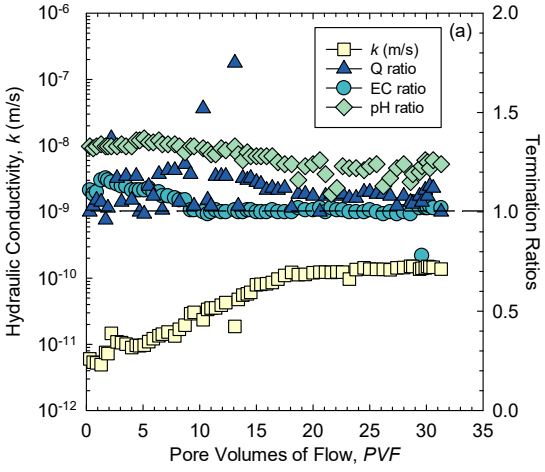

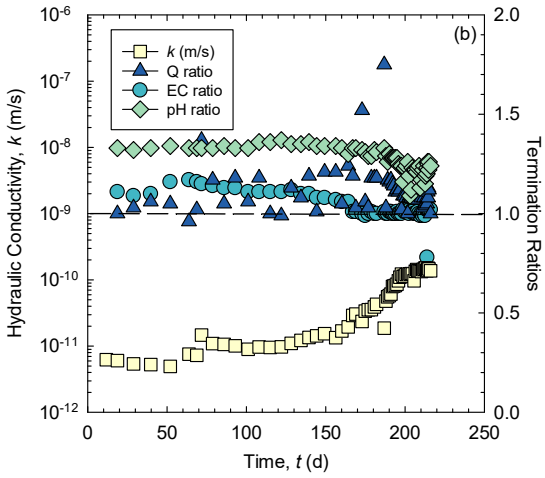

GCL Hydraulic Conductivity- Gravity Method

Test ID	B9		
GCL type	CMCHV5WM	**Terminated test results**	
Polymer type	CMCHV	*k* [D6766]	3.3×10^{-10} m/s
Mixing method	WM	PVF [D6766]	3.0
Permeant liquid	500 mM NaCl	time [D6766]	30.5 d
Permeant liquid EC	48.53 mS/cm	*k* [final]	2.3×10^{-11}m/s
Permeant liquid pH	6.17	PVF [final]	6.9
Specimen diameter	14.6 cm	time [final]	77.3 d
	5.7 in	Avg. EC	51.72 mS/cm
Specimen thickness	0.55 cm	Avg. pH	8.16
		Final sat.	112%
Avg. effective stress	27.3 kPa	Final porosity	0.70
	4.0 psi	Final void ratio	2.29
Avg. gradient	247	Final ρ_d	0.81 Mg/m^3
Avg. polymer content initial (%)	4.47	Final ω	0.96
Avg. polymer content final (%)	3.07	Hydrogel GCL	no
Preferential flow (Y/N)	Not Tested	Hydrogel effluent	yes

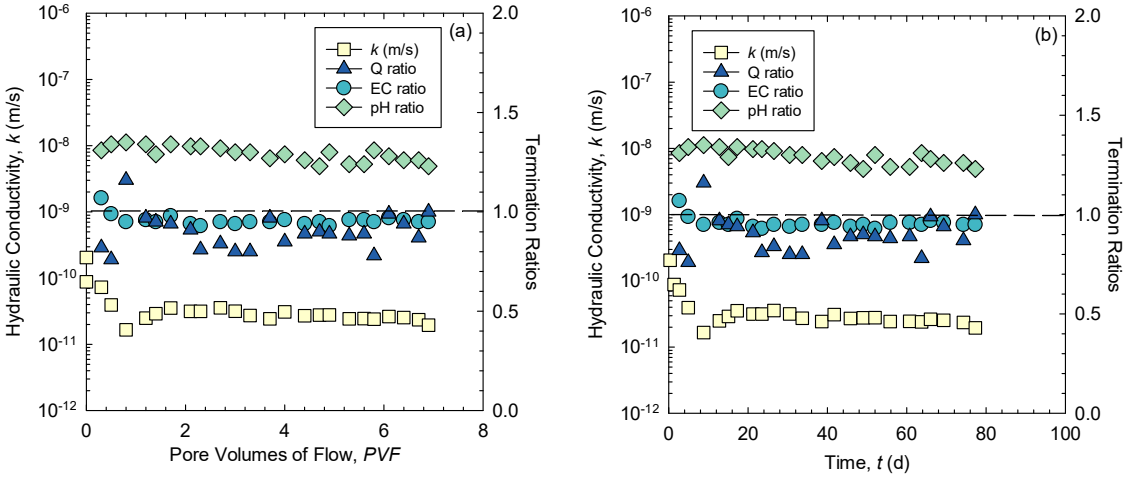

GCL Hydraulic Conductivity- Gravity Method

Test ID	B10		
GCL type	CMCLV5DM	**Terminated test results**	
Polymer type	CMCLV	*k* [D6766]	8.5×10^{-11} m/s
Mixing method	DM	PVF [D6766]	14.8
Permeant liquid	500 mM NaCl	time [D6766]	196 d
Permeant liquid EC	48.53 mS/cm	*k* [final]	1.2×10^{-10} m/s
Permeant liquid pH	6.17	PVF [final]	25.8
Specimen diameter	15.0 cm	time [final]	214 d
	5.9 in	Avg. EC	51.12 mS/cm
Specimen thickness	0.55 cm	Avg. pH	7.97
		Final sat.	100%
Avg. effective stress	27.3 kPa	Final porosity	0.71
	4.0 psi	Final void ratio	2.43
Avg. gradient	247	Final ρ_d	0.78 Mg/m^3
Avg. polymer content initial (%)	5	Final ω	0.91
Avg. polymer content final (%)	0.64	Hydrogel GCL	no
Preferential flow (Y/N)	Not Tested	Hydrogel effluent	yes

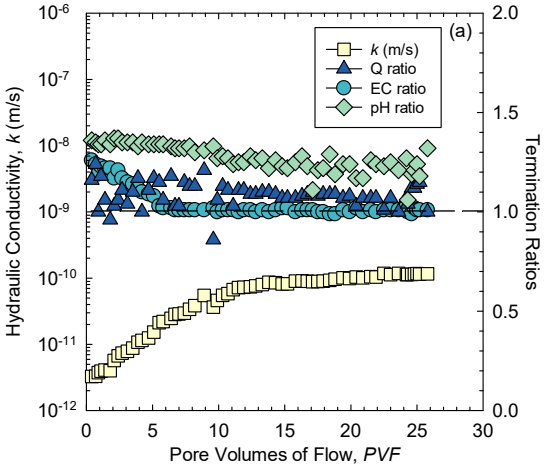

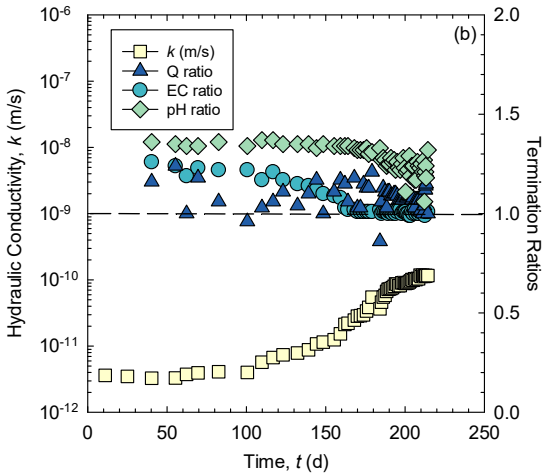

GCL Hydraulic Conductivity- Gravity Method

Test ID	B11		
GCL type	CMCLV5WM	**Terminated test results**	
Polymer type	CMCLV	*k* [D6766]	6.9×10^{-11} m/s
Mixing method	WM	PVF [D6766]	3.1
Permeant liquid	500 mM NaCl	time [D6766]	120 d
Permeant liquid EC	48.53 mS/cm	*k* [final]	6.7×10^{-11} m/s
Permeant liquid pH	6.17	PVF [final]	4.9
Specimen diameter	15.2 cm	time [final]	126 d
	6.0 in	Avg. EC	45.70 mS/cm
Specimen thickness	0.61 cm	Avg. pH	8.05
		Final sat.	99%
Avg. effective stress	27.5 kPa	Final porosity	0.74
	4.0 psi	Final void ratio	2.78
Avg. gradient	232	Final ρ_d	0.71 Mg/m^3
Avg. polymer content initial (%)	4.47	Final ω	1.03
Avg. polymer content final (%)	3.07	Hydrogel GCL	no
Preferential flow (Y/N)	Not Tested	Hydrogel effluent	yes

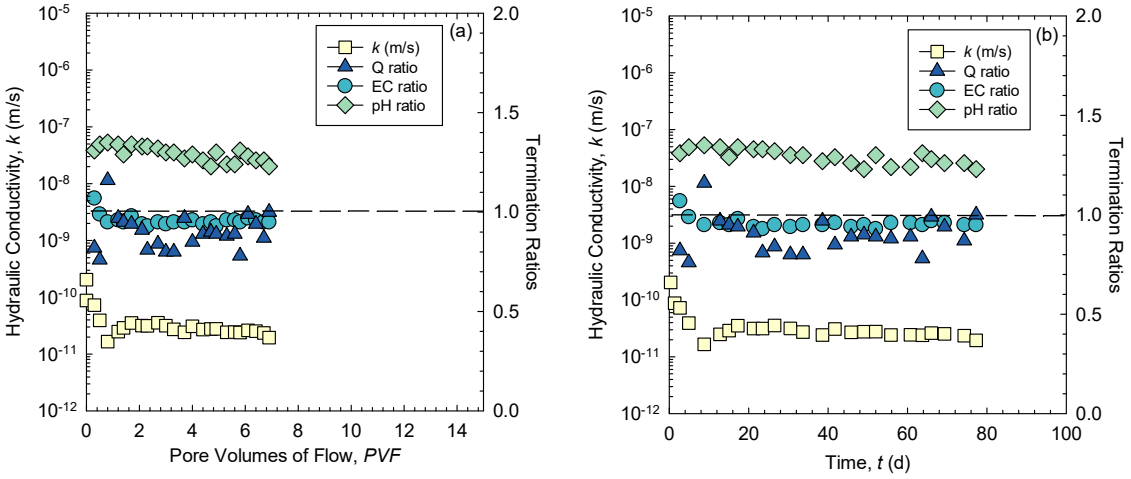

GCL Hydraulic Conductivity- Gravity Method

Test ID	B12		
GCL type	CMCLV5DS	**Terminated test results**	
Polymer type	CMCLV	*k* [D6766]	1.2×10^{-10} m/s
Mixing method	DS	PVF [D6766]	9.3
Permeant liquid	500 mM NaCl	time [D6766]	62.5 d
Permeant liquid EC	48.53 mS/cm	*k* [final]	1.4×10^{-10} m/s
Permeant liquid pH	6.17	PVF [final]	14.6
Specimen diameter	15.2 cm	time [final]	66.7 d
	6.0 in	Avg. EC	51.95 mS/cm
Specimen thickness	0.48 cm	Avg. pH	7.86
		Final sat.	107%
Avg. effective stress	27.3 kPa	Final porosity	0.66
	4.0 psi	Final void ratio	1.98
Avg. gradient	296	Final ρ_d	0.90 Mg/m^3
Avg. polymer content initial (%)	5	Final ω	0.79
Avg. polymer content final (%)	0.22	Hydrogel GCL	no
Preferential flow (Y/N)	Not Tested	Hydrogel effluent	yes

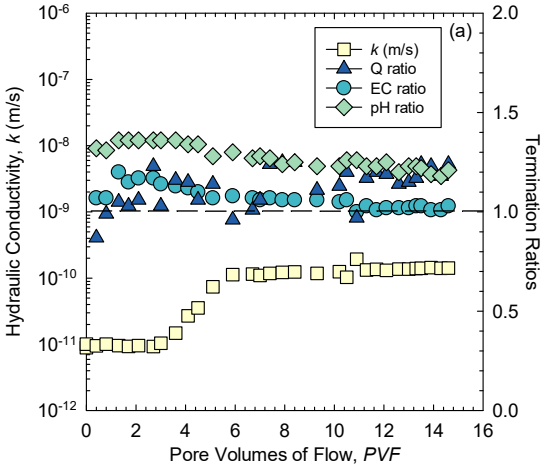

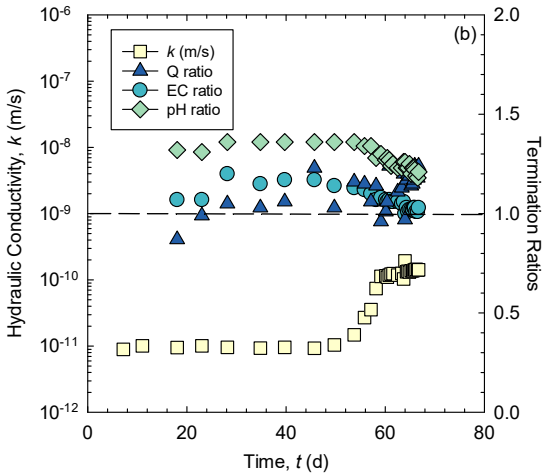

GCL Hydraulic Conductivity- Gravity Method

Test ID	B13		
GCL type	BPC	**Terminated test results**	
Polymer type	BPC	*k* [D6766]	NA
Mixing method	none	PVF [D6766]	NA
Permeant liquid	500 mM NaCl	time [D6766]	NA
Permeant liquid EC	48.53 mS/cm	*k* [final]	2.3×10^{-12} m/s
Permeant liquid pH	6.17	PVF [final]	0.9
Specimen diameter	14.9 cm	time [final]	85.5 d
	5.9 in	Avg. EC	51.95 mS/cm
Specimen thickness	0.56 cm	Avg. pH	7.86
		Final sat.	112%
Avg. effective stress	23.8 kPa	Final porosity	0.71
	3.5 psi	Final void ratio	2.47
Avg. gradient	296	Final ρ_d	0.77 Mg/m^3
Avg. polymer content initial (%)	28.5	Final ω	1.06
Avg. polymer content final (%)	7.69	Hydrogel GCL	no
Preferential flow (Y/N)	Not Tested	Hydrogel effluent	yes

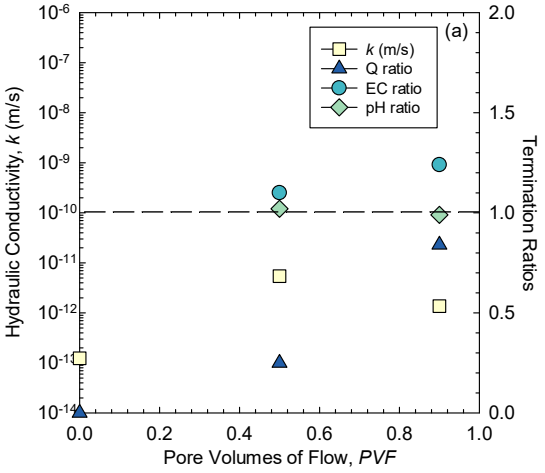

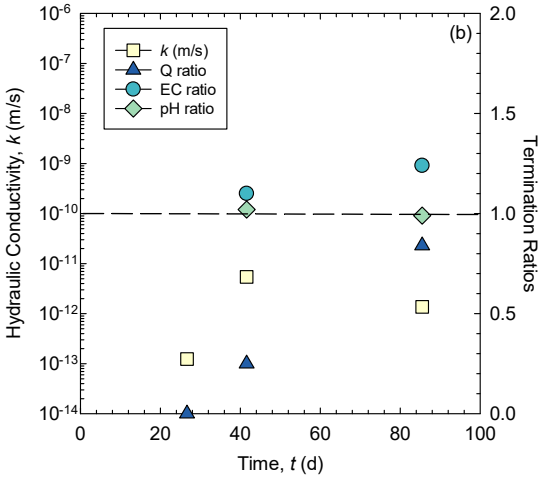

GCL Hydraulic Conductivity- Gravity Method

Test ID	B14		
GCL type	BPC5DM	**Terminated test results**	
Polymer type	BPC	*k* [D6766]	1.1×10^{-11} m/s
Mixing method	DM	PVF [D6766]	2.9
Permeant liquid	500 mM NaCl	time [D6766]	61.5 d
Permeant liquid EC	48.53 mS/cm	*k* [final]	1.9×10^{-11} m/s
Permeant liquid pH	6.17	PVF [final]	11.5
Specimen diameter	14.9 cm	time [final]	143 d
	5.9 in	Avg. EC	48.53 mS/cm
Specimen thickness	0.62 cm	Avg. pH	7.44
		Final sat.	82%
Avg. effective stress	24.7 kPa	Final porosity	0.73
	3.6 psi	Final void ratio	2.67
Avg. gradient	296	Final ρ_d	0.73 Mg/m^3
Avg. polymer content initial (%)	5	Final ω	0.82
Avg. polymer content final (%)	1.82	Hydrogel GCL	no
Preferential flow (Y/N)	Not Tested	Hydrogel effluent	yes

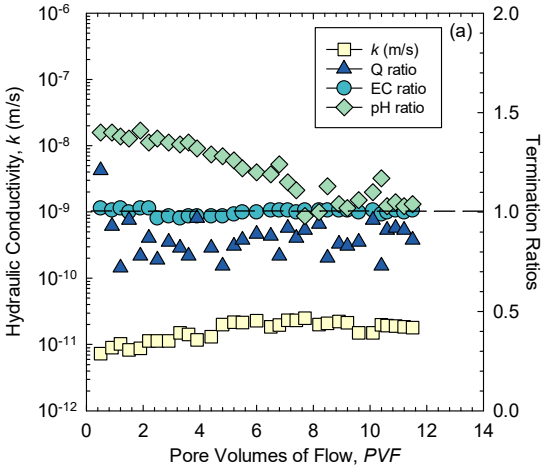

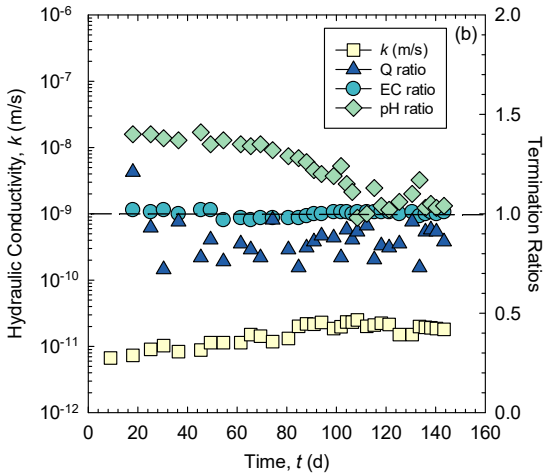

GCL Hydraulic Conductivity- Gravity Method

Test ID	B15		
GCL type	PAx5DS	**Terminated test results**	
Polymer type	PAx	*k* [D6766]	2.5×10^{-11} m/s
Mixing method	DS	PVF [D6766]	5.4
Permeant liquid	500 mM NaCl	time [D6766]	88.9 d
Permeant liquid EC	48.53 mS/cm	*k* [final]	2.5×10^{-11} m/s
Permeant liquid pH	6.17	PVF [final]	7.9
Specimen diameter	15.0 cm	time [final]	136 d
	5.9 in	Avg. EC	48.53 mS/cm
Specimen thickness	0.70 cm	Avg. pH	7.44
		Final sat.	78%
Avg. effective stress	30.1 kPa	Final porosity	0.76
	4.4 psi	Final void ratio	3.21
Avg. gradient	122	Final ρ_d	0.63 Mg/m^3
Avg. polymer content initial (%)	5	Final ω	0.95
Avg. polymer content final (%)	4.88	Hydrogel GCL	no
Preferential flow (Y/N)	Not Tested	Hydrogel effluent	yes

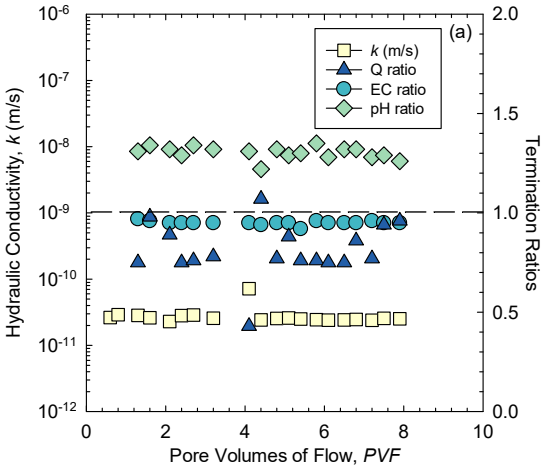

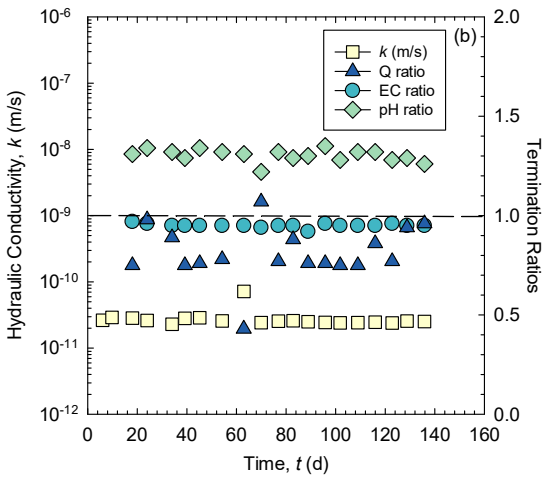

A2. Baseline GCLs (unenhanced)

GCL Hydraulic Conductivity- Gravity Method			
Test ID	**C1**		
GCL type	PNaB	**Terminated test results**	
Polymer type	none	*k* [D6766]	2.8×10^{-10} m/s
Mixing method	none	PVF [D6766]	2.6
Permeant liquid	500 mM NaCl	time [D6766]	1.7 d
Permeant liquid EC	48.53 mS/cm	*k* [final]	1.6×10^{-10} m/s
Permeant liquid pH	6.17	PVF [final]	5.9
Specimen diameter	15.2 cm	time [final]	4.8 d
	6.0 in	Avg. EC	53.8 mS/cm
Specimen thickness	0.61 cm	Avg. pH	7.07
		Final sat.	72%
Avg. effective stress	27.5 kPa	Final porosity	0.76
	4.0 psi	Final void ratio	3.18
Avg. gradient	236	Final ρ_d	0.64 Mg/m^3
Avg. polymer content initial (%)	0	Final ω	0.86
Avg. polymer content final (%)	0	Hydrogel GCL	no
Preferential flow (Y/N)	Not Tested	Hydrogel effluent	no

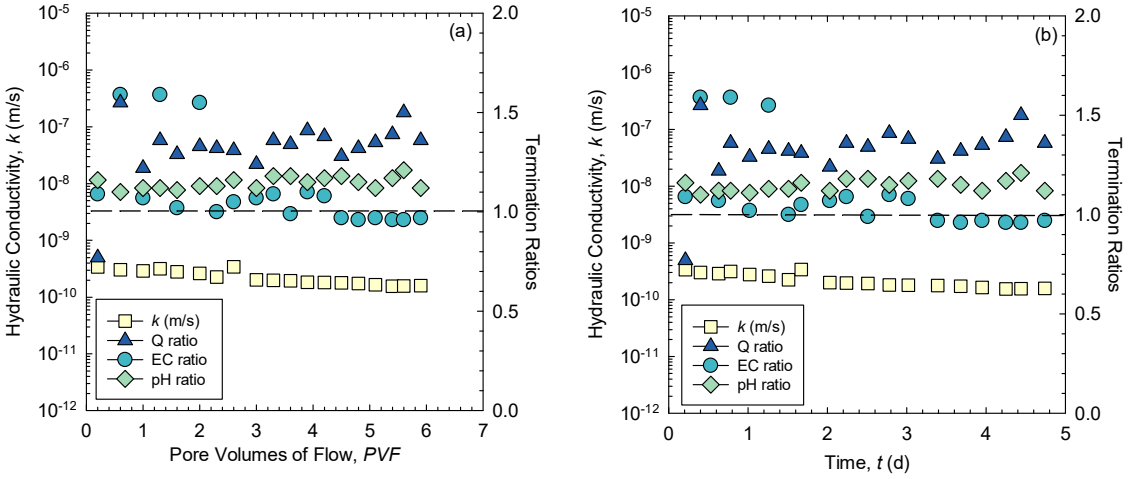

GCL Hydraulic Conductivity- Gravity Method

Test ID	C2		
GCL type	GNaB	**Terminated test results**	
Polymer type	none	*k* [D6766]	2.7×10^{-7} m/s
Mixing method	none	PVF [D6766]	2.2
Permeant liquid	500 mM NaCl	time [D6766]	<1 d
Permeant liquid EC	48.53 mS/cm	*k* [final]	2.6×10^{-11} m/s
Permeant liquid pH	6.17	PVF [final]	4.9
Specimen diameter	15.0 cm	time [final]	<1 d
	6.0 in	Avg. EC	44.6 mS/cm
Specimen thickness	0.64 cm	Avg. pH	6.80
		Final sat.	78%
Avg. effective stress	27.1 kPa	Final porosity	0.74
	4.0 psi	Final void ratio	2.89
Avg. gradient	237	Final ρ_d	0.69 Mg/m^3
Avg. polymer content initial (%)	0	Final ω	0.84
Avg. polymer content final (%)	0	Hydrogel GCL	no
Preferential flow (Y/N)	Not Tested	Hydrogel effluent	no

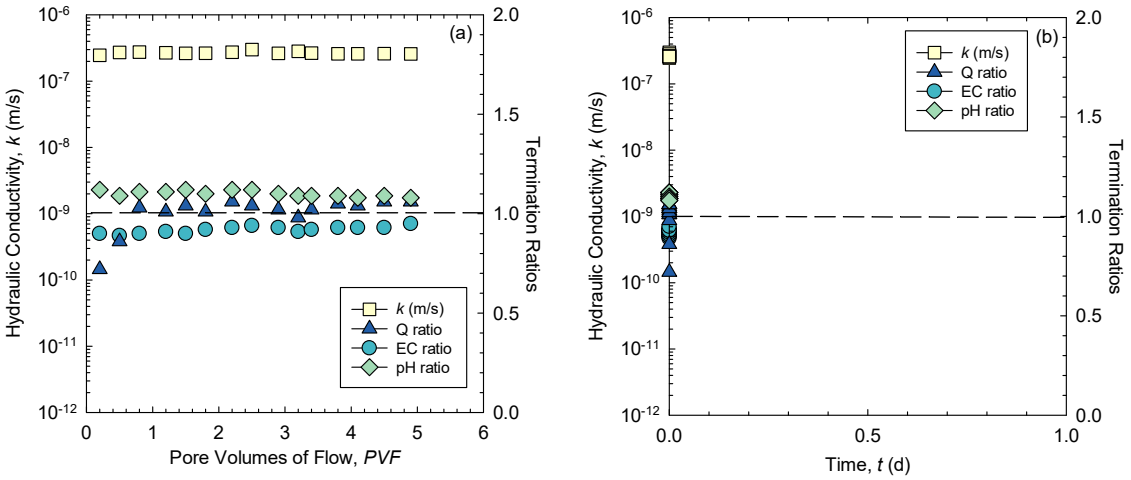

GCL Hydraulic Conductivity- Gravity Method

Test ID	C3		
GCL type	Pyrophyllite	**Terminated test results**	
Polymer type	none	*k* [D6766]	3.5×10^{-7} m/s
Mixing method	none	PVF [D6766]	5.6
Permeant liquid	500 mM NaCl	time [D6766]	<1 d
Permeant liquid EC	48.53 mS/cm	*k* [final]	3.2×10^{-7} m/s
Permeant liquid pH	6.17	PVF [final]	10.4
Specimen diameter	14.6 cm	time [final]	<1 d
	5.9 in	Avg. EC	46.47 mS/cm
Specimen thickness	0.44 cm	Avg. pH	5.75
		Final sat.	112%
Avg. effective stress	27.4 kPa	Final porosity	0.58
	4.1 psi	Final void ratio	1.37
Avg. gradient	321	Final ρ_d	1.13 Mg/m^3
Avg. polymer content initial (%)	0	Final ω	0.57
Avg. polymer content final (%)	0	Hydrogel GCL	no
Preferential flow (Y/N)	Not Tested	Hydrogel effluent	no

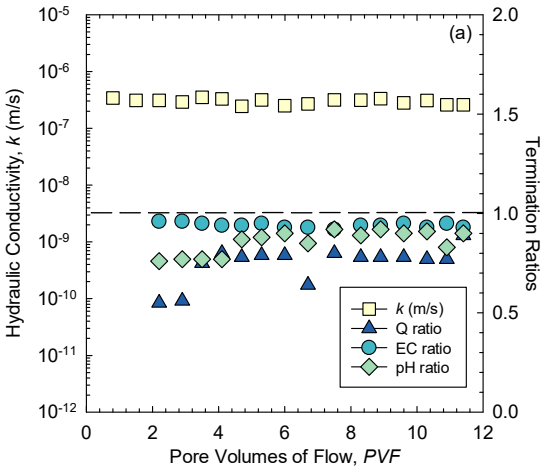

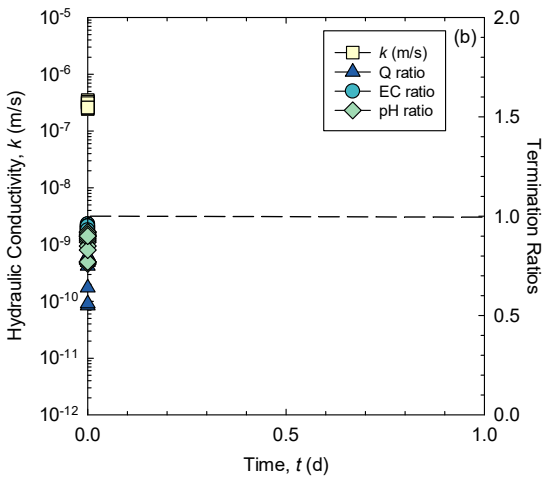

GCL Hydraulic Conductivity- Gravity Method

Test ID	**C4**		
GCL type	PNaB	**Terminated test results**	
Polymer type	none	*k* [D6766]	5.5×10^{-10} m/s
Mixing method	none	PVF [D6766]	3.0
Permeant liquid	167 mM$CaCl_2$	time [D6766]	1.6 d
Permeant liquid EC	31.70 mS/cm	*k* [final]	4.8×10^{-10} m/s
Permeant liquid pH	5.81	PVF [final]	9.2
Specimen diameter	15.0 cm	time [final]	5.6 d
	6.0 in	Avg. EC	33.80 mS/cm
Specimen thickness	0.68 cm	Avg. pH	6.53
		Final sat.	65%
Avg. effective stress	27.7 kPa	Final porosity	0.77
	4.0 psi	Final void ratio	3.28
Avg. gradient	205	Final ρ_d	1.11 Mg/m^3
Avg. polymer content initial (%)	0	Final ω	0.80
Avg. polymer content final (%)	0	Hydrogel GCL	no
Preferential flow (Y/N)	Not Tested	Hydrogel effluent	no

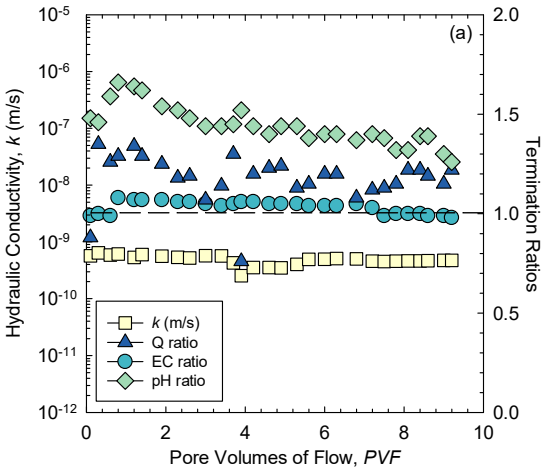

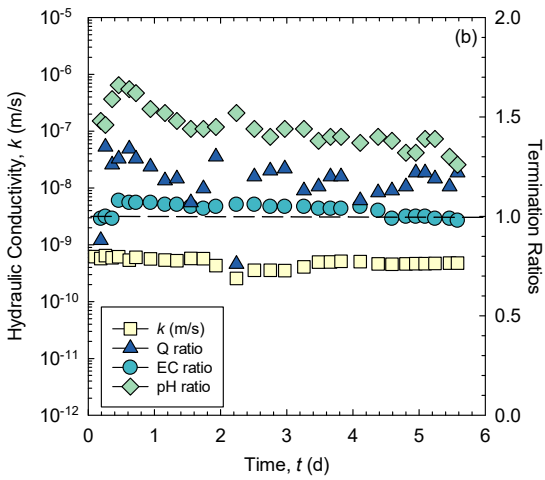

GCL Hydraulic Conductivity- Gravity Method

Test ID	C5		
GCL type	GNaB	**Terminated test results**	
Polymer type	none	*k* [D6766]	7.7×10^{-7} m/s
Mixing method	none	PVF [D6766]	2.2
Permeant liquid	167 mM$CaCl_2$	time [D6766]	<1 d
Permeant liquid EC	31.70 mS/cm	*k* [final]	6.7×10^{-7} m/s
Permeant liquid pH	5.81	PVF [final]	9.1
Specimen diameter	14.7 cm	time [final]	<1 d
	5.8 in	Avg. EC	30.94 mS/cm
Specimen thickness	0.64 cm	Avg. pH	6.28
		Final sat.	73%
Avg. effective stress	27.4 kPa	Final porosity	0.73
	4.1 psi	Final void ratio	2.70
Avg. gradient	224	Final ρ_d	0.72 Mg/m^3
Avg. polymer content initial (%)	0	Final ω	0.74
Avg. polymer content final (%)	0	Hydrogel GCL	no
Preferential flow (Y/N)	Not Tested	Hydrogel effluent	no

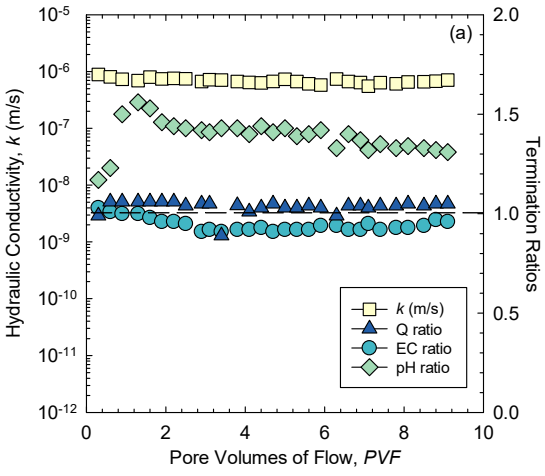

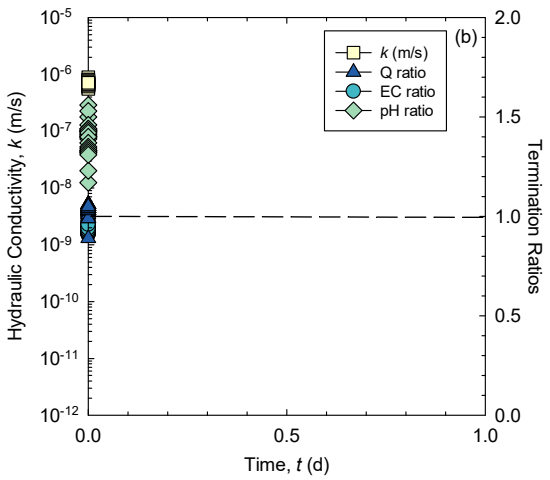

GCL Hydraulic Conductivity- Gravity Method

Test ID	**C6**		
GCL type	Pyrophyllite	**Terminated test results**	
Polymer type	none	*k* [D6766]	2.9×10^{-7} m/s
Mixing method	none	PVF [D6766]	6.0
Permeant liquid	167 mM$CaCl_2$	time [D6766]	<1 d
Permeant liquid EC	31.70 mS/cm	*k* [final]	2.8×10^{-7} m/s
Permeant liquid pH	5.81	PVF [final]	11.4
Specimen diameter	14.7 cm	time [final]	<1 d
	5.8 in	Avg. EC	29.86 mS/cm
Specimen thickness	0.43 cm	Avg. pH	4.97
		Final sat.	111%
Avg. effective stress	27.4 kPa	Final porosity	0.58
	4.1 psi	Final void ratio	1.40
Avg. gradient	325	Final ρ_d	1.11 Mg/m^3
Avg. polymer content initial (%)	0	Final ω	0.58
Avg. polymer content final (%)	0	Hydrogel GCL	no
Preferential flow (Y/N)	Not Tested	Hydrogel effluent	no

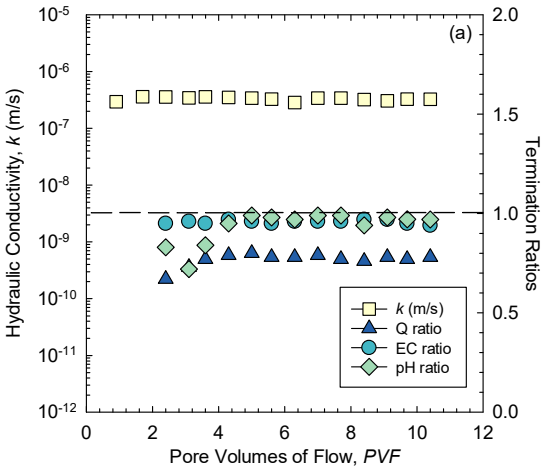

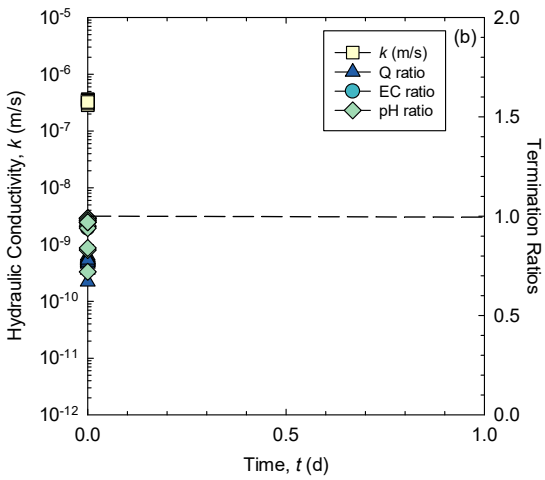

A3. Pyrophyllite EB-GCL hydraulic conductivity tests

GCL Hydraulic Conductivity- Gravity Method			
Test ID	**D1**		
GCL type	Pyro+PAHW5DS	**Terminated test results**	
Polymer type	PAHW	*k* [D6766]	1.8×10^{-7} m/s
Mixing method	DS	PVF [D6766]	6.6
Permeant liquid	167 mM$CaCl_2$	time [D6766]	<1 d
Permeant liquid EC	31.70 mS/cm	*k* [final]	1.6×10^{-7} m/s
Permeant liquid pH	5.81	PVF [final]	13.6
Specimen diameter	14.7 cm	time [final]	<1 d
	5.8 in	Avg. EC	31.61 mS/cm
Specimen thickness	0.34 cm	Avg. pH	2.72
		Final sat.	152%
Avg. effective stress	27.4 kPa	Final porosity	0.52
	4.0 psi	Final void ratio	1.08
Avg. gradient	411	Final ρ_d	1.28 Mg/m^3
Avg. polymer content initial (%)	5	Final ω	0.62
Avg. polymer content final (%)	1.84	Hydrogel GCL	no
Preferential flow (Y/N)	Not Tested	Hydrogel effluent	yes

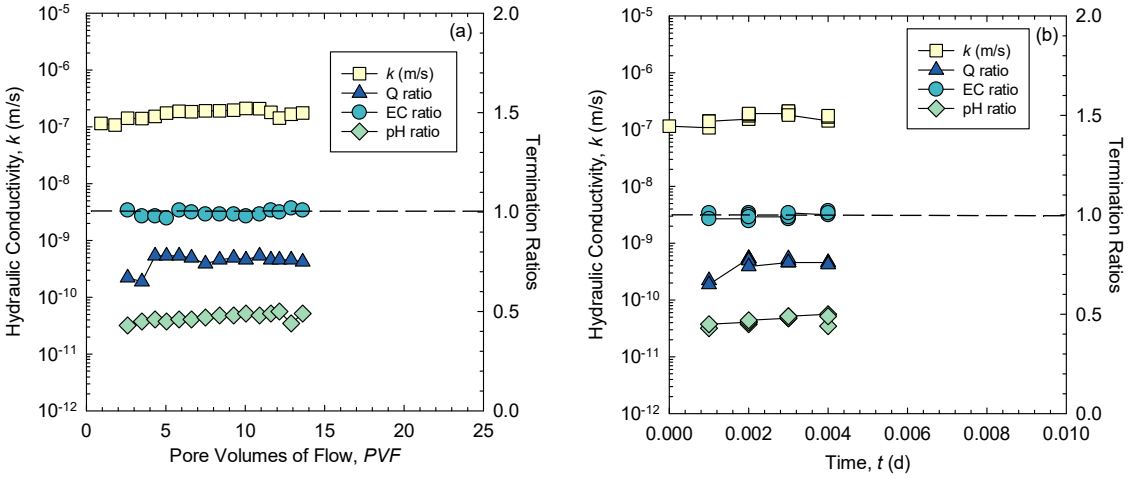

GCL Hydraulic Conductivity- Gravity Method

Test ID	**D2**		
GCL type	Pyro+PAMW8DS	**Terminated test results**	
Polymer type	PAMW	*k* [D6766]	6.7×10^{-8} m/s
Mixing method	DS	PVF [D6766]	8.4
Permeant liquid	167 mM$CaCl_2$	time [D6766]	<1 d
Permeant liquid EC	31.70 mS/cm	*k* [final]	1.1×10^{-7} m/s
Permeant liquid pH	5.81	PVF [final]	14.8
Specimen diameter	14.7 cm	time [final]	<1 d
	5.8 in	Avg. EC	31.61 mS/cm
Specimen thickness	0.49 cm	Avg. pH	2.72
		Final sat.	82%
Avg. effective stress	27.4 kPa	Final porosity	0.67
	4.0 psi	Final void ratio	1.99
Avg. gradient	411	Final ρ_d	0.89 Mg/m^3
Avg. polymer content initial (%)	8	Final ω	0.61
Avg. polymer content final (%)	0.43	Hydrogel GCL	no
Preferential flow (Y/N)	Not Tested	Hydrogel effluent	yes

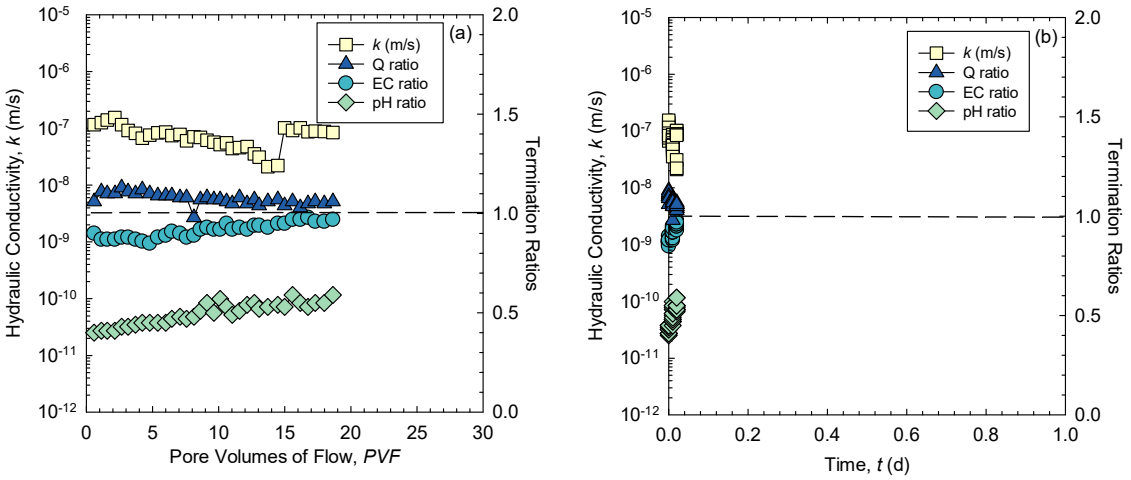

GCL Hydraulic Conductivity- Gravity Method

Test ID	D3		
GCL type	Pyro+PAHW32DS	**Terminated test results**	
Polymer type	PAHW	*k* [D6766]	NA
Mixing method	DS	PVF [D6766]	NA
Permeant liquid	167 mM$CaCl_2$	time [D6766]	NA
Permeant liquid EC	31.70 mS/cm	*k* [final]	3.3×10^{-7} m/s
Permeant liquid pH	5.81	PVF [final]	11.4
Specimen diameter	14.3 cm	time [final]	<1 d
	5.6 in	Avg. EC	31.34 mS/cm
Specimen thickness	0.59 cm	Avg. pH	2.63
		Final sat.	98%
Avg. effective stress	27.3 kPa	Final porosity	0.62
	4.0 psi	Final void ratio	1.62
Avg. gradient	473	Final ρ_d	1.02 Mg/m^3
Avg. polymer content initial (%)	32	Final ω	0.59
Avg. polymer content final (%)	0.52	Hydrogel GCL	no
Preferential flow (Y/N)	Not Tested	Hydrogel effluent	yes

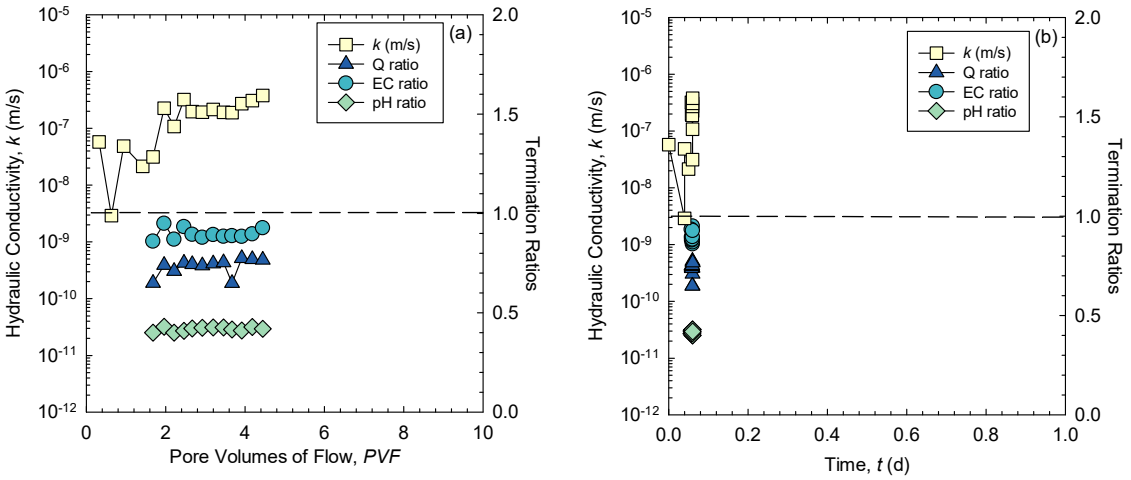

GCL Hydraulic Conductivity- Gravity Method

Test ID	D4		
GCL type	Pyro+PAHW5DS	**Terminated test results**	
Polymer type	PAHW	*k* [D6766]	1.8×10^{-7} m/s
Mixing method	DS	PVF [D6766]	6.6
Permeant liquid	500 mM NaCl	time [D6766]	<1 d
Permeant liquid EC	48.53 mS/cm	*k* [final]	1.6×10^{-7} m/s
Permeant liquid pH	6.17	PVF [final]	13.6
Specimen diameter	14.8 cm	time [final]	<1 d
	5.8 in	Avg. EC	47.79 mS/cm
Specimen thickness	0.40 cm	Avg. pH	2.96
		Final sat.	119%
Avg. effective stress	27.3 kPa	Final porosity	0.57
	4.0 psi	Final void ratio	1.32
Avg. gradient	360	Final ρ_d	1.15 Mg/m^3
Avg. polymer content initial (%)	5	Final ω	0.59
Avg. polymer content final (%)	1.84	Hydrogel GCL	no
Preferential flow (Y/N)	Not Tested	Hydrogel effluent	yes

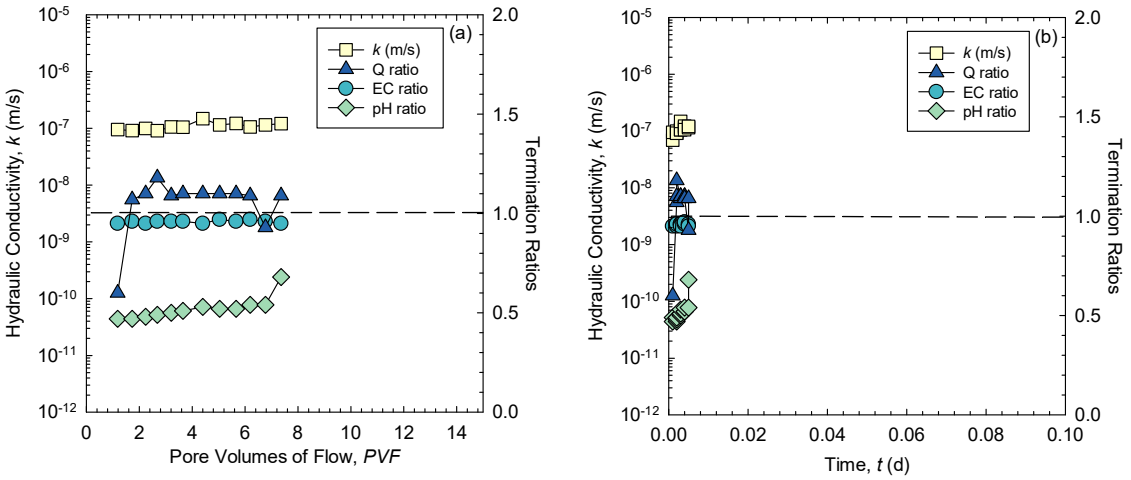

GCL Hydraulic Conductivity- Gravity Method

Test ID	**D5**		
GCL type	Pyro+PAMW8DS	**Terminated test results**	
Polymer type	PAMW	*k* [D6766]	3.4×10^{-7} m/s
Mixing method	DS	PVF [D6766]	4.6
Permeant liquid	500 mM NaCl	time [D6766]	<1 d
Permeant liquid EC	48.53 mS/cm	*k* [final]	3.4×10^{-7} m/s
Permeant liquid pH	6.17	PVF [final]	8.0
Specimen diameter	14.9 cm	time [final]	<1 d
	5.9 in	Avg. EC	44.89 mS/cm
Specimen thickness	0.51 cm	Avg. pH	3.10
		Final sat.	74%
Avg. effective stress	27.3 kPa	Final porosity	0.69
	4.0 psi	Final void ratio	2.20
Avg. gradient	278	Final ρ_d	0.83 Mg/m^3
Avg. polymer content initial (%)	8	Final ω	0.61
Avg. polymer content final (%)	0.42	Hydrogel GCL	no
Preferential flow (Y/N)	Not Tested	Hydrogel effluent	yes

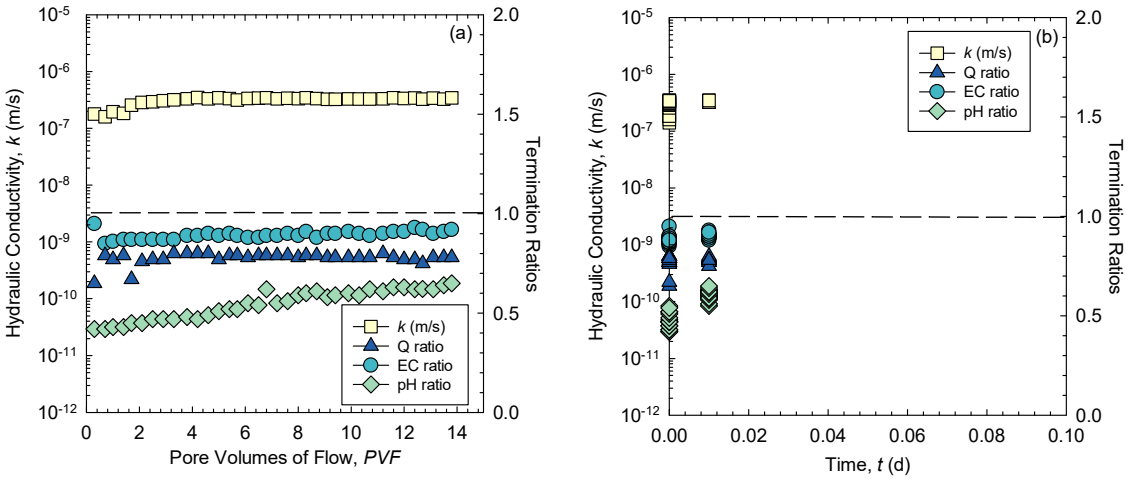

A4. Granular NaB EB-GCL hydraulic conductivity tests

GCL Hydraulic Conductivity- Gravity Method			
Test ID	**E1**		
GCL type	GNaB+PAHW5DS	**Terminated test results**	
Polymer type	PAHW	k [D6766]	5.4×10^{-7} m/s
Mixing method	DS	PVF [D6766]	2.6
Permeant liquid	500 mM NaCl	time [D6766]	<1 d
Permeant liquid EC	48.53 mS/cm	k [final]	3.0×10^{-7} m/s
Permeant liquid pH	6.17	PVF [final]	11.7
Specimen diameter	15.3 cm	time [final]	<1 d
	6.0 in	Avg. EC	49.09 mS/cm
Specimen thickness	0.51 cm	Avg. pH	4.17
		Final sat.	95%
Avg. effective stress	27.2 kPa	Final porosity	0.69
	4.0 psi	Final void ratio	2.22
Avg. gradient	283	Final ρ_d	0.83 Mg/m^3
Avg. polymer content initial (%)	5	Final ω	0.79
Avg. polymer content final (%)	1.12	Hydrogel GCL	no
Preferential flow (Y/N)	Not Tested	Hydrogel effluent	no

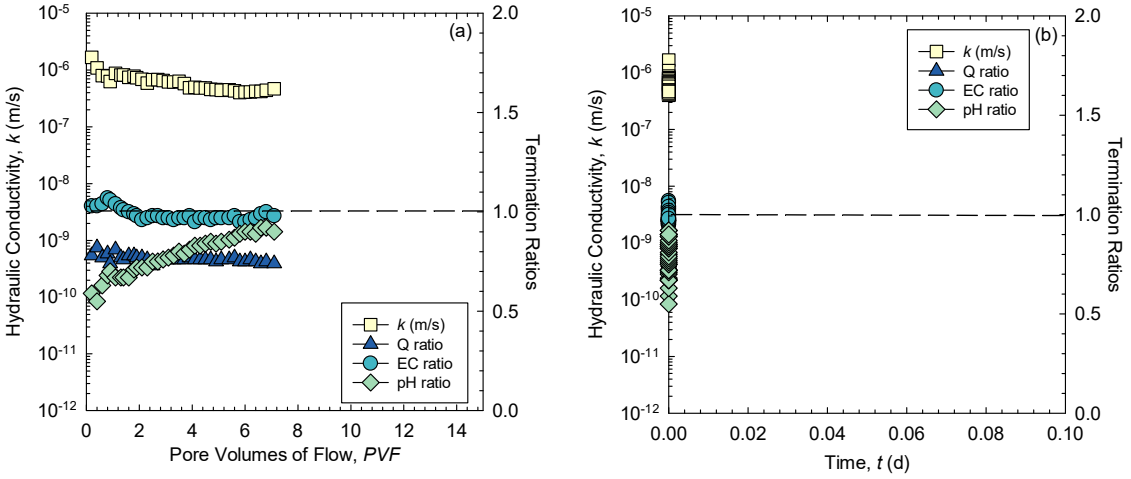

GCL Hydraulic Conductivity- Gravity Method

Test ID	E2		
GCL type	GNaB+PAHW5DS	**Terminated test results**	
Polymer type	PAHW	*k* [D6766]	7.8×10^{-7} m/s
Mixing method	DS	PVF [D6766]	4.0
Permeant liquid	167 mM$CaCl_2$	time [D6766]	<1 d
Permeant liquid EC	31.70 mS/cm	*k* [final]	6.3×10^{-7} m/s
Permeant liquid pH	5.81	PVF [final]	11.5
Specimen diameter	14.7 cm	time [final]	<1 d
	5.9 in	Avg. EC	31.49 mS/cm
Specimen thickness	0.56 cm	Avg. pH	4.08
		Final sat.	91%
Avg. effective stress	27.3 kPa	Final porosity	0.69
	4.0 psi	Final void ratio	2.25
Avg. gradient	253	Final ρ_d	0.82 Mg/m^3
Avg. polymer content initial (%)	5	Final ω	0.77
Avg. polymer content final (%)	0.96	Hydrogel GCL	no
Preferential flow (Y/N)	Not Tested	Hydrogel effluent	yes

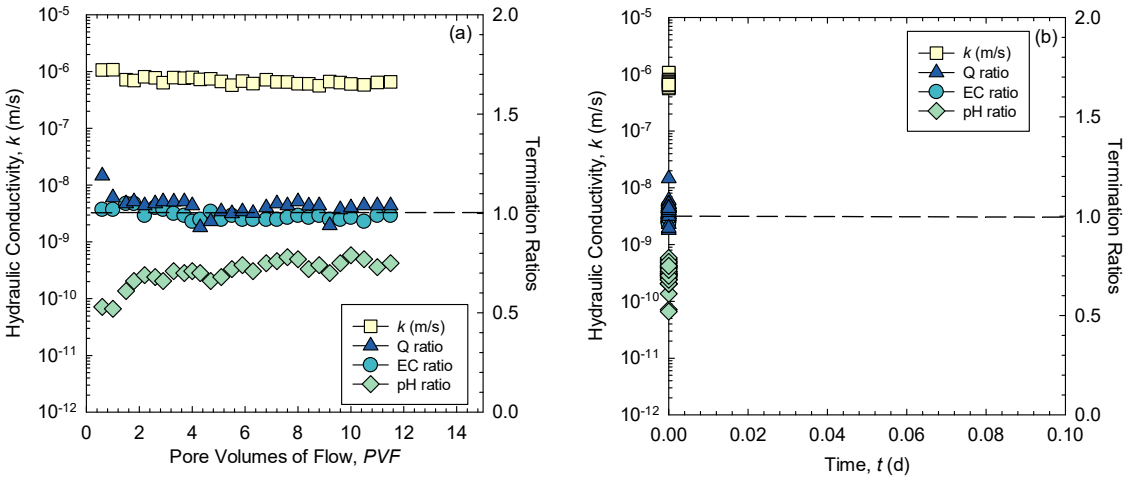

Appendix B: Batch Adsorption Sensitivity Analysis

B1.1 Batch adsorption and supernatant concentration sensitivity analysis

Two methods, (1) total organic carbon (TOC) analysis of the decanted supernatant, and (2) absorbance of the decanted supernatant via spectrophotometer were used to determine the adsorbed and non-adsorbed polymer factions of the batch adsorption experiments. A description and comparison of the methods is provided in the subsequent subsections. Before a complete method for batch adsorption was chosen, a sensitivity analysis was completed to determine the impacts of the following variables on PA adsorption: (1) soil:solution ratio, (2) mixing time, (3) centrifuge rate and (4) time, and (6) effective soil:solution separation (decanting/washing). The sensitivity analysis is presented in the subsequent subsection.

B1.2 Total organic carbon analysis

Total organic carbon analysis was completed using a Shimadzu TOC-L/TN analyzer (Shimadzu Corporation, Kyoto, Japan). Calibration of TOC was completed for PAHW in 167 mM $CaCl_2$, as shown in Figure B1. A 100-fold dilution was required due to the high TOC of the polymer (maximum calibrated at 100 ppm and minimum at 0.1 ppm for a 100ul injection) and the high salt concentration (maximum of 50 mM allowable).

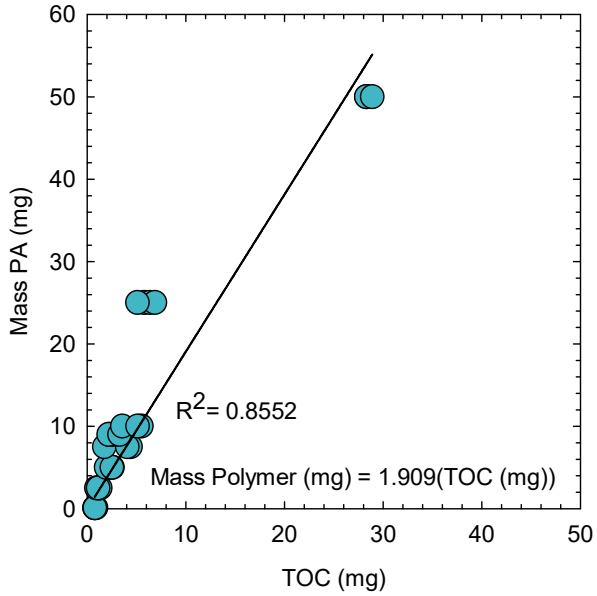

Figure B1: Calibration curve of mass of polymer (PA) (mg) plotted against measured total organic carbon content (mg) in 167 mM $CaCl_2$.

A sensitivity analysis of the TOC method of batch adsorption showed a wide spread of measured TOC that was affected by multiple variables, as shown in Figure A2. The highest variations in TOC were produced by changes in centrifuge rate and centrifuge time, and mixing time, as shown in Figure B2 (a) and (c), respectively. A "wash" of the NaB/PAHW mixture after the initial decant of the supernatant was completed to determine if there was mobile polymer that was not being captured in the initial draw. The resulting TOC data (as shown in Figure B2 (d,e)) indicated that the decant did not capture the entirety of the mobile TOC concentration. A single decant was not able to capture the liquid at the solid:solution interface of the NaB, which contained a fraction of unadsorbed polymer.

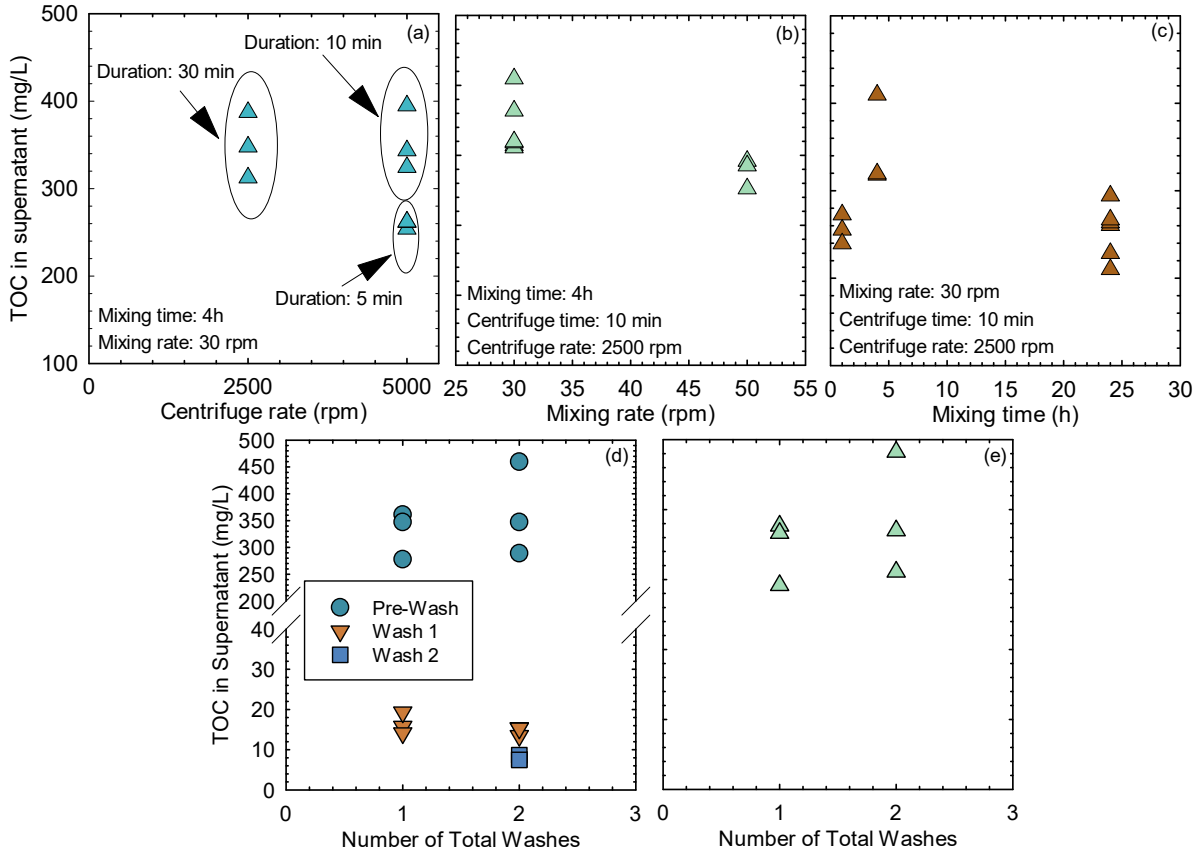

Figure B2: Measured total organic carbon (TOC) (mg/L) in decanted supernatant plotted against (a) centrifuge rate, (b) mixing rate, and (c) mixing time, and number of total washes (1 or 2) of (d) the prewash, first wash (wash 1), and second wash (wash 2) of each centrifuge tube and (e) the total TOC in the supernatant of each centrifuge tube (sum of prewash and washes for sensitivity analysis of batch adsorption variables).

The TOC analysis method used had a known allowable error of 10%. As shown in Figure B3, a large variation of % polymer (greater than 10% of the average) adsorbed was measured across all sensitivity analysis variables with no clear trend of a specific variable affecting the outcome. This variation led to the conclusion that either the collection of the supernatant or the TOC analysis was causing variability.

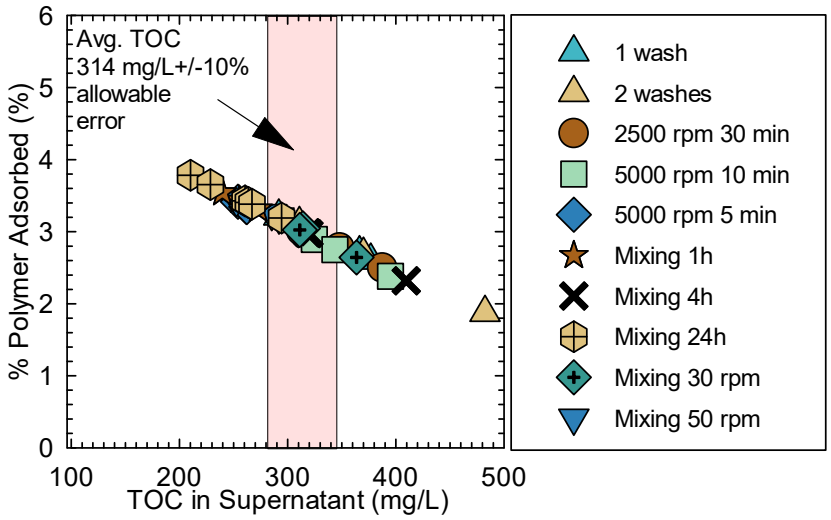

Figure B3: Calculated % polymer adsorbed plotted against total organic carbon (TOC) (mg/L) in decanted supernatant of all the following sensitivity analysis batch adsorption variables as indicated: total number of washes, centrifuge rate and time, and mixing rate and time.

As shown in Figure B4, the standard deviation per draw per sample in TOC analysis varied per draw, with standard deviations increasing with increasing polymer content. Due to the 100-fold dilution required for TOC analysis, the error in the diluted TOC readings was amplified when calculated for the actual sample concentration, as shown in Figure B5. The error could not be connected to any controlled variable and thus must be connected to the TOC analysis or the supernatant collection. The variability of the method was determined to be too high to obtain accurate batch adsorption results.

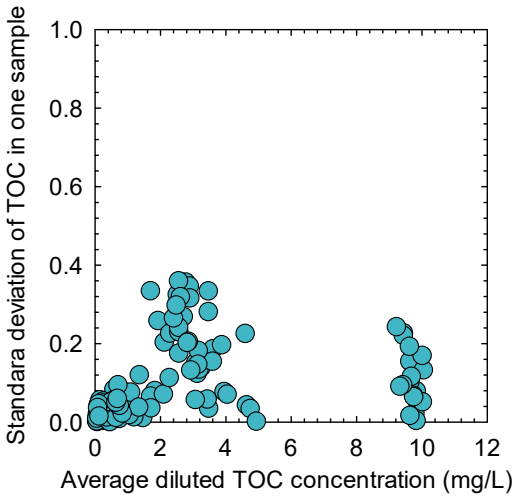

Figure B4: Standard deviation of TOC in a single sampling plotted against average 100-fold diluted total organic carbon (TOC) (mg/L). Results shown are for a range of tested TOC values (0-10 mg/L).

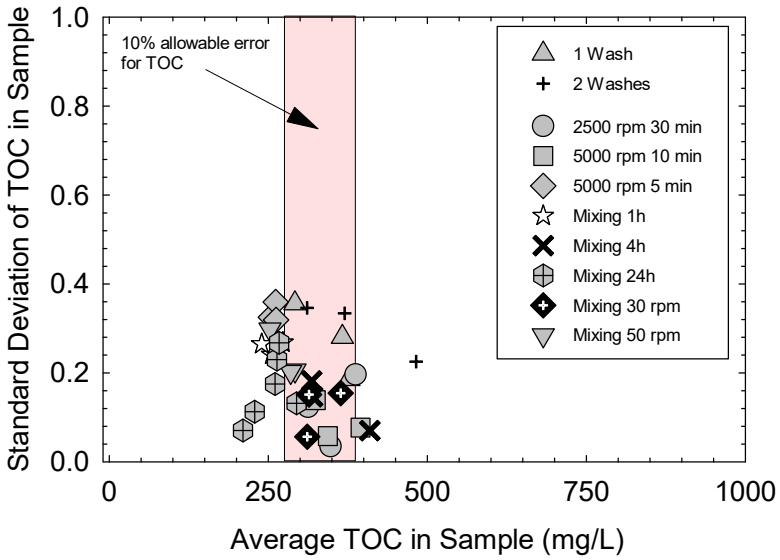

Figure B5: Standard deviation of TOC in a single sampling plotted against average total organic carbon (TOC) (mg/L) for each sample of batch adsorption method sensitivity analysis.

B1.3 Absorbance via spectrophotometer analysis

Polymers in solution produce an absorbance that is measurable via UV spectroscopy. Calibration of PAHW concentration in DIW produces a strong linear relationship ($r^2 = 0.994$) between measured absorbance at 190 nm and known PAHW concentration, as shown in Figure B6.

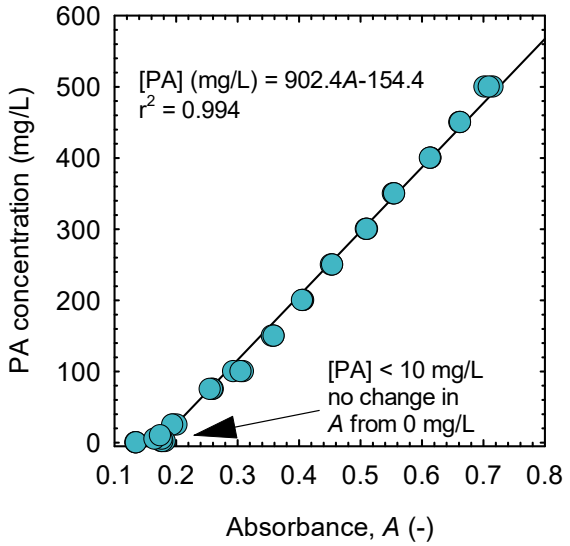

Figure B6: Poly(acrylic) acid (PA) concentration plotted against absorbance (-) measured at 190 nm in deionized water (DIW).

Unfortunately, chloride ions also produce an absorbance that is high enough to mask the change in absorbance due to change in polymer concentration when measured in the concentrated solutions this research is using (e.g., 500 mM NaCl), at the typically measured wavelength (190 nm) for polymer concentration identification, as shown in Figure B7.

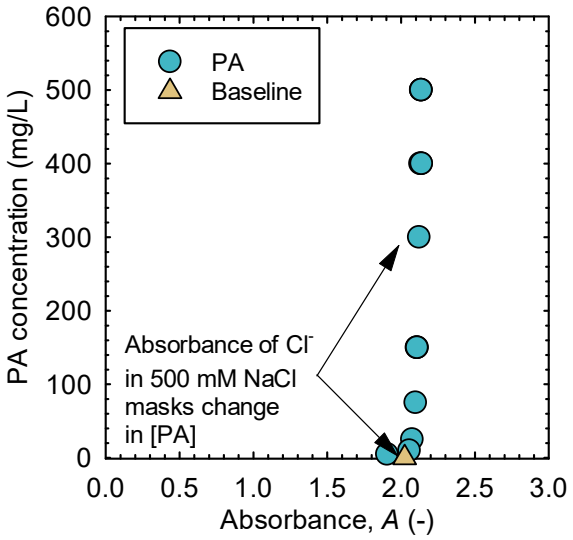

Figure B7: Poly(acrylic) acid (PA) concentration (mg/L) plotted against absorbance (-) measured at 190 nm in 500 mM NaCl.

To determine the wavelength in which chloride no longer masks changes in polymer concentrations, the scanning function of the UV spectrophotometer was used to determine the absorbance at 190-230 nm in a range of NaCl and $CaCl_2$ concentrations, as shown in Figure B8(a). The wavelength at which the chloride is no longer producing a measurable absorbance shifts to greater values (200 to 215 nm) depending on the concentration and the cations in solution (Na vs. Ca), best represented by ionic strength, as shown in Figure B8(b).

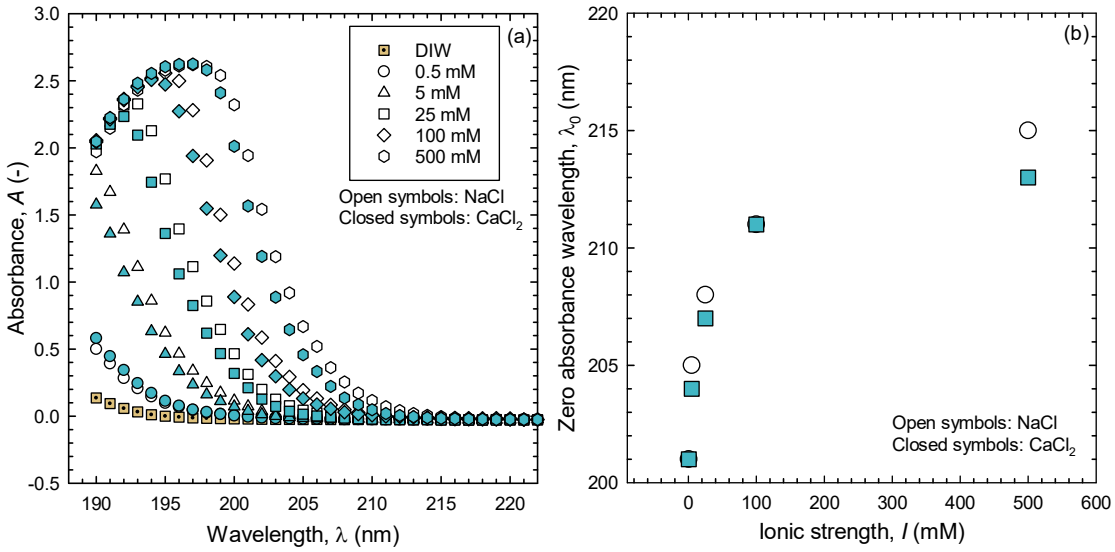

Figure B8: (a) Absorbance, *A* (-) plotted against wavelength, λ (nm) for DIW and sodium chloride (NaCl) and calcium chloride ($CaCl_2$) solutions at ionic strengths (*I*) of 0.5 mM, 5 mM, 25 mM, 100 mM, 500 mM, and (b) zero absorbance wavelength, λ_0 (nm) plotted against ionic strength, *I* (nm) of NaCl and $CaCl_2$ solutions.

As shown in Figure B9, Batch adsorption experiments with NaB (1:40 soil:solution ratio) also produce a change in measured absorbance. Sodium bentonite contains soluble salts and has a cation exchange capacity that results in a higher measured absorbance than the base 167 mM $CaCl_2$ solution and a positive, non-zero absorbance at values where the 167mM $CaCl_2$ produces a zero or negative absorbance. This increase is reduced back to zero by dilution at 0.6:3 mL and 0.3:3 mL.

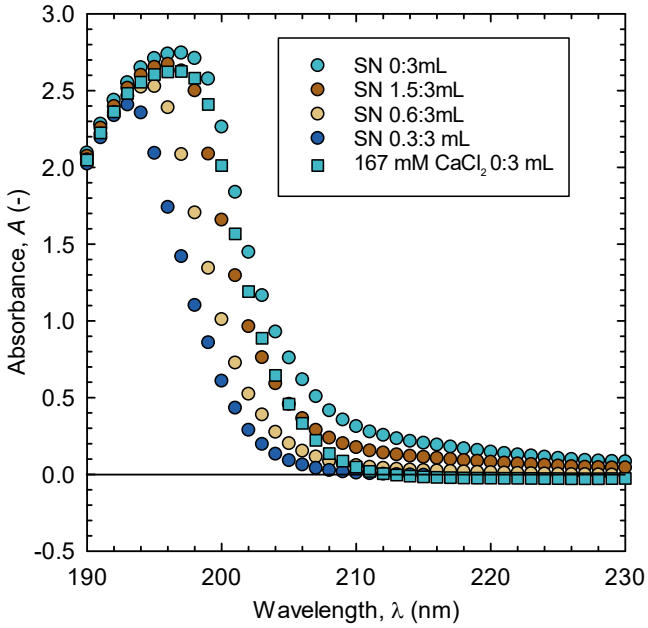

Figure B9: Absorbance, *A* (-) plotted against wavelength, λ (nm) for supernatant (SN) of sodium bentonite (NaB) 1:40 batch adsorption tests with 167 mM calcium chloride ($CaCl_2$) at 0:3 mL (no dilution), 1.5:3 mL, 0.6:3 mL, and 0.3:3 mL dilutions with deionized water (DIW) compared to 167 mM $CaCl_2$ solution with no dilution.

In accordance with EPA batch adsorption methods, the soil:solution ratio needs to be verified. Ratios 1:4, 1:10, 1:100, and 1:500 were considered and are summarized in Figure B10(a). Ratios 1:4 and 1:10 produced cloudiness (suspended NaB) even after centrifugation and 2 h rest (Figure B10(a)) that resulted in an absorbance well above the blank (167 mM $CaCl_2$, no NaB) absorbance. While 1:40 showed an increase in absorbance with no rest after centrifugation (Figure B10(a)), 2 h rest allowed enough time for suspended NAB to settle and resulted in an absorbance similar to the blank (no NaB). Ratios 1:100 and 1:500 produced similar absorbances to the blank with no rest and 2h rest. However, the polymer concentrations of interest would be too difficult to weigh out with such a low amount of NaB (i.e., 1% by mass of polymer in 1:100 in 50 ml centrifuge tube is 0.5g NaB and 0.005g polymer). A soil:solution ratio of 1:40 was chosen for batch adsorption analysis with measurement after 2h. This method produced a clear differentiation between tested polymer concentrations at 1250 and 5000 mg/L in the presence of NaB (Figure B10(b)).

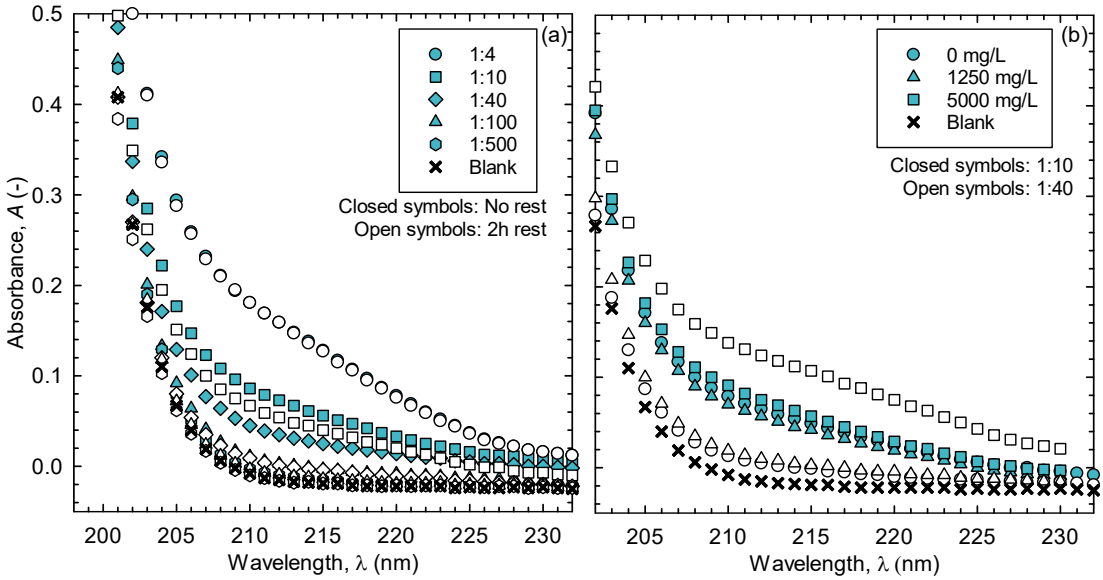

Figure B10: Absorbance, *A* (-) plotted against wavelength, λ (nm) for supernatant (SN) of sodium bentonite (NaB) batch adsorption tests with 167 mM calcium chloride ($CaCl_2$) at 0.3:3 mL dilutions with deionized water (DIW) at soil (g):solution (mL) ratios of (a) 1:4, 1:10, 1:40, 1:100, and 1:500 mixed for 24h at 30 rpm, centrifuged at 2500 rpm for 10 min and then immediately sampled (no rest, closed symbols) or rested for 2h before sampling (open symbols) and (b) 1:10 and 1:40 at 0, 1250, and 5000 mg/L of PA compared to diluted (0.3:3 mL) 167 mM $CaCl_2$ (blank).

To verify that the batch adsorption tests captured the adsorption capacity and no physical (mechanical) entrapment of polymer due to centrifugation. The absorbance of NaB in solution was compared with pyrophyllite in solution. Pyrophyllite is a neutral mineral with no adsorption capacity. If polymer was not entrapped in the batch adsorption experiment, the absorbance of the polymer solutions without soil should be equivalent to the absorbance of the vials mixed with pyrophyllite and centrifuged. As shown in Figure B11, pyrophyllite produced the same absorbance as blank vials (no soil) while NaB indicated adsorption capacity by a reduction in measured absorbance. These results indicated that no mechanical entrapment occurred during mixing/centrifugation.

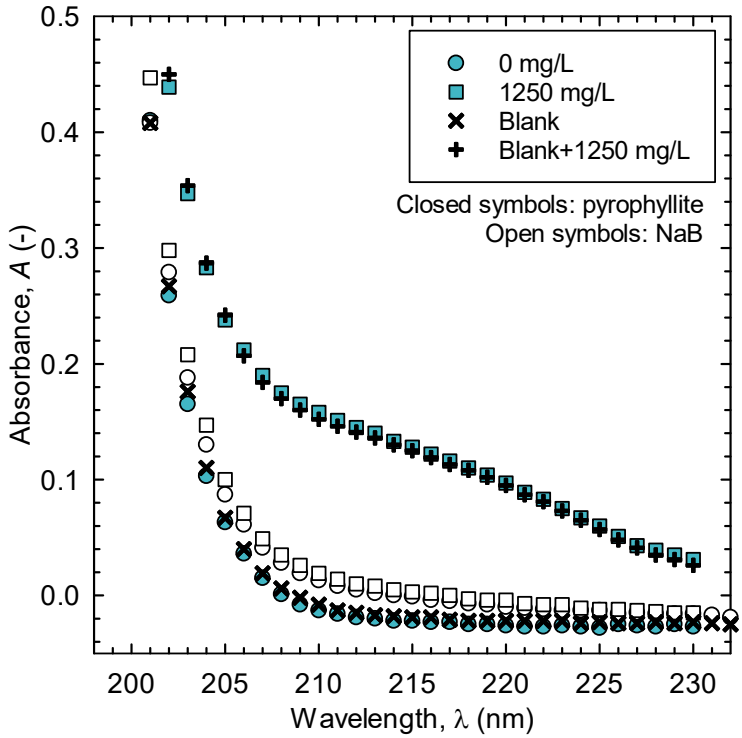

Figure B11: Absorbance, *A* (-) plotted against wavelength, λ (nm) for supernatant (SN) of batch adsorption tests with 167 mM calcium chloride ($CaCl_2$) at 0.3:3 mL dilutions with deionized water (DIW) at 1:40 soil:solution ratio mixed for 24h at 30 rpm, centrifuged at 2500 rpm for 10 min and then rested for 2h before sampling with NaB (open symbols) and pyrophyllite (closed symbols) at 0 mg/L and 1250 mg/L of PA compared to diluted (0.3:3 mL) 167 mM $CaCl_2$ at 0 mg/L (blank) and 1250 mg/L (blank+1250 mg/L).

B1.4 Batch adsorption sensitivity analysis

Polymer stock solutions were prepared by mixing the dried and ground PA into inorganic salt solutions in a sealed beaker for at least 2 h via a magnetic mixer and then mixed with the NaB in 50 ml centrifuge tubes, end over end at 30 rpm in a tumbler. After mixing, the tubes were centrifuged at 2500 rpm for 10 min. The tubes were rested for 2 h. The supernatant was tested to determine polymer content. As shown in Figure B12, sensitivity analysis of the batch adsorption method variables indicated the following: (1) rest for at least 2 h is crucial to remove suspended bentonite and reduce variability (Figure 12 (a,b)), and (2) mixing beyond 24 h creates a cloudiness (bentonite suspension) that is very difficult to remove (Figure 12 (c)),

even with 24 h resting of the tube, (3) centrifuge rate and time do not have large effect on results (Figure 12 (d))).

A mixing time of 24h was chosen due to ease of set up/measurement so that set up and measurement spanned over two days and did not require an entire day of setup and measurement. A centrifuge rate of 2500 rpm and time of 10 min were chosen.

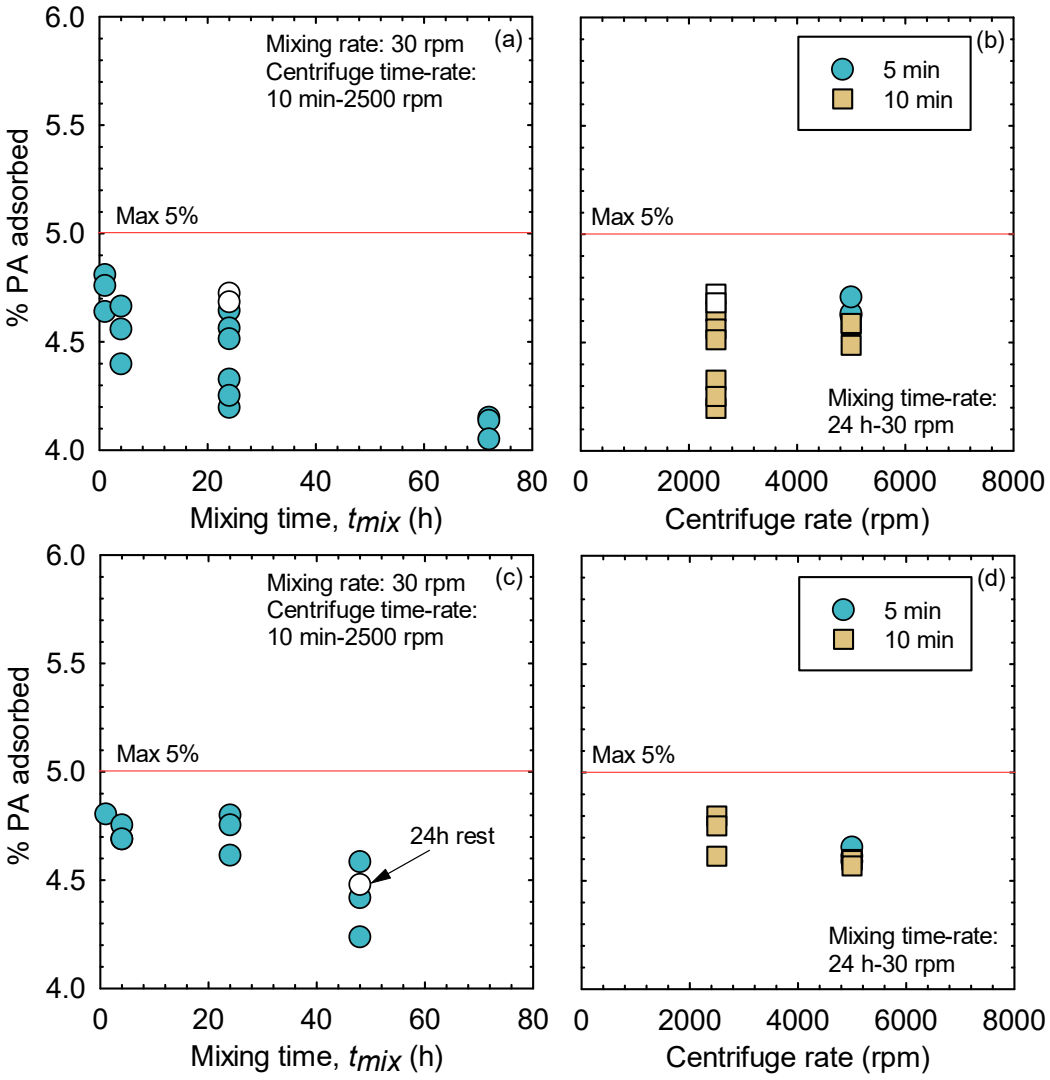

Figure B12: Absorbance, *A* (-) plotted against (a,c) mixing time and (b,d) centrifuge rate for sensitivity analysis of batch adsorption tests of PAHW and NaB in 167 mM $CaCl_2$, undiluted, with (a,b) no rest or (c,d) 2h (or 24h) rest before sampling.

B1.5 Calibration curves

Calibration curves were developed for polymer solutions of PAHW and collected supernatant of NaB by mixing the solution of interest (i.e., 167 mM $CaCl_2$) with the base NaB following the same procedure for batch adsorption but with 0 mg/L PAHW. The resulting supernatant was collected and mixed to produce a bulk store of supernatant. The supernatant was then used to prepare polymer solutions at the concentrations of interest. The polymer solutions were then tested for absorbance at 215-220 nm either with no dilution or at a 0.3:3.0 mL dilution with DIW for higher polymer concentrations. At least three data points were collected for each polymer concentration. The data was used to create calibration curves that covered the entirety of the concentrations of interest. The generated equations were used to evaluate batch adsorption results.

As shown in Figure B13, calibration curves across the 215-220 nm wavelengths produced very similar values of R^2 and average percent standard error, regardless of dilution. The 215 nm wavelength consistently produced a low average percent standard error and R^2 close to one, so this wavelength was used to create the calibration curves used in calculating the polymer concentrations for the batch adsorption experiments. The calibration curves for diluted (0.3:3 mL) and undiluted polymer concentrations for the solutions tested are provided in Figures B14-B18. Each plot for a given solution contains blank calibration curves (containing no NaB) and supernatant curves generated with either no dilution or 0.3:3 mL dilution with DIW.

As shown previously, increases in absorbance compared to the base solution occur due to the release of soluble salts and cation exchange when the concentrated calcium or sodium chloride solutions mix with the NaB. This behavior can be seen Figures B14-B18, where the calibration curves for both the blank (no mixing with NaB) solution and the supernatant solution are compared in the five tested salt solutions. Dilution of the supernatant with DIW at 0.3mL to 3 mL largely removed this variation.

Test points were created by mixing a known mass of PAHW into a centrifuge tube containing a measured volume of 20-40 mL of supernatant solution. The tube was shaken and mixed using a (vibratory plate mixer) for one minute before immediate testing.

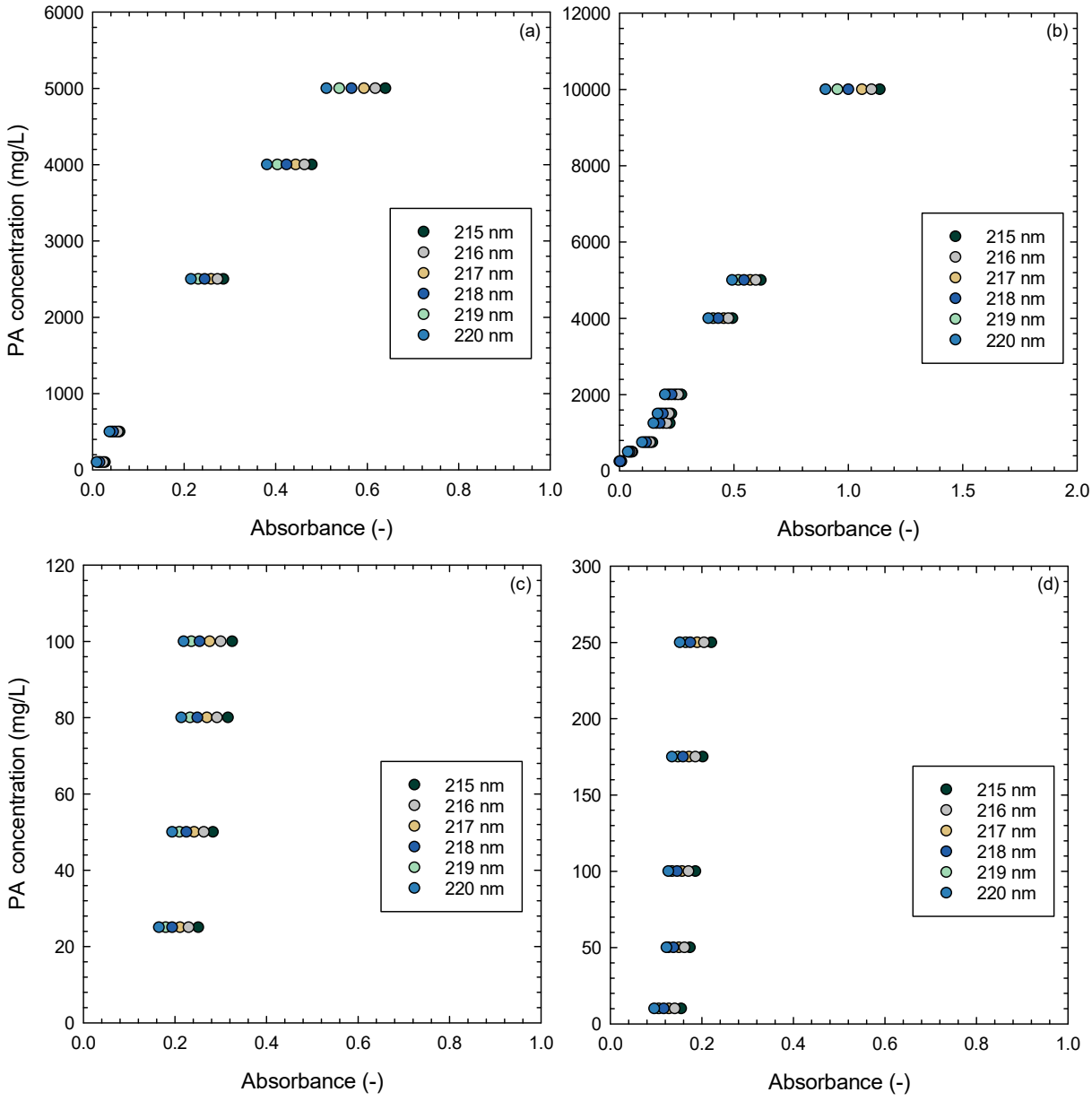

Figure B13: Absorbance, *A* (-) plotted against PA concentration (mg/L) for calibration of PA concentration in (a,c) 500 mM NaCl and (b,d) 167 mM $CaCl_2$ supernatant (mixed with NaB then centrifuged and decanted) with (a,b) 0.3:3 mL dilution and (c,d) no dilution.

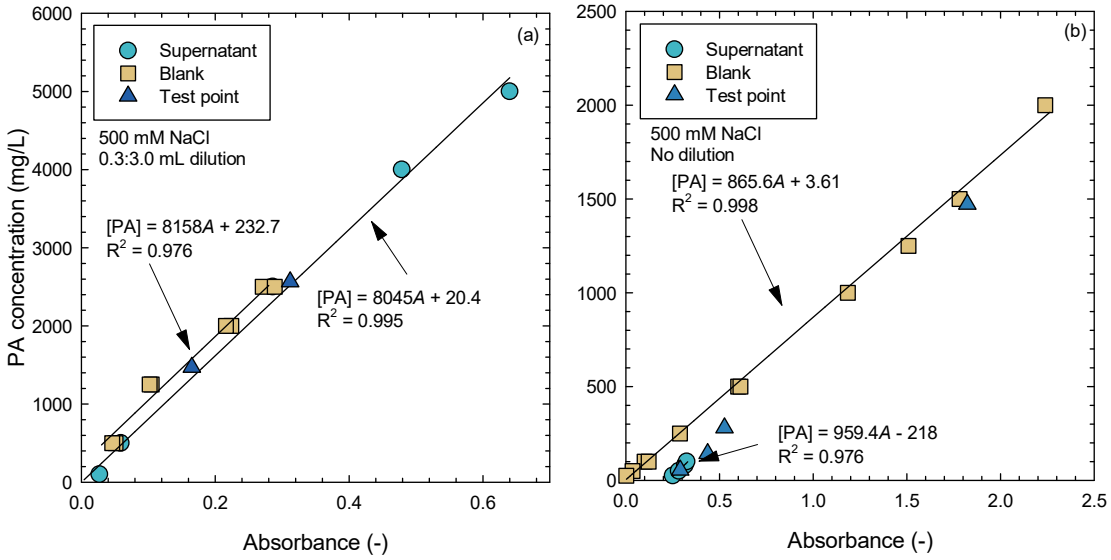

Figure B14: Absorbance, *A* (-) plotted against PA concentration (mg/L) for calibration of PA concentration in 500 mM NaCl supernatant (mixed with NaB then centrifuged and decanted) and blank (only 500 mM NaCl) with (a) 0.3:3 mL dilution or (b) no dilution.

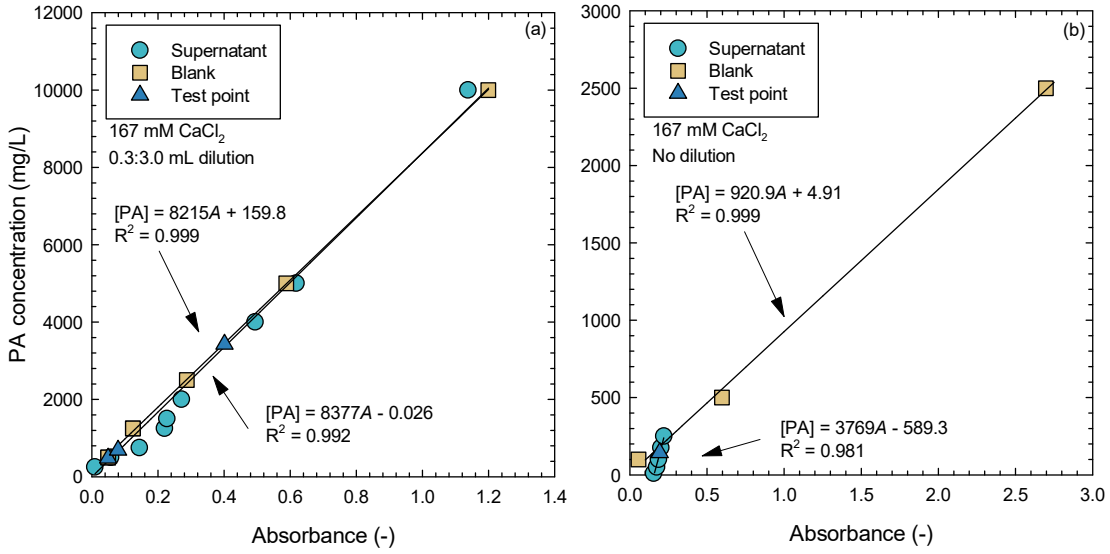

Figure B15: Absorbance, *A* (-) plotted against PA concentration (mg/L) for calibration of PA concentration in 167 mM $CaCl_2$ supernatant (mixed with NaB then centrifuged and decanted) and blank (only 167 mM $CaCl_2$) with (a) 0.3:3 mL dilution or (b) no dilution.

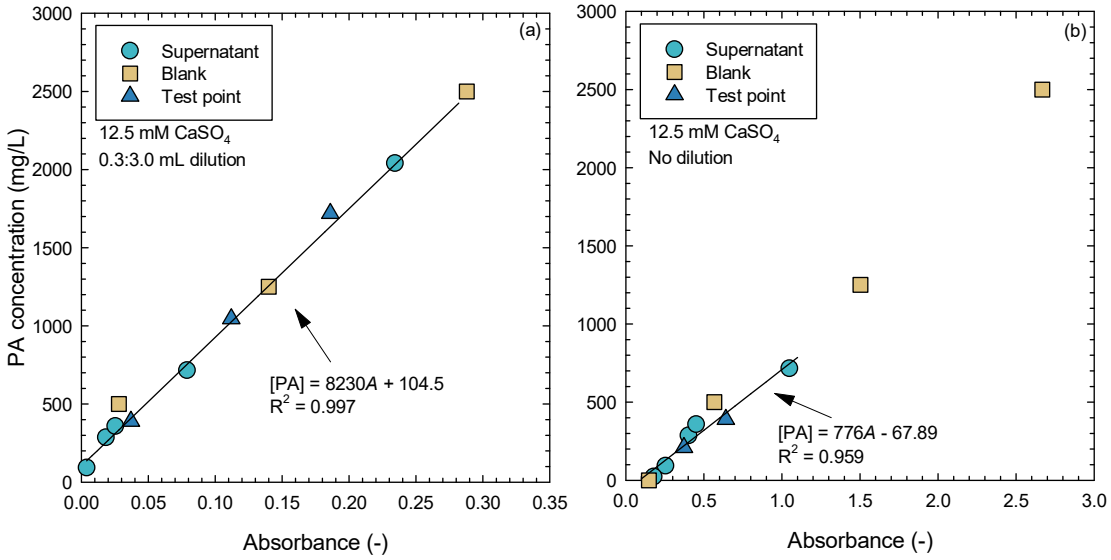

Figure B16: Absorbance, *A* (-) plotted against PA concentration (mg/L) for calibration of PA concentration in 12.5 mM $CaSO_4$ supernatant (mixed with NaB then centrifuged and decanted) and blank (only 12.5 mM $CaSO_4$) with (a) 0.3:3 mL dilution or (b) no dilution.

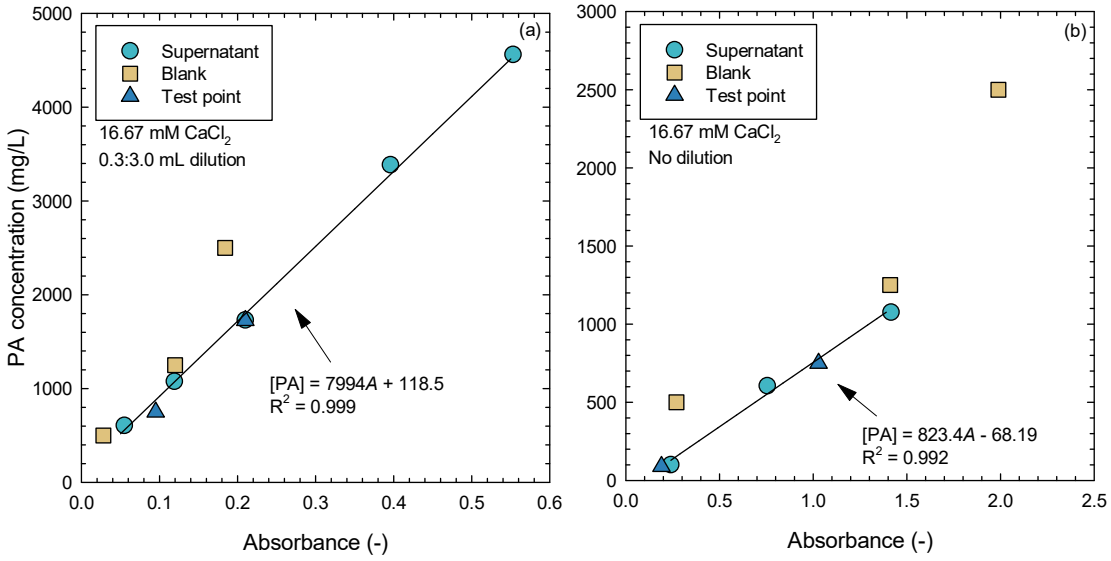

Figure B17: Absorbance, *A* (-) plotted against PA concentration (mg/L) for calibration of PA concentration in 16.67 mM $CaCl_2$ supernatant (mixed with NaB then centrifuged and decanted) and blank (only 16.67 mM $CaCl_2$) with (a) 0.3:3 mL dilution or (b) no dilution.

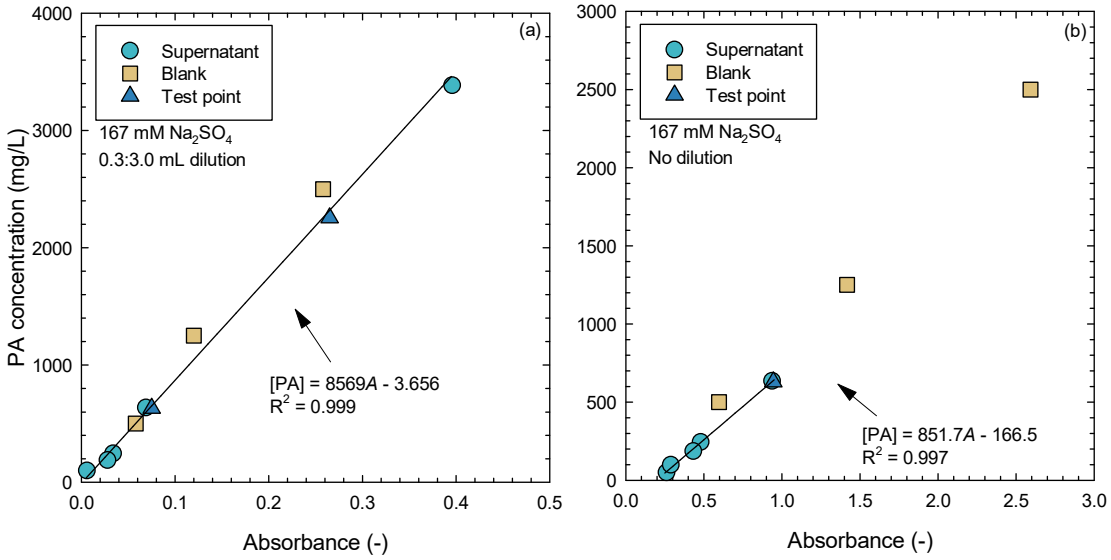

Figure B18: Absorbance, *A* (-) plotted against PA concentration (mg/L) for calibration of PA concentration in 167 mM Na_2SO_4 supernatant (mixed with NaB then centrifuged and decanted) and blank (only 167 mM Na_2SO_4) with (a) 0.3:3 mL dilution or (b) no dilution.

Appendix C: Pyrophyllite

C1.1 Gradations

Particle size distributions prepared via dry sieve analysis, for the pyrophyllite, granular NaB, and powdered NaB tested in this study are shown in Figure C1.

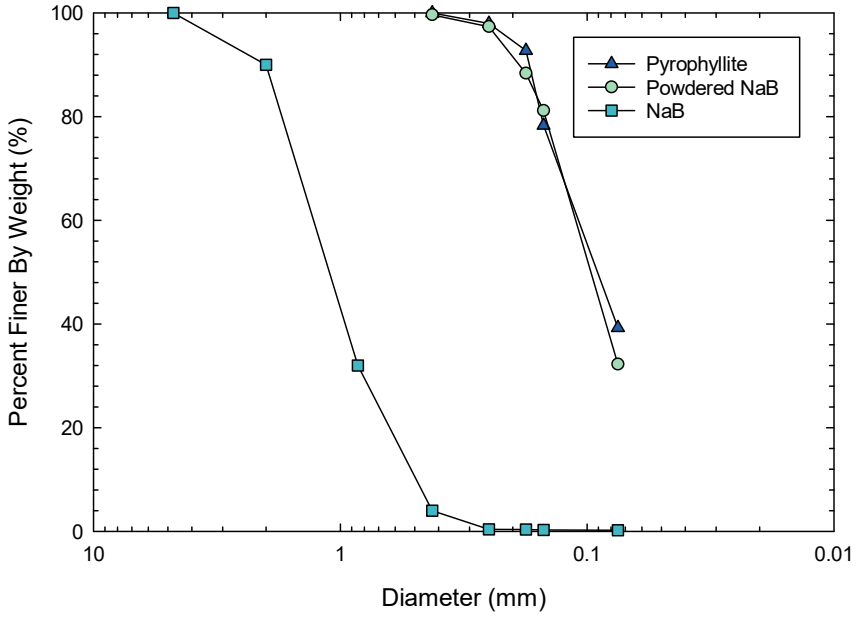

Figure C1: Particle size distribution (dry sieve) of pyrophyllite and granular NaB compared to powdered NaB.

C1.2 Pyrophyllite structure

Pyrophyllite has the same structure as montmorillonite. However, pyrophyllite has only aluminum octahedral cations. The lack of isomorphic substitution in pyrophyllite results in no net layer charge and thus, no interlayer cations. A schematic comparison of the structures of montmorillonite and pyrophyllite is provided in Figure C2.

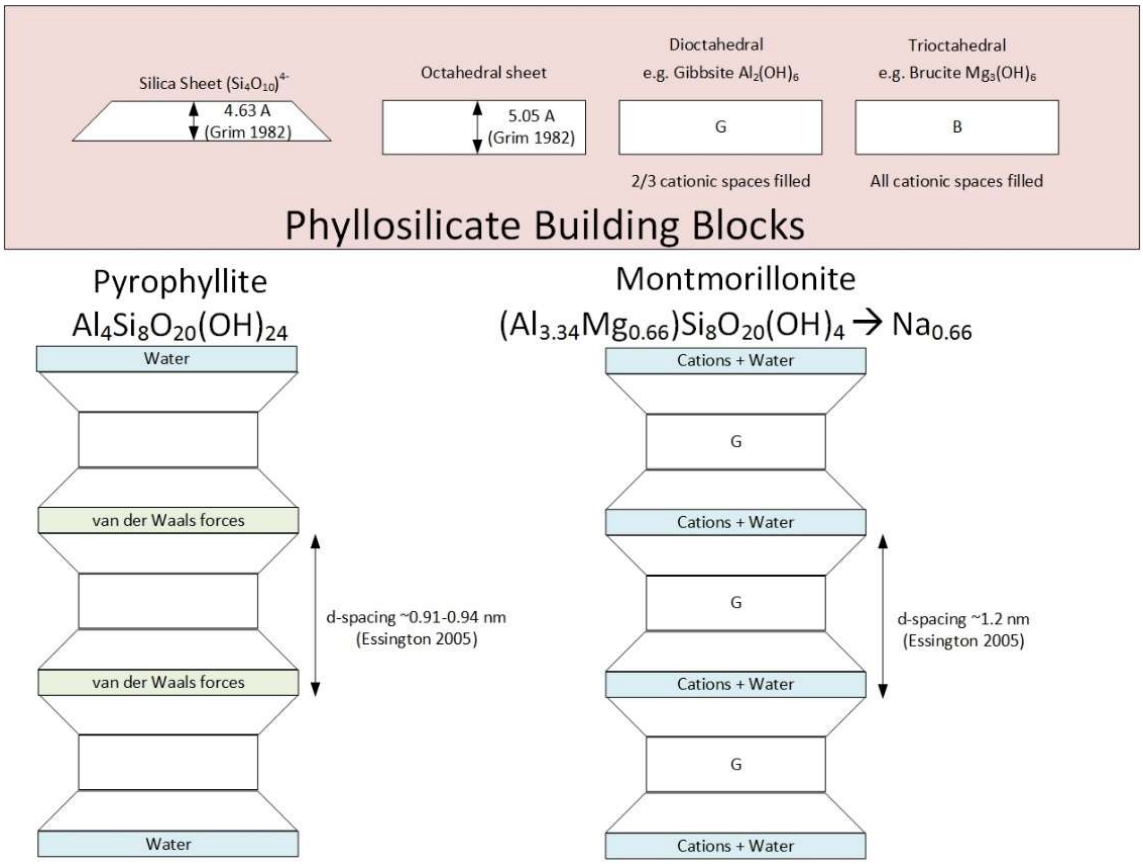

Figure C2: Schematic of structural differences between powdered NaB and pyrophyllite.

Appendix D: Photo Library
D1 Post permeation GCL specimens

Figure D1-1: Post permeation hydrogel on inflow side of Sample A1, PAHW5DS permeated with 167 mM $CaCl_2$.

Figure D1-2: Post permeation hydrogel inside Sample A1, PAHW5DS permeated with 167 mM $CaCl_2$.

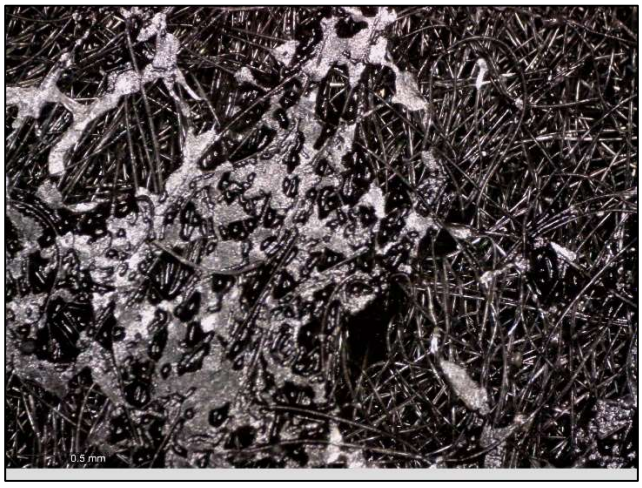

Figure D1-3: Post permeation hydrogel on inflow side geotextile of Sample A1, PAHW5DS permeated with 167 mM $CaCl_2$.

Figure D1-4: Post permeation cross section of Sample A1, PAHW5DS permeated with 167 mM $CaCl_2$.

Figure D1-5: Post permeation cross section of Sample A1, PAHW5DS permeated with 167 mM $CaCl_2$.

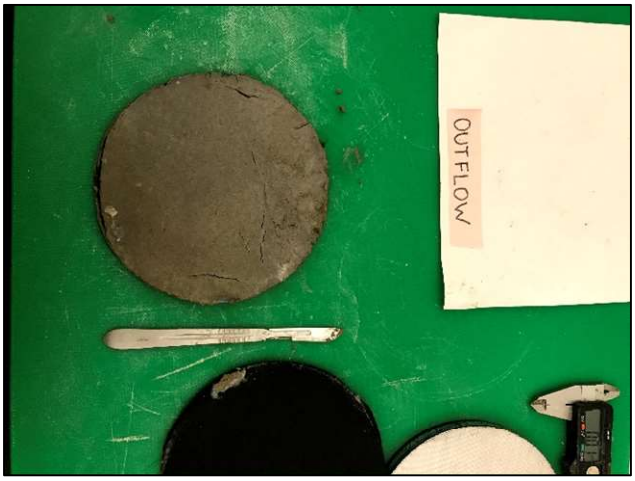

Figure D1-6: Post permeation outflow side of Sample A2, PAHW8DS permeated with 167 mM $CaCl_2$.

Figure D1-7: Post permeation inflow side of Sample A3, PAHW5WM permeated with 167 mM $CaCl_2$.

Figure D1-8: Post permeation cross section of Sample A3, PAHW5WM permeated with 167 mM $CaCl_2$.

Figure D1-9: Post permeation cross section of Sample A3, PAHW5WM permeated with 167 mM $CaCl_2$.

Figure D1-10: Post permeation cross section of Sample A4, PAMW5DS permeated with 167 mM $CaCl_2$.

Figure D1-11: Post permeation cross section of Sample A4, PAMW5DS permeated with 167 mM $CaCl_2$.

Figure D1-12: Post permeation outflow side of Sample A5, PAMW8DS permeated with 167 mM $CaCl_2$ with visible indications of hydrogel formation.

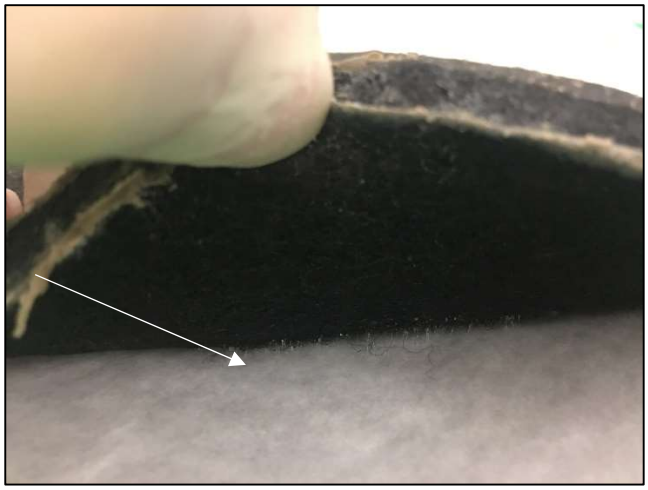

Figure D1-13: Post permeation of Sample A5, PAMW8DS permeated with 167 mM $CaCl_2$ with visible indications of hydrogel formation within GCL.

Figure D1-14: Post permeation of Sample A5, PAMW8DS permeated with 167 mM $CaCl_2$ with visible indications of hydrogel formation on inflow side base plate of permeameter.

Figure D1-15: Post permeation outflow side of Sample A6, PAMW10DS permeated with 167 mM $CaCl_2$. White layer is filter paper adhered to hydrogel.

Figure D1-16: Post permeation outflow side geotextile of Sample A7, PALW5DS permeated with 167 mM $CaCl_2$.

Figure D1-17: Post permeation outflow side of Sample A7, PALW5DS permeated with 167 mM $CaCl_2$.

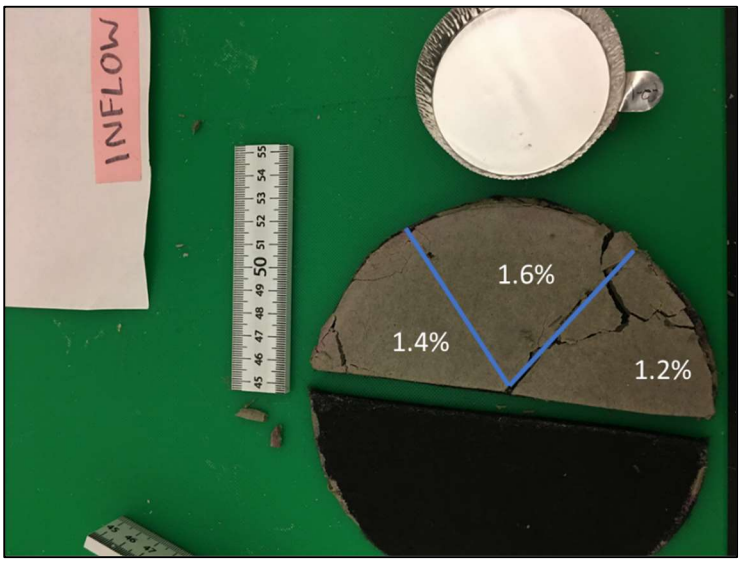

Figure D1-18: Post permeation inflow side of Sample A7, PALW5DS permeated with 167 mM $CaCl_2$. Post permeation polymer contents measured via TC-IC analysis are labeled for each sampled section.

Figure D1-19: Post permeation inflow side of Sample A8, PALW10DS permeated with 167 mM $CaCl_2$.

Figure D1-20: Post permeation cross section of Sample A8, PALW10DS permeated with 167 mM $CaCl_2$.

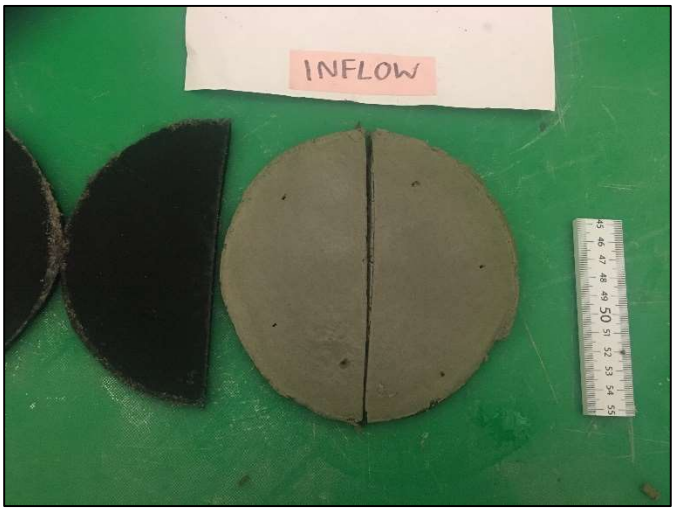

Figure D1-21: Post permeation cross section of Sample A9, PALW5WM permeated with 167 mM $CaCl_2$.

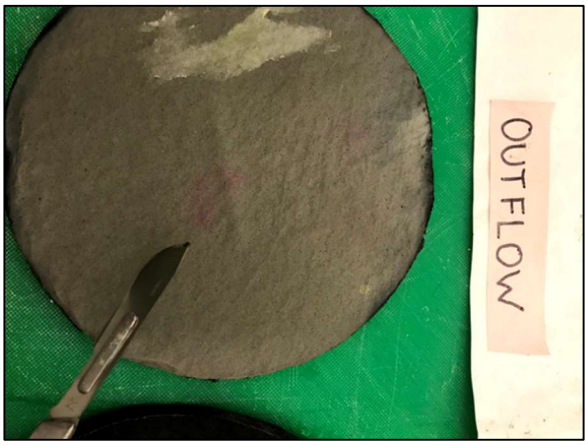

Figure D1-22: Post permeation outflow side of Sample A10, CMCHV5DM permeated with 167 mM $CaCl_2$ and dyed for identification of preferential flow.

Figure D1-23: Post permeation outflow side of Sample A11, CMCHV5WM permeated with 167 mM $CaCl_2$.

Figure D1-24: Post permeation inflow side of Sample A12, CMCLV5DM permeated with 167 mM $CaCl_2$ and dyed for identification of preferential flow.

Figure D1-25: Post permeation outflow side of Sample A12, CMCLV5DM permeated with 167 mM $CaCl_2$ and dyed for identification of preferential flow.

Figure D1-25: Post permeation cross section of Sample A12, CMCLV5DM permeated with 167 mM $CaCl_2$ and dyed for identification of preferential flow.

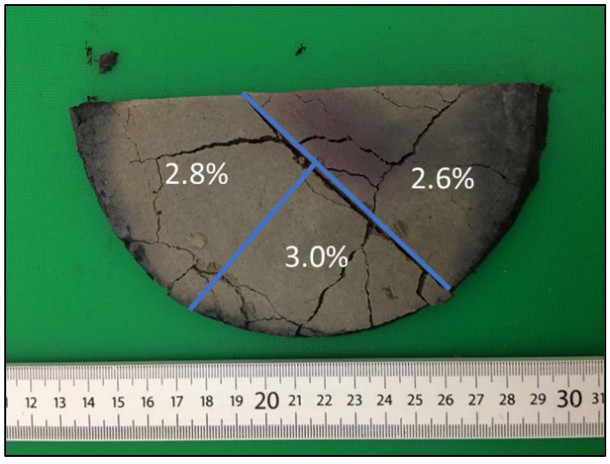

Figure D1-25: Post permeation outflow side of Sample A12, CMCLV5DM permeated with 167 mM $CaCl_2$ and dyed for identification of preferential flow. Post permeation polymer contents measured via TC-IC analysis are labeled for each sampled section.

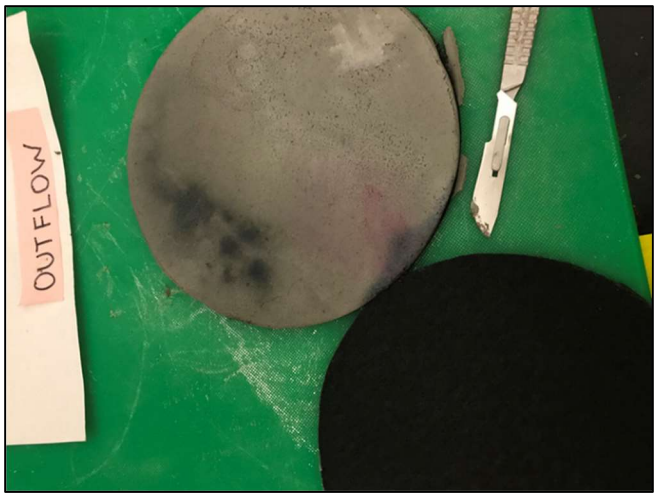

Figure D1-26: Post permeation outflow side of EB-GCL CMCLV5WM permeated with 167 mM $CaCl_2$ and dyed for identification of preferential flow. (Failed test due to geotextile pinching).

Figure D1-27: Post permeation cross section of Sample A13, BPC permeated with 167 mM $CaCl_2$ and dyed for identification of preferential flow. Sample exhibited a cohesive flexibility that allowed holding/bending without breakage.

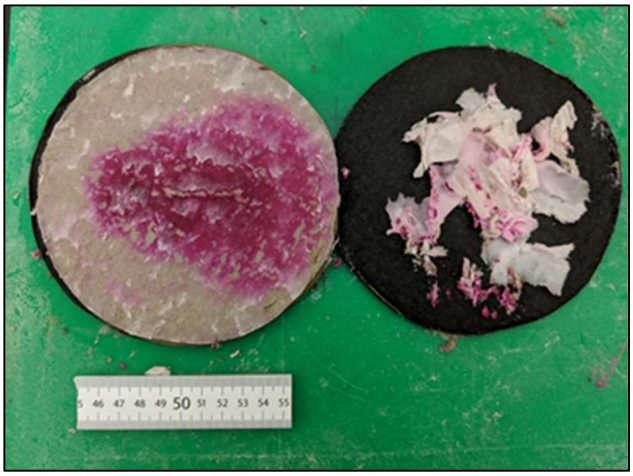

Figure D1-28: Post permeation inflow side of Sample A13, BPC permeated with 167 mM $CaCl_2$ and dyed for identification of preferential flow.

Figure D1-29: Post permeation outflow side of Sample A13, BPC permeated with 167 mM $CaCl_2$ and dyed for identification of preferential flow.

Figure D1-30: Post permeation hydrogel present inside inflow tubing of Sample A13, BPC permeated with 167 mM $CaCl_2$, dyed for identification of preferential flow.

Figure D1-31: Post permeation hydrogel attached to inflow geotextile of Sample A13, BPC permeated with 167 mM $CaCl_2$, dyed for identification of preferential flow.

Figure D1-32: Post permeation outflow side Sample A14, BPC5DM permeated with 167 mM $CaCl_2$.

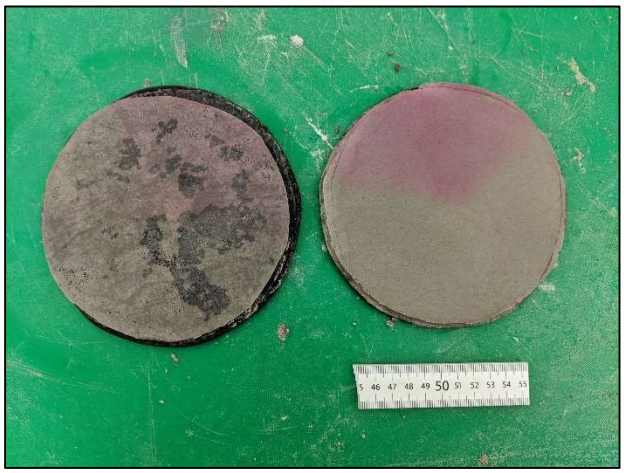

Figure D1-33: Post permeation outflow side of Sample A15, PAx5DS, permeated with 167 mM $CaCl_2$, dyed for preferential flow.

Figure D1-34: Post permeation inflow side of Sample A15, PAx5DS, permeated with 167 mM $CaCl_2$, dyed for preferential flow. Large amount of hydrogel present on inflow side of GCL.

Figure D1-35: Post permeation inflow side of Sample B1, PAHW5DS, permeated with 500 mM NaCl.

Figure D1-36: Post permeation inflow side of Sample B2, PAHW5WM, permeated with 500 mM NaCl.

Figure D1-37: Post permeation of Sample B2, PAHW5WM permeated with 500 mM NaCl exhibiting a cohesive flexibility, allowing GCL to be slightly bent without breaking.

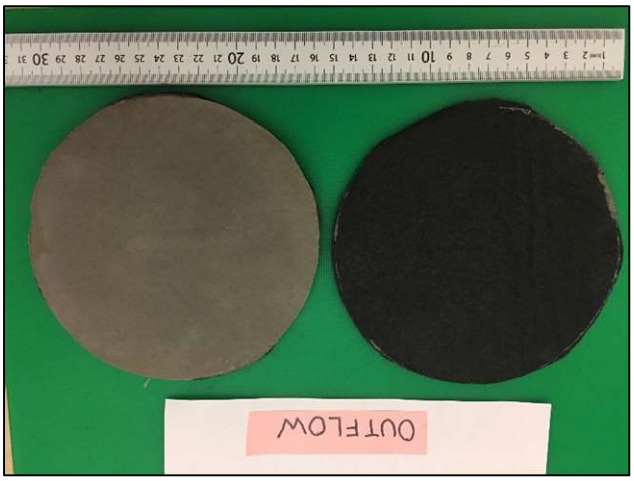

Figure D1-38: Post permeation outflow side of Sample B3, PAMW5DS permeated with 500 mM NaCl.

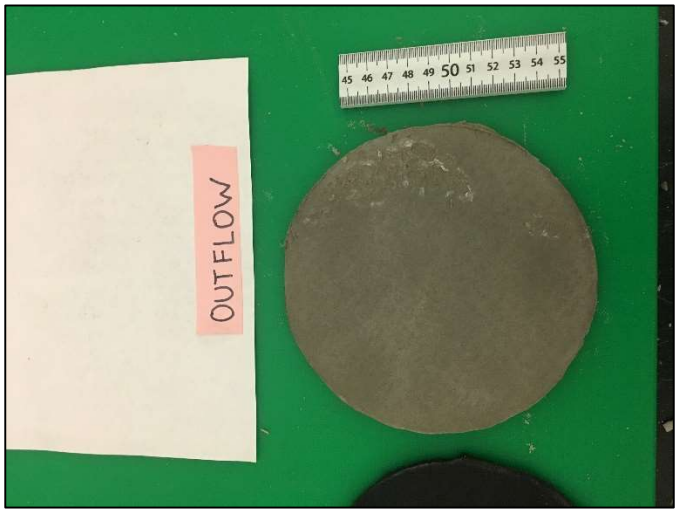

Figure D1-39: Post permeation outflow side of Sample B4, PAMW8DS permeated with 500 mM NaCl.

Figure D1-40: Post permeation outflow side of Sample B5, PAMW5WM permeated with 500 mM NaCl.

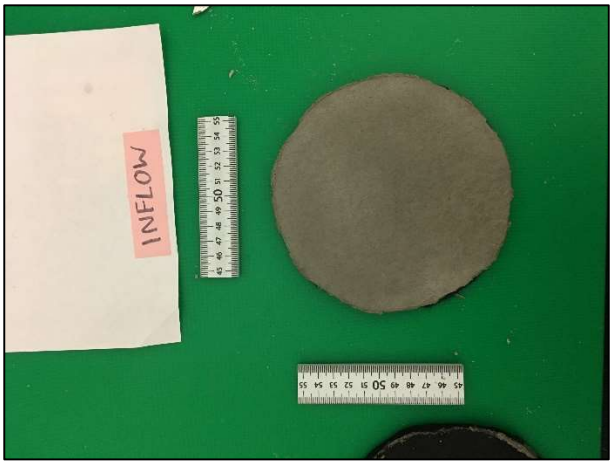

Figure D1-41: Post permeation outflow side of Sample B6, PALW5DS permeated with 500 mM NaCl.

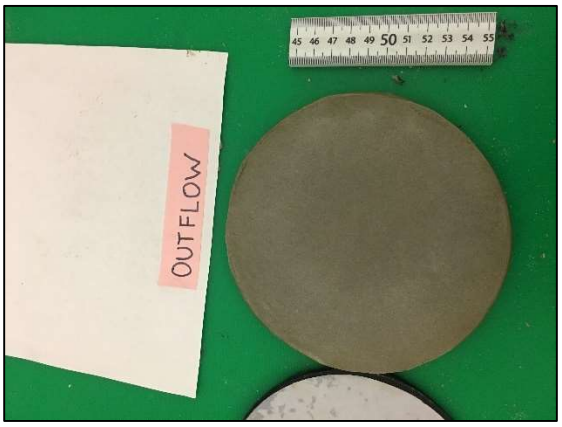

Figure D1-42: Post permeation outflow side of Sample B7, PALW5WM permeated with 500 mM NaCl.

Figure D1-43: Post permeation outflow side of Sample B8, CMCHV5DM permeated with 500 mM NaCl, dyed for preferential flow.

Figure D1-44: Post permeation outflow side of Sample B8, CMCHV5DM permeated with 500 mM NaCl, dyed for preferential flow.

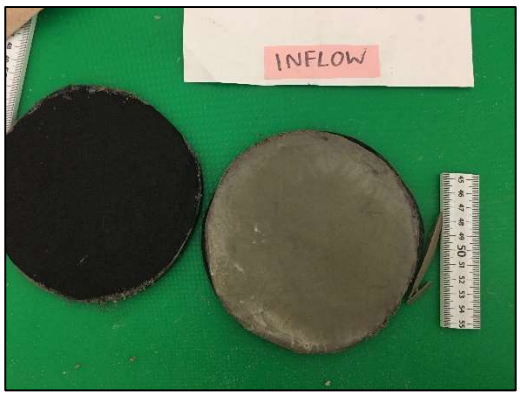

Figure D1-45: Post permeation inflow side of Sample B9, CMCHV5WM permeated with 500 mM NaCl.

Figure D1-46: Post permeation outflow side of Sample B10, CMCLV5DM permeated with 500 mM NaCl.

Figure D1-47: Post permeation inflow side of Sample B11, CMCLV5WM permeated with 500 mM NaCl.

Figure D1-48: Post permeation inflow side of Sample B12, CMCLV5DS permeated with 500 mM NaCl.

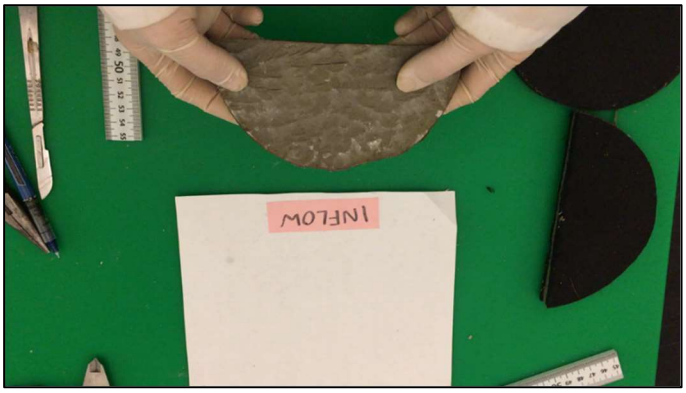

Figure D1-49: Post permeation inflow side of Sample B13, BPC permeated with 500 mM NaCl.

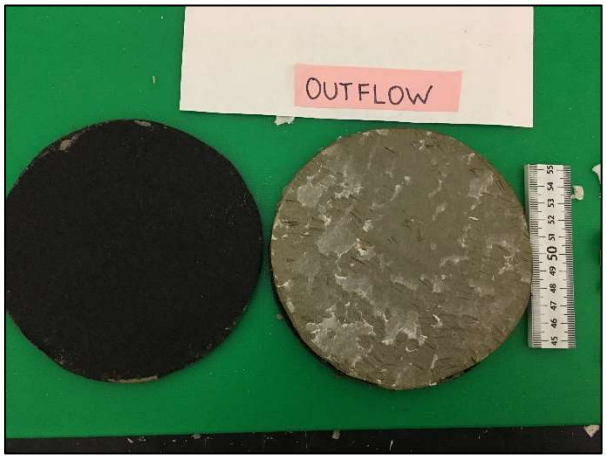

Figure D1-50: Post permeation outflow side of Sample B13, BPC permeated with 500 mM NaCl.

Figure D1-51: Effluent of Sample B13, BPC permeated with 500 mM NaCl.

Figure D1-52: Post permeation outflow side of Sample B14, BPC5DM permeated with 500 mM NaCl.

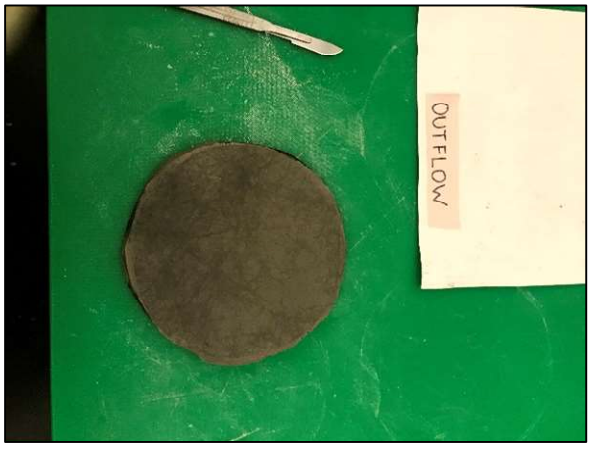

Figure D1-53: Post permeation outflow side of Sample B15, PAx5DS permeated with 500 mM NaCl.

Figure D1-54: Post permeation cross section of Sample B15, PAx5DS permeated with 500 mM NaCl.

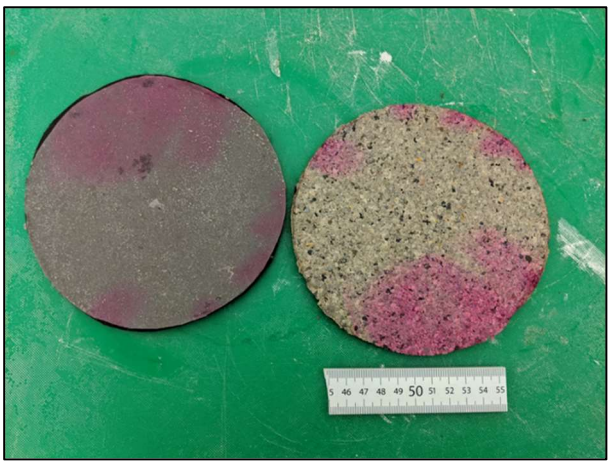

Figure D1-55: Post permeation inflow side of Sample E1, PAHW5DS prepared with granular NaB and permeated with 500 mM NaCl. Specimen dyed for identification of preferential flow.

Figure D1-56: Post permeation inflow side of Sample E2, PAHW5DS prepared with granular NaB and permeated with 167 mM $CaCl_2$. Specimen dyed for identification of preferential flow.

Figure D1-57: Post permeation outflow side of EB-GCL PAHW5DS prepared with granular NaB and permeated with 167 mM $CaCl_2$. Specimen dyed for identification of preferential flow.

Figure D1-58: Post permeation outflow side of EB-GCL PAHW5DS prepared with granular NaB and permeated with 167 mM $CaCl_2$. Specimen dyed for identification of preferential flow. Post permeation polymer contents measured via TC-IC analysis are labeled for each sampled section.

D2. Batch adsorption

Figure D2-1: Batch adsorption tube, 10,000 mg/L PAHW in 167 mM $CaCl_2$ with NaB, 1:40 ratio.

Figure D2-2: Batch adsorption tube, 7500 mg/L PAHW in 167 mM $CaCl_2$ with NaB, 1:40 ratio.

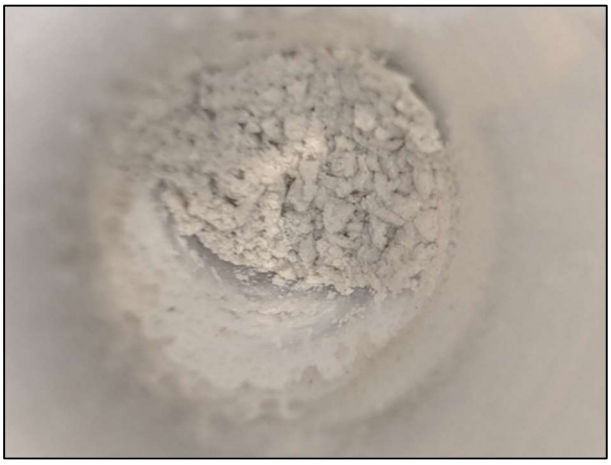

Figure D2-3: Batch adsorption tube, 5000 mg/L PAHW in 167 mM $CaCl_2$ with NaB, 1:40 ratio.

Figure D2-4: Batch adsorption tube, 2500 mg/L PAHW in 167 mM $CaCl_2$ with NaB, 1:40 ratio.

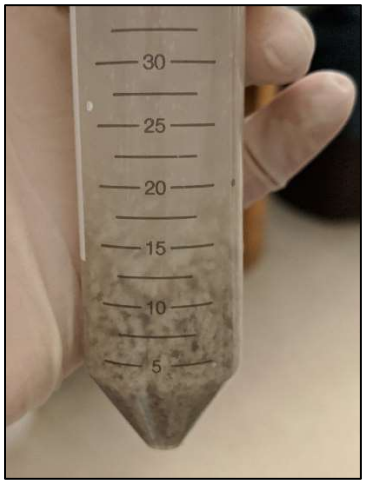

Figure D2-5: Batch adsorption tube, 10,000 mg/L PAHW in 167 mM $CaCl_2$ with NaB, 1:40 ratio.

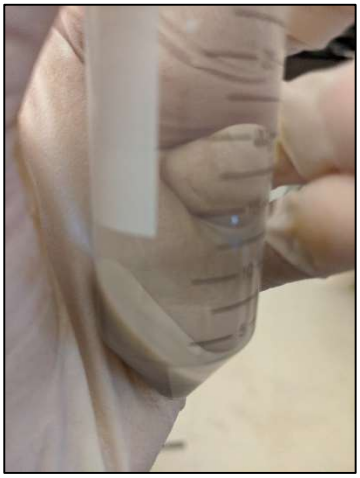

Figure D2-6: Batch adsorption tube, 0 mg/L PAHW in 167 mM $CaCl_2$ with NaB, 1:40 ratio.

Figure D2-7: Batch adsorption tube, 10,000 mg/L PAHW in 167 mM $CaCl_2$ with pyrophyllite, 1:40 ratio.

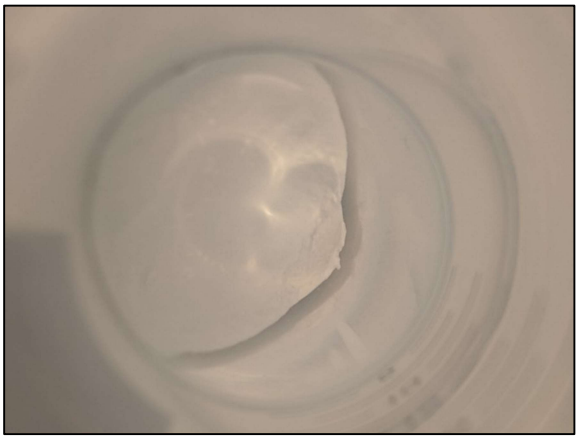

Figure D2-8: Batch adsorption tube, 5000 mg/L PAHW in 167 mM $CaCl_2$ with pyrophyllite, 1:40 ratio.

Figure D2-9: Batch adsorption tube, 2500 mg/L PAHW in 167 mM $CaCl_2$ with pyrophyllite, 1:40 ratio.

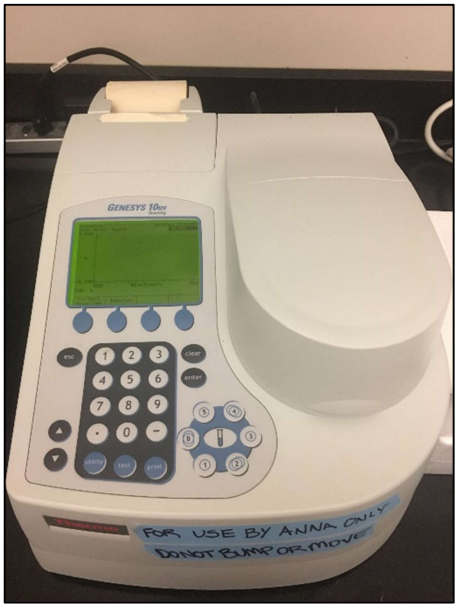

Figure D2-10: UV-Vis Spectrophotometer used for batch adsorption testing.

D3. Materials and methods

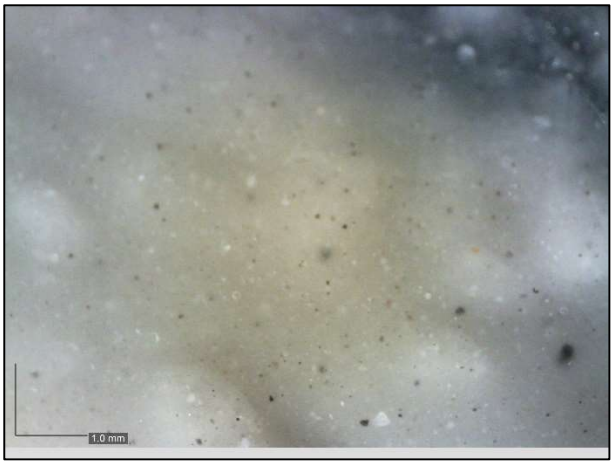

Figure D3-1: Powdered NaB hydrated with tap deionized water.

Figure D3-2: Powdered HVCMC, air-dry.

Figure D3-3: Oven dried PAMW5WM before grinding.

Figure D3-4: Oven dried CMCHV5WM, before grinding.

Figure D3-5: Hydrophobicity of pyrophyllite. Deionized water droplets added are not absorbed.

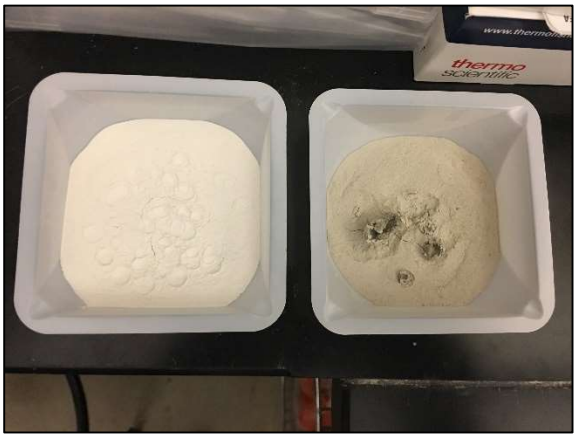

Figure D3-5: Hydrophobicity of pyrophyllite. Deionized water droplets added are not absorbed, compared to addition of deionized water to powdered NaB.

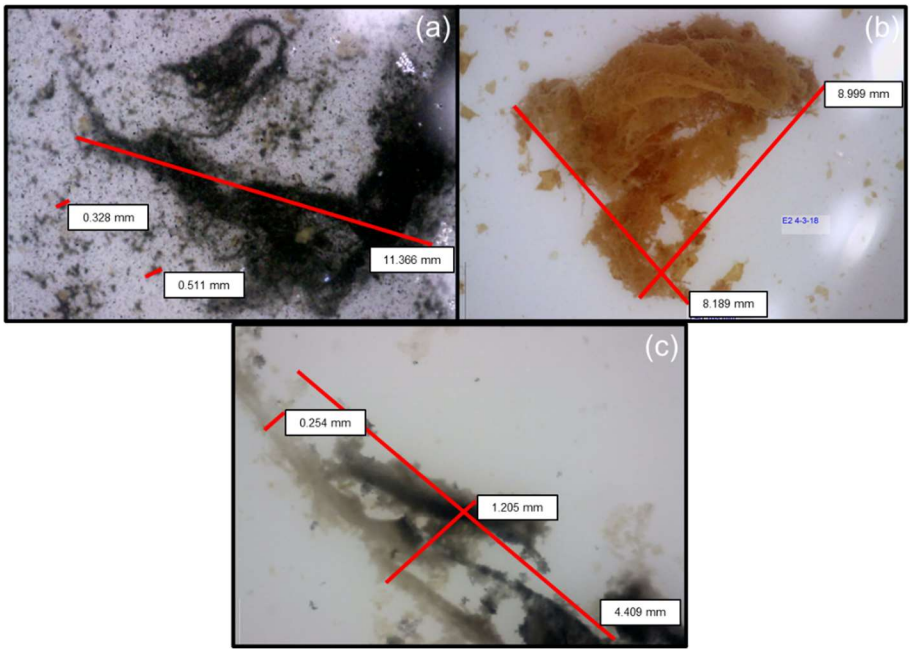

Figure D3-6: Hydrogel in effluent samples collected during permeation.

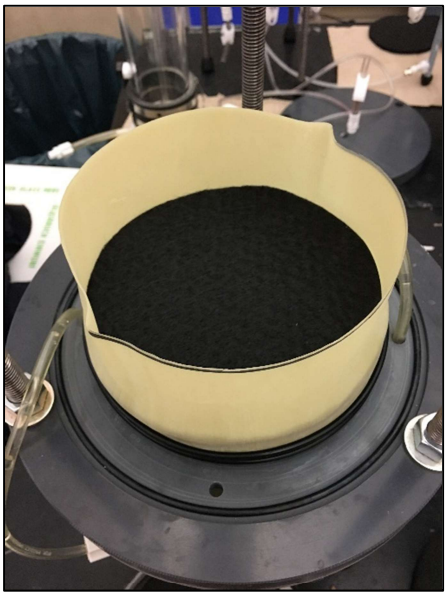

Figure D3-7: EB-GCL assembly, placement of inflow side, nonwoven geotextile.

Figure D3-8: EB-GCL assembly, placement of inflow side calendered, nonwoven geotextile.

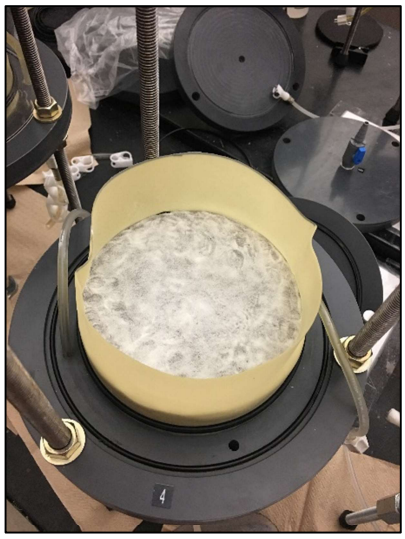

Figure D3-9: EB-GCL assembly, placement of dry-sprinkled polymer on inflow side, on top of calendered, nonwoven geotextile.

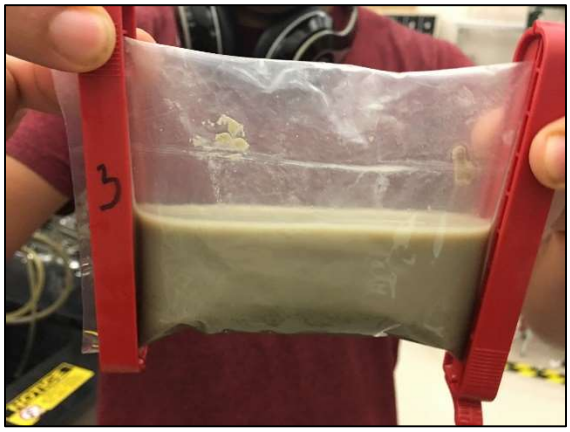

Figure D3-10: Slurry of bentonite at 2 M NaCl after homoionization.

Figure D3-11: Homionized NaB after rinsing with deionized water.

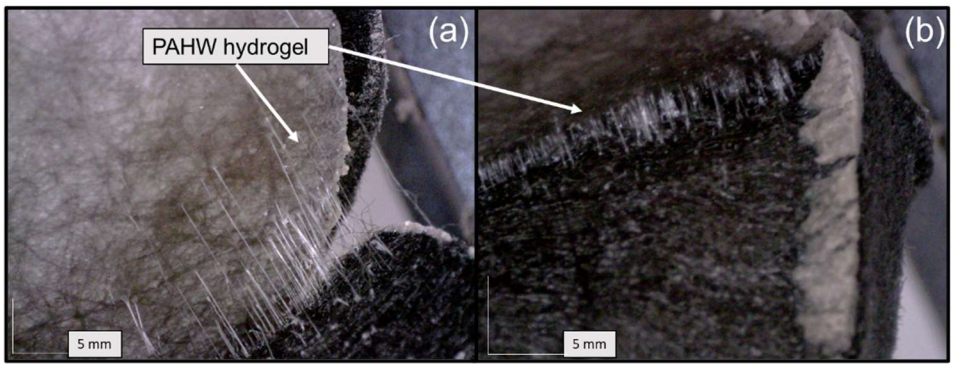

Figure D3-12: Inflow side of EB-GCL PAHW5DS hydrated with 500 mM NaCl and broken down. Visible hydrogel formation during hydration.

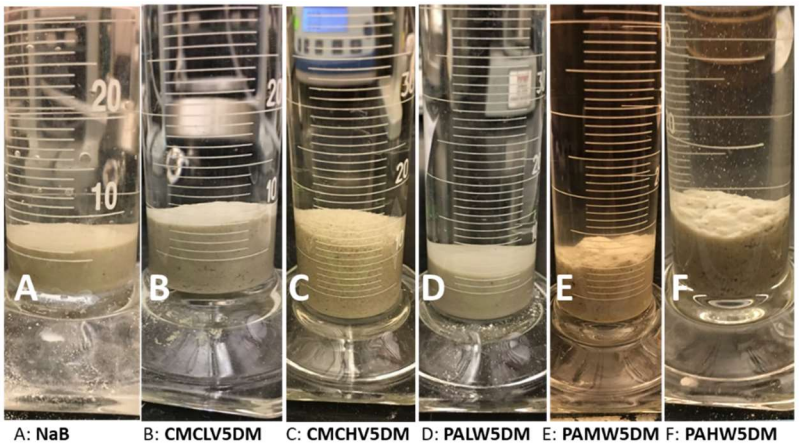

Figure D3-13: Swell index testing of NaB and DM EBs in 167 mM $CaCl_2$.

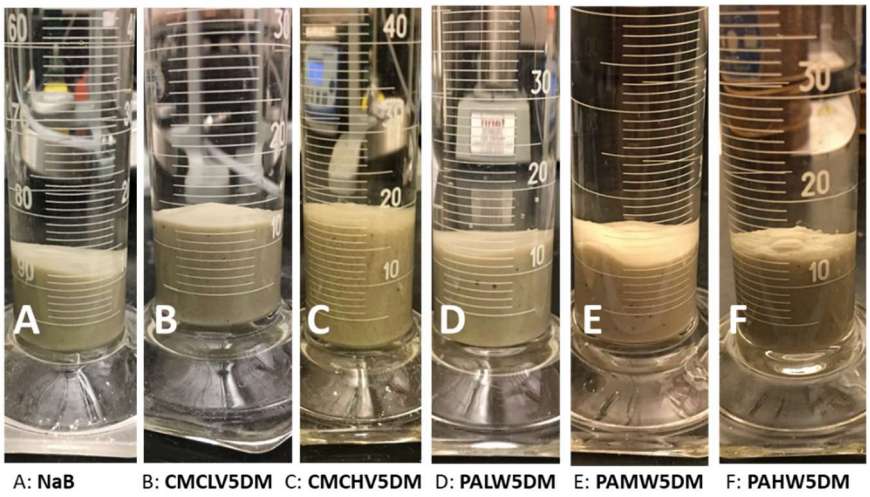

Figure D3-14: Swell index testing of NaB and DM EBs in 500 mM NaCl.

Figure D3-15: Swell index testing of NaB in tap water, 500 mM NaCl, and 167 mM $CaCl_2$.

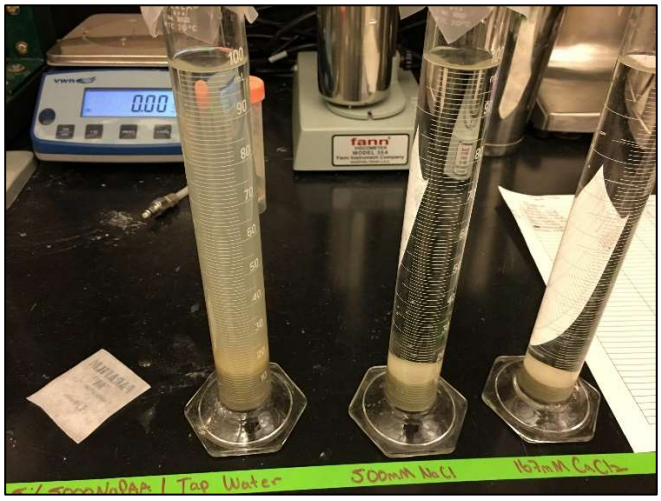

Figure D3-16: Swell index testing of PALW5DM in tap water, 500 mM NaCl, and 167 mM $CaCl_2$.

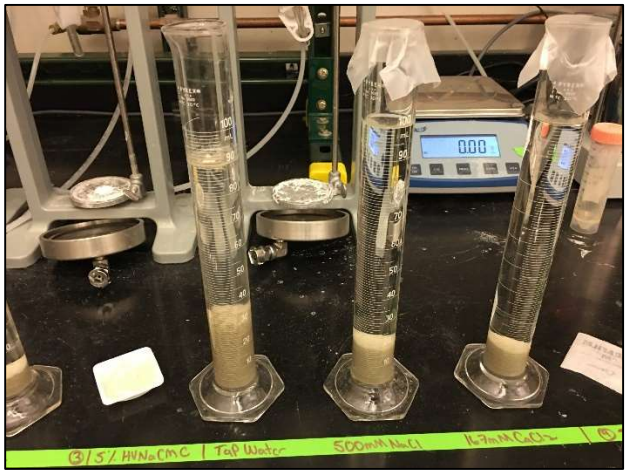

Figure D3-17: Swell index testing of CMCHV5DM in tap water, 500 mM NaCl, and 167 mM $CaCl_2$.

Figure D3-18: Swell index testing of CMCLV5DM in tap water, 500 mM NaCl, and 167 mM $CaCl_2$.

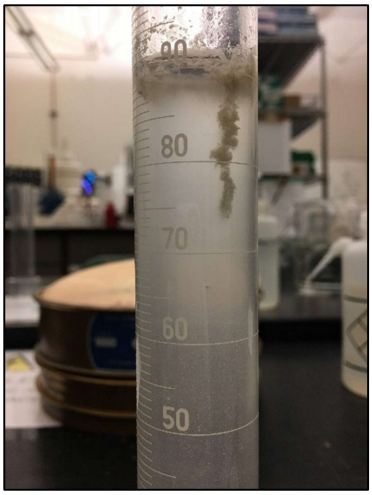

Figure D3-19: Swell index testing of PAHW5DM in 167 mM $CaCl_2$.

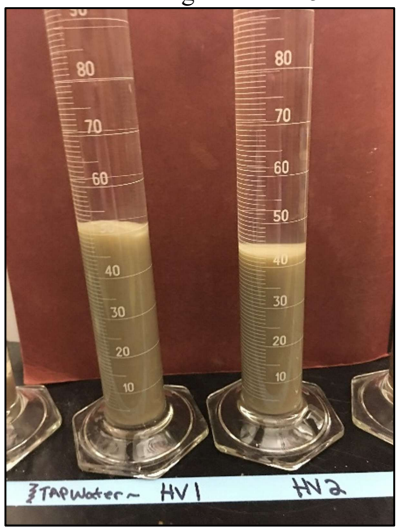

Figure D3-20: Swell index testing of CMCHV5WM in tap water.

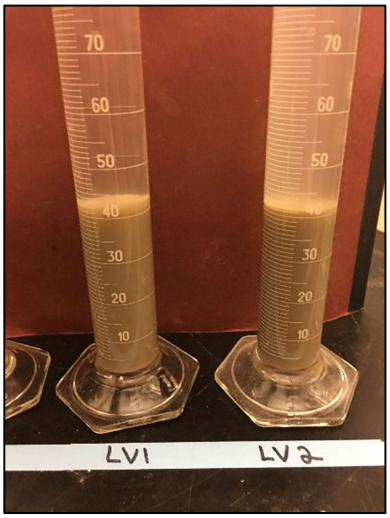

Figure D3-21: Swell index testing of CMCLV5WM in tap water.

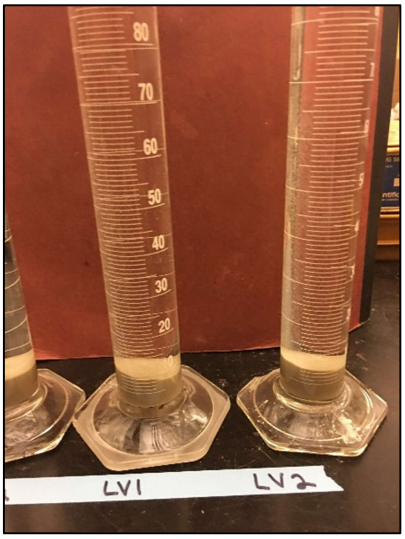

Figure D3-22: Swell index testing of CMCLV5WM in 167 mM $CaCl_2$.

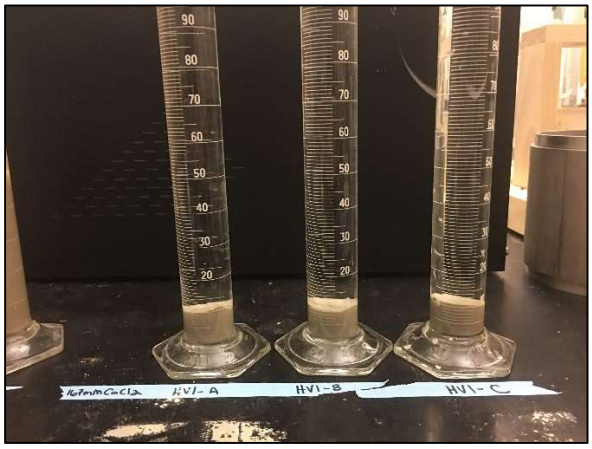

Figure D3-23: Swell index testing of CMCHV5WM in 167 mM $CaCl_2$.

Figure D3-24: Electrical conductivity and pH meter.

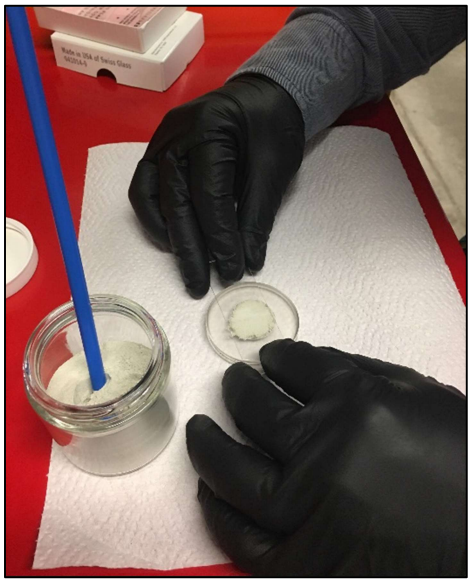
Figure D3-25: Sample preparation for powder X-ray diffraction.

Figure D3-26: Sample preparation for powder X-ray diffraction.

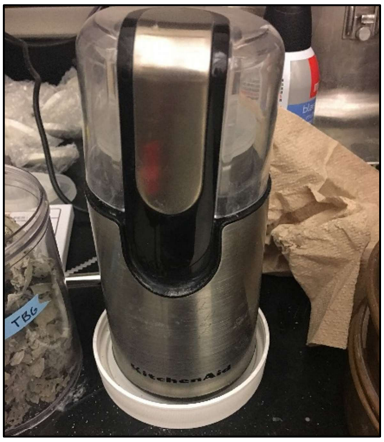

Figure D3-27: Rotary grinder for grinding of dried polymers and wet mixed EBs.

Figure D3-28: Addition of rhodamine dye in inflow burette for preferential flow testing.

Figure D3-29: Inflow burettes for falling head permeation.

Figure D3-30: Elevated water tank for application of cell pressure via gravity head.

Figure D3-31: Desiccator (left) and muffle furnace (right) for loss on ignition testing.

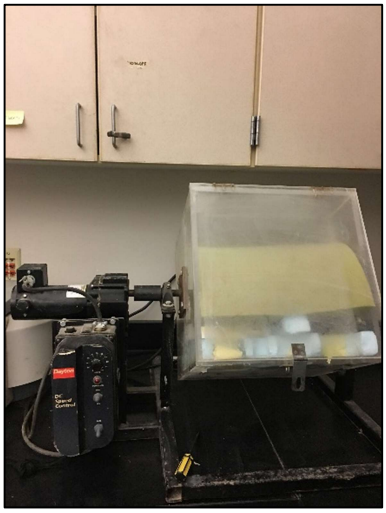

Figure D3-32: Rotary mixer for end over end mixing of batch adsorption samples.

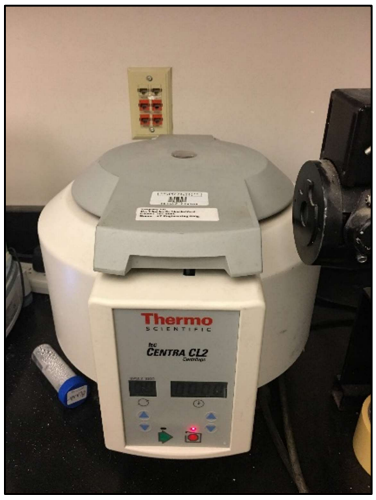

Figure D3-33: Centrifuge used for batch adsorption testing.

Figure D3-34: Mixture of NaB and polymer post ignition in loss on ignition testing.

Figure D3-35: CMCLV (top) and PAHW (bottom) polymer post ignition in loss on ignition testing.

LIST OF ABBREVIATIONS

BPC	Bentonite Polymer Composite
CETCO	Colloid Environmental Technologies Company
CMC	Sodium Carboxymethylcellulose
COO-	Unprotonated Carboxyl Group
COOH	Protonated Carboxyl Group
CRC	Contaminant Resistant Clay
DDL	Diffuse Double Layer
DM	Dry Mix
DOI	Degree of Ionization
DOP	Degree of Polymerization
DoS	Degree of Substitution
DPH-GCL	Densely Pre-hydrated Geosynthetic Clay Liner
DS	Dry Sprinkle
EB	Enhanced Bentonite
EB-GCL	Enhanced Bentonite Geosynthetic Clay Liner
GCL	Geosynthetic Clay Liner
HC	HYPER Clay
HV	High Viscosity
HW	High Molecular Weight
LOI	Loss on Ignition
LV	Low Viscosity
LW	Low Molecular Weight
MMT	Montmorillonite
MSB	Multi-Swellable Bentonite
MW	Medium Molecular Weight
NaB	Sodium Bentonite
PA	Sodium Poly(acrylic acid)
PAx	Crosslinked Sodium Polyacrylate
R	Repeating Unit
SEM	Scanning Electron Microscopy
TC	Total Carbon
TIC	Total Organic Carbon
TOC	Total Organic Carbon
WM	Wet Mix
XRD	X-ray Diffraction